

8-21-2015

Polydopamine Modified Thin Film Composite Membranes for Engineered Osmosis

Jason T. Arena

University of Connecticut - Storrs, arena.jason.t@gmail.com

Follow this and additional works at: <https://opencommons.uconn.edu/dissertations>

Recommended Citation

Arena, Jason T., "Polydopamine Modified Thin Film Composite Membranes for Engineered Osmosis" (2015). *Doctoral Dissertations*. 869.

<https://opencommons.uconn.edu/dissertations/869>

Polydopamine Modified Thin Film Composite Membranes for Engineered Osmosis

Jason Thomas Arena, PhD

University of Connecticut, 2015

The ever expanding human population and improving standards of living have driven the development of new technologies to incorporate into civil infrastructure. The new technologies will augment or replace pre-existing technologies to sustainably deliver life essential goods and services worldwide. Forward osmosis processes represent a fraction of the new ideas being cultivated to meet these needs. These processes are driven by natural forces that exist when solutions of differing osmotic pressures are separated by a semi-permeable membrane. Through the use of a semi-permeable membrane and high osmotic pressure solution, forward osmosis processes offer new ways to produce clean energy and water. Most recent efforts in forward osmosis research have focused on the development of high productivity membranes design for reduced diffusion limitation within the support layer of asymmetric membrane structures which have become the norm in pressure driven aqueous membrane separations. This study differs in that it examines the role of membrane chemistry in improving interactions between membranes and aqueous

electrolyte systems. Membranes were modified for enhanced hydrophilicity to improve wettability of a membrane's structure. After the observation of a unique cation exchange behavior this study branched into the investigation of alternative monomers for the synthesis of semi-permeable membranes. Ultimately, this created a hydrophilic cation exchange resistant polyamide for forward osmosis.

Polydopamine Modified Thin Film Composite Membranes for Engineered Osmosis

Jason Thomas Arena

B.S., Polytechnic University, 2008

M.S., University of Connecticut, 2013

A Dissertation

Submitted in Partial Fulfillment of the

Requirements for the Degree of

Doctor of Philosophy

at the

University of Connecticut

2015

Copyright by
Jason Thomas Arena

2015

APPROVAL PAGE

Doctor of Philosophy Dissertation

Polydopamine Modified Thin Film Composite Membranes for Engineered Osmosis

Presented by

Jason Thomas Arena, B.S., M.S.

Major Advisor _____
Jeffrey R. McCutcheon

Associate Advisor _____
Benny D. Freeman

Associate Advisor _____
Richard S. Parnas

Associate Advisor _____
Leslie M. Shor

Associate Advisor _____
Luyi Sun

University of Connecticut

2015

Acknowledgments

Of the entire proceeding dissertation I am finding this section to be the most challenging for it is with great trepidation do I dare embark on offering up the enormity of the gratitude which I have for the innumerable people who have helped me along this most daunting of paths. The most straightforward sentiment I can offer up is best summed up in the quote attributed to Isaac Newton, "If I have seen further, it is by standing on the shoulders of giants." In all fairness the first people I should acknowledge are those who shoulders I may have in fact stood or at the least sat upon are my parents James and Elizabeth. After them, and by no means of lesser standing is my wife Crystal without who's encouragement I would have never set upon this path. Standing with my her I must also acknowledge my newborn son Nialls and my in-laws Deokie and Ruben. I must also acknowledge my grandparents James,

Joan, Beverly, and Michael, a chemical engineering to boot; they have all proved to be an inspiration in my life. Next, there are the many furry friends who have given me consolation along the way my cat Chewbacca and my parents cats Stormy, Minnie, and Honey. There are so many other members of my family who have also helped and inspired me along this path; there are my uncles (John, Craig, and Rob), my aunts (Bridget, Mary, and Kim), my sister Kristin, my sisters-in-law (Marsha and Asha), and my brothers-in-law (Robert, Reynold, Earrol, Dave, and Drew).

Professionally I have also received immense guidance and help from simple suggestions to insightful intellectual discussion. I first need to acknowledge my research advisor Dr. Jeffrey McCutcheon, followed my committee Dr. Benny Freeman, Dr. Richard Parnas, Dr. Leslie Shor, and Dr. Luyi Sun. Extra special acknowledgment must be given to my committee's sixth ranger Dr. Ranjan Srivastava. Besides my committee members there are the innumerable contacts I have made through my involvement with the American Membrane Technology Association (Dr. Harold Fravel, Mr. Jeff Mosher, Mr. Stuart McClellan) and the North American Membrane Society (Dr. Uwe Beuscher, Dr. Fred Steward, Dr. Aaron Wilson). An extra special gratitude has to been given to funding source which have been personally extend to me the American

Membrane Technology Association and the National Water Research Institute for the membrane technology research fellowship which was awarded to me for 2013-2014 and 2014-2015 academic years. I must also acknowledge the National Science Foundation and the University of Connecticut for the GK-12 fellowship extended to me for the 2010-2011 and 2011-2012 academic year; the GK-12 program manager Ms. Aida Ghiaei and principle investigators Dr. Doug Cooper and Dr. Kazem Kazerounian. There innumerable others both within and without the University of Connecticut who helped to contribute to this work (in no intended order) Mr. Joe Csiki, Mr. Mark Drobney, Mr. John Pudelkiewicz, Mr. Steve Massey, Mr. Russ Casey , Mr. Bernie Plantz, Mrs. Susan Soucy, Mrs. Leah Winterberger, Mrs. Carol Ruel, Ms. Charlene Fuller, Dr. Bryan McCloskey, Dr. James Arena (yes my Dad, if the reader has free time check out his dissertation it should be only a few shelves over), Dr. Joseph Cook, Dr. Ryan Lively, Dr. Dan Miller, Dr. Chad Johnston, Dr. Abhay Vaze, Dr. Maria Chrysochoou, and Dr. Dan Burkey. Additionally there my lab colleague who have been a source of support and stimulating discussion over these many years (in alphabetical order, so do not read too much into the order guys) Dr. Dan Anastasio, Mr. Maqsud Chowdhury, Ms. Malgorzata Chwatko, Ms. Emily Cole, Dr. Seetha Manickam, Ms. Breanne Muratori, Mr. Kevin Reimund,

Ms. Jian Ren, Dr. Ngoc Bui, Mr. Justin Durelli, Dr. Liwei Huang, Mr. Brendan O'Grady, and Ms. Ling Ling Xia.

And finally there are the people who helped get me on the path being a chemical engineering graduate student at the University of Connecticut in the first place. I must acknowledge my undergraduate research advisor Dr. Edward Ziegler. Special gratitude must be extended to the funding for my undergraduate education all person associated with the the Walter J. Kenny scholarship. I have to acknowledge my high school teacher who pushed me into the engineering discipline in the first place, Mr. Paul Argassi. While I have tried to be as expansive as possible I must end this acknowledgment by acknowledge, thank, and apologize to any I have forgotten. One final extra special acknowledgment goes out to any who one who feels I should have acknowledgement more. To all the aforementioned, the unmentioned, and you the reader, "Thank you!"

Table of Contents

Chapter 1

Membranes in reverse and forward osmosis	1
--	---

Chapter 2

The ammonia-carbon dioxide draw solution	35
--	----

Chapter 3

Polydopamine modification of commercial thin film composite membranes for pressure retarded osmosis.....	57
--	----

Chapter 4

Pressure retarded osmosis performance of polydopamine modified membranes with differing permselectivities and structure	85
---	----

Chapter 5

Solute and water transport in forward osmosis using polydopamine modified thin film composite membranes	133
---	-----

Chapter 6

Comparison of polydopamine modified thin film composite membranes reverse osmosis membranes to forward osmosis membranes available commercially.....	166
--	-----

Chapter 7

pH sensitivity of ion exchange through a commercial thin film composite membrane in forward osmosis.....	190
--	-----

Chapter 8

Alternative and post-treated polyamide chemistries for the mitigation of ion exchange in forward osmosis	213
--	-----

Concluding Remarks	252
 Appendix 1	
Speciation of the ammonia-carbon dioxide draw solution	254
 Appendix 2	
Design and iteration of the dopamine coating containers.....	258
 Appendix 3	
Titration of chloride within the ammonia-carbon dioxide draw solution.....	278
 Appendix 4	
Numerical simulation of membrane performance and calculation of effective structural parameter	282
 Appendix 5	
Character and performance relationships for a high water flux commercial thin film composite membrane in forward osmosis desalination and pressure retarded osmosis	295
 Appendix 6	
Numerical simulation of water flux and simultaneous determination of membrane transport parameters in forward osmosis.....	333

Chapter 1

Membranes in reverse and forward osmosis

1.1. Water resources

Accessible and sustainable water and energy resources are critical to the further development of the human species. Despite the fact that over 70% of the planet is covered with water there are many regions worldwide where freshwater is or will soon become a scarce resource. Water scarcity with increasing concerns about the impact of current energy production technologies to human and environmental well-being necessitates the investigation and maturation of new water and energy production technologies.¹⁻³ Any investigation into the availability of water sources and their availability will, ignoring economics, arrive at the competition between water consumption for energy production and energy consumption for water production.^{1,4} The link between water and energy has received increased attention from

growth in the use of unconventional water sources such as saline waters (brackish groundwater and seawater) or wastewater to meet local and regional water needs.^{2,4,5} These unconventional water sources have increased energy requirements over conventional centralized distribution of freshwater resources.¹

Desalination (the separation dissolved salts from water) has large innate energy costs because of thermodynamic restrictions limiting the efficiency or recovery of water from a saline water source.⁶ The specific limitations in water recovery and energy usage will vary from one desalination process to another.⁷ The energy usage and its associated costs limit the applicability of readily available desalination technologies. Thermal processes, which remove water vapor from a saline solution containing a nonvolatile electrolyte, boil water and condense water vapor in their operation. Amongst the primary drawback of distillation for seawater desalination are scaling and corrosion of the process equipment and high energy costs.⁸ Electrochemical desalination process such as electrodialysis are limited to feed solution concentrations below $5000 \text{ mg}\cdot\text{L}^{-1}$. Additionally, eletrodialysis can only remove ions from the product water. This limitation means uncharged contaminants to remain in the product water making it undesirable for potable water supply.^{8,9} Meanwhile membrane separation processes

like reverse osmosis (RO) apply a large hydrostatic pressure to a saline feed solution to force water through a semi-permeable membrane.^{3,6,8} RO processes have been improved to be the most energy efficient of the matured desalination processes;⁷ however, even efficient RO processes have substantially higher capital and operating costs than a conventional centralized water distribution system.¹ The presence of solutes within saline waters sources influence the colligative properties of the water in which they are dissolved such as a reduction in the water vapor pressure over the solution and increasing the solutions osmotic pressure.¹⁰

1.2. Osmotic pressure

What is osmotic pressure?

When a solution, e.g. of sugar in water, is separated from the pure solvent - in this case water - by a membrane which allows water but not sugar to pass through it, then water forces its way through the membrane into the solution.

This process naturally results in greater pressure on that side of the membrane to which the water is penetrating, i.e. to the solution side.

This pressure is osmotic pressure.

-Jacobus H. van't Hoff, 1901¹¹

The osmotic pressure of an aqueous solution is affected by the concentration of dissolved chemical species within.^{10,12} A number of relationships have been developed which relate solute concentrations to osmotic pressure of a solution. The van't Hoff equation approximates the osmotic pressure of a solution from the molar concentrations of solutes, shown in Eq. (1.1).^{10,13}

$$\pi = \sum_{i \neq W} c_i R_{\text{const}} T \quad (1.1)$$

Many early studies which calculated the osmotic pressure of solutions experimentally noted deviations from the osmotic pressure which was calculated using the van't Hoff equation.^{14,15} This led to the derivation of the Morse equation, which differs from the van't Hoff equation in that it uses molality rather than molarity for the concentrations of the solutes within solution, shown in Eq. (1.2).¹⁴

$$\pi = \sum_{i \neq W} \frac{m_i}{\rho} R_{\text{const}} T \quad (1.2)$$

Further refinements to the calculation of the osmotic pressure of a solution led to relationships that can calculate the osmotic pressure of a solution from the activity of water. The use of water activity introduces other approaches for the calculation of osmotic pressure such as freezing point depression or boiling point elevation osmometry which calculates the

activity of water as influenced by colligative properties. They can calculate the osmotic pressure of complex solutions without necessarily knowing the concentration of solutes within solution. The equation for calculation of osmotic pressure from water activity is shown in Eq.

(1.3).^{10,16,17}

$$\pi = -\frac{1}{v_w} \ln(a_w) R_{\text{const}} T \quad (1.3)$$

The osmotic pressures created by solutes within solution can be immense, equivalent to many hundreds of bar of hydrostatic pressure¹¹ and this creates a substantial opposing potential which makes reverse processes so energy intensive.

1.3. Transport through dense semi-permeable membranes

Transport through semi-permeable membranes commonly encountered in water separations is governed by the solution-diffusion behavior. In solution-diffusion, chemical species that permeate through a membrane must first dissolve into the polymer and diffuse through it.¹⁸ Membrane selectivity or the capacity of semi-permeable membranes to retain or impede the transport of dissolve solutes across a membrane's selective layer requires that a salt have a lower solubility and/or lower diffusivity through a membrane than the solvent in

which it is dissolved or suspended. Coinciding with the solubility and diffusivity of salt within a membrane there is the added limitation of electroneutrality when considering the transport of dissociating salts.¹⁹ Electroneutrality or the balance between positive and negative charges requires that a cation or anion diffusing through a membrane must carry with it its counterion. For membranes in pressure driven applications this means that a membrane separating a single salt from water need only be impermeable (or have low permeability) to either the cation or anion of a salt and electroneutrality will prevent its' counterion from also crossing the membrane.^{20,21}

Water moves through a membrane's selective layer with the same restrictions as salts, needing to dissolve into the polymer phase of the selective layer and diffuse through it. The rate of transport through a dense membrane's selective layer for both water and dissolve salts is lower for thicker membranes since the distance that these chemical species must diffuse through to cross a membrane is increased.¹⁸ The importance of thickness in its contribution to membrane resistance (the inverse of water permeance). To minimize the resistance of a dense membrane practical membranes are asymmetric structures having a thin dense selective layer (the actual membrane) supported by thicker porous materials. The porous support layers allow

for the formation of membrane with good mechanical properties for membrane applications without having a high resistance to water transport.

1.4. Reverse osmosis

Reverse osmosis (RO) is the application of hydrostatic pressure overcome the osmotic pressure of an aqueous solution and force water across a semi-permeable membrane. In a pressure driven separation of solvent from a solution, water must overcome the resistance to water transport by membrane and the osmotic pressure potential that opposes the hydrostatic pressure applied to it.^{3,20,21} The governing equation for water flux in a hydrostatic pressure driven membrane process is shown in Eq. (1.4).^{13,21}

$$J_w = A(\Delta P - \Delta \pi) \quad (1.4)$$

With a RO system there are three principles stream: the feed, the solution pressurized against a membrane, the permeate, the solution or ideally pure solvent which crosses the membrane, and the retentate, the solution or brine concentrated by RO containing solute that were rejected or retained by the membrane.²¹ The osmotic pressure exerted across a membrane ($\Delta \pi$) is affected by the selectivity of a membrane or its solute permeability (B). The

solute permeability being is a function of the solubility and diffusivity of solutes within a membrane.^{3,22,23}

$$J_s = B(\Delta C) \quad (1.5)$$

The governing equation for solute flux across a membrane is shown in Eq. (1.5). Both the water permeance (A) and solute permeability (B) are intrinsic properties of a membrane impacted by the thickness of a dense selective layer and the material from which it is formed. A description of the mechanism by which water and solute move through the selective layer is in Section 1.5. The dense selective layer of the membrane mediates the transport of water and salts across the complete membrane structure and each solute has a unique B for a given membrane selective layer (i.e. the B value of a membrane for sodium chloride is different from the B value for magnesium sulfate). The osmotic pressure exerted across a membrane is directly impacted by solute permeability. A membrane having a low permeability to a solute will have an osmotic pressure exerted across it close to the osmotic pressure of the pressurized feed solution because in a RO type experiment a low B will result in a sharp concentration difference across the membrane's selective layer.²¹

$$R = \frac{C_f - C_p}{C_f} \quad (1.6)$$

Rather than measure solute permeability directly, the rejection (R) of the membrane in a RO process is commonly calculated first. The rejection then used to calculate solute permeability. Rejection represents the percentage of feed solute which crosses the membrane and is the attribute of membrane performance directly calculated in RO style characterization experiments. From rejection measured in an RO experiment the solute permeability can then be used to calculate the solute permeability by Eq. (1.7).²⁴

$$B = \frac{(1-R)A(\Delta P - \Delta \pi)}{R} = \frac{(1-R)J_w}{R} \quad (1.7)$$

1.5. Forward osmosis

Forward osmosis (FO) processes are a pool of technologies seeking to harness the potentials of osmotic pressure difference between two aqueous systems separated by a semi-permeable membrane.^{13,24-26} FO processes can take the form of waste or solution concentration (direct osmotic concentration), draw solution dilution from an impaired water source (direct osmotic dilution), energy production (pressure retarded osmosis), or water

desalination (forward osmosis desalination).

The general governing equation for water flux in an FO process can be expressed by Eq.

(1.8).^{13,27}

$$J_w = A(\Delta\pi - \Delta P) \quad (1.8)$$

In an FO process, water flows from a low osmotic pressure feed solution to a higher osmotic pressure draw solution when these solutions are separated by a semi-permeable membrane.

Water permeates through the membrane into the draw solution leaving solutes (if present) behind within a concentrated feed stream.²⁸⁻³¹ This separation requires no energy input, as it is driven by the spontaneous thermodynamic tendency towards osmotic equilibrium. The earliest work in FO for water purification uses used a concentrated sugar draw solution to draw water across a cellulose acetate reverse osmosis (RO) membranes. These studies used a consumable draw solution unsuitable for a continuous FO process.^{28,29}

Alongside the flow of water through a membrane in FO, solutes transport bidirectionally across membranes in an FO process.³²⁻³⁴ In addition to water flux feed solute cross the membrane into the draw solution and draw solutes cross the membrane into the feed. Like RO, the permeability of solutes across the membrane, shown in Eq. (1.5), impacts this behavior

with solute flux occurring along the direction of concentrations differences across the membrane. As shown in Fig. 1.1, reverse solute flux is the flux of draw solute across the membrane occurring opposite the direction of water flux, and forward solute flux is the flux of feed solutes in the direction of water flux.

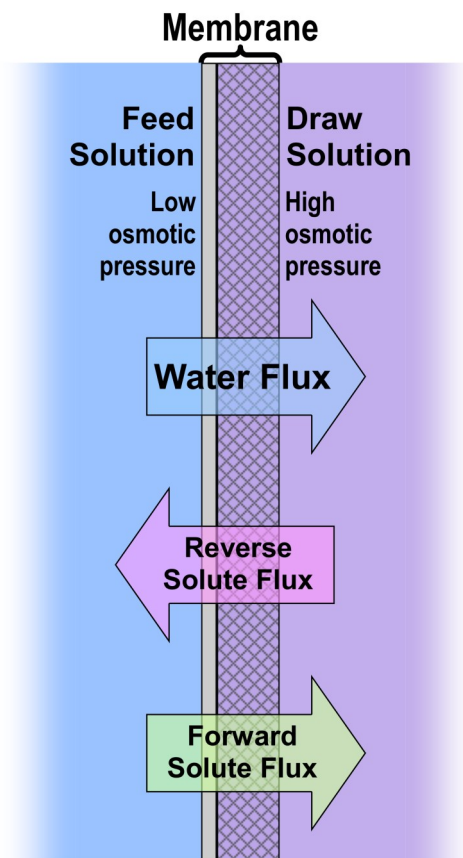


Fig. 1.1. Direction of water and solute flux across a membrane in forward osmosis.

An ideal draw solute for a FO process is one which can be easily removed from the draw solution.

The only significant energy input into the process is used for the separation of the draw solute and water^{7,30,35}. A variety of draw solutes have been proposed for FO desalination processes. Amongst these are surface modified nano-particle,³⁶⁻³⁸ switchable polarity solvents,³⁵ polymers which display a thermal sensitivity to water solubility,³⁹ and electrolytes.^{30,40-47} Electrolyte draw solutes offer generally lower viscosities and higher diffusivities over other proposed draw solutes. Sodium chloride

(NaCl) is commonly used as draw solute for FO/RO processes where an FO is used to dilute a NaCl stream that is subsequently concentrated in a following RO step.^{43,48} Another branch of electrolyte draw solutions considered are those based upon thermolytic draw salts, which consists of water soluble gases forming ionic species within solution.^{7,49,50} This allows for a sufficiently high concentration of draw solute to desalinate waters with high amounts of dissolved solids.⁴⁶ A draw solution initially proved for seawater desalination by McCutcheon is a mixture of ammonia (NH_3) and carbon dioxide (CO_2) gases.³⁰

When present in solution these gases form ammonium (NH_4^+) cations and carbonate (CO_3^{2-}), bicarbonate (HCO_3^-), and carbamate (NH_2COO^-) anions.^{7,49} A thermolytic salt solution is comprised of dissolved gases that can be removed from solution using with heat.^{7,41} The stripped gases can then be absorbed into water, recycling them within a closed loop process.⁴⁶ A detailed discussion of draw solutions and the $\text{NH}_3\text{-CO}_2$ draw solution can be found in Chapter 2.

1.6. Semi-permeable membranes

1.6.1. Thin film composite membranes

The current industrial standard in reverse osmosis membranes is the thin film composite (TFC) membrane chemistry.^{21,51} TFC membranes employ polymers resilient to many chemicals within three distinct layers. The base layer that rest of the membrane is built upon is a non-woven polyethyleneterephthalate (PET) fabric. This layer provides mechanical strength to the final membrane structure and serves as a substrate for the phase inverted polymer mid-layer. In commercial applications this is typically polysulfone (PSu) or polyethersulfone

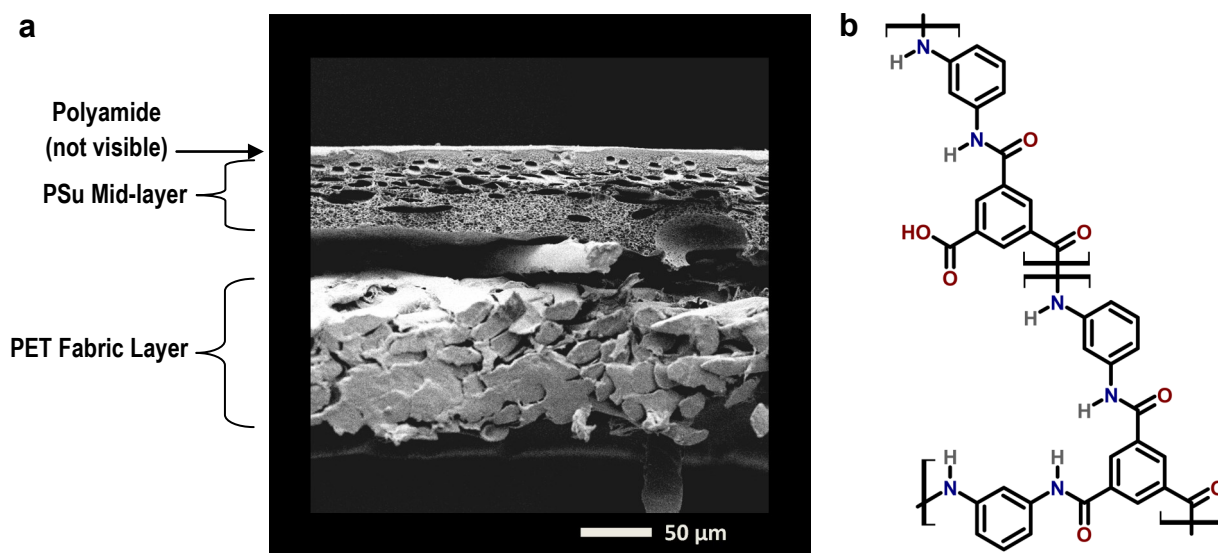


Fig. 1.2. Scanning electron microscope image of the cross-section of a SW30-HR from Dow Water and Process Solutions (a). This shows the three principle layer in the construction of thin film composite RO membranes. Chemical structural of the polyamide selective layer used in TFC for salt water desalination (b).

(PES) as these polymers have been found to give good permselectivity and are physicochemically stable.^{51,52} The topmost layer is almost exclusively a dense cross-linked polyamide made from a condensation reaction between a diamine or polyamine and acid chloride.⁵¹ Fig. 1.2 shows the structure of the SW30-HR high rejection seawater reverse osmosis membrane from Dow Water and Process Solutions.

The formation of a polyamide selective layer is synthesized in an interfacial polymerization (IP) reaction. In IP, a polymer film is formed at the interface between two immiscible solvents. For the formation of polyamide selective layers, an acyl chloride is dissolved within a nonpolar organic solvent and reacted with an aqueous diamine or polyamine. The most common TFC polyamide in both FO and RO applications is synthesized from m-phenylenediamine (MPD) in water and 1,3,5-benzenetricarbonyl trichloride (alternatively trimesoylchloride or TMC) in an alkane.⁵²⁻⁵⁶ The use of these monomers in interfacially polymerized TFC membrane was first reported by Cadotte et al.,⁵² preceded by many years of study in the preparation of polyamides for the separation of dissolved solids and water. An early polyamide using ethylene diamine (ED) instead of MPD within the aqueous phase and TMC within the organic phase and was observed having 95-97% sodium chloride rejection at 13.8 bar (200 psi).⁵¹

1.6.2. Asymmetric cellulosic membranes

The Loeb-Sourirajan dry/wet process was initially developed in the 1960s for the preparation of asymmetric reverse osmosis membrane.⁵⁷ Like TFC membranes, commercial cellulose RO membranes are prepared upon a fabric support layer for mechanical strength and to serve as the initial substrate in the preparation of the membranes.⁵⁸ In the original embodiment of cellulosic membrane preparation a solution of cellulose acetate is dissolved in acetone with magnesium perchlorate and drawn out upon a glass plate at a thickness of 250 μm (0.01 in). The drawn polymer solution was permitted to air dry for 2-4 min. Drying the cast polymer solution forms a dense film which later serves as the selective layer of the final membrane. After drying, the film is immersed into a water bath.⁵⁷ Cellulose acetate is insoluble in water and the mixing of solvent within the polymer solution and water results in the precipitation of polymer which forms a porous polymer film with a dense topmost skin layer. The final step of the Loeb-Sourirajan process is annealing the membrane at temperature of 77-83 °C. Annealing densifies the selective layer of a cellulose acetate membrane improving its rejection of electrolytes and low-molecular weight compounds.^{59,60} Since the initial discovery of polymeric cellulose based RO membranes a number of different cellulosic polymers can be

employed in the preparation of membrane for both RO and FO including cellulose acetate, cellulose acetate butyrate, cellulose acetate propionate, and cellulose triacetate.^{60,61}

1.7. Membrane orientations in osmotic flow

1.7.1. Forward osmosis orientation

The forward osmosis membrane orientation is commonly used in processes which employ feed solutions having a high fouling propensity. This includes many of the large scale continuous FO processes which handle suspensions or emulsions such as wastewater or produced waters from hydrocarbon excavation.^{42,46,48} The FO orientation describes when the draw solution contacts the support layer of the membrane and the feed solution is in contact with the selective layer of a membrane. In this orientation water permeating along the concentration gradient first passes through the selective layer and then moves through the membrane support layers.

1.7.2. Pressure retarded osmosis orientation and process

Pressure retarded osmosis (PRO) is a renewable energy technology to harness the latent energy of an osmotic pressure difference between two solutions. In PRO processes the draw

solution is pressurized to a hydrostatic pressure less than its osmotic pressure so osmosis can still occur into the draw solution through a semi-permeable membrane. The water flux through the membrane from osmosis produces a constant pressure volumetric increase of the draw solution. This increase in volume at constant pressure is converted to work by relieving the pressure through a hydroturbine.^{45,62} Commonly the volumetric increase of the draw solution is expressed as the membranes water flux. Water flux combines with the draw solution hydrostatic pressure to calculate a membrane's power density, shown in Eq. (1.9). Power density is often used as the defining metric of a membrane in PRO.

$$\eta = J_w \cdot \Delta P \quad (1.9)$$

Membranes in PRO are oriented so its selective layer faces the draw solution.^{13,63} This orientation gives maximum water flux, needed for high power high power density, and also imparts a degree of pressure tolerance. The applied hydrostatic pressure compacts the selective and support layers against the fabric layer, which provides asymmetric membranes with much of their mechanical strength.

1.8. Mass Transport Limitation in Osmosis

Semi-permeable membranes used in FO are asymmetric structures consisting of a dense selective layer, which mediates solute and water transport, and porous support layer(s), which provide mechanical reinforcement for a membrane's selective layer. Osmosis occurs only through the membrane support layer. The dependence of osmosis on an osmotic pressure gradient leaves it affected by the dilution of the draw solution and concentration of the feed solution as water flows from the latter to the former. In addition to the unmixed external boundary layer encountered in a RO type process, the support layer(s) of the membrane also behave similarly to an unmixed boundary layer. Here convection the solution (as water flux through the membrane) and the diffusion of solutes are transport limitations to the membranes interface.^{22,23,27,64} In the preparation of the governing equation for water flux in forward osmosis water is treated as a continuum through which solutes travel towards and away from the selective layer. The concentration of solutes at the selective layer is crucial to osmosis since osmotic pressure is the driving potential for water flux through the membrane. That leaves only salt diffusion both through the selective layer and related diffusion limited distances to be considered. Yip²³ and Tiraferri²² have derived rigorous governing equations for water flux

based upon bulk feed and draw solute concentrations.

$$J_w = A \left\{ \frac{\pi_{d,b} \exp\left(-\frac{J_w}{k}\right) - \pi_{f,b} \exp(J_w K)}{1 + \frac{J_w}{B} \left[\exp(J_w K) - \exp\left(-\frac{J_w}{k}\right) \right]} - \Delta P \right\} \quad (1.10)$$

$$J_w = A \left\{ \frac{\pi_{d,b} \exp(-J_w K) - \pi_{f,b} \exp\left(\frac{J_w}{k}\right)}{1 + \frac{J_w}{B} \left[\exp\left(\frac{J_w}{k}\right) - \exp(-J_w K) \right]} - \Delta P \right\} \quad (1.11)$$

Eq. (1.10) and Eq. (1.11) illustrate the differences in water flux through a membrane as affected by membrane orientation. The first of these two orientations is called the PRO mode where the selective layer is contacting the draw solution (show in Fig. 1.3a and Eq. (1.10)). The other orientation is called the FO mode where the selective layer contacts in the feed solutions (show in Fig. 1.3b and Eq. (1.11)). It should be noted that Eq. (1.10) and Eq. (1.11) assumes an ideal van't Hoff relationship between solute concentration and osmotic pressure. K is the solute resistivity which describes the diffusion rate of solute through the membrane support layer(s). The effective distance through which solute diffusion occurs is referred to as

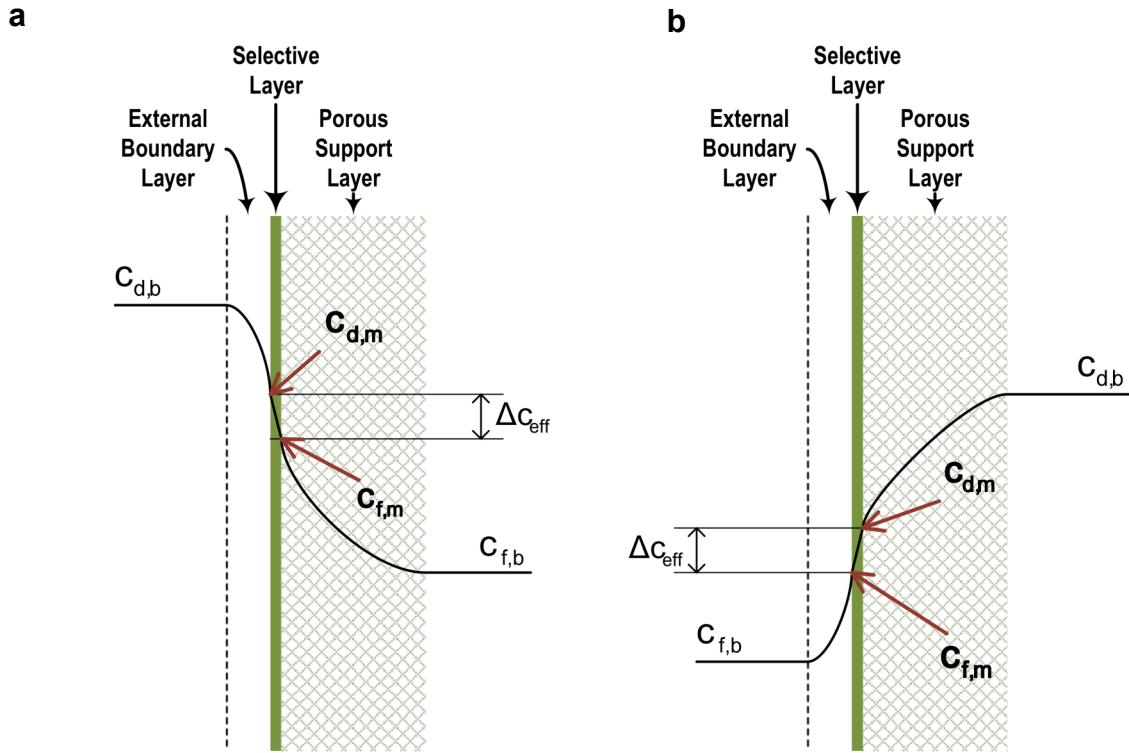


Fig. 1.3. Concentration gradients across asymmetric membranes in the PRO (a) and FO (b) membrane orientations.

the structural parameter of the membrane, which ideal relates to the structural morphology of an asymmetric membranes support layer, shown in Eq. (1.12).¹³

$$S = K \cdot D = \frac{t \cdot \tau}{\varepsilon} \quad (1.12)$$

The structural parameter (S) along with the water permeance (A) and solute permeability (B) comprise the three intrinsic properties of the membrane which dictate how the membrane

behaves in osmosis. Ideal membrane structures are those which have a high water permeance (A), low solute permeability (B), and low structural parameter (S). A lower solute permeability is desirable since it increases the usable osmotic pressure for osmosis by mitigating reverse solute permeation diffusion limitations. An experimental and theoretical study on the role of selectivity in PRO is in Chapter 4.

1.9. Limitations and improved membranes for forward osmosis

One widely available FO membrane is produced by Hydration Technology Innovations (HTI). This membrane is made from cellulose triacetate, formed through a Loeb-Sourirajan type wet casting process.⁶¹ While this has produced a membrane with sufficient permeability, selectivity and chemical resilience to operate in a number of processes,^{24,30,38,48,65-69} cellulose acetates are vulnerable to hydrolysis which results in the replacement of acetyl groups with hydroxyl degrading membrane selectivity.^{21,70} Additionally, membranes made from cellulose acetates characteristically tend to have lower water permeance than a similar thin film composite membrane.²¹ These limitations encouraged the development of alternative membrane chemistries for FO. Thin film composite (TFC) membranes have been considered as the logical replacement for cellulose derived membranes in FO; however, early studies

observing commercial TFC reverse osmosis membranes in forward osmosis reported low water fluxes.^{30,67} TFC membranes typically employ a cross-linked polyamide selective layer that, while susceptible to degradation by hypochlorous acid and hypochlorite salts,⁷¹ exhibits stability over a broader pH range than cellulose acetate based membranes.²¹

Numerous studies have sought to design an improved TFC membrane for FO by developing optimized morphologies to minimize membrane structural parameters. One of the earliest recent studies from Yip et al. examined techniques to improve support layer morphology with hand cast PSu membranes by using a blended solvent system of

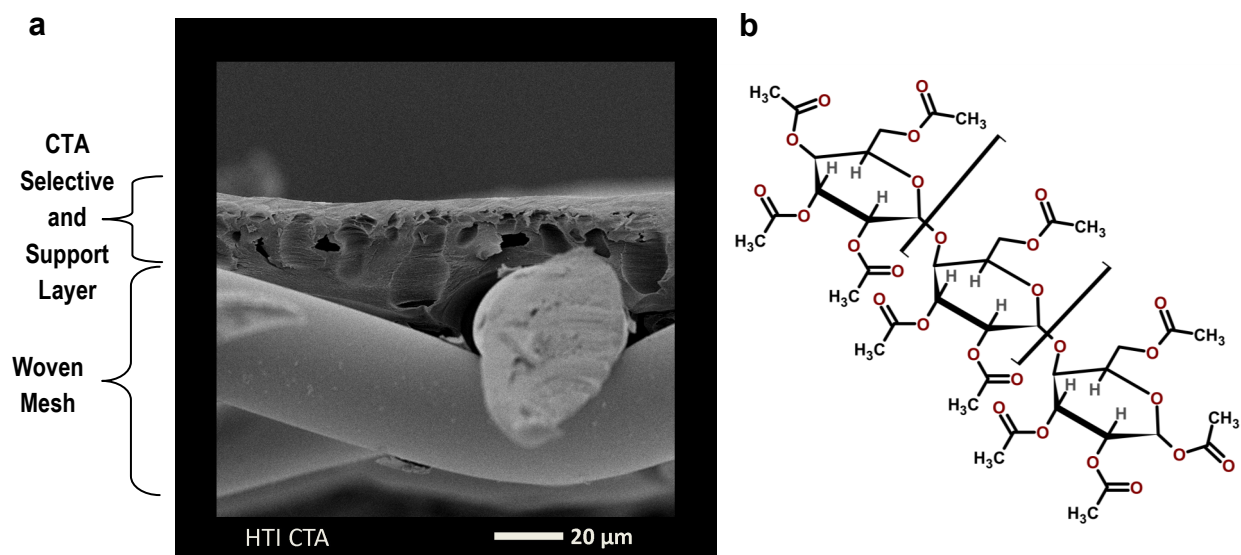


Fig. 1.4. Scanning electron microscope cross-section of the cellulose triacetate forward osmosis membrane made by Hydration Technology Innovations (a). Chemical structure of cellulose triacetate (b).

1-methyl-2-pyrrolidinone (NMP) and dimethylformamide (DMF).⁵⁶ Subsequent studies have examined differing morphologies created by altering solvent ratios⁷² or doing a post fabrication hypochlorite degradation of the polyamide.²³ Wei examined the effects of lithium chloride as a pore former using cast solutions of NMP and polysulfone.⁷³ In general studies seeking to reduce mass transport limitation in FO seek supports with straight finger-like pores.^{26,56,72} A different approach was employed by Widjojo et al. who fabricated spongy PES support through the blending of sulfonated polyethersulfone into the casting solution.⁷⁴ Using a polyimide Han demonstrated the fabrication of a spongy pore structure capable of high pressure tolerances for PRO.⁸⁵ A radically different technique for TFC synthesis was presented by Bui et al. who used electrospun nanofibers as a support for TFCs.⁷⁵ Electrospinning allows for the fabrication of thin, highly porous membrane supports with low tortuosity. Hoover also examined electrospinning as a synthesis route for PET non-wovens to eliminate the need for conventional PET non-wovens which has a significant mass transport limitation in conventional TFCs for FO.²⁶

Many early studies examining TFC membranes for EO applications yielded water fluxes significantly lower than expected based on membrane water permeance and solute

permeability.^{30,66,67} This was later identified to be a result of the inherent hydrophobicity of the materials commonly used in TFC membrane support fabrication (PSu and PES).⁵⁸ Subsequent research focus has indentified polyacrylonitrile (PAN) as a viable support for TFC membranes using conventional m-phenylenediamine and trimesoyl chloride selective layer chemistry. PAN has been used as a TFC support in both the cast and electrospun morphologies.^{76,77} PAN can also be blended with cellulose acetate to fabricate nanofiber suitable for TFC membrane supports.⁷⁶ Huang has demonstrated the ability to synthesize PAs on commercial nylon 6,6 microfiltration membranes, presenting another path for hydrophilic TFC supports.⁷⁸

In addition to the use of inherently hydrophilically supported TFC membranes there has been studies which explored the use of surface modified hydrophobic supports for TFC membrane construction. Arena undertook the first studies using polydopamine as a hydrophilicizing surface modifier. PDA was applied to the PSu support layers of conventional TFC RO membranes to examine water flux improvements imparted to membrane support layers for PRO (Chapter 3).⁸⁰ This technique applied can be applied to membrane following their fabrication allowing for a continuation of optimized polyamide chemistries becoming dominate since their initial inception. Follow up work examined these membrane performances

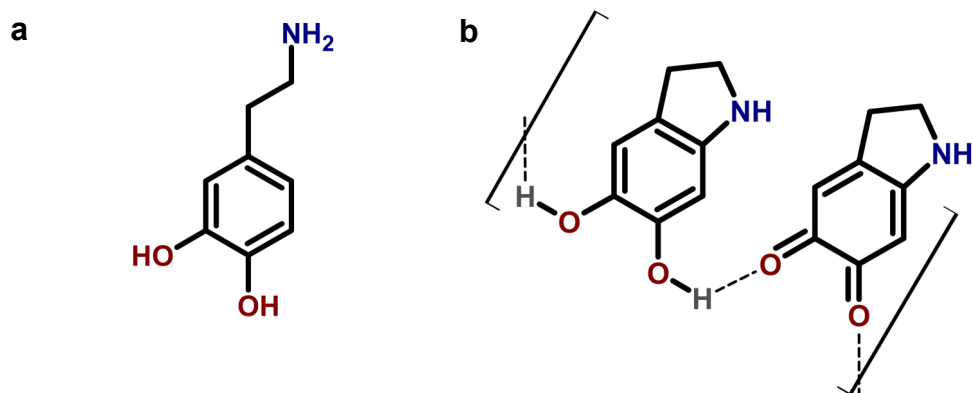


Fig. 1.5. Structures of dopamine (a) and polydopamine (b). The structure of polydopamine proposed by Dreyer et al. is held together through the hydrogen bonding of different moieties of the dopamine monomer formed from its molecular rearrangement at alkaline pH.⁷⁹

in FO as well as their desalination potential (Chapter 5)⁸¹ using the patented ammonia-carbon dioxide draw solution,^{82,83} which has also been implemented in Oasys's produce water treatment plant.⁴⁶ Additional work on PDA modification examined the use of PDA to hydrophilize PSu supports prior to polyamide synthesis.⁸⁴

List of Symbols

A	water permeance of a membrane
a_w	activity of water
B	solute permeability of a membrane
c_i	concentration of solute i
c_p	concentration of permeate

C_f	concentration of feed
J_w	water flux through a membrane
J_s	solute flux through a membrane
k	external mass transfer coefficient
K	solute resistivity
m_i	molality of solute i
R	rejection of a membrane
R_{const}	ideal gas constant ($0.08314 \text{ L} \cdot \text{bar} \cdot \text{mol}^{-1} \cdot \text{K}^{-1}$)
T	absolute temperature
v_w	molar volume of water ($0.018018 \text{ L} \cdot \text{mol}^{-1}$)
W	power density of a membrane
Δc	concentration gradient across a membrane ($c_{d,m} - c_{f,m}$)
ΔP	hydrostatic pressure gradient across a membrane ($P_f - P_p$) or ($P_d - P_f$)
$\Delta \pi$	osmotic pressure difference across a membrane
π	osmotic pressure of a solution
$\pi_{d,b}$	bulk osmotic pressure of the draw

$\pi_{f,b}$ bulk osmotic pressure of the feed

ρ density of a pure solvent

References

1. Hall, M. R.; West, J.; Sherman, B.; Lane, J.; de Haas, D. Long-Term Trends and Opportunities for Managing Regional Water Supply and Wastewater Greenhouse Gas Emissions. *Environ. Sci. Technol.* **2011**, *45*, 5434-5440.
2. Blackhurst, M.; Hendrickson, C.; Vidal, J. S. I. Direct and Indirect Water Withdrawals for U.S. Industrial Sectors. *Environ. Sci. Technol.* **2011**, *44*, 2126-2130.
3. Greenlee, L. F.; Lawler, D. F.; Freeman, B. D.; Marrot, B.; Moulin, P. Reverse osmosis desalination: Water sources, technology, and today's challenges. *Water Res.* **2009**, *43*, 2317-2348.
4. Schnoor, J. L. Water-Energy Nexus. *Environ. Sci. Technol.* **2011**, *45*, 5065-5065.
5. Scott, C. A.; Pierce, S. A.; Pasqualetti, M. J.; Jones, A. L.; Montz, B. E.; Hoover, J. H. Policy and institutional dimensions of the water–energy nexus. *Energy Policy* **2011**, *39*, 6622-6630.
6. Elimelech, M.; Phillip, W. A. The Future of Seawater Desalination: Energy, Technology, and the Environment. *Science* **2011**, *333*, 712-717.
7. McGinnis, R. L.; Elimelech, M. Energy requirements of ammonia–carbon dioxide forward osmosis desalination. *Desalination* **2007**, *370-382*, 207.
8. Van der Bruggen, B.; Vandecasteele, C. Distillation vs. membrane filtration: overview of process evolutions in seawater desalination. *Desalination* **2002**, *143*, 207-218.
9. Strathmann, H. Electrodialysis, a mature technology with a multitude of new applications. *Desalination* **2010**, *264*, 268-288.
10. Robinson, R. A.; Stokes, R. H. *Electrolyte Solutions*, 2nd ed.; Dover Publications: Mineola, 2002.
11. van't Hoff, J. H. Osmotic pressure and chemical equilibrium, December 13, 1901. Nobel Lecture. http://www.nobelprize.org/nobel_prizes/chemistry/laureates/1901/hoff-lecture.pdf.

12. Wilson, A. D.; Stewart, F. F. Deriving osmotic pressures of draw solutes used in osmotically driven membrane processes. *J. Membr. Sci.* **2013**, *431*, 205-211.
13. Cath, T. Y.; Childress, A. E.; Elimelech, M. Forward osmosis: Principles, applications, and recent developments. *J. Membr. Sci.* **2006**, *281*, 70-87.
14. Lewis, G. N. The osmotic pressure of concentrated solutions, and the laws of perfect solution. *J. Am. Chem. Soc.* **1908**, *30*, 668-683.
15. Frazer, J. C. W.; Myrick, R. T. The osmotic pressure of sucrose solutions at 30°. *J. Am. Chem. Soc.* **1916**, *38*, 1907-1922.
16. Prausnitz, J. M.; Lichtenthaler, R. N.; de Azevedo, E. G. *Molecular Thermodynamics of Fluid-Phase Equilibria*, 3rd ed.; Prentice-Hall, Inc.: Upper Saddle River, 1999.
17. Grattoni, A.; Merlo, M. Osmotic Pressure beyond Concentration Restrictions. *J. Phys. Chem. Part B* **2007**, *111*, 11770-11775.
18. Wijmans, J. G.; Baker, R. W. The solutions-diffusion model: a review. *J. Membr. Sci.* **1995**, *107*, 1-21.
19. Coday, B. D.; Heil, D. M.; Xu, P.; Cath, T. Y. Effects of Transmembrane Hydraulic Pressure on Performance of Forward Osmosis Membranes. *Environ. Sci. Technol.* **2013**, *47*, 2386-2393.
20. Van Wagner, E. M.; Sagle, A. C.; Sharma, M. M.; Freeman, B. D. Effect of crossflow testing conditions, including feed pH and continuous feed filtration, on commercial reverse osmosis membrane performance. *J. Membr. Sci.* **2009**, *345*, 97-109.
21. Baker, R. W. *Membrane Technology and Applications*, 2nd Edition; John Wiley & Sons Ltd: West Sussex, 2004.
22. Tiraferri, A.; Yip, N. Y.; Straub, A. P.; Castrillon, S. R.-V.; Elimelech, M. A method for the simultaneous determination of transport and structural parameters of forward osmosis membranes. *J. Membr. Sci.* **2013**, *444*, 523-538.
23. Yip, N. Y.; Tiraferri, A.; Phillip, W. A.; Schiffman, J. D.; Hoover, L. A.; Kim, Y. C.; Elimelech, M. Thin-Film Composite Pressure Retarded Osmosis Membranes for Sustainable Power Generation from Salinity Gradients. *Environ. Sci. Technol.* **2011**, *45*, 4360-4369.

24. Chung, T. S.; Zhang, S.; Wang, K. Y.; Su, J.; Ling, M. M. Forward osmosis processes: Yesterday, today, and tomorrow. *Desalination* **2012**, *287*, 78-81.
25. McGinnis, R. L.; Elimelech, M. Global challenges in energy and water supply: the promise of engineered osmosis. *Environ. Sci. Technol.* **2008**, *42*, 8625-8629.
26. Hoover, L. A.; Schiffman, J. D.; Elimelech, M. Nanofibers in thin-film composite membrane support layers: Enabling expanded application of forward and pressure retarded osmosis. *Desalination* **2013**, *308*, 73-81.
27. McCutcheon, J. R.; Elimelech, M. Modeling Water Flux in Forward Osmosis: Implications for Improved Membrane Design. *AIChE J.* **2007**, *53*, 1736-1744.
28. Kravath, R. E.; Davis, J. A. Desalination of sea water by direct osmosis. *Desalination* **1975**, *16*, 151-155.
29. Kessler, J.; Moody, C. Drinking water from sea water by forward osmosis. *Desalination* **1976**, *18*, 297-306.
30. McCutcheon, J. R.; McGinnis, R. L.; Elimelech, M. A novel ammonia-carbon dioxide forward (direct) osmosis desalination process. *Desalination* **2005**, *174*, 1-11.
31. McCutcheon, J. R.; McGinnis, R. L.; Elimelech, M. Desalination by ammonia-carbon dioxide forward osmosis: Influence of draw and feed solution concentrations on process performance. *J. Membr. Sci.* **2006**, *278*, 114-123.
32. Hancock, N. T.; Phillip, W. A.; Elimelech, M.; Cath, T. Y. Bidirectional Permeation of Electrolytes in Osmotically Driven Membrane Processes. *Environ. Sci. Technol.* **2011**, *45*, 10462-10651.
33. Hancock, N. T.; Cath, T. Y. Solute Coupled Diffusion in Osmotically Driven Membrane Processes. *Environ. Sci. Technol.* **2009**, *43*, 6769-6775.
34. Phillip, W. A.; Yong, J. S.; Elimelech, M. Reverse draw solute permeation in forward osmosis: modeling and experiments. *Environ. Sci. Technol.* **2010**, *44*, 5170-5176.
35. Stone, M. L.; Rae, C.; Stewart, F. F.; Wilson, A. D. Switchable polarity solvents as draw solutes for forward osmosis. *Desalination* **2013**, *312*, 124-129.

36. Ge, Q.; Su, J.; Chung, T.-S.; Amy, G. Hydrophilic Superparamagnetic Nanoparticles: Synthesis, Characterization, and Performance in Forward Osmosis Processes. *Ind. Eng. Chem. Res.* **2011**, *50*, 382-288.
37. Ling, M. M.; Wang, K. Y.; Chung, T. S. Highly water-soluble magnetic nanoparticles as novel draw solutes in forward osmosis for water reuse. *Ind. Eng. Chem. Res.* **2010**, *49*, 5869-5876.
38. Ling, M. M.; Chung, T.-S. Desalination process using super hydrophilic nanoparticles via forward osmosis. *Desalination* **2011**, *278*, 194-202.
39. Carmignani, G.; Sitkiewitz, S.; Webley, J. W. Recovery of retrograde soluble solute for forward osmosis water treatment. US 2012/0267308 A1, October 25, 2012.
40. McGinnis, R. L. Osmotic Desalinization Process. US 6,391,205 B1, May 21, 2002.
41. Achilli, A.; Cath, T. Y.; Childress, A. E. Selection of inorganic-based draw solutions for forward osmosis applications. *J. Membr. Sci.* **2010**, *364*, 233-241.
42. Hancock, N. T.; Black, N. D.; Cath, T. Y. A comparative life cycle assessment of hybrid osmotic dilution desalination and established seawater desalination and wastewater reclamation process. *Water Research* 2012, *46*, 1145-1154.
43. Hickenbottom, K. L.; Hancock, N. T.; Hutchings, N. R.; Appleton, E. W.; Beaudry, E. G.; Xu, P.; Cath, T. Y. Forward osmosis treatment of drilling mud and fracturing wastewater from oil and gas operations. *Desalination* **2013**, *312*, 60-66.
44. Lin, S.; Yip, N. Y.; Cath, T. Y.; Osuji, C. O.; Elimelech, M. Hybrid Pressure Retarded Osmosis–Membrane Distillation System for Power Generation from Low-Grade Heat: Thermodynamic Analysis and Energy Efficiency. *Environ. Sci. Technol.* **2014**, *48*, 5306-5313.
45. Anastasio, D. D.; Arena, J. T.; Cole, E. A.; McCutcheon, J. R. Impact of temperature on power density in closed-loop pressure retarded osmosis for grid storage. *J. Membr. Sci.* **2015**, *479*, 240-245.
46. McGinnis, R. L.; Hancock, N. T.; Nowosielski-Slepowron, M. S.; McGurgan, G. D. Pilot Demonstration of the NH₃/CO₂ forward osmosis desalination process on high salinity brines. *Desalination* **2013**, *312*, 67-74.

47. McGinnis, R. L.; McCutcheon, J. R.; Elimelech, M. A novel ammonia–carbon dioxide osmotic heat engine for power generation. *J. Membr. Sci.* **2007**, *305*, 13-19.
48. Cath, T. Y.; Hancock, N. T.; Lundin, C. D.; Hoppe-Jones, C.; Drewes, J. E. A multi-barrier osmotic dilution process for simultaneous desalination and purification of impaired water. *J. Membr. Sci.* **2010**, *362*, 417-436.
49. Edwards, T. J.; Maurer, G.; Newman, J.; Prausnitz, J. M. Vapor-Liquid Equilibria in Multicomponent Aqueous Solutions of Volatile Weak Electrolytes. *AIChE J.* **1978**, *24*, 966-976.
50. Boo, C.; Khalil, Y. F.; Elimelech, M. Performance evaluation of trimethylamine–carbon dioxide thermolytic draw solution for engineered osmosis. *J. Membr. Sci.* **2015**, *473*, 302-309.
51. Petersen, R. J. Composite reverse osmosis and nanofiltration membranes. *J. Membr. Sci.* **1993**, *83*, 81-150.
52. Cadotte, J. E.; Petersen, R. J.; Larson, R. E.; Erickson, E. E. A New Thin-Film Composite Seawater Reverse Osmosis Membrane. *Desalination* **1980**, *32*, 25-31.
53. Dow Water and Process Solutions. FILMTEC™ Reverse Osmosis Membranes Technical Manual, Form No. 609-00071-1009. http://msdssearch.dow.com/PublishedLiteratureDOWCOM/dh_08db/0901b803808db77d.pdf.
54. Ren, J.; McCutcheon, J. R. A new commercial thinfilm composite membrane for forward osmosis. *Desalination* **2014**, *343*, 187-193.
55. McGinnis, R.; McGurgan, G. Forward osmosis membranes. United States Patent No. US 8,181,794, May 22, 2012.
56. Yip, N. Y.; Tiraferri, A.; Phillip, W. A.; Schiffman, J. D.; Elimelech, M. High Performance Thin Film Composite Forward Osmosis Membrane. *Environ. Sci. Technol.* **2010**, *44*, 3812-3818.
57. Loeb, S.; Sourirajan, S.; Weaver, D. E. High flow porous membranes for separating water from saline solutions. US 3,133,137 A, May 12, 1964.
58. McCutcheon, J. R.; Elimelech, M. Influence of membrane support layer hydrophobicity on water flux in osmotically driven membrane processes. *J. Membr. Sci.* **2008**, *318*, 458-466.

59. Sairam, M.; Sereewatthanawut, E.; Li, K.; Bismarck, A.; Livingston, A. G. Method for the preparation of cellulose acetate flat sheet composite membranes for forward osmosis—Desalination using MgSO_4 draw solution. *Desalination* **2011**, *273*, 299-307.
60. Zhang, S.; Wang, K. Y.; Chung, T. S.; Jean, Y. C.; Chen, H. Molecular design of the cellulose ester-based forward osmosis membranes for desalination. *Chem. Eng. Sci.* **2011**, *66*, 2008-2018.
61. Herron, J. Asymmetric forward osmosis membranes. United States Patent No. US 7,445,712, Nov. 4, 2008.
62. Achilli, A.; Cath, T. Y.; Childress, A. E. Power generation with pressure retarded osmosis: An experimental and theoretical investigation. *J. Membr. Sci.* **2009**, *343*, 42-52.
63. Gray, G. T.; McCutcheon, J. R.; Elimelech, M. Internal concentration polarization in forward osmosis: role of membrane orientation. *Desalination* **2006**, *197*, 1-8.
64. McCutcheon, J. R.; Elimelech, M. Influence of concentrative and dilutive internal concentration polarization on flux behavior in forward osmosis. *J. Membr. Sci.* **2006**, *284*, 237-247.
65. Cath, T. Y.; Childress, A. E.; Elimelech, M. Forward osmosis: Principles, applications, and recent developments. *J. Membr. Sci.* **2006**, *281*, 70-87.
66. Cath, T. Y.; Adams, D.; Childress, A. E. Membrane contactor processes for wastewater reclamation in space II. Combined direct osmosis, osmotic distillation, and membrane distillation for treatment of metabolic wastewater. *J. Membr. Sci.* **2005**, *257*, 111-119.
67. Cath, T. Y.; Gormly, S.; Beaudry, E. G.; Flynn, M. T.; Adams, V. D.; Childress, A. E. Membrane contactor processes for wastewater reclamation in space Part I. Direct osmotic concentration as pretreatment for reverse osmosis. *J. Membr. Sci.* **2005**, *257*, 85-98.
68. Ge, Q.; Su, J.; Chung, T.-S.; Amy, G. Hydrophilic Superparamagnetic Nanoparticles: Synthesis, Characterization, and Performance in Forward Osmosis Processes. *Ind. Eng. Chem. Res.* **2011**, *50*, 382-288.
69. She, Q.; Jin, X.; Tang, C. Y. Osmotic power production from salinity gradient resource by pressure retarded osmosis: Effects of operating conditions and reverse solute diffusion. *J. Membr. Sci.* **2012**, *401-402*, 262-273.

70. Vos, K. D.; Burris, F. O.; Riley, R. L. Kinetic Study of the Hydrolysis of Cellulose Acetate in the pH Range of 2-10. *J. Appl. Polym. Sci.* **1966**, *10*, 825-832.
71. Watters, J. C.; Klein, E.; Fleischman, M.; Roberts, J. S.; Hall, B. Rejection Spectra of Reverse Osmosis Membranes Degraded by Hydrolysis of Chlorine Attack. *Desalination* **1986**, *60*, 93-110.
72. Tiraferri, A.; Yip, N. Y.; Phillip, W. A.; Schiffman, J. D.; Elimelech, M. Relating performance of thin-film composite forward osmosis membranes to support layer formation and structure. *J. Membr. Sci.* **2011**, *367*, 340-352.
73. Wei, J.; Qiu, C.; Tang, C. Y.; Wang, R.; Fane, A. G. Synthesis and characterization of flat-sheet thin film composite forward osmosis membranes. *J. Membr. Sci.* **2011**, *372*, 292-302.
74. Widjojo, N.; Chung, T. S.; Weber, M.; Maletzko, C.; Warzelhan, V. The role of sulphonated polymer and macrovoid-free structure in the support layer for thin-film composite (TFC) forward osmosis (FO) membranes. *J. Membr. Sci.* **2011**, *383*, 214-223.
75. Bui, N. N.; Lind, M. L.; Hoek, E. M. V.; McCutcheon, J. R. Electrospun nanofiber supported thin film composite membranes for engineered osmosis. *J. Membr. Sci.* **2011**, *385-386*, 10-19.
76. Bui, N. N.; McCutcheon, J. R. Hydrophilic Nanofibers as New Supports for Thin Film Composite Membranes for Engineered Osmosis. *Environ. Sci. Technol.* **2013**, *47*, 1761-1769.
77. Low, S. C. Preliminary studies of seawater desalination using forward osmosis. *Desalin. Water Treat.* **2009**, *7*, 41-46.
78. Huang, L.; McCutcheon, J. R. Hydrophilic nylon 6,6 nanofibers supported thin film composite membranes for engineered osmosis. *J. Membr. Sci.* **2014**, *457*, 162-169.
79. Dreyer, D. R.; Miller, D. J.; Freeman, B. D.; Paul, D. R.; Bielawski, C. W. Elucidating the structure of poly(dopamine). *Langmuir* **2012**, *28*, 6428-6435.
80. Arena, J. T.; McCloskey, B.; Freeman, B. D.; McCutcheon, J. R. Surface modification of thin film composite membrane support layers with polydopamine: Enabling use of reverse osmosis membranes in pressure retarded osmosis. *J. Membr. Sci.* **2011**, *375*, 55-62.

81. Arena, J. T.; Manickam, S. S.; Reimund, K. K.; Freeman, B. D.; McCutcheon, J. R. Solute and water transport in forward osmosis using polydopamine modified thin film composite membranes. *Desalination* **2014**, *343*, 8-16.
82. Neff, R. A. Solvent extractor. US 3,130,156 A, April 21, 1964.
83. McGinnis, R. Osmotic Desalination Process. US 8,753,514 B2, June 17, 2014.
84. Han, G.; Zhang, S.; Li, X.; Widjojo, N.; Chung, T. S. Thin film composite forward osmosis membranes based on polydopamine modified polysulfone substrates with enhancements in both water flux and salt rejection. *Chem. Eng. Sci.* **2012**, *80*, 219-231.
85. Han, G.; Wang, P.; Chung, T.S. Highly robust thin-film composite pressure retarded osmosis (PRO) hollow fiber membrane with high power densities for renewable salinity-gradient energy generation. *Environ. Sci. Technol.* **2013**, *47*, 8070-8077.

Chapter 2

The ammonia-carbon dioxide draw solution

2.1. Draw solutions and processes

2.1.1. Draw solutions in forward osmosis

Forward osmosis (FO) processes are driven by the osmotic pressure difference between two solutions separated by a membrane permeable to water and not solutes within solution.¹⁻⁵

The solution having the higher osmotic pressure of these solutions is called a draw. The osmotic flow of water concentrates the feed solution while draw solution is diluted till osmotic equilibrium, or the point at which the osmotic pressure of the feed solution equals the osmotic pressure of the draw solution.^{6,7} The flow of water across the membrane occurs spontaneously and requires no energy input. The energy input in a FO process occurs in the recovery and/or

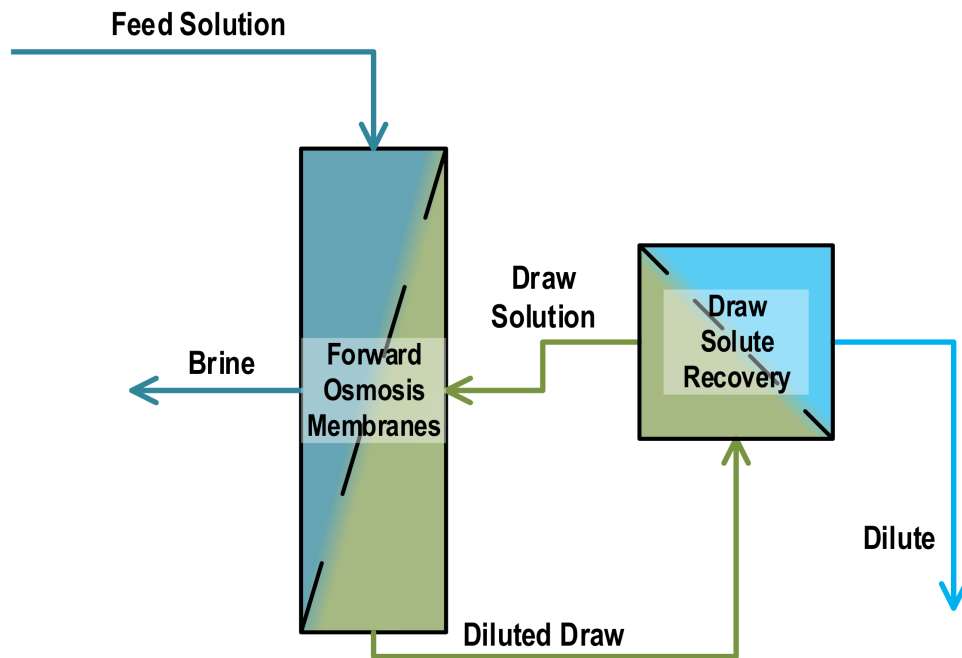


Fig. 2.1. A forward osmosis process consisting of forward osmosis and draw solute recovery steps.

preparation of the draw solution.^{8,9}

Draw solute selection for an FO process varies depending on application of water or solutions managed by the process. In the case of direct osmotic dilution (DOD) processes, the draw solution will be used directly after its dilution by osmosis. This type of FO process was detailed in the earliest work on the use of FO for water purification and used concentrated sugar solutions to drive osmosis across a cellulose acetate reverse osmosis membranes.^{1,2} An extended form of this draw solution is used in the hydration products sold by Hydration

Technology Innovations™ which adds electrolytes to the sugar solution.^{5,10} In another direct use FO process, a concentrated fertilizer solution is used as a draw solution which is osmotically diluted by brackish groundwater and blended with freshwater for fertigation.^{11,12}

Not all FO processes make direct use of a dilute draw solution; other FO processes such as direct osmotic concentration¹³⁻¹⁵ and desalination^{3,9,16-18} require a draw solution/solute concentration/recovery step or steps as a part of the FO process. The particular technique employed varies depending on physicochemical aspects of the draw solution. Typically this will be a thermal separation,^{3,8,19} a membrane separation,^{18,20,21} or both.¹⁴ Since a significant energy input into a FO process is used for the separation of the draw solute(s) from water, one critical aspect of draw solute design includes the selection of a draw solution which can be easily separated.

A variety of draw solutes have been proposed for FO desalination and concentrator processes. Amongst these are surface modified nano-particles,^{16,22} switchable polarity solvents,²³ polymers which display a thermal sensitivity to water solubility,²⁴ and electrolytes.^{3,4,19,20,25,26} Electrolyte draw solutes offer lower viscosities and higher diffusivities than proposed alternatives. Sodium chloride (NaCl) is commonly used as draw solute for

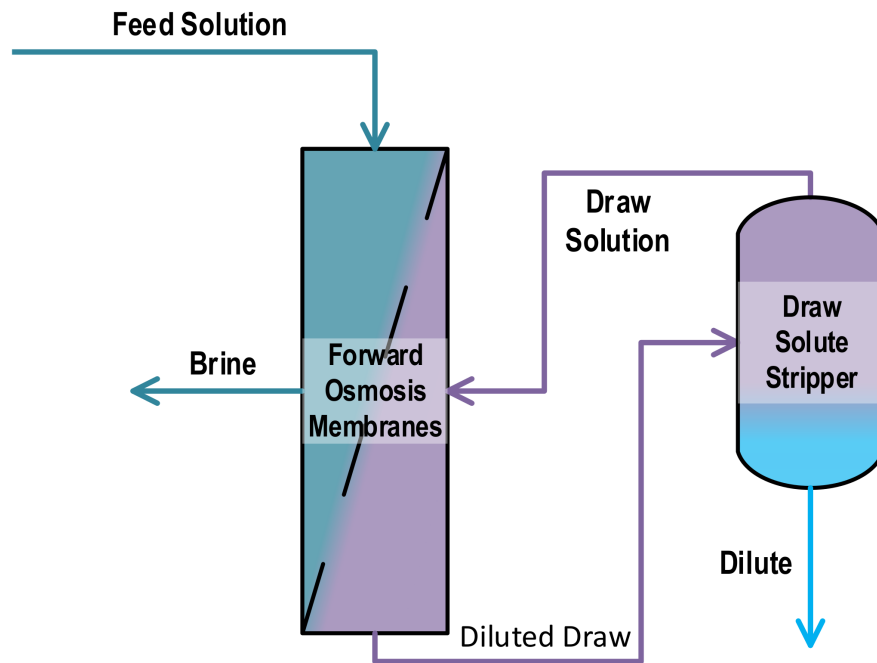


Fig. 2.2. Forward osmosis processes using a thermolytic draw solute where a distillation or stripping system separates a draw solute from the draw solution diluted by osmosis.

FO-RO processes where an FO is used to dilute a NaCl stream that is subsequently concentrated in a following reverse osmosis (RO) step.^{20,27}

Another branch of electrolyte draw solutions often considered are those based upon thermolytic draw solutes, which consists of water soluble gases forming ionic species within solution.^{3,4,8,14,19,25,28} The high solubility and thermal recovery of these draw solutes allows for draw solution of sufficiently high osmotic pressure to dewater feed solutions with very high amounts of dissolved solids.¹⁴ One thermolytic draw solution studied for seawater desalination

by McCutcheon from a mixture of ammonia (NH_3) and carbon dioxide (CO_2) gases.³ Fig. 2.2 illustrates the simplest design of an $\text{NH}_3\text{-CO}_2$ FO desalination process.

2.1.2. Draw solutions in pressure retarded osmosis

Draw solutes in pressure retarded osmosis processes are almost exclusively electrolytes. The electrolyte selected does alter how a PRO process is specifically configured. The oldest embodiment of a PRO process uses seawater and river water as the draw and feed solutions respectively.²⁹⁻³¹ This PRO configuration has become known as an open-loop process since the draw and feed solutions are withdrawn from this naturally occurring salinity gradient

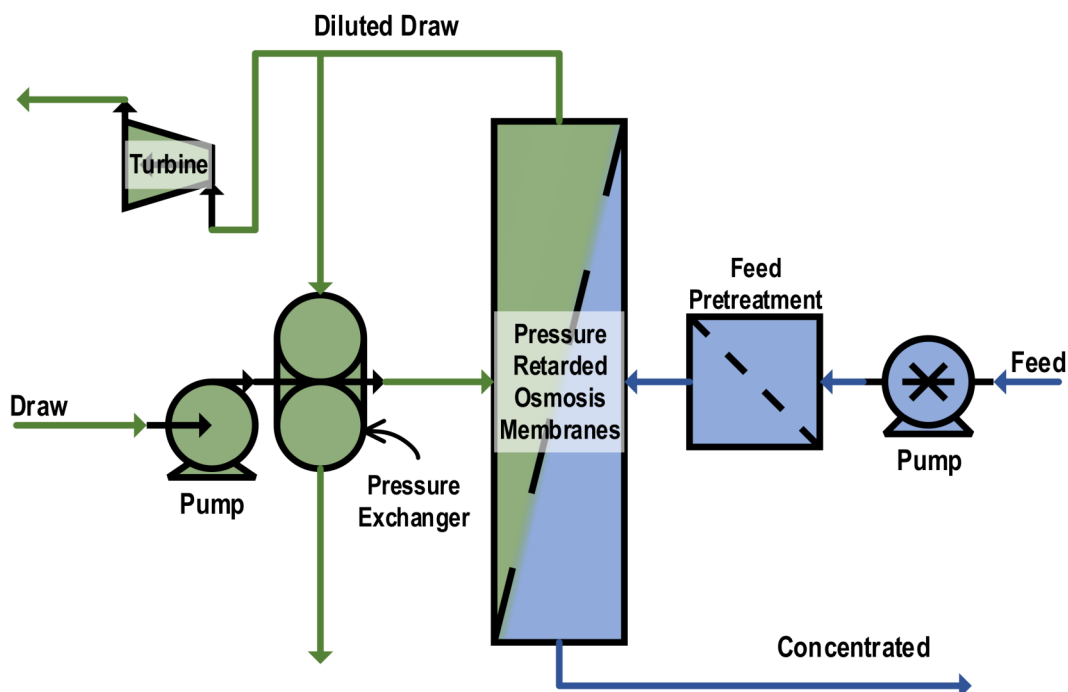


Fig. 2.3. Open-loop pressure-retarded osmosis process.

diluted/concentrated and discharged.³² Some variety does exist amongst open-loop PRO processes in the source of the draw and feed solutions; however, they still are closely related to natural salinity gradients. Amongst the high salinity draw solutions proposed was water from the Dead Sea,³³ Great Salt Lake,³⁴ or reverse osmosis (RO) brine as alternatives to seawater.³⁵⁻³⁹ These more saline waters have higher osmotic pressures for increase energy production^{40,41} or greater flexibility in feed solution selection including the use of seawater.^{33,39}

As an alternative to open-loop PRO process, there are also closed-loop PRO processes³² or osmotic heat engines (OHE)^{9,42} in which the draw solute and solvent (typically water) are within a closed process containing a draw solute/solvent separation. OHEs commonly use waste heat in the solute/solvent separation and the integration of a solute/solvent separation allows for the use of higher osmotic pressure draw solutions and lower osmotic pressure (close to deionized water) feed solutions.^{8,32,42} One proposed draw solution for use in an OHE by McGinnis, et al. is also the $\text{NH}_3\text{-CO}_2$ draw solution.⁸

2.2. The ammonia-carbon dioxide draw solution

Of the available draw solutions presently available for use in forward osmosis water treatment processes few have received a broader variety of study than the ammonia-carbon

dioxide ($\text{NH}_3\text{-CO}_2$) draw solution.^{3,4,8,9,14,25,43,44} The $\text{NH}_3\text{-CO}_2$ draw solution has been envisaged being prepared from the absorption of ammonia and carbon dioxide gases in water.¹⁴ Contrasting this, in laboratory scale studies the draw solution is more typically prepared from mixing ammonium bicarbonate, ammonia hydroxide, and water.^{3,43,45} Within a prepared $\text{NH}_3\text{-CO}_2$ draw solutes solution there exist two primary chemical species the dissolved gases and ions formed in reversible reactions with water.^{46,47} The four primary ionic components of this draw solution are: ammonium (NH_4^+) cations and bicarbonate (HCO_3^-), carbonate (CO_3^{2-}), and carbamate (NH_2COO^-) anions.^{8,46,48} Additionally, the natural equilibrium of water also introduces hydrogen cations (H^+ or H_3O^+) and hydroxide (OH^-). The chemical equilibria impacting the speciation of this draw solution are shown in Table 1.1. As prepared, this draw solution is typically alkaline having pHs > 7 .^{4,43} Chemically speaking the $\text{NH}_3\text{-CO}_2$ draw solution represents one of the more complex draw solutions proposed for FO as it has nine

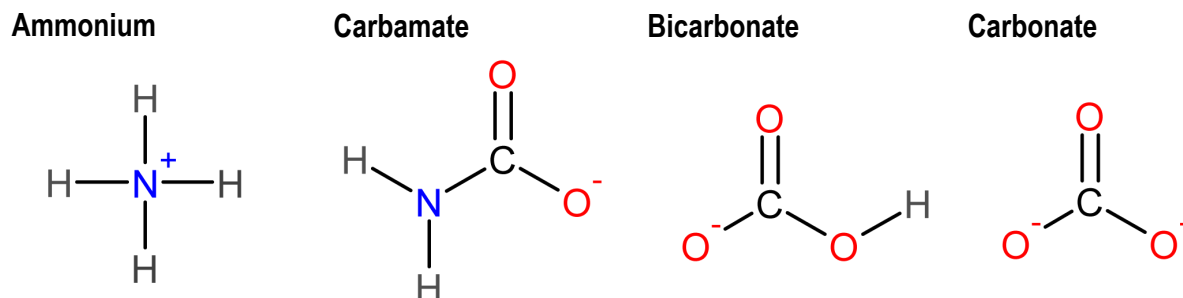
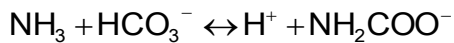
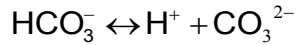
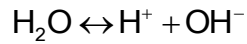
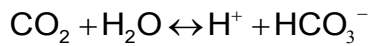


Fig. 2.4. Ionic species of ammonia and carbon dioxide in water.

Table 2.1. Equilibria describing the species formed from ammonia and carbon dioxide in solution.



components within solution (including water) each of which influences the concentrations of other components.⁴⁷ The formation of carbamates, observed at higher aqueous ammonia concentrations, increases the complexity of this

draw solution when compared to other amine based draw solutions such as trimethylammonium bicarbonate and n,n-dimethylcyclohexylammonium bicarbonate.^{23,28}

2.2.1. Interactions defining speciation of the ammonia-carbon dioxide draw solution

Numerous studies on the equilibrium relationships between NH_3 and CO_2 gases within solution have been performed.^{46-48,50,51} While these studies primarily focus on the use of ammonia for carbon dioxide scrubbing, empirical expressions used to calculate ion interactions, solubility, and equilibrium exist for the 20°C-50°C range likely encountered in FO processes.^{3,46,52} Intermolecular interactions between water, the dissolve gases, cations, and anions play a role in the speciation of this draw solution,⁴⁶ and the concentrations needed to exert sufficient osmotic pressure for an $\text{NH}_3\text{-CO}_2$ draw solution to function in an FO process are sufficiently high such that ideality cannot be assumed.⁴⁵

Amongst the most important empirical relationships to approximate the activity coefficients of mixed electrolyte solutions include parameters relating the interactions amongst chemical species present within solution. These interaction parameters are used in the approximation of both the activity coefficients for the dissolve species and the activity of water. Edwards et al. approximated activity coefficient for weak electrolytes using an expression derived from Pitzer's theory.⁴⁶

$$\ln(\gamma_i) = -A_\phi z_i^2 \left[\frac{\sqrt{I}}{1 + 1.2\sqrt{I}} + \frac{2}{1.2} \ln(1 + 2\sqrt{I}) \right] + \sum_{j \neq w} m_j \left\{ \beta_{ij}^{(0)} + \frac{\beta_{ij}^{(1)}}{2I} \left[1 - (1 + 2\sqrt{I}) e^{(-2\sqrt{I})} \right] \right\} - \frac{z_i^2}{4I^2} \sum_{j \neq w} \sum_{k \neq w} m_j m_k \beta_{jk}^{(1)} \left\{ 1 - (1 + 2\sqrt{I} + 2I) e^{(-2\sqrt{I})} \right\} \quad (2.1)$$

$$I = \frac{1}{2} \sum_j z_j^2 m_j \quad (2.2)$$

$$A_\phi = 2.303 \frac{A_v}{3} \quad (2.3)$$

The interaction parameters $\beta^{(0)}$ and $\beta^{(1)}$ represent the effect of short range forces⁵³ affecting the activity coefficient of all species and the activity of water. A_ϕ is the Debye-Hückel parameter, shown in Eq. (2.3) and calculated from A_v , which is the Debye-Hückel limiting constant for water at 1 atm and tabulated from 0°C to 100°C in Appendix 4 of Lewis et al.⁵⁴

In addition to 5 chemical equilibria shown in Table 2.1, draw solute speciation is also affected by a mass balance upon the total aqueous nitrogen species, a mass balance upon the total aqueous carbon species, solution electroneutrality, and the activity of water. Edwards et al. determined the activity of water for a solution of weak electrolytes from the Gibbs-Duhem equation Eq (2.4).⁴⁶

$$\ln(a_w) = M_w \left\{ \frac{2A_\phi I^{3/2}}{1 + 1.2\sqrt{I}} - \sum_{i \neq W} \sum_{j \neq W} m_i m_j [\beta_{ij}^{(0)} + \beta_{ij}^{(1)} e^{(-2\sqrt{I})}] \right\} - M_w \sum_{i \neq W} m_i \quad (2.4)$$

Using the relationships shown in Table 2.2 and Eq. (2.4) a numerical determination for the concentration of ionic and neutral species within solution can be obtained. This calculation was performed in a Mathematica programe created by the author, which can be found in Appendix 1. This program accounts for ion and molecular interactions parameters given by Edwards et al.,⁴⁶ NH_3 and CO_2 equilibrium constants from Kawazuishi and Prausnitz,⁴⁷ and water self-dissociation equilibrium constants from Robinson and Stokes.⁴⁹ In solving for the speciation of the $\text{NH}_3\text{-CO}_2$ draw solution a direct calculation of the osmotic pressure of these solutions can be obtain from the water activity in solution by Eq. (2.5).^{49,55,56}

Table 2.2. Constraints to consider for the calculation of ammonia and carbon dioxide species present within an $\text{NH}_3\text{-CO}_2$ draw solution. For the calculation of electroneutrality since the concentration of both H^+ and OH^- are low relative to the ions present within solution those concentrations were neglected in the actual calculation of solution electroneutrality.⁴⁶

Chemical Equilibria

$$K_1 = \frac{a_{\text{NH}_4^+} a_{\text{OH}^-}}{a_{\text{NH}_3} a_{\text{H}_2\text{O}}} = \frac{m_{\text{NH}_4^+} m_{\text{OH}^-}}{m_{\text{NH}_3} m_{\text{H}_2\text{O}}} \times \frac{\gamma_{\text{NH}_4^+} \gamma_{\text{OH}^-}}{\gamma_{\text{NH}_3} \gamma_{\text{H}_2\text{O}}}$$

$$K_2 = \frac{a_{\text{H}^+} a_{\text{HCO}_3^-}}{a_{\text{CO}_2} a_w} = \frac{m_{\text{H}^+} m_{\text{HCO}_3^-}}{m_{\text{CO}_2}} \times \frac{\gamma_{\text{H}^+} \gamma_{\text{HCO}_3^-}}{\gamma_{\text{CO}_2}} \times \frac{1}{a_w}$$

$$K_3 = \frac{a_{\text{H}^+} a_{\text{OH}^-}}{a_w} = \frac{m_{\text{H}^+} \gamma_{\text{H}^+} m_{\text{OH}^-} \gamma_{\text{OH}^-}}{a_w}$$

$$K_4 = \frac{a_{\text{H}^+} a_{\text{OH}^-}}{a_{\text{HCO}_3^-}} = \frac{m_{\text{H}^+} m_{\text{OH}^-}}{m_{\text{HCO}_3^-}} \times \frac{\gamma_{\text{H}^+} \gamma_{\text{OH}^-}}{\gamma_{\text{HCO}_3^-}}$$

$$K_5 = \frac{a_{\text{NH}_2\text{COO}^-} a_w}{a_{\text{NH}_3} a_{\text{HCO}_3^-}} = \frac{m_{\text{NH}_2\text{COO}^-}}{m_{\text{NH}_3} m_{\text{HCO}_3^-}} \times \frac{\gamma_{\text{NH}_2\text{COO}^-}}{\gamma_{\text{NH}_3} \gamma_{\text{HCO}_3^-}} \times a_w$$

Mass Balances

$$m_{\text{Total-N}} = m_{\text{NH}_3} + m_{\text{NH}_4^+} + m_{\text{NH}_2\text{COO}^-}$$

$$m_{\text{Total-C}} = m_{\text{CO}_2} + m_{\text{HCO}_3^-} + m_{\text{CO}_3^{2-}} + m_{\text{NH}_2\text{COO}^-}$$

Electroneutrality

$$m_{\text{NH}_4^+} + m_{\text{H}^+} = m_{\text{HCO}_3^-} + m_{\text{NH}_2\text{COO}^-} + m_{\text{OH}^-} + 2m_{\text{CO}_3^{2-}}$$

$$\pi = -\frac{1}{v_w} \ln(a_w) R_{\text{const}} T \quad (2.5)$$

2.2.2. Limitations on the solubility of the ammonia-carbon dioxide draw solution

The speciation of the $\text{NH}_3\text{-CO}_2$ draw solution is significant in considering solubility limitations and their impact on the stability of a concentrated $\text{NH}_3\text{-CO}_2$ draw solution. The ability of the gases to remain in solution is inversely related to their Henry's Law coefficient which is strongly a function of temperature, increasing for both NH_3 and CO_2 over the range of 0-100°C. Edwards et al. presented semi-empirical constants for the calculation of Henry's Law constants

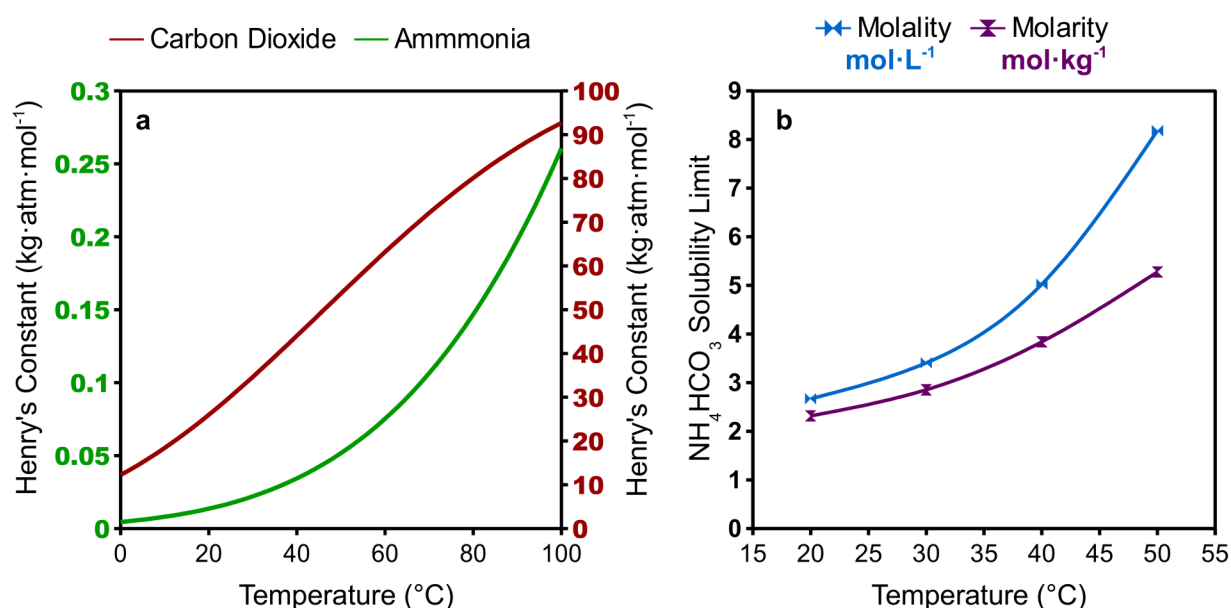


Fig. 2.5. (a) Constraints on the solubility of the $\text{NH}_3\text{-CO}_2$ draw solution showing the Henry's Law constants for ammonia and carbon dioxide in water over the range of 0-100°C,⁴⁶ and (b) solubility of ammonium bicarbonate over the range of 20-50°C.⁵²

base off of literature data;⁴⁶ plots of the Henry's Law coefficients for NH_3 and CO_2 are shown in Fig. 2.5a.

The Henry's law constants become significant when considering the molar (or molal) ratio of NH_3 to CO_2 within solution. Typically the draw solution is prepared with an excess of NH_3 with the purpose of keeping the concentration of dissolved CO_2 low,^{3,4,14,43} since the Henry's Law constant of CO_2 is 10-100x higher than it is for NH_3 , this means that NH_3 is less likely to escape an open draw solution tank over short tests. In addition to considerations of gas solubility, attention must also be given to the solubility of ammonium salts present within this draw solution. While these ammonium salts are highly soluble in water (i.e. ammonium carbonate is $2.4 \text{ mol}\cdot\text{L}^{-1}$, ammonium carbamate is $10.1 \text{ mol}\cdot\text{L}^{-1}$ and ammonium bicarbonate is $2.8 \text{ mol}\cdot\text{L}^{-1}$ at 20°C),⁴⁸ the solubility of ammonium bicarbonate is important in the preparation and chemical characteristic of the draw solution since ammonium bicarbonate can be considered the base form of this draw solution. It is the primary salt formed for $\text{NH}_3:\text{CO}_2$ ratios less than 1:1, and since the chemical equilibrium defined in Table 2.1 and Table 2.2 are for aqueous species, formation of the ammonium carbamate and ammonium carbonate from mixing ammonium bicarbonate, water, and ammonium hydroxide requires ammonium

bicarbonate to mostly or completely go into solution. As ammonium bicarbonate is the base salt of the $\text{NH}_3:\text{CO}_2$ draw solution its solubility should be considered in selecting the upper limit a given CO_2 species concentration for a given $\text{NH}_3:\text{CO}_2$. This is supported over a temperature range from 20-50°C in work by Trypuć and Kielkowska, shown in Fig. 2.5b.⁵²

2.2.3. Speciation and osmotic pressures of ammonia-carbon dioxide draw solution

Fig. 2.6 shows the increasing osmotic pressure over a range of increasing CO_2 species concentrations at 20°C. Higher osmotic pressures can be generated by the $\text{NH}_3\text{-CO}_2$ draw solution with increasing $\text{NH}_3:\text{CO}_2$ ratio, which increases the concentration of carbamate and the overall solubility of the draw solution (Fig. 2.6a). While the osmotic pressure of the draw solution is substantially higher at increased $\text{NH}_3:\text{CO}_2$ ratios the total ion concentration (ignoring solubility constraints for lower $\text{NH}_3:\text{CO}_2$ ratios) of these solutions follows a linear trend. This shows that increases in osmotic pressure with increasing $\text{NH}_3:\text{CO}_2$ ratios (Fig. 2.6a) is largely the result of increased aqueous ammonia concentrations (Fig. 2.6c). Osmotic pressure from aqueous ammonia cannot be effectively leveraged by the membrane as these membranes tend to be fairly permeable to uncharged chemical species,⁵⁷ particularly ammonia due to its flexible hydration shell and similar polarity to water.⁵⁸ With regards to specific ion concentration

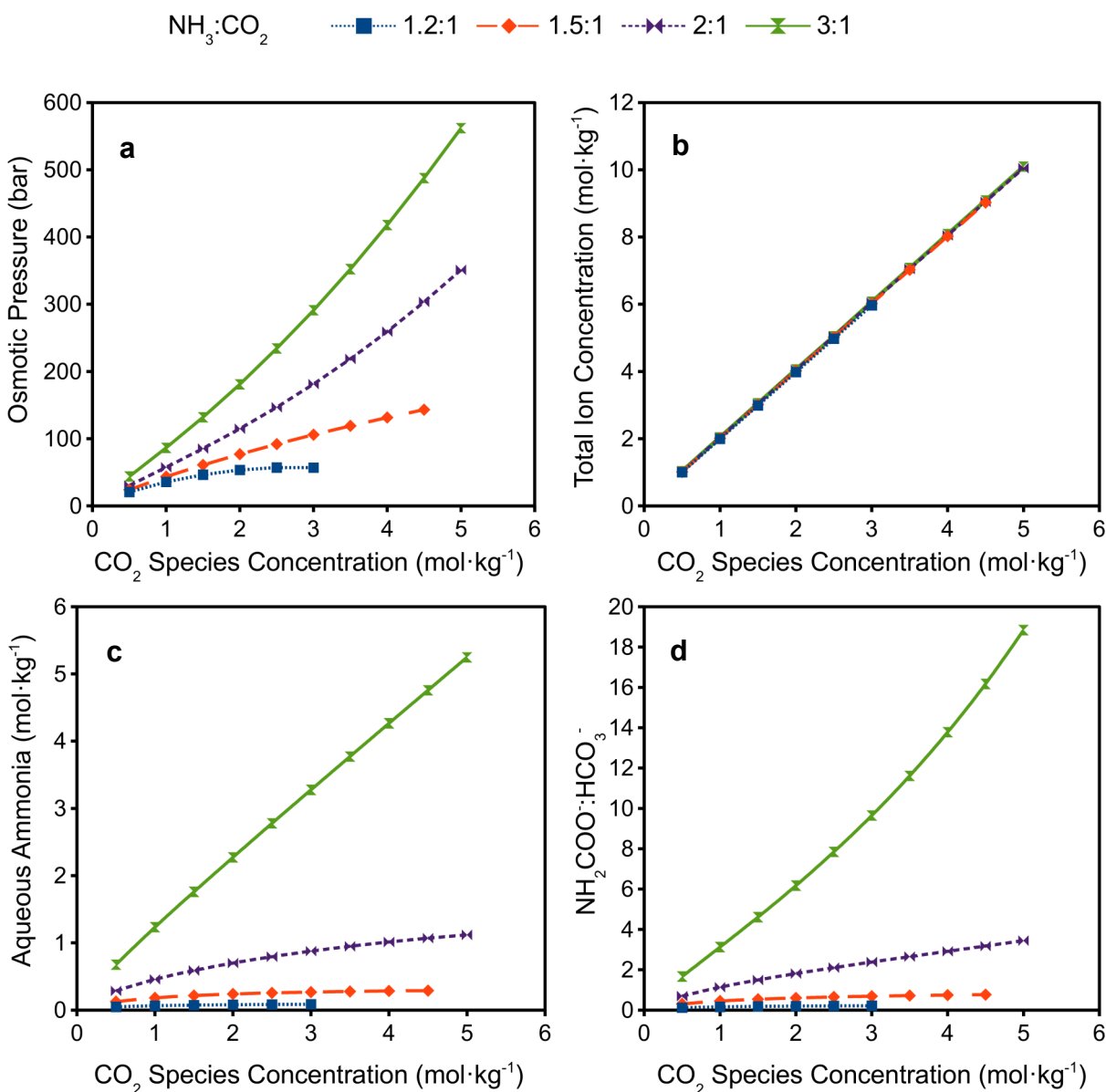


Fig. 2.6. Osmotic pressure (a), total ion concentration (b), aqueous ammonia concentration (c), and $\text{HCO}_3^-:\text{NH}_2\text{COO}^-$ ratios for differing $\text{NH}_3:\text{CO}_2$ ratios of the $\text{NH}_3\text{-CO}_2$ draw solution at 20°C limited by the solubility of ammonium bicarbonate. Curves which terminate suddenly are due to the draw solution having a concentration of ammonium bicarbonate above its solubility limit.

increasing the $\text{NH}_3:\text{CO}_2$ ratio does not promote the formation of carbonate instead bicarbonate is converted to carbamate, while the ammonium concentration is approximately the same at all the total CO_2 species concentrations. At high $\text{NH}_3:\text{CO}_2$ ratios the mole fraction of bicarbonate to carbamate increase sharply illustrating the solubility advantage (or disadvantage) which can be leveraged through the tailoring of $\text{NH}_3:\text{CO}_2$ ratios, desired osmotic pressure, and solubility limitations of the salts present within the $\text{NH}_3\text{-CO}_2$ draw solution. Some of the broader implications $\text{NH}_3:\text{CO}_2$ ratios and a membrane experimentally observed membrane performance can be found in Appendix 5.

List of Symbols

A_ϕ	Debye-Hückel parameter
A_γ	Debye-Hückel limiting constant at 1 atm
a_i	activity of species i
a_w	activity of water
I	ionic strength of solution
m_i	molality of solute i
M_w	molecular weight of water ($0.018018 \text{ kg}\cdot\text{mol}^{-1}$)

R_{const}	ideal gas constant ($0.08314 \text{ L} \cdot \text{bar} \cdot \text{mol}^{-1} \cdot \text{K}^{-1}$)
T	absolute temperature
v_w	molar volume of water ($0.018018 \text{ L} \cdot \text{mol}^{-1}$)
z_i	ionic charge of species i
$\beta_{ij}^{(0)}$	interaction parameter between species i and j
$\beta_{ij}^{(1)}$	interaction parameter between species i and j
γ_i	activity coefficient of species i

References

1. Kravath, R. E.; Davis, J. A. Desalination of sea water by direct osmosis. *Desalination* **1975**, *16*, 151-155.
2. Kessler, J.; Moody, C. Drinking water from sea water by forward osmosis. *Desalination* **1976**, *18*, 297-306.
3. McCutcheon, J. R.; McGinnis, R. L.; Elimelech, M. A novel ammonia-carbon dioxide forward (direct) osmosis desalination process. *Desalination* **2005**, *174*, 1-11.
4. McCutcheon, J. R.; McGinnis, R. L.; Elimelech, M. Desalination by ammonia-carbon dioxide forward osmosis: Influence of draw and feed solution concentrations on process performance. *J. Membr. Sci.* **2006**, *278*, 114-123.
5. Cath, T. Y.; Childress, A. E.; Elimelech, M. Forward osmosis: Principles, applications, and recent developments. *J. Membr. Sci.* **2006**, *281*, 70-87.

6. Cath, T. Y.; Childress, A. E.; Elimelech, M. Forward osmosis: Principles, applications, and recent developments. *J. Membr. Sci.* **2006**, *281*, 70-87.
7. Phuntsho, S.; Hong, S.; Elimelech, M.; Shon, H. K. Osmotic equilibrium in the forward osmosis process: Modelling, experiments and implications for process performance. *J. Membr. Sci.* **2014**, *453*, 240-252.
8. McGinnis, R. L.; Elimelech, M. Energy requirements of ammonia–carbon dioxide forward. *Desalination* **2007**, *207*, 370-382.
9. McGinnis, R. L.; McCutcheon, J. R.; Elimelech, M. A novel ammonia–carbon dioxide osmotic heat engine for power generation. *J. Membr. Sci.* **2007**, *305*, 13-19.
10. Hydration Technology Innovations Personal Desalination & Water Filters: About. http://www.htiwater.com/divisions/personal_hydration/about.html.
11. Phuntsho, S.; Shon, H. K.; Majeed, T.; Saliby, I. E.; Vigneswaran, S.; Kandasamy, J.; Hong, S.; Lee, S. Blended Fertilizers as Draw Solutions for Fertilizer-Drawn Forward Osmosis Desalination. *Environ. Sci. Technol.* **2012**, *46*, 4567-4575.
12. Hoover, L. A.; Phillip, W. A.; Tiraferri, A.; Yip, N. Y.; Elimelech, M. Forward with Osmosis: Emerging Applications for Greater Sustainability. *Environ. Sci. Technol.* **2011**, *45*, 9824–9830.
13. Garcia-Castello, E. M.; McCutcheon, J. R. Dewatering press liquor derived from orange production by forward osmosis. *J. Membr. Sci.* **2011**, *372*, 97-101.
14. McGinnis, R. L.; Hancock, N. T.; Nowosielski-Slepowron, M. S.; McGurgan, G. D. Pilot Demonstration of the NH₃/CO₂ forward osmosis desalination process on high salinity brines. *Desalination* **2013**, *312*, 67-74.
15. Hickenbottom, K. L.; Hancock, N. T.; Hutchings, N. R.; Appleton, E. W.; Beaudry, E. G.; Xu, P.; Cath, T. Y. Forward osmosis treatment of drilling mud and fracturing wastewater from oil and gas operations. *Desalination* **2013**, *312*, 60-66.
16. Ling, M. M.; Chung, T.-S. Desalination process using super hydrophilic nanoparticles via forward osmosis. *Desalination* **2011**, *278*, 194-202.
17. Ge, Q.; Su, J.; Amy, G. L.; Chung, T. S. Exploration of polyelectrolytes as draw solutes in forward osmosis processes. *Water Res.* **2012**, *46*, 1318-1326.

18. Tan, C. H.; Ng, H. Y. A novel hybrid forward osmosis – nanofiltration (FO-NF) process for seawater desalination: Draw solution selection and system configuration. *Desalin. Water Treat.* **2010**, *13*, 356-361.
19. McGinnis, R. Osmotic Desalination Process. US 2005/0145568 A1, July 7, 2005.
20. Cath, T. Y.; Hancock, N. T.; Lundin, C. D.; Hoppe-Jones, C.; Drewes, J. E. A multi-barrier osmotic dilution process for simultaneous desalination and purification of impaired water. *J. Membr. Sci.* **2010**, *362*, 417-436.
21. Zhao, S.; Zou, L.; Mulcahy, D. Brackish water desalination by a hybrid forward osmosis–nanofiltration system using divalent draw solute. *Desalination* **2012**, *284*, 175-181.
22. Ge, Q.; Su, J.; Chung, T.-S.; Amy, G. Hydrophilic Superparamagnetic Nanoparticles: Synthesis, Characterization, and Performance in Forward Osmosis Processes. *Ind. Eng. Chem. Res.* **2011**, *50*, 382-288.
23. Stone, M. L.; Rae, C.; Stewart, F. F.; Wilson, A. D. Switchable polarity solvents as draw solutes for forward osmosis. *Desalination* **2013**, *312*, 124-129.
24. Carmignani, G.; Slitkiewitz, S.; Webley, J. W. Recovery of retrograde soluble solute for forward osmosis water treatment. US2012/0267308 A1, April 23, 2012.
25. Achilli, A.; Cath, T. Y.; Childress, A. E. Selection of inorganic-based draw solutions for forward osmosis applications. *J. Membr. Sci.* **2010**, *364*, 233-241.
26. McGinnis, R. L. Osmotic Desalinization Process. US 6,391,205 B1, May 21, 2002.
27. Hancock, N. T.; Black, N. D.; Cath, T. Y. A comparative life cycle assessment of hybrid osmotic dilution desalination and established seawater desalination and wastewater reclamation process. *Water Res.* **2012**, *46*, 1145-1154.
28. Boo, C.; Khalil, Y. F.; Elimelech, M. Performance evaluation of trimethylamine–carbon dioxide thermolytic draw solution for engineered osmosis. *J. Membr. Sci.* **2015**, *473*, 302-309.
29. Lee, K. L.; Baker, R. W.; Lonsdale, H. K. Membranes for power generation by pressure-retarded osmosis. *J. Membr. Sci.* **1981**, *8*, 141-171.

30. Yip, N. Y.; Tiraferri, A.; Phillip, W. A.; Schiffman, J. D.; Hoover, L. A.; Kim, Y. C.; Elimelech, M. Thin-Film Composite Pressure Retarded Osmosis Membranes for Sustainable Power Generation from Salinity Gradients. *Environ. Sci. Technol.* **2011**, *45*, 4360-4369.
31. Yip, N. Y.; Elimelech, M. Thermodynamic and Energy Efficiency Analysis of Power Generation from Natural Salinity Gradients by Pressure Retarded Osmosis. *Environ. Sci. Technol.* **2012**, *46*, 5230-5239.
32. Logan, B. E.; Elimelech, M. Membrane-based processes for sustainable power generation using water. *Nature* **2012**, *488*, 313-319.
33. Loeb, S. Energy production at the Dead Sea by pressure-retarded osmosis challenge or chimera? *Desalination* **1998**, *120*, 247-262.
34. Loeb, S. One hundred and thirty benign and renewable megawatts from Great Salt Lake? The possibilities of hydroelectric power by pressure-retarded osmosis. *Desalination* **2001**, *141*, 85-91.
35. Song, X.; Liu, Z.; Sun, D. D. Energy recovery from concentrated seawater brine by thin-film nanofiber composite pressure retarded osmosis membranes with high power density. *Energy Environ. Sci.* **2013**, *6*, 1199-1210.
36. Kim, J.; Park, M.; Snyder, S. A.; Kim, J. H. Reverse osmosis (RO) and pressure retarded osmosis (PRO) hybrid processes: Model-based scenario study. *Desalination* **2013**, *322*, 121-130.
37. Achilli, A.; Prante, J. L.; Hancock, N. T.; Maxwell, E. B.; Childress, A. E. Experimental Results from RO-PRO: A Next Generation System for Low-Energy Desalination. *Environ. Sci. Technol.* **2014**, *48*, 6437-6443.
38. Prante, J. L.; Ruskowitz, J. A.; Childress, A. E.; Achilli, A. RO-PRO desalination: An integrated low-energy approach to seawater desalination. *Appl. Energ.* **2014**, *120*, 104-114.
39. Kim, Y. C.; Elimelech, M. Potential of osmotic power generation by pressure retarded osmosis using seawater as feed solution: Analysis and experiments. *J. Membr. Sci.* **2013**, *429*, 330-337.

40. Straub, A. P.; Yip, N. Y.; Elimelech, M. Raising the Bar: Increased Hydraulic Pressure Allows Unprecedented High Power Densities in Pressure-Retarded Osmosis. *Environ. Sci. Technol. Lett.* **2014**, *1*, 55-59.
41. Anastasio, D. D.; Arena, J. T.; Cole, E. A.; McCutcheon, J. R. Impact of temperature on power density in closed-loop pressure retarded osmosis for grid storage. *J. Membr. Sci.* **2015**, *479*, 240-245.
42. Lin, S.; Yip, N. Y.; Cath, T. Y.; Osuji, C. O.; Elimelech, M. Hybrid Pressure Retarded Osmosis–Membrane Distillation System for Power Generation from Low-Grade Heat: Thermodynamic Analysis and Energy Efficiency. *Environ. Sci. Technol.* **2014**, *48*, 5306-5313.
43. Arena, J. T.; Manickam, S. S.; Reimund, K. K.; Freeman, B. D.; McCutcheon, J. R. Solute and water transport in forward osmosis using polydopamine modified thin film composite membranes. *Desalination* **2014**, *343*, 8-16.
44. Low, S. C. Preliminary studies of seawater desalination using forward osmosis. *Desalin. Water Treat.* **2009**, 41-46.
45. McCutcheon, J. R.; McGinnis, R. L.; Elimelech, M. Desalination by ammonia-carbon dioxide forward osmosis: Influence of draw and feed solution concentrations on process performance. *J. Membr. Sci.* **2006**, *278*, 114-123.
46. Edwards, T. J.; Maurer, G.; Newman, J.; Prausnitz, J. M. Vapor-Liquid Equilibria in Multicomponent Aqueous Solutions of Volatile Weak Electrolytes. *AIChE J.* **1978**, *24*, 966-976.
47. Kawazuishi, K.; Prausnitz, J. M. Correlation of Vapor-Liquid Equilibria for the System of Ammonia-Carbon Dioxide-Water. *Ind. Eng. Chem. Res.* **1987**, *26*, 1482-1485.
48. Mani, F.; Peruzzini, M.; Stoppioni, P. CO₂ absorption by aqueous NH₃ solutions: speciation of ammonium. *Green Chem.* **2006**, *8*, 995-1000.
49. Robinson, R. A.; Stokes, R. H. *Electrolyte Solutions*, 2nd ed.; Dover Publications: Mineola, 2002.
50. Pawlikowski, E. M.; Newman, J.; Prausnitz, J. M. Phase Equilibria for Aqueous Systems of Ammonia and Carbon Dioxide. *Ind. Eng. Chem. Proc. Des. Dev.* **1982**, *21*, 764-770.

51. Buetler, D.; Renon, H. Representation of NH₃-H₂S-H₂O, NH₃-CO₂-H₂O, and NH₃-SO₂-H₂O Vapor-Liquid Equilibria. *Ind. Eng. Chem. Proc. Des. Dev.* **1978**, *17*, 220-230.
52. Trypuć, M.; Kielkowska, U. Solubility in the NH₄HCO₃ + NaHCO₃ + H₂O system. *J. Chem. Eng. Data* **1998**, *43*, 201-204.
53. Pitzer, K. S. Thermodynamic of Electrolytes. I. Theoretical Basis and General Equations. *J. Phys. Chem.* **1973**, *77*, 268-277.
54. Lewis, G. N.; Randall, M.; Pitzer, K. S.; Brewer, L. *Thermodynamics*, 2nd ed.; McGraw-Hill Book Company: New York, 1961.
55. Grattoni, A.; Merlo, M. Osmotic Pressure beyond Concentration Restrictions. *J. Phys. Chem. Part B* **2007**, *111*, 11770-11775.
56. Prausnitz, J. M.; Lichtenthaler, R. N.; de Azevedo, E. G. *Molecular Thermodynamics of Fluid-Phase Equilibria*, 3rd ed.; Prentice-Hall, Inc.: Upper Saddle River, 1999.
57. Baker, R. W. *Membrane Technology and Applications*, 2nd ed; John Wiley & Sons Ltd: West Sussex, England, 2004.
58. Hesske, H.; Gloe, K. Hydration Behavior of Alkyl Amines and Their Corresponding Protonated Forms. 1. Ammonia and Methylamine. *J. Phys. Chem.* **2007**, *111*, 9848-9853.
59. Coday, B. D.; Xu, P.; Beaudry, E. G.; Herron, J.; Lampi, K.; Hancock, N. T.; Cath, T. Y. The sweet spot of forward osmosis: Treatment of produced water, drilling wastewater, and other complex and difficult liquid streams. *Desalination* **2014**, *333*, 23-35.
60. Cui, Y.; Lui, X. Y.; Chung, T. S. Enhanced osmotic energy generation from salinity gradients by modifying thin film composite membranes. *Chem. Eng. J.* **2014**, *242*, 195-203.
61. She, Q.; Jin, X.; Tang, C. Y. Osmotic power production from salinity gradient resource by pressure retarded osmosis: Effects of operating conditions and reverse solute diffusion. *J. Membr. Sci.* **2012**, *401-402*, 262-273.

Chapter 3

Polydopamine modification of commercial thin film composite membranes for pressure retarded osmosis

Arena et al. *J. Membr. Sci.* 2011, 375, 55-62. doi:10.1016/j.memsci.2011.01.060

3.1. Introduction

Forward (or engineered) osmosis (FO) offers the possibility for utilizing osmotic pressure gradients for a wide range of applications. These include water desalination, pressure retarded osmosis (PRO) for power generation and direct osmotic concentration (DOC) for dewatering; however, poor performance of existing membrane technology has limited the growth of this emerging platform technology.¹⁻⁶

Current thin film composite (TFC) membrane has resulted in highly selective and permeable membranes for hydraulically driven flow, such as nanofiltration (NF) and reverse osmosis (RO).⁷⁻⁹ The performance of TFC membranes far exceeds that of integrated

asymmetric membranes for pressure driven flow,⁹ but these benefits do not translate to FO processes. Poor performance of commercial TFC RO membranes is attributed to severe internal concentration polarization (ICP) caused by the thick porous support layers that are universal to these type of membranes.^{10,11} Recent efforts reported that ICP may be enhanced by the hydrophobic nature of typical TFC support layers. The intrinsic hydrophobicity of the polysulfone (PSu) support mid-layer and the polyester (PET) nonwoven prevents complete wetting of the pore structure. The reduction in 'wetted porosity' of the support layer reduces solute diffusivity and available pathways for water transport.¹² This is one reason that, as of 2009, the only commercially available forward osmosis (FO) membrane from Hydration Technologies Innovations (HTI) is comprised of cellulose acetate, a hydrophilic polymer.¹³

3.1.1. Using membranes with intrinsically hydrophilic support layers

Several groups reported on the fabrication of integrated membranes for forward osmosis using hydrophilic polymers such as polybenzimidazole (PBI) and cellulose acetate (CA).¹⁴⁻¹⁷ While hydrophilic polymers may be suitable for integrated membrane fabrication they are not likely to function as an adequate TFC membrane support. If the entire porous support membrane were hydrophilic, it could absorb water, swell and soften (plasticize).¹⁸ Additionally,

if the membrane support were hydrophilic, it might swell differently in different media (e.g., pure water vs. saltwater), contributing to mechanical instability of the support.¹⁹ Support layer swelling may also cause post-fabrication perforation or delamination of the selective layer. It is therefore advantageous to use hydrophobic and tough thermoplastics for membrane supports.

Additionally, other complications may arise if hydrophilic polymers are used as supports for TFC membranes. According to a recent study, support layer hydrophobicity may be important during the interfacial polymerization due to the shape of the meniscus that forms between the organic and aqueous phase. The hydrophilicity of the support will alter the shape of the meniscus which will affect the resulting polyamide properties.²⁰ The surface chemistry of the support layer may also interact with the amine monomer during interfacial polymerization. These phenomena cause changes in the resulting thin film properties and a reduction in selectivity.

Research on using hydrophilic polymers in thin film composite membranes is at the time of this writing still in its infancy. Nevertheless, these early efforts have indicated that if TFC membranes having a hydrophilic support layer are desirable, imparting the hydrophilic character to the support layer *after* the composite structure has been fully formed may be a

preferred approach. This allows for the advantageous use of the superior permselectivity of the polyamide selective layer that has been optimized for performance for the past thirty years.

3.1.2. Use of polydopamine for increasing hydrophilicity of surfaces

Polydopamine (PDA) is a novel bio-inspired polymer sharing similar properties to the adhesive secretions of mussels and is capable of adhering to substrates underwater and without surface preparation.^{21,22} PDA is formed by a polymerization/precipitation reaction using low concentrations of dopamine in an aerated aqueous solution at basic pHs. Though the mechanism of PDA formation is still undergoing investigation, one proposed mechanism consists of three primary steps; the first is the requisite oxidation of the catechol functionality to a benzoquinone, cyclization of the primary amine yielding 5,6-dihydroxindole, and the polymerization of this monomer.²¹⁻²³ The 5,6-dihydroxindole can then adsorb onto the substrate's surface as a result of excessive hydrogen bonding permissible because of the catechol moiety. This process results in a layer-by-layer assembly of PDA onto the substrate²⁴. Various studies have examined the thickness of the PDA coating; upon termination of the polymerization step PDA layer thicknesses of between 20 to 65 nm were reported.^{22,25,26}

PDA can be applied to wide variety of materials including those which are considered

highly resistance to adhesion such as polytetrafluoroethylene (PTFE).²¹ Additionally, inorganic materials such as metals and metal oxides can be coated with PDA.^{22,24,25} Another unique and useful property of PDA is its ability to scavenge metals out of solution and incorporate them into a PDA surface coating via an electroless metallization.²⁴ Furthermore when PDA is applied to a material its surface properties dominate over those of the substrate allowing for the compatibilization of organic fibers or carbon nanotubes.^{27,28}

Recently, PDA has been used to impart fouling resistance to ultrafiltration and RO membranes.^{22,26} In these investigations, the PDA was applied to the selective layer and shown to increase hydrophilicity. This resulted in reduced adhesion to the surface by proteins and other foulants. In addition to this direct application of hydrophilic PDA surface layers to impart fouling resistance; amine functionalized polyethylene glycol (PEG) can be covalently bonded to a membrane surface further enhancing its fouling resistance.^{22,26}

3.2 Materials and methods

3.2.1. Selected membranes and chemicals

The membranes selected for this investigation are the Dow Water & Process Solutions BW30 and SW30-XLE membranes. Both membranes support layers are made of PSu

Table 3.1. Varieties of BW30 and SW30-XLE membranes examined in this study.

Name	Description
Neat	Used as received
No PET	PET fabric backing layer removed
PDA 1h	PDA modified with 1h coating time
PDA 42h	PDA modified with 42h coating time

supported by a PET nonwoven.⁸ They were chosen for their well documented ability of rejecting sodium chloride ions as well as the inherent benefits of being able to source consistent substrates for PDA modification.^{29,30} The membranes were tested in four different varieties descriptions of which can be found in Table 3.1. Sodium chloride, Tris-HCl, and sodium hydroxide were purchased from Fisher Scientific (Pittsburgh, PA). The dopamine-hydrochloride was purchased from Sigma-Aldrich (St. Louis, MO). The water used was ultrapure Milli-Q water produce by a Millipore Integral 10 water system, (Millipore Corporation Billerica, MA).

3.2.2. Scanning electron microscope imaging of thin film composite membranes

The TFC membrane PSu layer pore structures were imaged with a FEI Phenom scanning electron microscope (SEM) from FEI Company (Hillsboro, OR). These samples were prepared

using a freeze fracturing technique involving liquid nitrogen^{31,32,33} after removal of the PET support layer. This method allows for clean, straight edges preserving the internal pore structure for observation.

3.2.3. Preparation of membranes for coating

The membranes were taken as is from Dow and prepared for coating. First, the polyester (PET) fabric layer was removed by carefully peeling the layer from the porous PSu layer while taking care to not damage the selective layers of the membrane.¹² This was done to expose the more hydrophobic Psu directly to the PDA coating solution. The membranes with no PET were then placed in deionized water for storage.

Prior to coating the membrane with PDA, the membrane is soaked in isopropyl alcohol (IPA) at room temperature for 1 h to wet out the pore structure. Wetting of the Psu pore structure with water is essential for coating the pore with PDA because current understanding indicates PDA polymerization occurs only within aqueous solution as a result of the need for hydroxide groups to facilitate functionalization of dopamine for polymerization.²² The IPA is then rinsed out of the membranes using a series of three deionized (DI) water baths of 1 L volume for forty-five minutes each.²⁶ The DI water rinsing baths are refrigerated to prevent the

nucleation of air bubbles on the surface and into the pores of the membranes and thus jeopardize the pore wetting. After the IPA has been washed out of the membranes they are stored at 5°C in deionized water.

3.2.4. Method for coating membrane support layers with polydopamine

The coating step takes place at room temperature and was performed in a custom designed coating device which limits coating to only one side of the membrane (for more information see Appendix 2). The container has two reservoirs separated by the membrane. The PDA coating solution is placed in the reservoir exposed to the PSu layer and is added as two components: 100 mL of a pH 8.7 Tris-HCl buffer and 2 mL of a 100 g·L⁻¹ solution of

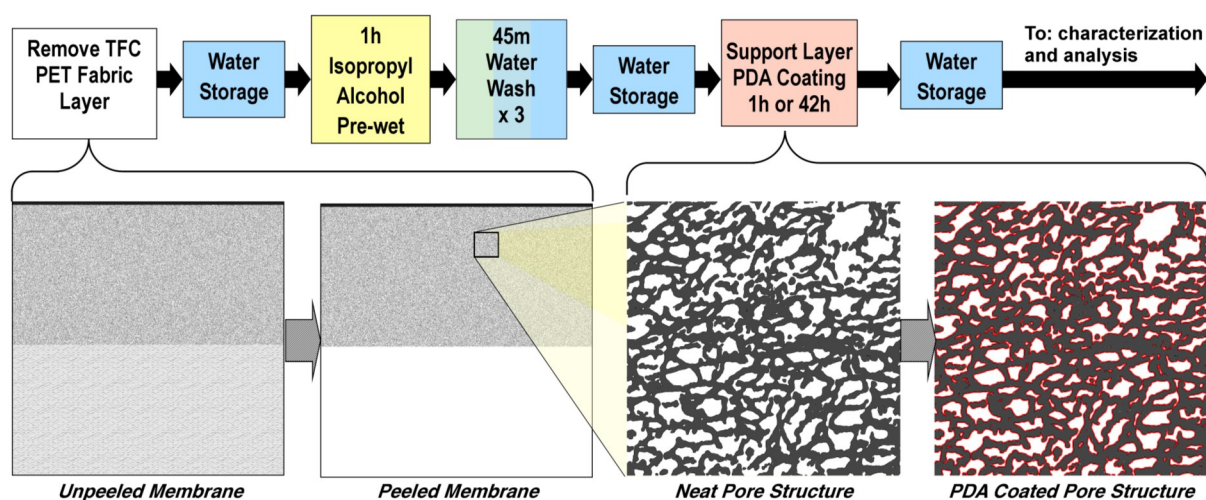


Fig. 3.1. Flowchart showing the process for modifying a TFC RO membrane with PDA.

dopamine.^{21,22,24-28} The reservoir in contact with the selective layer contains the same pH 8.7 Tris-HCl buffer solution, without dopamine-HCl, to balance out a majority of concentration gradients across the membrane. Having a solution in contact with the selective layer is essential to ensure that the membranes selective layer remains hydrated.

Coating times for PDA can vary but this investigation was limited to a short coating time of 1 h and a long coating time of 42 h. 42 h hours should be sufficient for the PDA coating thickness to have attained a maximum given the reagents.^{21,25,26} A diagram showing the membrane preparation and coating process is provided in Fig. 3.1.

3.2.5.Measurement of surface contact angles

The contact angles of the peeled and PDA modified membranes PSu support layers were measured using the sessile drop method on a CAM 101 series contact angle goniometer (KSV Company, Linthicum Heights, MD). The values were taken as an average of at least four points with a volume of $10 \pm 1 \mu\text{L}$.

3.2.6. Testing hydrostatic pressure driven flux of membranes

The peeled and PDA modified membranes were subjected to cross-flow RO tests to

determine if the PET removal or PDA coating process altered the membrane permselectivity. Previous work has indicated that PET removal, if done carefully resulted in no significant loss of selectivity.¹² Moreover, it is unlikely that PDA modification of the support layer would damage the polyamide selective layer and reduce selectivity. To ensure these results, pure water permeability and salt rejection tests were performed on the neat and modified membranes in a lab-scale cross-flow RO system, show in Fig. 3.2. For these tests, the removed PET was inserted behind the membrane to serve as additional support. This

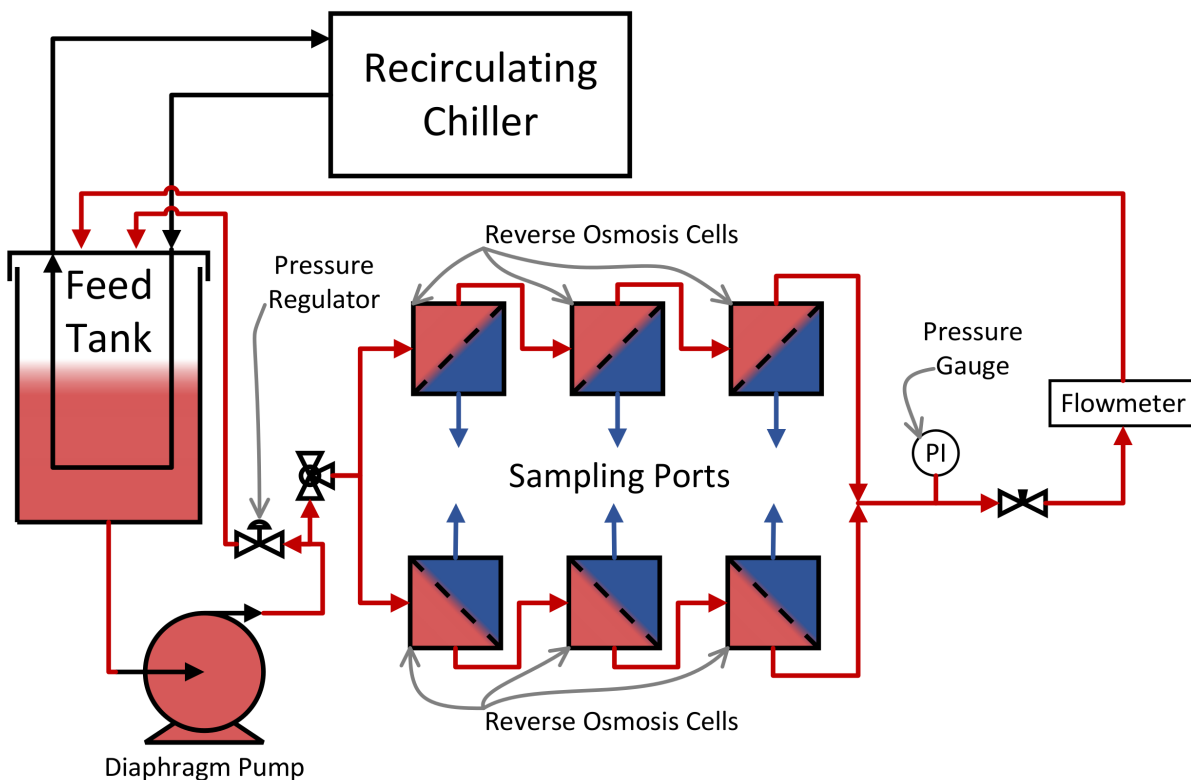


Fig. 3.2. Schematic of the reverse osmosis test system used in this study.

additional support does not contribute significantly to the hydraulic resistance of the membrane and will not impact the pure water permeability. Pure water permeability tests were conducted at 25°C at five pressures ranging from 10.3 bar to 31.0 bar. Flux was measured in duplicate with very close agreement as observable by the small error bars. The salt rejection tests were conducted with a feed of 2000 ppm sodium chloride at 25°C at a cross-flow velocity of 0.125 m·s⁻¹. Permeate for the salt rejection tests were collected at 15.5 bar and 31.0 bar. The conductivity of the bulk permeate and feed were measured to determine the rejection.

3.2.7. Testing osmotically driven flux of modified membranes

The modified TFC RO membranes were tested under osmotic flux conditions using a method similar to previous investigations.^{5,33} In these tests, the membrane was oriented in the PRO mode, with the selective layer facing the draw solution.¹⁰ Sodium chloride was used as the draw solute at concentrations of 0.05 M, 0.1 M, 0.5 M, 1.0 M, and 1.5 M. The system, shown in Fig. 3.3, incorporated a recirculating chiller and temperature was maintained at 23±1°C. Tests were run in triplicate using fresh membrane samples in each of the four varieties listed in Table 3.1.

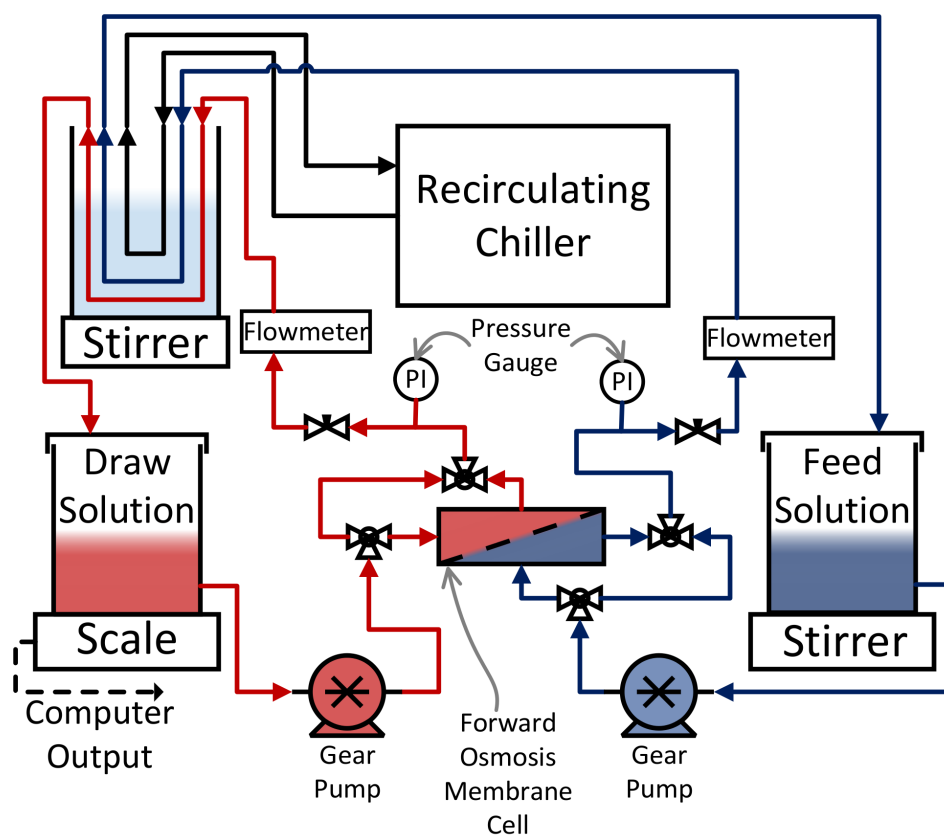


Fig. 3.3. Schematic of the forward osmosis test system used in this study.

3.2.8. Flux modeling for evaluating coating efficacy

A model was developed to compare the actual performance of the PDA modified membranes to that of an ideal membrane with a fully wetted support layer and perfect selectivity. The model was developed in previous investigations.^{10,34} Since the membrane was oriented in the PRO mode, negligible salt passage through the membranes selective layer was assumed. Water flux predicted in this way is based solely on the pure water permeability, the

draw solution osmotic pressure, and the external concentration polarization modulus.³³

$$J_w = A \cdot \pi_D \exp\left(-\frac{J_w}{k}\right) \quad (3.1)$$

In Eq. 3.1 J_w is the water flux, A is the hydraulic permeability, π_D is the osmotic pressure of the draw solution and k is the external mass transfer coefficient on the draw side of the membrane.

Given a known mass transfer coefficient, hydraulic permeance, and draw solution osmotic pressure, flux is solved iteratively using a Mathematica program coded by the author.

Author's note: The original publication used code that was written in MatLab; however, the data shown later used values generated from the code in Appendix 4 assuming for a structural parameter equaling zero.

3.3. Results and discussion

3.3.1. Polysulfone pore structure

SEM Images of the PSu layers of the BW30 and SW30-XLE membranes are shown in Fig.

3.4. The SW30-XLE's PSu layer is more porous and contains large numbers of macrovoids.

The BW30's PSu layer contains fewer macrovoids and in general smaller pores.

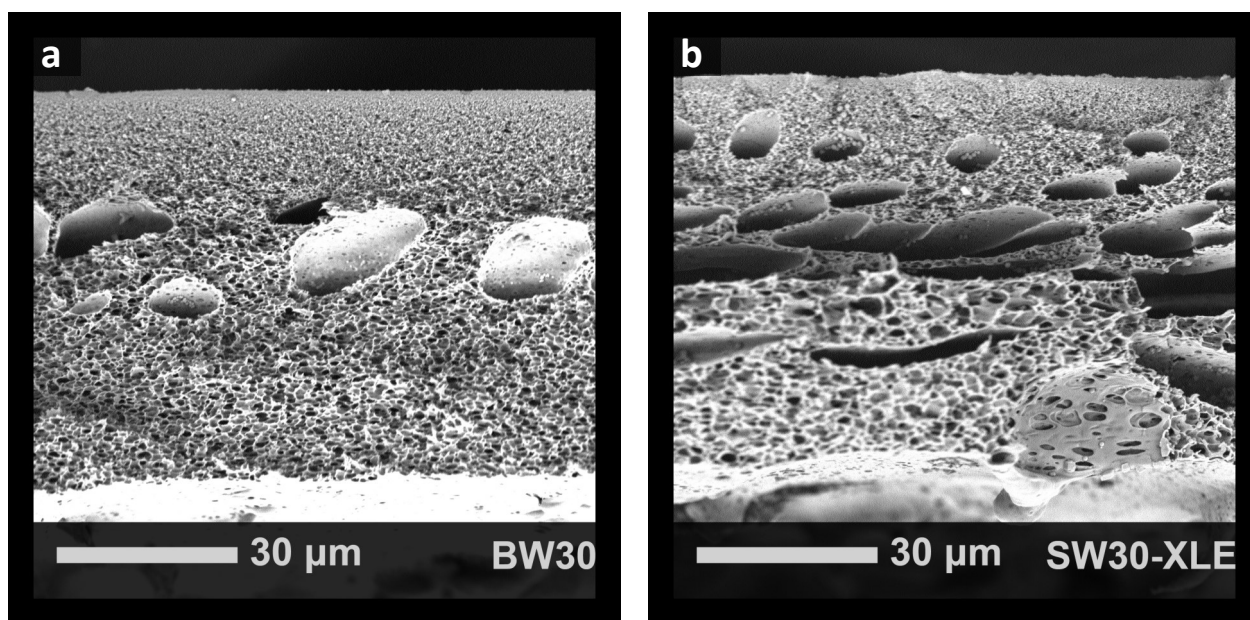


Fig. 3.4. SEM of BW30 (a) and SW30-XLE (b) membranes showing the pore structure of the porous PSu support layer. The polyamide selective layers are at the top of the images.

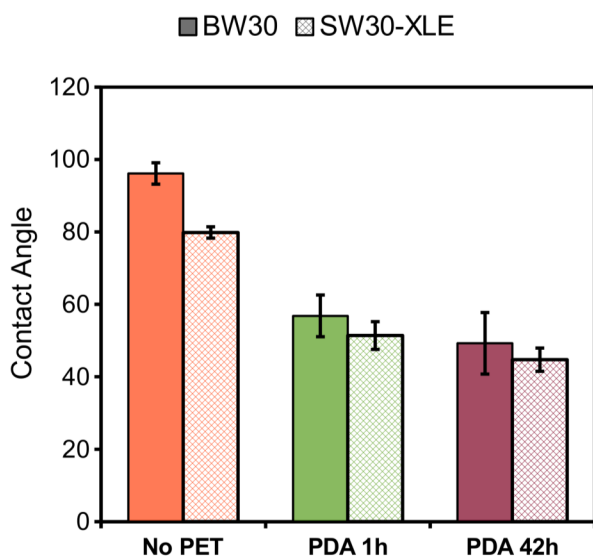


Fig. 3.5. Contact angles for the porous support layers of neat and PDA modified BW30 (solid) and SW30-XLE (cross-hatched) membranes. These values represent an average of at least four locations using a droplet size of approximately 10 μL.

3.3.2. Contact angles

Fig. 3.5 shows that the PDA coating resulted in a decrease in contact angle for the both the BW30 and SW30-XLE PSu layers, indicating increased hydrophilicity. It is noted that this technique does not determine changes in hydrophilicity *within* the support layer and only measures the PSu interface

exposed to the coating solution. Contact angles of the PDA 42h membranes were only marginally less than those of the PDA 1h membranes, indicating that short coat times effectively cover the PSu substrate at its surface.

3.3.3. Membrane characterization

3.3.3.1. Water permeance

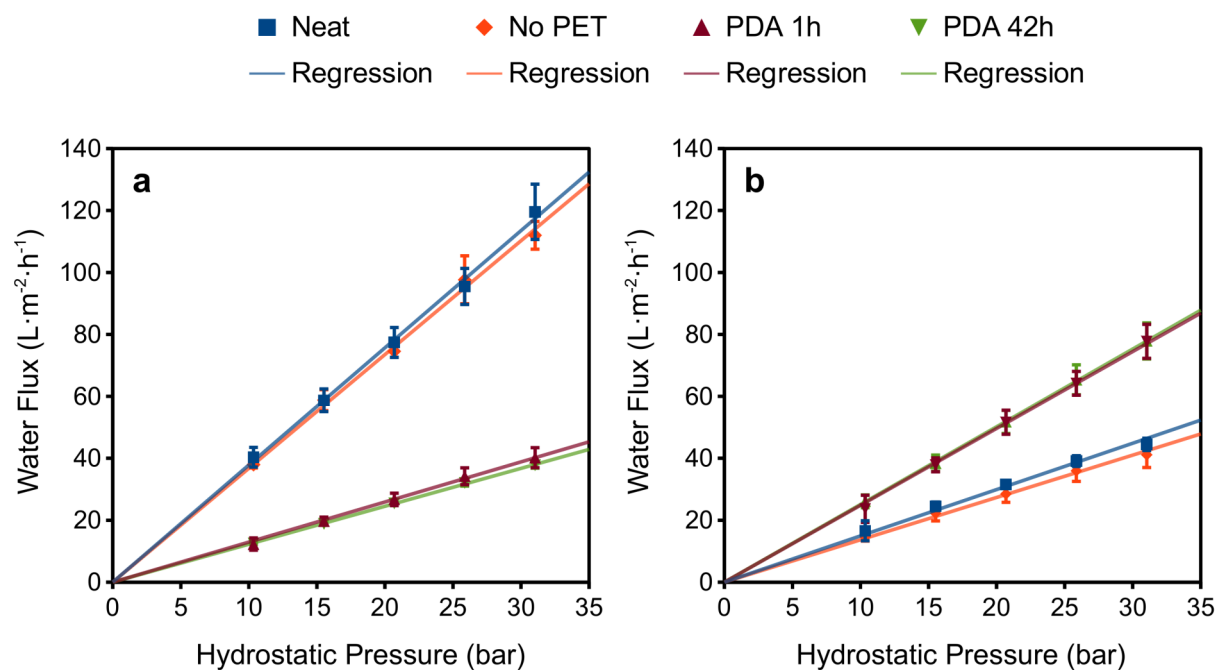


Fig. 3.6. Pure water flux of the BW30 (a) and SW30-XLE (b) membranes using a pure water feed at a temperature of 25°C. Descriptions of the membrane varieties are in Table 3.1. Slope of the regression line represents the water permeance of a membrane.

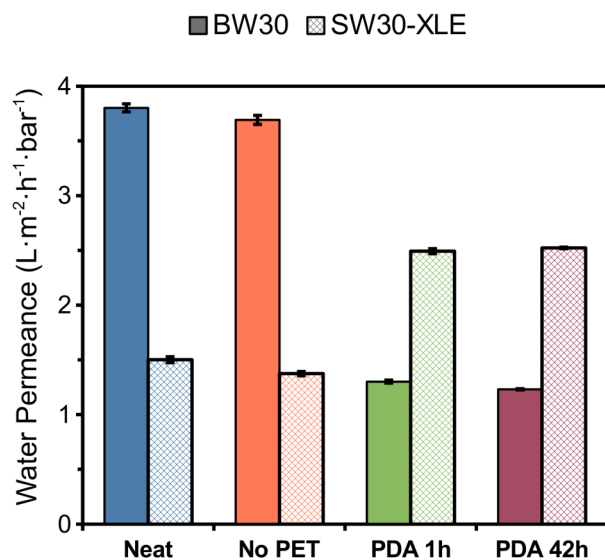


Fig. 3.7. Pure permeance of the BW30 (solid) and SW30-XLE (cross-hatched) membranes measured in reverse osmosis, using a pure water feed at a temperature of 25°C. Descriptions of the membrane varieties are in Table 3.1.

The pure water flux results for the modified membranes were interesting and unexpected. The modified BW30 membranes exhibited a decreased water permeance while the SW30-XLE exhibited an increase in water permeance (Fig. 3.6 & Fig. 3.7). The increased permeance of the SW30-XLE is likely due to the hydrophilization of the

support layer at the interface of the PSu layer and the polyamide selective layer. By increasing the hydrophilic character of this interface, transport of water from the polyamide layer is more favorable. It may be that water transporting through the now hydrophilic support layer encounters less surface energy resistance than normally associated with an unmodified hydrophobic PSu support. This may allow for easier water access to smaller pores in the support layer which may have been inaccessible prior to hydrophilization.

The same effect is not seen with a PDA coated BW30 membrane support. This may be

due to the lower porosity and fewer number of macrovoids in the PSu mid-layer. PDA will polymerize in the bulk solution to form aggregates which can adsorb to the pore surfaces and clog them. SEM imaging shows no observable fouling, though the blocking likely occurs at narrow junctions between interconnected pores. This internal fouling is more likely to take place when the pores are smaller and the PDA aggregates can intersect a pore junction and block it. Compared to the SW30-XLE, the BW30 has smaller pores near the coating solution and lacks many large macrovoids. These macrovoids reduce tortuosity and facilitate deeper penetration by diffusion of PDA into the support structure prior to deposition on a pore wall or pore junction. Thus we see internal fouling by PDA in the BW30 membrane result in reduced permeance and less hydrophilization of the PSu/polyamide interface.

3.3.3.2. Salt rejection

Average salt rejections for the modified membranes are shown in Fig. 3.8. The fluxes for the tests can be found in Table 3.2. These results show that the PDA modified membranes have comparable selectivity to the unaltered membranes.

Table 3.2. Water flux for a 2000 ppm sodium chloride solution for neat and modified membranes at 25 °C with a cross-flow velocity of 0.125 m·s⁻¹. Flux are in L·m⁻²·h⁻¹.

	SW30-XLE Neat	SW30-XLE No PET	SW30-XLE PDA 1h	SW30-XLE PDA 42h
15.5 bar	21.67 ± 2.33	18.40 ± 0.59	28.83 ± 4.36	31.25 ± 2.57
31.0 bar	45.82 ± 4.92	54.55 ± 1.23	66.87 ± 5.21	63.80 ± 3.97

	BW30 Neat	Bw30 No PET	BW30 PDA 1h	BW30 PDA 42h
15.5 bar	43.74 ± 3.97	43.15 ± 2.45	16.21 ± 1.37	15.85 ± 0.34
31.0 bar	91.94 ± 9.19	91.73 ± 7.57	36.18 ± 1.81	33.36 ± 0.47

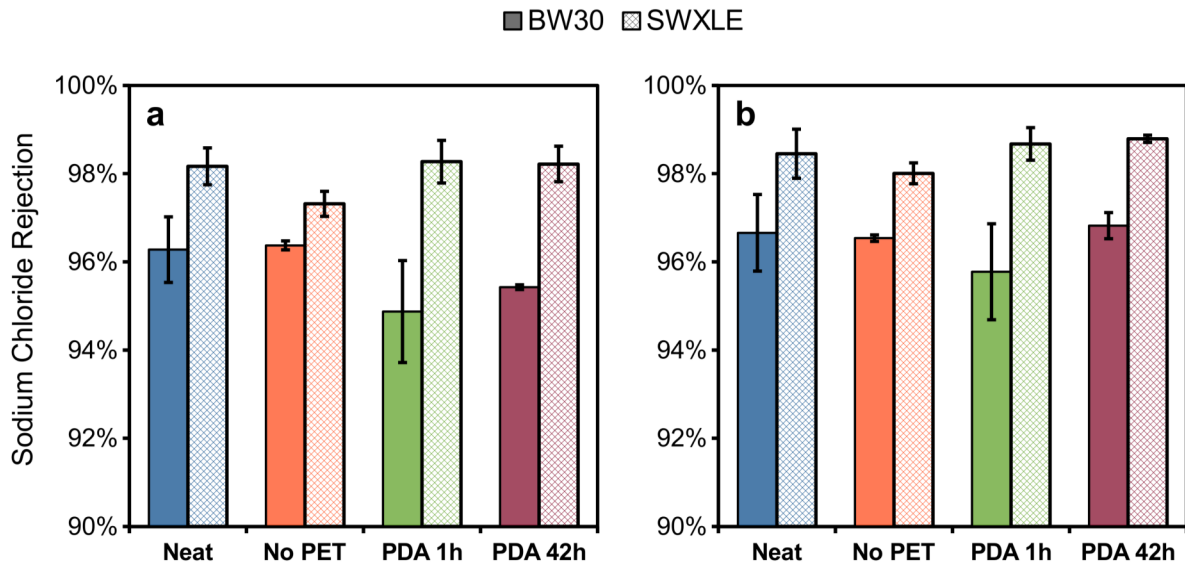


Fig. 3.8. Salt rejection for the BW30 (solid) and SW30-XLE (cross-hatched) membranes measured in reverse osmosis using a 2000 ppm sodium chloride feed solution at 15.5 bar (a) and 31.0 bar (b) , temperature of 25°C, cross-flow velocity of 0.125 m·s⁻¹. The cross-hatched and solid bars represent the BW30 and SW30-XLE membranes, respectively. Descriptions of the membrane varieties are in Table 3.1.

3.3.4. Osmotically driven flux testing in the pressure retarded osmosis mode

3.3.4.1. Water flux

To evaluate the impact of PDA coating on the commercial membranes for PRO applications, the membranes were tested for osmotic flux in the PRO mode. The coated membranes were compared to the neat membranes both with and without the PET layer. The observed water flux for the BW30 and SW30-XLE membranes are shown in Fig. 3.9a and Fig. 3.9b respectively.

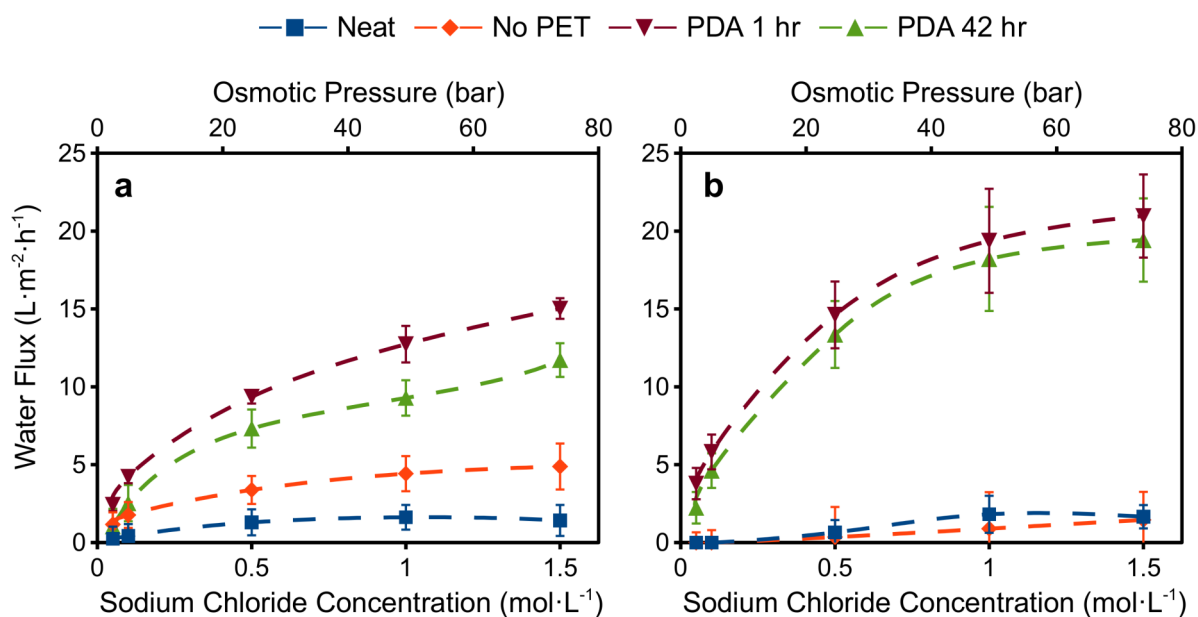


Fig. 3.9. Osmotic flux performance of BW30 (a) and SW30-XLE (b) membranes using a sodium chloride draw solution. Descriptions of the membrane varieties are in Table 3.1. Tests were run at 23°C with a cross-flow velocity of $0.25 \text{ m} \cdot \text{s}^{-1}$. The membranes were oriented in the PRO mode.

For both membranes, the neat and peeled membranes performed poorly (water flux less than $4\text{L}\cdot\text{m}^{-2}\cdot\text{h}^{-1}$). This result is consistent with other studies using RO membranes in osmotic flux tests.^{5,12} The PDA modified membrane exhibited substantial flux improvement, indicative of an increase in the 'wetted porosity' of the membrane support layer. This increased wetting promotes water transport through the support layer and to the interior interface of the polyamide layer.

The increased wetted porosity also promotes salt diffusion through the support layer and away from this interface. Internal concentration polarization occurs as a result of solute crossover.^{10,12,33} Draw solutes are not permitted to easily diffuse out of the membrane support, they will increase in concentration and drastically reduce water flux. Since no salt is present in the dilute solution at the start of the test, solute crossover would be the only source of internal concentration polarization under these test conditions.

Significant water flux improvements were observed for both the BW30 and SW30-XLE membranes, following a PDA modification; however, the less permeable SW30-XLE membrane shows approximately 20% higher flux when compared to the BW30 (Fig. 3.9). It is thought that this has to do with the macrovoids present in the SW30 membrane, which results

in a decreased tortuosity and larger pore sizes when compared to the BW30. This results in decreased internal concentration polarization induced by salt crossover.³³

There are also flux differences between the PDA 1h and PDA 42h membrane varieties. The SW30-XLE membrane exhibits similar flux performance for both coat times, while the BW30 indicates reduction in flux for increased coat times. This supports the hypothesis that the macroporous structure of the BW30 membrane support is prone to pore clogging during the coating process. Some of the BW30 pores are blocked during the coating process, increasing the tortuosity of the structure and enhancing internal CP in addition to hampering water transport to the PSu/polyamide interface.

3.3.4.2. Salt flux

The conductivity of the initially deionized feed solution was measured before and after each flux measurement. This value was correlated to a salt concentration and used to determine the reverse draw solute (sodium chloride) flux across these membranes (Fig. 3.10). Generally, increased flux performance has been correlated with increased salt flux. This is not unexpected given that salt generates the driving force for water flux. Such results have also been observed by others.^{32,35} It is worth noting that an increased sodium chloride flux into the

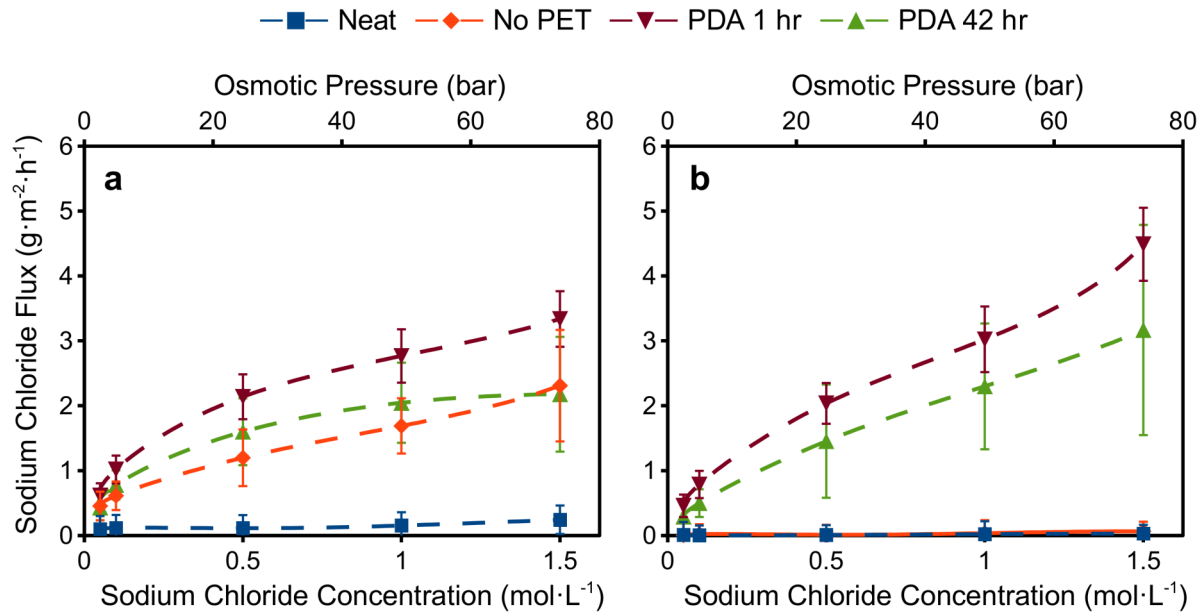


Fig. 3.10. Salt flux during the osmotic flux tests for the neat and modified BW30 membranes using a NaCl draw solution at 0.05 M, 0.1 M, 0.5 M, 1.0 M, and 1.5 M concentration. Descriptions of the membrane varieties are in Table 3.1. Tests were run at 23°C with a cross-flow velocity of 0.25 m·s⁻¹. The membranes oriented in the PRO mode.

feed solution is indicative of less internal concentration polarization. If salts are diffusing out of the support layer with greater ease, they are not residing in the support layer thus resulting in a reduced osmotic driving force. Increasing the wetted porosity thus increases both water *and* reverse solute flux.

3.3.4.3. Flux modeling

Flux was modeled based on the pure water permeance of the neat and modified BW30 and SW30-XLE membranes as determined from RO. Mass transfer coefficients on the draw side

were calculated with appropriate Sherwood number correlations as has been done in previous investigations.^{34,36} Eq. (3.1) was used to predict flux given these known values.

Since we are not certain whether the neat or PDA modified membrane water permeance is the effective permeance for osmotically driven water flux, the modeled flux data contains a range of values for both water permeance values based upon the averages of neat-no PET and PDA 1h-PDA 42h water permeance. Though the model does not take into account salt

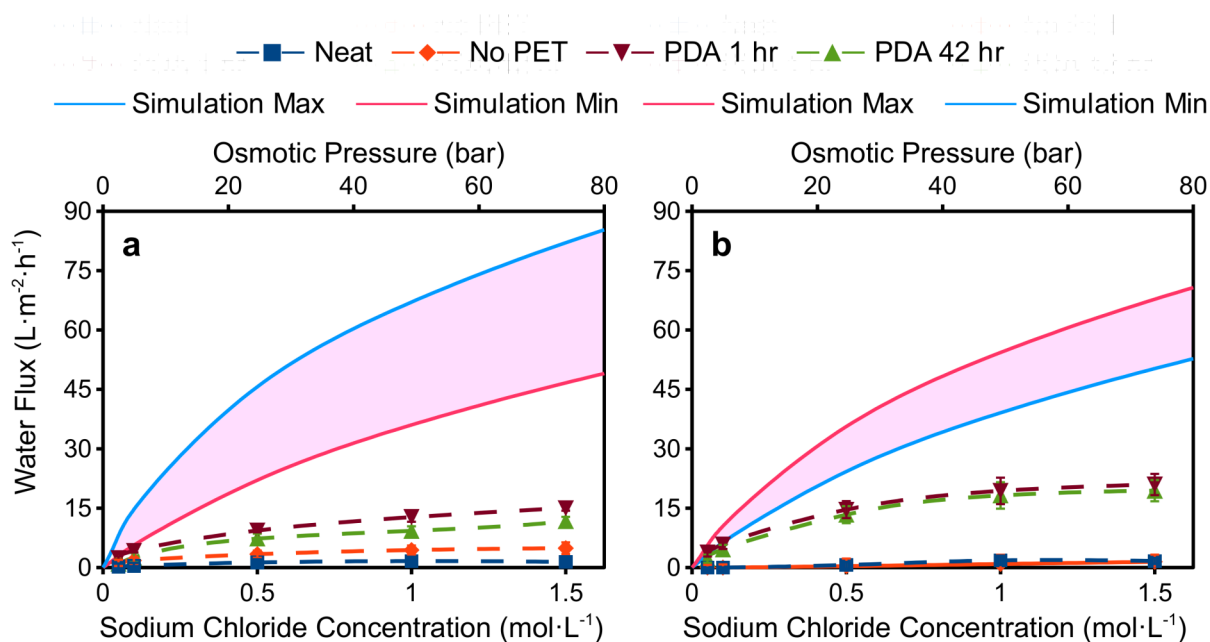


Fig. 3.11. Comparison between the osmotically driven water flux data in Fig. 3.5 and the modeled ideal water flux for the BW30 and SW30-XLE membranes. The modeled data assumes water flux is only limited by external concentration polarization is present. The shaded area indicates the expected flux for a membrane based upon the water permeance for unmodified and modified membranes from RO tests. The red curve is the modeled flux using the water permeance of PDA modified membrane and the blue curve is the modeled flux using the water permeance of unmodified membranes.

crossover induced internal CP, Fig. 3.11 indicates that there is significant room for further flux enhancement for both membranes through improved PDA coating protocol.

3.4. Conclusions

The data shows that modifying the support layers of commercial thin film composite membranes with polydopamine resulted in significant improvement in osmotic flux performance of these membranes when oriented in the PRO mode. This flux enhancement is due to a radically increased 'wetted porosity' which facilitates water transport through the support layer and decreased internal CP caused by salt crossover from the draw solution. The increased hydrophilicity also results in a two times higher hydraulic permeability for the SW30-XLE membrane but a reduction in water permeability for the BW30 caused by the difference in porous support structure

The scalability of this process renders it viable for modification of traditional thin film composite membranes after fabrication. It is the authors' hope that refinement and enhancement to the PDA coating methodology will produce further improvements to membrane performance in PRO.

References

1. McGinnis, R. L.; Elimelech, M. Global challenges in energy and water supply: the promise of engineered osmosis. *Environ. Sci. Technol.* **2008**, *42*, 8625-8629.
2. Kravath, R. E.; Davis, J. A. Desalination of sea water by direct osmosis. *Desalination* **1975**, *16*, 151-155.
3. Kessler, J.; Moody, C. Drinking water from sea water by forward osmosis. *Desalination* **1976**, *18*, 297-306.
4. Lee, K. L.; Baker, R. W.; Lonsdale, H. K. Membranes for power generation by pressure-retarded osmosis. *J. Membr. Sci.* **1981**, *8*, 141-171.
5. McCutcheon, J. R.; McGinnis, R. L.; Elimelech, M. A novel ammonia-carbon dioxide forward (direct) osmosis desalination process. *Desalination* **2005**, *174*, 1-11.
6. Cath, T. Y.; Childress, A. E.; Elimelech, M. Forward osmosis: Principles, applications, and recent developments. *J. Membr. Sci.* **2006**, *281*, 70-87.
7. Petersen, R. J. Composite reverse osmosis and nanofiltration membranes. *J. Membr. Sci.* **1993**, *83*, 81-150.
8. Dow Water and Process Solutions. FILMTEC™ Reverse Osmosis Membranes Technical Manual, Form No. 609-00071-1009. http://msdssearch.dow.com/PublishedLiteratureDOWCOM/dh_08db/0901b803808db77d.pdf.
9. Cadotte, J. E.; Petersen, R. J.; Larson, R. E.; Erickson, E. E. A New Thin-Film Composite Seawater Reverse Osmosis Membrane. *Desalination* **1980**, *32*, 25-31.
10. McCutcheon, J. R.; Elimelech, M. Influence of concentrative and dilutive internal concentration polarization on flux behavior in forward osmosis. *J. Membr. Sci.* **2006**, *284*, 237-247.
11. McCutcheon, J. R.; McGinnis, R. L.; Elimelech, M. Desalination by ammonia-carbon dioxide forward osmosis: Influence of draw and feed solution concentrations on process performance. *J. Membr. Sci.* **2006**, *278*, 114-123.

12. McCutcheon, J. R.; Elimelech, M. Influence of membrane support layer hydrophobicity on water flux in osmotically driven membrane processes. *J. Membr. Sci.* **2008**, *318*, 458-466.
13. Herron, J. Asymmetric forward osmosis membranes. United States Patent No. US 7,445,712, Nov. 4, 2008.
14. Zhang, S.; Wang, K. Y.; Chung, T. S.; Chen, H.; Jean, Y. C.; Amy, G. Well-constructed cellulose acetate membranes for forward osmosis: minimized internal concentration polarization with an ultra-thin selective layer. *J. Membr. Sci.* **2010**, *360*, 522-535.
15. Wang, K. Y.; Chung, T. S.; Chen, H.; Qin, J. J. Polybenzimidazole (PBI) nanofiltration hollow fiber membranes applied in forward osmosis process. *J. Membr. Sci.* **2007**, *300*, 6-12.
16. Wang, K. Y.; Yang, Q.; Chung, T. S.; Rajagopalan, R. Enhanced forward osmosis from chemically modified polybenzimidazole (PBI) nanofiltration hollow fiber membranes with a thin wall. *Chem. Eng. Sci.* **2009**, *64*, 1577-1584.
17. Wang, K. Y.; Ong, R. C.; Chung, T. S. Double-skinned forward osmosis membranes for reducing internal concentration polarization within the porous sublayer. *Ind. Eng. Chem. Res.* **2010**, *49*, 4824-4831.
18. Eaton, R. F.; Roe, R. J.; Wilkes, G. L.; Tobolsky, A. V. Thermodynamics of Hydrophilic Polymer Membranes: The Degree of Swelling and Salt Partition Coefficient. *American Chemical Society, Division of Organic Coatings and Plastics* **1975**, *35*, 503-508.
19. Bert, J. L.; Fatt, I.; Saraf, D. Dynamics of water transport in cellulose acetate, The Swelling Phenomenon. **1970**, *13*, 105-119.
20. Ghosh, A. K.; Hoek, E. M. V. Impacts of support membrane structure and chemistry on polyamide-polysulfone interfacial composite membranes. *J. Membr. Sci.* **2009**, *336*, 140-148.
21. Lee, H.; Rho, J.; Messersmith, P. B. Facile conjugation of biomolecules onto surfaces via mussel adhesive protein inspired coatings. *Adv. Mater.* **2009**, *21*, 431-434.
22. Lee, H.; Dellatore, S. M.; M, M. W.; Messersmith, P. B. Mussel-inspired surface chemistry for multifunctional coating. *Science* **2007**, *318*, 426-430.

23. Messersmith, P. B.; Lee, H. Surface-Independent, Surface-Modifying, Multifunctional Coatings and Applications Thereof. US 2008/0149566A1, June 26, 2008.
24. Lee, H.; Lee, Y.; Statz, A. R.; Rho, J.; Park, T. G.; Messersmith, P. B. Substrate-independent layer-by-layer assembly by using mussel-adhesive-inspired polymers. *Adv. Mater.* **2008**, *20*, 1619-1623.
25. Potsma, A.; Yan, Y.; Wang, Y.; Zelikin, A. N.; Tjijto, E.; Caruso, F. Self-polymerization of dopamine as a versatile and robust technique to prepare polymer capsules. *Chem. Mater.* **2009**, *21*, 3042-3044.
26. McCloskey, B. D.; Park, H. B.; Ju, H.; Rowe, B. W.; Miller, D. J.; Chun, B. J.; Kin, K.; Freeman, B. D. Influence of polydopamine deposition conditions on pure waterflux and foulant adhesion resistance of reverse osmosis, ultrafiltration, and microfiltration membranes. *Polymer* **2010**, *51*, 3472-3485.
27. Bourmand, A.; Riviere, J.; Le Duigou, A.; Raj, G.; Baley, C. Investigations of the use of a mussel-inspired compatibilizer to improve the matrix-fiber adhesion of a biocomposite. *Polym. Test.* **2009**, *28*, 668-672.
28. Fei, B.; Qian, B.; Yang, Z.; *, W. R.; Liu, W. C.; Mak, C. L.; Xin, J. H. Coating carbon nanotubes by spontaneous oxidative polymerization of dopamine. *Carbon* **2008**, *46*, 1795-1797.
29. Dow Water and Process Solutions. DOW FILMTEC BW30-400 High Rejection, High Surface Area Brackish Water RO Element, Form No. 609-00091-0910. http://msdssearch.dow.com/PublishedLiteratureDOWCOM/dh_090d/0901b8038090d9a2.pdf.
30. Dow Water and Process Solutions. DOW™ FILMTEC SW30XLE-440i Seawater Reverse Osmosis Element with iLECInterlocking Endcaps, Form No. 609-03003-1109.
31. Ferlita, R. R.; Phipps, D.; Safarik, J.; Yeh, D. H. Cryo-snap: a simple modified freeze-fracture method for SEM imaging of membrane cross-sections. *Environ. Prog.* **2008**, *27*, 204-209.
32. Phillip, W. A.; Yong, J. S.; Elimelech, M. Reverse draw solute permeation in forward osmosis: modeling and experiments. *Environ. Sci. Technol.* **2010**, *44*, 5170-5176.

33. Gray, G. T.; McCutcheon, J. R.; Elimelech, M. Internal concentration polarization in forward osmosis: role of membrane orientation. *Desalination* **2006**, *197*, 1-8.
34. McCutcheon, J. R.; Elimelech, M. Modeling Water Flux in Forward Osmosis: Implications for Improved Membrane Design. *AIChE J.* **2007**, *53*, 1736-1744.
35. Hancock, N. T.; Cath, T. Y. Solute Coupled Diffusion in Osmotically Driven Membrane Processes. *Environ. Sci. Technol.* **2009**, *43*, 6769-6775.
36. Mulder, M. *Basic Principles of Membrane Technology*, 2nd ed.; Kluwer Academic Publishers: Dordrecht, 2003.

Chapter 4

Pressure retarded osmosis performance of polydopamine modified membranes with differing permselectivities and structure

4.1. Introduction

Forward osmosis (FO) processes are driven by the selective permeation of water between two solutions of differing osmotic pressure separated by a semi-permeable membrane.¹⁻⁵ The osmotic pressure is developed through concentration differences between two solutions, a concentrated draw solution and a more dilute feed solution. Many have published on the use of forward osmosis for separations, including concentrate dilution,^{1,2,6} dewatering,^{7,8} and water purification and desalination.⁹⁻¹¹ The potential that drives osmosis can also be harnessed to generate power.¹²⁻¹⁴ This process is referred to as pressure retarded osmosis (PRO). PRO harnesses the potential energy of osmotic pressure differences, making use of energy released from the mixing of dilute and concentrated solutions.¹⁵ An important

part of any PRO process is the draw solution used. The most common PRO process uses a draw solution of seawater and feed solution river water.¹²⁻¹⁷ Other processes consider using reverse osmosis brine in as the draw solution to take advantage of the higher osmotic pressure.¹⁸⁻²⁰ Osmotic heat engines are another form of the PRO process uses a draw solute which is recovered within the process, ideally using some form of low temperature (~40-60°C) heat.^{21,22}

In a PRO process the draw solution is pressurized to a hydrostatic pressure less than its osmotic pressure. The hydrostatic pressure applied to the draw solution retards osmosis through a semi-permeable membrane. The osmotic flow of water creates a constant pressure volumetric expansion of draw solution which generates power by releasing the pressure of the draw solution through a hydroturbine Eq. (4.1).

$$W = J_w \cdot \Delta P \quad (4.1)$$

For PRO processes that use seawater as the draw solution, the available osmotic pressure is effectively fixed at the osmotic pressure of available seawater and so for a membrane to be capable of high power densities a suitable membrane should give high water fluxes at elevated transmembrane pressure. A common effect attributed to low water flux is internal concentration

polarization (ICP) resulting from either the membrane structure^{9,23,24} or chemistry.^{25,26} In PRO ICP occurs from the entrainment of dissolved solutes within support layer of an asymmetric membrane due to imperfect selectivity. For PRO, membrane selectivity is an important parameter impacting water flux since selective membranes can mediate some of the deleterious effects of ICP by reducing reduced solute transport through the selective layer.

4.1.1. Membranes for pressure retarded osmosis

The broader application of forward osmosis (FO) processes have been hampered by limitations to membrane design, resulting in low water fluxes^{9,27,26} or deeper incompatibilities between desirable process conditions and membrane chemistry.^{11,28} A widely studied membrane for forward osmosis (FO) is the cellulose triacetate (CTA) membrane made by Hydration Technologies Innovations (HTITM).^{1,13,14,18,29,30,31} This is an asymmetric membrane made through a wet-dry casting processes specially designed for FO processes;³² however, CTA membranes have a characteristically lower water permeance when compared to a similarly selective thin film composite (TFC) membrane.^{29,33} Mirroring the adoption of TFC membranes in reverse osmosis (RO), TFC membranes have been viewed by some as the logical replacement for CTA FO membrane due to their higher water permeance and superior

chemical resilience.^{5,9,34}

TFC membranes typically consist of three principle layers: a fabric layer for mechanical strength (typically a polyethylene terephthalate non-woven), a phase inverted mid-layer (typically polysulfone), and a polyamide selective layer, which mediates the flow of water and ions through a TFC membrane structure.³⁵ The polyamide of a TFC membrane has been formed using a number of differing monomers.^{17,35,36} The classical polyamide formulation is prepared from an aqueous diamine (typically m-phenylene diamine) and an acid chloride dissolved in a non-polar solvent (typically trimesoyl chloride).^{37,36}

The three tiered structure of TFC membranes allow for the specific tailoring of each layer, and TFC membranes tailored specifically for FO have recently become available.^{30,38} This is outwardly done through a specific redesign of the support layer to be thinner, more porous, and/or less tortuous.^{24,39} Currently, and unlike their RO and nanofiltration (NF) counterparts, FO TFC membranes are available with limited permselectivity options; therefore, in order to study variations between membrane selectivity and performance a modification of commercial RO membrane support layers for better FO performance offers an accessible approach. One such modification initially utilized by Arena et al., is the application of polydopamine (PDA) to TFC

RO membranes.^{11,26,41} The PDA modification helps to mitigate the detrimental effects of poor support layer wetting due to the innate hydrophobicity of polysulfone.²⁵

This study seeks to incorporate experimental and numerical techniques to evaluate the properties and performance of Dow Water and Process Solutions nanofiltration, brackish water and seawater reverse osmosis membranes with focusing upon:

- I. The impact of PDA modification on hydrophilicity and transport properties of these membranes.
- II. Differentiate between selective layer and support layer parameters and their impact on water flux through numerical simulation.
- III. Experimentally observe membrane performance in seawater/river water PRO while identifying mass transport effects causing observed behavior to deviate from ideal conditions.

4.2. Materials and methods

4.2.1 Selected membranes and chemicals

The membranes selected for this investigation are the Dow Water & Process Solutions™

NF270, NF90, BW30, SW30-XLE, and SW30-HR membranes. All membranes' support layers are made of polysulfone (PSu) supported by a polyethylene terephthalate (PET) nonwoven. The selective layer of the NF270 is a piperazine based polyamide, which gives higher permeance at the cost of reduced selectivity.³⁵ All other membranes used in this study had fully aromatic polyamide selective layers.^{36,42} These membranes were chosen for their availability and reported properties.^{36,43-47} Within the scope of this work each of these membranes were studied in three varieties described in Table 4.1. Sodium chloride, tris-HCl and sodium

Table 4.1. Description of the membrane varieties used in this study

Label	Description
Neat	Stored in deionized water at 4°C Otherwise used as received from manufacturer
No PET	Stored in deionized water at 4°C PET fabric backing layer carefully removed Stored in deionized water at 4°C Subjected to no additional pre-wet prior to testing
PDA 1h	Stored in deionized water at 4°C PET fabric backing layer carefully removed PDA modified according to procedure described in Section 4.2.2 Stored in deionized water at 4°C

hydroxide were purchased from Fisher Scientific (Pittsburgh, PA). Dopamine-HCl was purchased from Sigma-Aldrich (St. Louis, MO). Isopropanol was purchased from Acros Organics (Geel, Belgium). Water used in this study was ultrapure Milli-Q water produced by a Millipore Integral 10 water system, (Millipore Corporation, Billerica, MA).

4.2.2. PDA modification of TFC membranes

The PDA modification follows the procedure, including pretreatment, set forth in prior work by Arena.^{11,26} The pretreatment includes removal of the membrane's PET and soaking the membrane in isopropyl alcohol (IPA) for one hour. The membrane is then soaked in a series of three deionized water baths for 45 minutes each. Following the IPA wetting and deionized water rinsing, membranes were stored in deionized water at 4°C before being modified with PDA. As in prior studies, the dopamine polymerization took place within a custom device to avoid coating the selective layer with polydopamine which can reduce water permeance.^{11,26,48-}

⁵⁰ Both sides of the membrane were placed in contact with a pH 8.8 Tris buffer solution. Dopamine-HCl was added to the solution in contact with the membranes' PSu support layers to bring the support layer coating solution to a concentration of 2 g·L⁻¹ dopamine. The formation of PDA occurred at room temperature within non-agitated solutions exposed to the

air for 1 hour.

4.2.3. Scanning electron microscopy of studied membranes

The cross sections of the TFC membranes were imaged with a FEI Phenom scanning electron microscope (SEM) from (FEI Company Hillsboro, OR). These samples were prepared using a freeze fracturing technique after removal of the PET support layer. To freeze fracture, the membranes are submerged beneath liquid nitrogen, making the PSu layer brittle and allowing it to be easily fractured. This prepares samples having clean, straight edges preserving the internal pore structure for observation. This technique has been used elsewhere to image the cross-sections of membranes.^{17,24,26,39,40,51}

4.2.4. Contact angle testing

The contact angles of the no PET and PDA membranes PSu support layers were measured with deionized water using the sessile drop method, reflecting the technique used previously.²⁶ A CAM 101 series contact angle goniometer (KSV Company Linthicum Heights, MD). The values were taken as an average of at least four points with a volume of $7 \pm 1 \mu\text{L}$.

4.2.5. Reverse osmosis testing

The water permeance and sodium chloride rejection of these membranes was measured for the neat and PDA varieties in a lab scale reverse osmosis system maintained at a temperature of 20°C. RO characterization were not performed for the no PET membranes. Prior study by Arena et al. has shown negligible changes in the RO performance of these TFC membrane upon removal of their fabric backing layer.²⁶ Water permeance was measured from the linear regression of water flux measured at pressures ranging from 8.6 bar to 29.3 bar (125 psi to 425 psi) using a feed of deionized water.

Rejection tests were carried out using conductivity measurements at 15.5 bar (225 psi) with a 2000 ppm sodium chloride (NaCl) feed at 20 °C with a cross flow velocity of 0.25 m·s⁻¹. Intrinsic rejections were then calculated after accounting for concentration polarization using well-established mass transfer correlations^{1,52} based on hydrodynamic conditions and empirical data for diffusivity.^{53,54} The intrinsic rejections were used to determine the sodium chloride permeability for these membranes, calculated from Eq. (4.2).¹

$$B = \frac{(1-R) A (\Delta P - \Delta \pi)}{R} = \frac{(1-R) J_w}{R} \quad (4.2)$$

4.2.5.1. Calculation of transport properties from manufacturer reported values

From product information sheets supplied by the manufacturer water permeance and solute permeability.^{36,44-47} The information sheets specify sodium chloride feed concentration, sodium chloride rejection, permeate flow rate, feed pressure, active membrane area, and recovery. From the reported information solute permeability can be calculated from Eq. (4.2). Water permeance was calculated using Eq. (4.3) from the governing equation for water flux in reverse osmosis solved for the water permeance.¹

$$A = \frac{J_w}{\Delta P - \Delta \pi} \quad (4.3)$$

In calculating the water permeance, the water fluxes (J_w) and pressure difference ($\Delta P - \Delta \pi$) across the membrane are needed. Water flux was calculated by dividing the permeate flowrate by membrane area. The hydrostatic pressure difference across the membrane was assumed to be the inlet feed pressure. The osmotic pressure difference was calculated using Eq. (4.4).

$$\Delta \pi = \frac{C_{f,i} \cdot R \cdot \exp(0.7Y_i)}{58.45 \cdot 1000} \cdot R_{\text{const}} \cdot T \quad (4.4)$$

The inclusion of rejection in Eq. (4.4) accounts for the imperfect selectivity of the membrane and the exponential term corrects for concentration polarization as defined by these membranes manufacturer.³⁶

4.2.6 Osmotic water flux testing

4.2.6.1. PRO membrane orientation

In a PRO process power density is linked to water flux (Eq. (4.1)) requiring a hydrostatic pressure across the membrane with the draw solution having the higher hydrostatic pressure. Membranes within a PRO process are commonly oriented so the membrane's selective (or active) layer is facing the draw solution. This orientation, described in literature as the PRO mode,^{16,55} prevents damage to the selective layer by orienting the pressure toward the selective layer which is properly supported by the porous support. In the PRO mode a perfectly selective semi-permeable membrane would experience no ICP if the feed solution was pure water. As membrane selectivity decreases the severity of ICP will increase. The membrane's selectivity partially mitigates the effect of ICP and this effect on water flux as mitigated by membrane selectivity is present within the governing equations for water flux in PRO. A governing equation for water flux was derived by Yip et al. and presented here as Eq. (4.5).¹⁶

$$J_w = A \left\{ \frac{C_{d,b} \exp\left(-\frac{J_w}{k}\right) i R_{\text{const}} T - C_{f,b} \exp\left(\frac{J_w \cdot S}{D_{f,b}}\right) i R_{\text{const}} T}{1 + \frac{J_w}{B} \left[\exp\left(\frac{J_w \cdot S}{D_{f,b}}\right) - \exp\left(-\frac{J_w}{k}\right) \right]} - \Delta P \right\} \quad (4.5)$$

Likewise the equation for the reverse solute flux as influenced by the effect of water flux on mass transfer limitations is represented by Eq.(4.6).¹⁶

$$J_s = B \left\{ \frac{C_{d,b} \exp\left(-\frac{J_w}{k}\right) - C_{f,b} \exp\left(\frac{J_w \cdot S}{D_{f,b}}\right)}{1 + \frac{B}{J_w} \left[\exp\left(\frac{J_w \cdot S}{D_{d,b}}\right) - \exp\left(-\frac{J_w}{k}\right) \right]} \right\} \quad (4.6)$$

From Eq. (4.5), the membrane's intrinsic properties, water permeance (A), solute permeability (B), and structural parameter (S), directly impact the observable water flux across a membrane under osmotic flow. Likewise in Eq. (4.6), the coupled nature of water flux, reverse solute fluxes, ICP, and ECP are illustrated. Specifically, as water flux decreases from increasing hydrostatic pressure the reverse solute flux should increase due to higher draw solute concentration at the membrane selective layer interface.

4.2.6.2. Zero transmembrane pressure water flux

Osmotic water flux was measured in our lab scale test systems using the PRO membrane orientation. The membranes were tested in each of variations described in Table 4.1. Each membrane variety was tested in triplicate using fresh samples for each test in PRO mode at $20\pm 1^\circ\text{C}$ with a feed and draw flow velocity of $0.25\text{ m}\cdot\text{s}^{-1}$ and no transmembrane pressure. The feed and draw solutions were under a minimal amount of hydrostatic pressure ($\sim 0.2\text{ bar}$) and for all tests the transmembrane pressure was zero. Osmotic flux performance was measured at 0.05 M, 0.1 M, 0.5 M, 1.0 M and 1.5 M NaCl. The effective structural parameters of these membranes were calculated from a numerical solution to Eq. (4.5) using the observed water fluxes at 1.5 M and membrane properties determined from the RO characterization.

4.2.6.3. Water flux comparison from the numerical decoupling of membrane properties

Comparison amongst membranes for FO can be challenging due to the coupling of test conditions, selective layer and support layer properties. While a publication by Cath et al. suggests standardized testing conditions increases the compatibility of comparison between differing membrane structures²⁹ a more rigorous approach is needed to decouple selective layer and support layer properties in relation to water flux. To correct for structural parameter

Table 4.2. Data matrix showing experimentally and simulated water flux for combinations of membrane selective layer properties and effective structural parameters.

Selective Layer Properties (A & B)	Effective Structural Parameter (S)				
	NF270	NF90	BW30	SW30-	SW30-HR
	NF270	Exp & Sim	Sim	Sim	Sim
	NF90	Sim	Exp & Sim	Sim	Sim
	BW30	Sim	Sim	Exp & Sim	Sim
	SW30-XLE	Sim	Sim	Sim	Exp & Sim
	SW30-HR	Sim	Sim	Sim	Exp & Sim

Exp denotes values observed experimentally

Sim denotes water flux calculated from selective layer properties and structural parameter

differences water fluxes for the studied membranes were calculated using Eq. (4.5). In these calculations, Eq. (4.5) was solved using the water permeance (A) and solute permeability (B) for a specified membrane (i.e. NF270) and effective structural parameters (S) for each membrane studied (i.e. NF270, NF90, BW30, SW30-XLE and SW30-HR).). This simulates what would happen if, for example, a BW30 selective layer were placed on a SW30-HR support. This is important because the support layers of the five membranes are similar, but not identical. This normalization approach is depicted in Table 4.2. Simulation was performed assuming draw solution concentrations from 0 M to 2 M NaCl at 20°C and 1 L·min⁻¹. This

mathematical analysis allows for the comparison of the relative importance of both selective layer and support layer properties for membrane PRO and experimental data provides a comparative benchmark across the span of selective layer and support layer properties.

4.2.6.2. PRO testing procedure

Membranes modified with PDA were tested in triplicate on a bench scale pressure retarded osmosis test system. PRO system layout is shown in Fig. 4.1. has been described

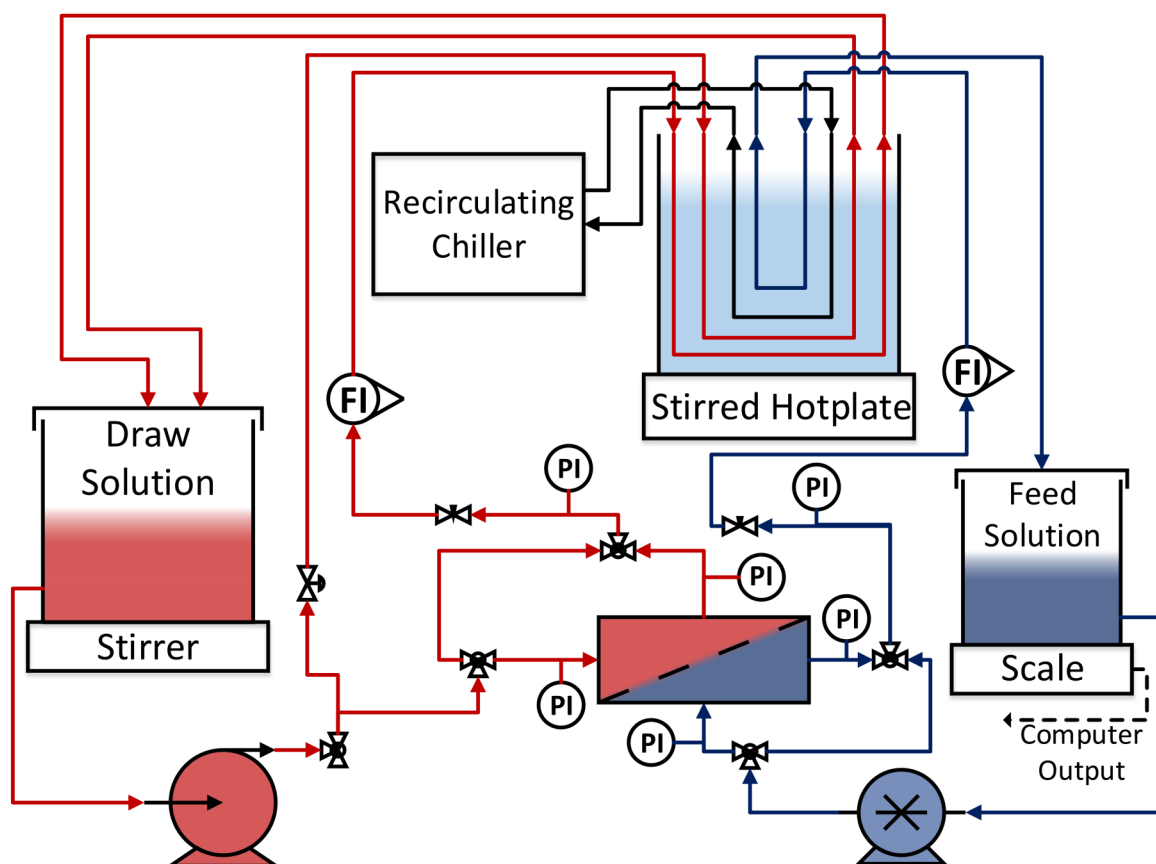


Fig. 4.1. Schematic of the pressure retarded osmosis test system used in this study.

elsewhere.^{14,17} Tests were run at an operating temperature of 20°C using a 0.5 M NaCl draw solution. The draw solution was circulated co-currently against a deionized water feed with a cross-flow velocity of 0.25 m·s⁻¹ for both the draw and feed solutions. The PDA membranes were supported by a piece of Cooltexx PET non-woven⁵⁶ atop a feed channel packed with tricot RO permeate spacer. Water flux was measure gravimetrically, and reverse solute flux was monitored by measuring feed solution conductivity. The inlet and outlet pressure of both the feed and draw solution were monitored with pressure gauges for both the inlet and outlet of the PRO cell. Under experimental conditions the tricot feed spacer generated a large feed pressure drop with an inlet pressure of approximately 1.9 bar (27 psi) and an outlet pressure of 0.2 bar (3 psi). An average feed pressure of 1 bar was assumed, being the rounded linear average of the inlet and outlet pressures, for the calculation of power density and modelling of water flux. As no noticeable pressure drop was observed for the draw solution, the transmembrane pressure was treated as the pressure of the draw solution minus the 1 bar average pressure of the feed within the feed channel.

PRO tests were begun with a draw solution hydrostatic pressure of 2.8 bar (40 psi) and increased in 2.8 bar (40 psi) increments until the observed water flux was approximately zero.

Water fluxes observed as the draw solution hydrostatic pressure increases are referred to the ascending pressure ramp. After data was collected at near zero water flux, pressures were decreased in 2.8 bar (40 psi) increments to 2.8 bar (40 psi), Water flux observed as the draw solution hydrostatic pressure decreases are referred to as the descending pressure ramp. Operating the membrane through both ascending and descending pressures allows for the examination of irreversible membrane damage as a result of high pressures employed within the PRO system.

Similar to PRO mode FO tests with zero transmembrane pressure, the effective structural parameters for these membranes was calculated from a numerical solution of Eq. (4.5) for the effective structural parameter. This calculation was performed assuming constant water permeance and solute permeability for water fluxes observed during the PRO test and plotted as effective structural parameters versus applied transmembrane pressures. Due to the applied hydrostatic pressures employed it is possible that selective layer damage can occur from testing. To test the assumption of constant solute permeability an expected reverse solute flux was calculated for changing structural parameters with increasing transmembrane pressure, external mass transfer coefficient, and solute permeability using Eq. (4.6). A

comparison of these values to those measured experimentally tests the assumption of constant solute permeability. Deviation from expected behavior would suggest that some alteration to the selective layer's properties and incorrect effective structural parameters.

4.3. Results and discussion

4.3.1. Modified membrane contact angles

Contact angle measurements of the membranes' support layers are shown in Fig. 4.2. All membranes exhibit a twenty to thirty degree reduction in the contact angle following a one hour

modification of these membranes with

PDA. These data show that a PDA

modification will render the surfaces of

the membrane support layer more

hydrophilic. Similar improvements in

surface hydrophilicity of PSu membranes

following PDA modification have been

observed elsewhere.^{26,48}

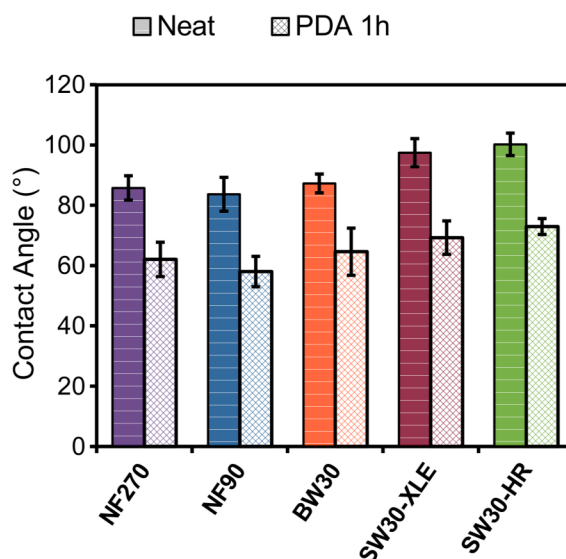


Fig. 4.2. Support layer contact angles for PET removed (horizontal lined bars) and PDA modified (cross-hatched bars) membranes using a KSV Cam 101 contact angle goniometer with the sessile drop method and water droplet size of 7 μ L.

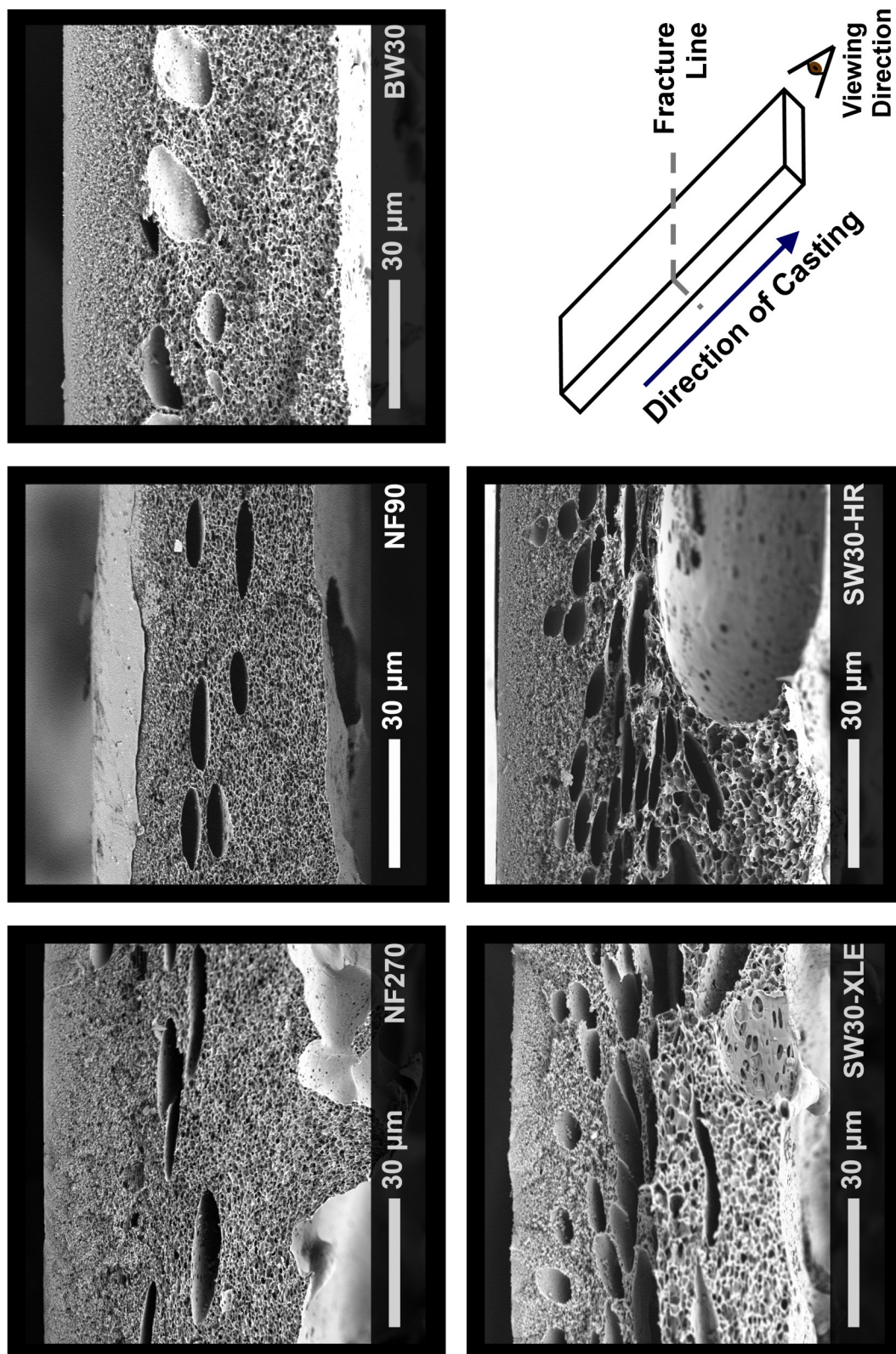


Fig. 4.3. Cross section SEMs for membranes following PET removal. The membranes were fractured perpendicular to casting direction.

4.3.2. SEM images of cross-sectioned membranes

The SEM images showing the cross-sectioned membranes are showing in Fig. 4.3, and they illustrate the differing support layer structures of these membranes. The structures of these membranes can be separated into one of two narrow categories. The seawater RO membranes appear to have a greater quantity of macrovoids along the middle of the membrane support. The brackish water and nanofiltration membranes have fewer macrovoids and in general have a spongier pore structure. These structural differences could play a significant role in how the membrane will perform when tested in PRO as the membrane is compacted from the transmembrane hydrostatic pressure.

4.3.3. Membrane water permeance and solute permeability

Waterpermeance for the neat and PDA membranes can be seen in Fig. 4.4a. In addition to the water permeance measured in lab tests, values calculated from manufacturer's specifications are also presented. The experimentally measured water permeance of the neat membranes was found to be equal to or slightly lower than the values calculated from data supplied by the manufacturers. A slight to significant drop in the water permeance was observed for the NF270, NF90, and BW30 membranes. The water permeance of the BW30

was attributed to the blockage of small pores within membrane support layer impairing water flux from a loss of porosity following the PDA modification.^{11,26} As these membranes (the NF270, NF90 and BW30) have qualitatively similar structures (Fig. 4.3) the same effect may be occurring for the NF270 and NF90. As noted in our previous work, the SW30-XLE and SW30-HR membrane experienced an increase water permeance after modification.²⁶

Solute permeability for neat and PDA membranes are presented in Fig. 4.4b. The draw solute used throughout this study was sodium chloride (NaCl). Differences in the solute permeability between lab tests and Dow specifications show striking disparities. In most instances the calculated solute permeabilities are much lower than those measured in lab

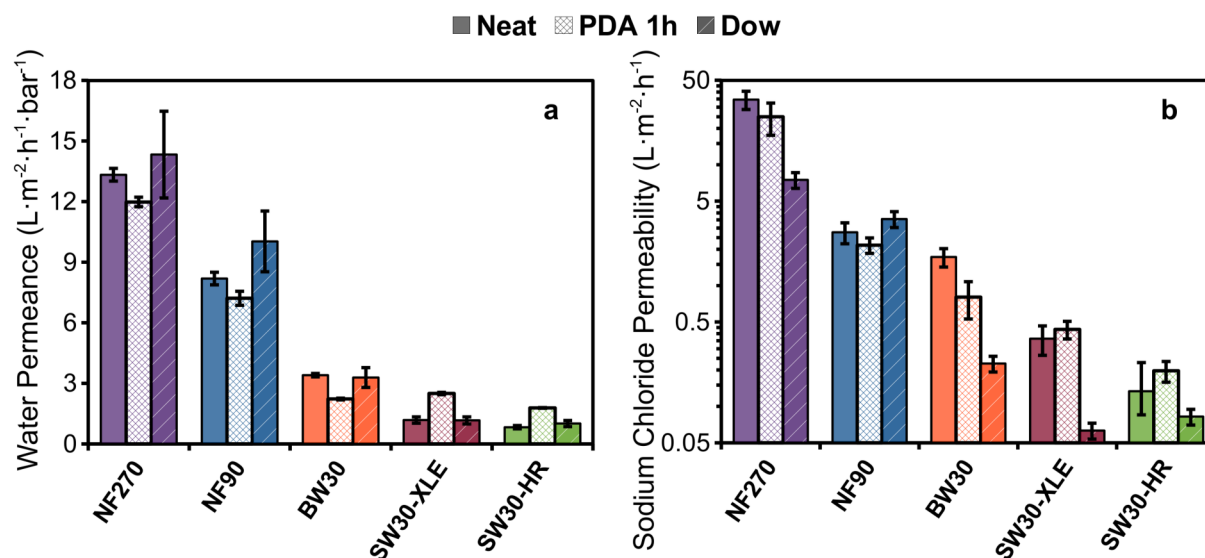


Fig. 4.4. Pure water permeance (a) and solute permeability (b) for neat (solid bars and lined bars) and PDA modified (cross-hatched bars) membranes (lined bar denotes water permeance calculate from manufacture specification sheets).

tests. This is likely the result of pH differences between the two tests.^{35,57} Dow provides specifications for pH 8 where lab tests were conducted at ambient pHs (~6.5-7). Solution pH affects the surface charge of a TFC membrane; at alkaline pHs carboxylic acid functional groups within the polyamide selective layer will deprotonated give the membrane a negative surface charge. A negative surface charge will electrostatically repel anions and prevent salts (since electroneutrality must be preserved) from passing through the selective layer, enhancing the rejection of a TFC membrane at basic pHs.^{57,58} PDA modification of the membranes yielded a small change in their solute permeability compared to their unmodified counterparts; the changes were statistically insignificant except for the BW30. As shown in Fig. 4.4b, the lack of a sharp increase in the solute permeability of these membranes' illustrates that the PDA modification did not damage the membranes' selective layer.

4.3.4. PRO mode performance under no hydrostatic pressure

4.3.4.1. Water flux

Water fluxes for PRO mode osmotic flux tests with no transmembrane pressure are shown in Fig. 4.5. Here similar trends in the performance of neat, no PET and PDA membranes can be observed. In all instances (neat, no PET, and PDA varieties) the most selective membrane

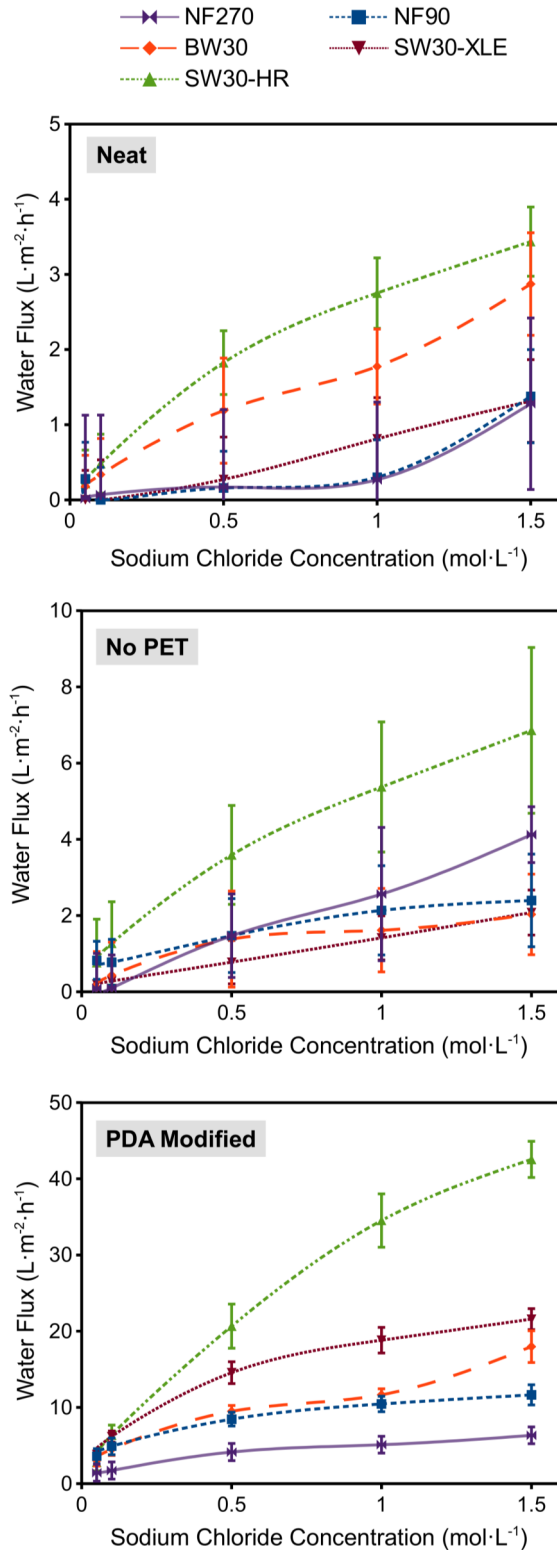


Fig. 4.5. Zero transmembrane pressure PRO water flux for membranes at 20°C and 0.25 m·s⁻¹ draw and feed solution cross flow velocities.

studied, the SW30-HR, had the highest water flux. All neat membranes exhibited low fluxes (less than 4 L·m⁻²·hr⁻¹), which contributed to the large errors shown in Fig. 4.5. Observed water flux increase slightly upon removal of the PET but generally remained low. The large error bars impair the statistical significance of these data but for both the neat and no PET membrane varieties the SW30-HR has the highest observable water flux.

The PDA membranes, with the exception of the NF270, showed at minimum, a doubling of the water flux when compared to those with just the PET removed. Here the SW30-HR had the

highest water fluxes of all the modified membranes producing a peak water flux of approximately $45 \text{ L}\cdot\text{m}^{-2}\cdot\text{hr}^{-1}$ at 1.5 M NaCl . This value is still noticeably less than peak water fluxes produced by membranes whose structures have been designed for optimum performance in osmotic processes under similar testing conditions (temperatures of $23\text{-}25^{\circ}\text{C}$, cross-flow velocities of $15\text{-}21 \text{ m}\cdot\text{s}^{-1}$).^{16,17,39}

4.3.4.2. Effective structural parameters

Effective structural parameters for the neat, no PET, and PDA membranes are shown in Fig. 4.6. These data were calculated from the osmotic water flux data (Fig. 4.5), water permeance (Fig. 4.4a) and solute permeability (Fig. 4.4b); a numerical solution to Eq. (4.5) calculates the effective structural parameter (S_{eff}). All of the unmodified membranes have effective structural parameters greater than $9000 \mu\text{m}$. These high structural parameters are a combination of the added thickness of the PET fabric layer and poor wetting of the PSu layer. PET removal did significantly decrease the effective structural parameters of the NF270 and NF90, the least selective membranes. A slight decrease the effective structural parameter of the SW30-HR was also observed; however, removal of the PET did not significantly change the effective structural parameter of the BW30 and SW30-XLE. Following PDA modifications

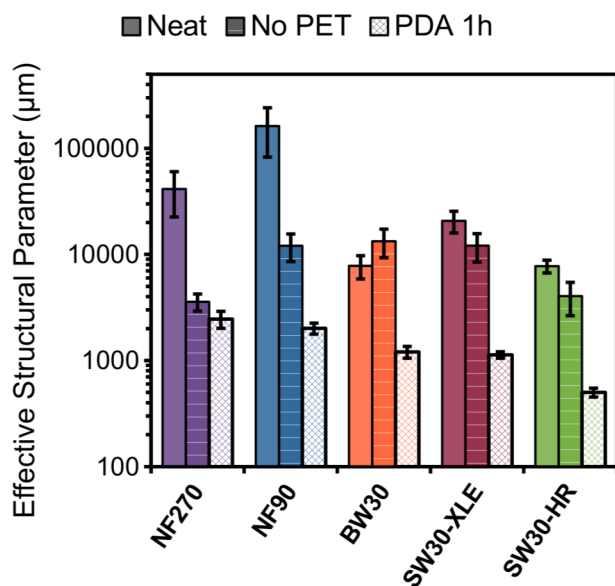


Fig. 4.6. Structural parameters for neat (solid bars), no PET (lined bars) and PDA modified (cross-hatched bars) for zero transmembrane pressure PRO at 20°C.

only the NF270 had a significant observable decrease in its effective structural parameters. The lowest effective structural parameter was approximately 500 μm for the PDA modified SW30-HR. The effective structural parameter of the SW30-HR is comparable to reported values for

the CTA FO membrane made by HTITM under identical test conditions.^{29,32}

4.3.4.3. Reverse solute flux

Reverse solute fluxes for the neat, no PET, and PDA membranes are shown in Fig. 4.7. In all instances the NF270 had noticeably higher reverse salt fluxes than other membranes. This high reverse solute flux is the cause of low water flux as increased solute leakage decreases transmembrane osmotic pressures across the selective layer. Increasing solute fluxes would occur from the decreased structural parameters, as the increased transmembrane osmotic pressure results from an increased effective concentration gradient across a membrane's

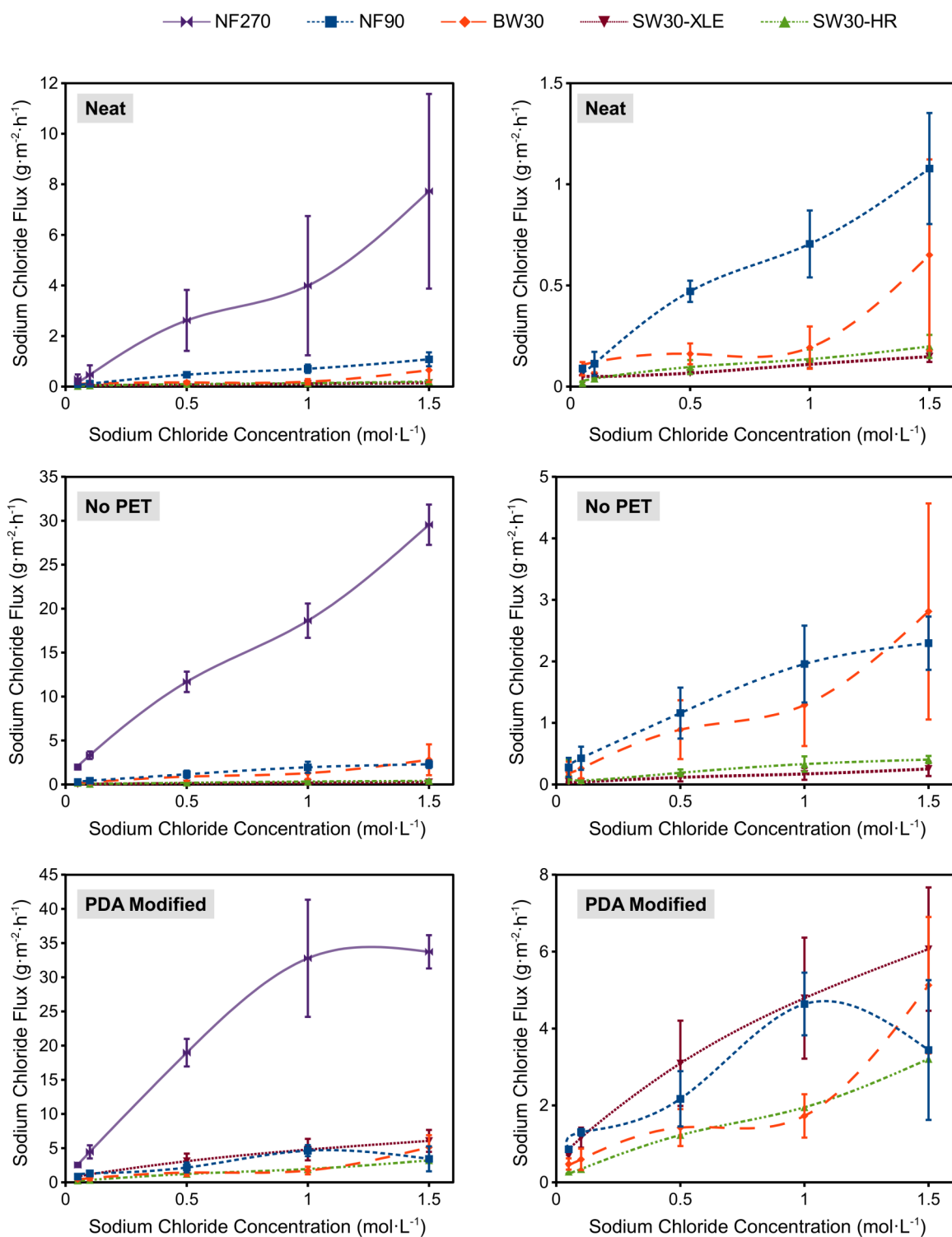


Fig. 4.7. Zero transmembrane pressure PRO salt flux for membranes at 20°C and 0.25 m·s⁻¹ draw and feed solution cross flow velocities.

selective layer.^{16,26} The SW30-HR, in all variants, had reverse solute fluxes less than $2 \text{ g}\cdot\text{m}^{-2}\cdot\text{hr}^{-1}$ while still producing high water fluxes. In general all of the aromatic polyamides had reverse solute fluxes lower than the HTITM's CA membrane.²⁹

4.3.4.2. De-coupling of TFC support layer and selective layer influence on water flux

The differing effective structural parameters for these membranes as illustrated in Fig. 4.6 means that a direct comparison of the water fluxes for the whole membrane structure do not allow for discrete isolation of competing solute transport behaviors, specifically competition between selectivity and ICP. Numerical simulation of water flux (Eq. (4.5)) from selective layer properties (Fig. 4.4) and effective structural parameter (Fig. 4.6) makes an evaluation of the competing transport limitation for PRO feasible. The data generated from this simulation is shown in Fig. 4.8. Experimental data for membranes with the same effective structural parameters are also shown to observe agreement between experimental and simulated data. For all of the structural parameters characterized, the piperazine based NF270 underperformed all of the aromatic polyamides. Membranes with aromatic polyamide selective layers are grouped more closely together. At with higher draw solute concentrations the

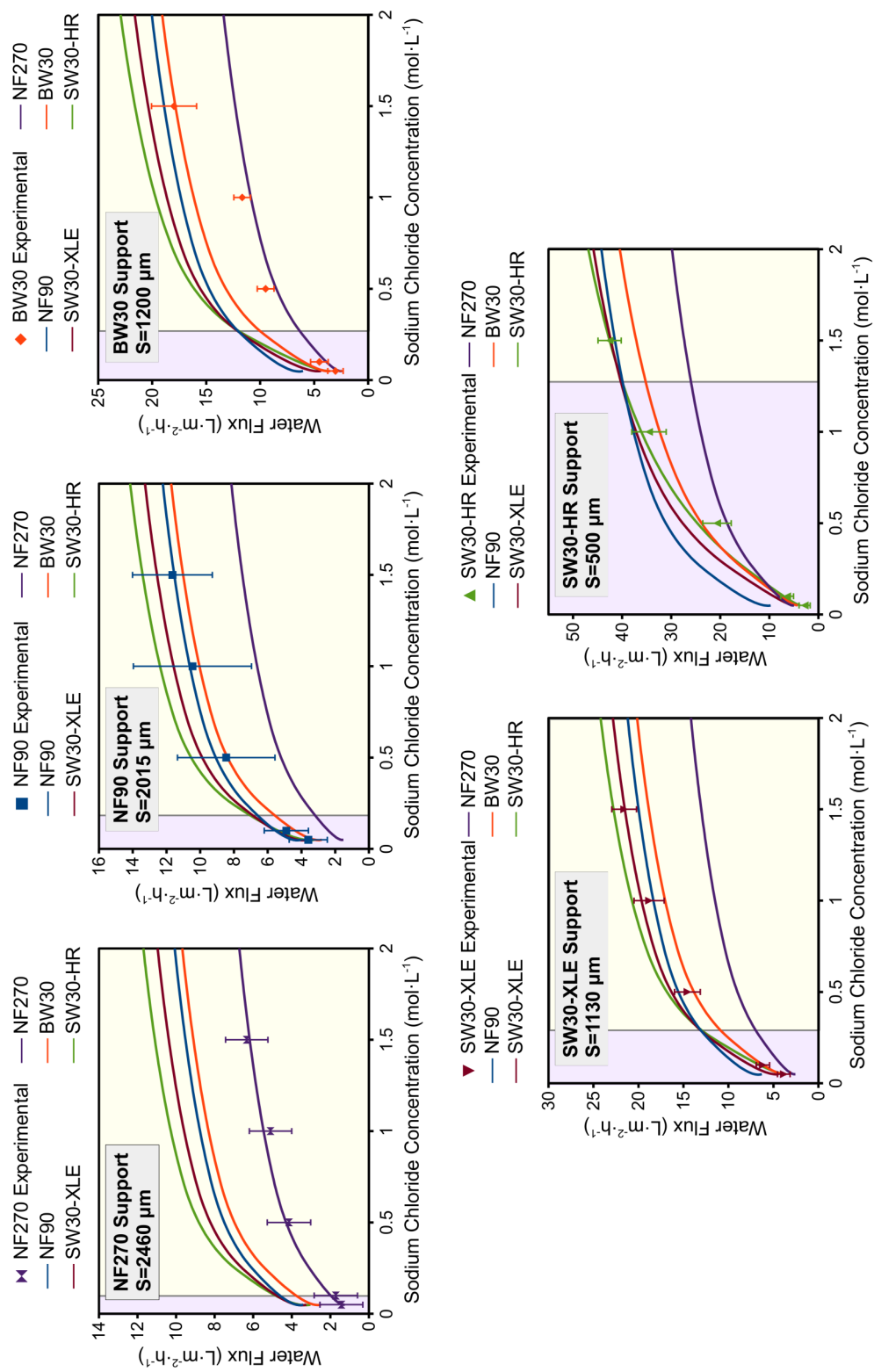


Fig. 4.8. Simulated water flux data for membranes with fixed structural parameters at 20°C and 0.25 m·s⁻¹ draw solution cross flow velocities. Water permeance and solute permeability used for this calculator are presented in Fig. 4.3 .

seawater RO membranes (i.e. the SW30-XLE and SW30-HR) showed a higher water flux from their lower solute permeability.

The fully aromatic polyamides are closely grouped, and the water flux profiles at all of the effective structural parameters studied can be split into two regions. At lower draw solute concentrations, the less selective NF90 showed the highest water flux, and this can be described as a permeance dominated region of the water flux profile. This region (shaded purple in Fig. 4.8) represents the higher water permeance overcoming the effect of solute transport through the selective layer in reducing the osmotic pressure difference across the membrane. Opposite the permeance dominant region, these water flux profiles have a selectivity dominated region. The selectivity dominant region describes where water flux for the higher permeance less selective membranes are depressed by reverse solute transport through the selective layer and ICP causes a large reduction of the osmotic pressure difference across the membrane's selective layer. This region is represented by the lower permeance membrane's having highest water flux (shaded yellow in Fig. 4.8)

One relationship visible in Fig. 4.8 is the draw solute concentration where water flux shifts from permeance dominant to selectivity dominant. For water fluxes evaluated from structural

parameters higher than 1000 μm the permeance dominate region only exists at draw solution concentrations below 0.5 M. As the effective structural parameter decreases the region of permeance dominated water flux grows. These findings allow for the reconciliation of data as present here with findings by Yip et al.⁵⁹ In this study water flux was predicted for PRO after experimentally measuring water flux at zero transmembrane hydrostatic pressure using 3 polyamides of different permselectivities synthesized onto identical support layers. It was reported that the membrane having an intermediate permselectivity and gave the highest power density in PRO;⁵⁹ however, the permeance to selectivity trade-off suggests some variability in what permselectivity is optimal for a given draw solution composition. Additionally, as the draw solution is diluted, the optimal membrane permselectivity may change creating continuum of optimal permselectivity which changes as draw solution concentration decreases.

4.3.5. PRO performance under hydrostatic pressure

4.3.5.1. Water flux

PRO water flux data using a 0.5 M NaCl draw solution (osmotic pressure ~ 22.4 bar) is shown in Fig. 4.9. It should be noted that the NF270 is absent because even at the lowest transmembrane pressures tested the membrane exhibited reverse osmosis behavior (water

flux into the feed solution). Of all the membranes examined in this study, only for the NF90 were water fluxes measured near values predicted from simulation only at the initial hydrostatic pressure of 1.7 bar. The other membranes exhibited 80% or less than the predicted water flux (Eq. (4.5)). The SW30-HR had the highest water flux for both the ascending and descending

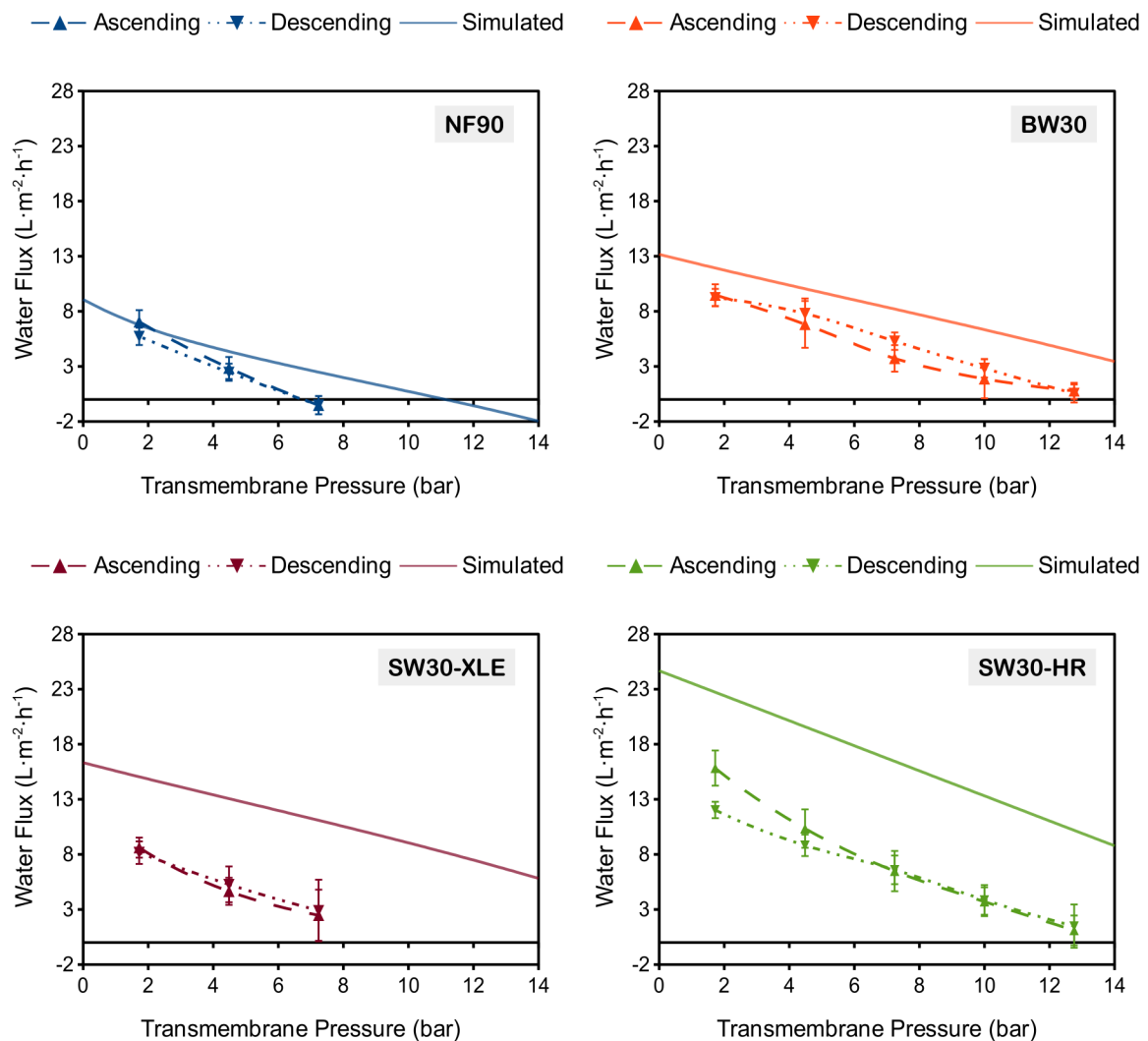


Fig. 4.9. Water flux for PRO tests using PDA modified TFC membranes at 20°C, cross-flow velocities of $0.25 \text{ m} \cdot \text{s}^{-1}$, and draw solution concentration of 0.5 M NaCl.

pressure ramp; however, at 1.7 bar on the descending pressure ramp a 76% reduction in water flux was observed for SW30-HR when compared to the observed water flux at 1.7 bar on the ascending pressure ramp. For the other membranes studied similar water fluxes were observed along the ascending and descending pressure ramps, implying that no measureable damage is occurring to these membranes' selective layers and the membranes' support layers have been reversibly compacted.

For all of the membranes in this study, statistically zero (error range overlaps zero) water flux was observed at a draw solution hydrostatic pressure lower than simulation predicts. Table 4.3 shows this pressure as determined from both experimentally observed and simulated water fluxes for PRO. All of the studied membranes were observed at zero water flux at hydrostatic

Membrane	Theoretical Zero Flux Pressure (bar)	Experimental Zero Flux Pressure (bar)	Percent of Utilized Pressure
NF90	11.1	6.7	60.4%
BW30	18.2	13.2	72.5%
SW30-XLE	20.0	9.7	48.5%
SW30-HR	21.9	13.6	62.1%

Table 4.3. Theoretical and experimental flux inversion points of the four membranes characterized in this study. Percent of utilized pressure refers specifically to ratio experimental/theoretical pressures.

pressures 48.5% to 72.5% lower than expected from the membranes' transport properties (Table 4.3). This suggests that although membrane performance is mostly recovered by decreasing the draw solution pressure other competing phenomena are inhibiting water flux causing poor performance.

4.3.5.2. Power densities

Ideal and experimental power densities for membranes tested in PRO can be seen in Fig. 4.10. The power densities presented here were calculated using Eq. (4.1). Simulated power densities were calculated from the numerical solutions for water flux (Fig. 4.9). Here all experimentally measured power densities were lower than values predicted from simulation. Coinciding with water fluxes only the NF90 was observed operating at an expected power density at 1.7 bar of transmembrane pressure. At higher transmembrane pressures expected power density dropped sharply corresponding to a decline in observed water flux. Other membranes tested experimentally demonstrated the capacity to achieve 20% to 50% of the simulated power density. This difference between predicted and experimentally measured power densities was observed in previous study by She et al. who studied PRO performance using HTITM's CTA membrane platform and concluded that lower water fluxes were the result

of enhance solute permeation through the selective layer from the applied hydrostatic pressures.¹⁸ This enhanced reverse solute flux increases the deleterious effects of ICP and decreases water flux.

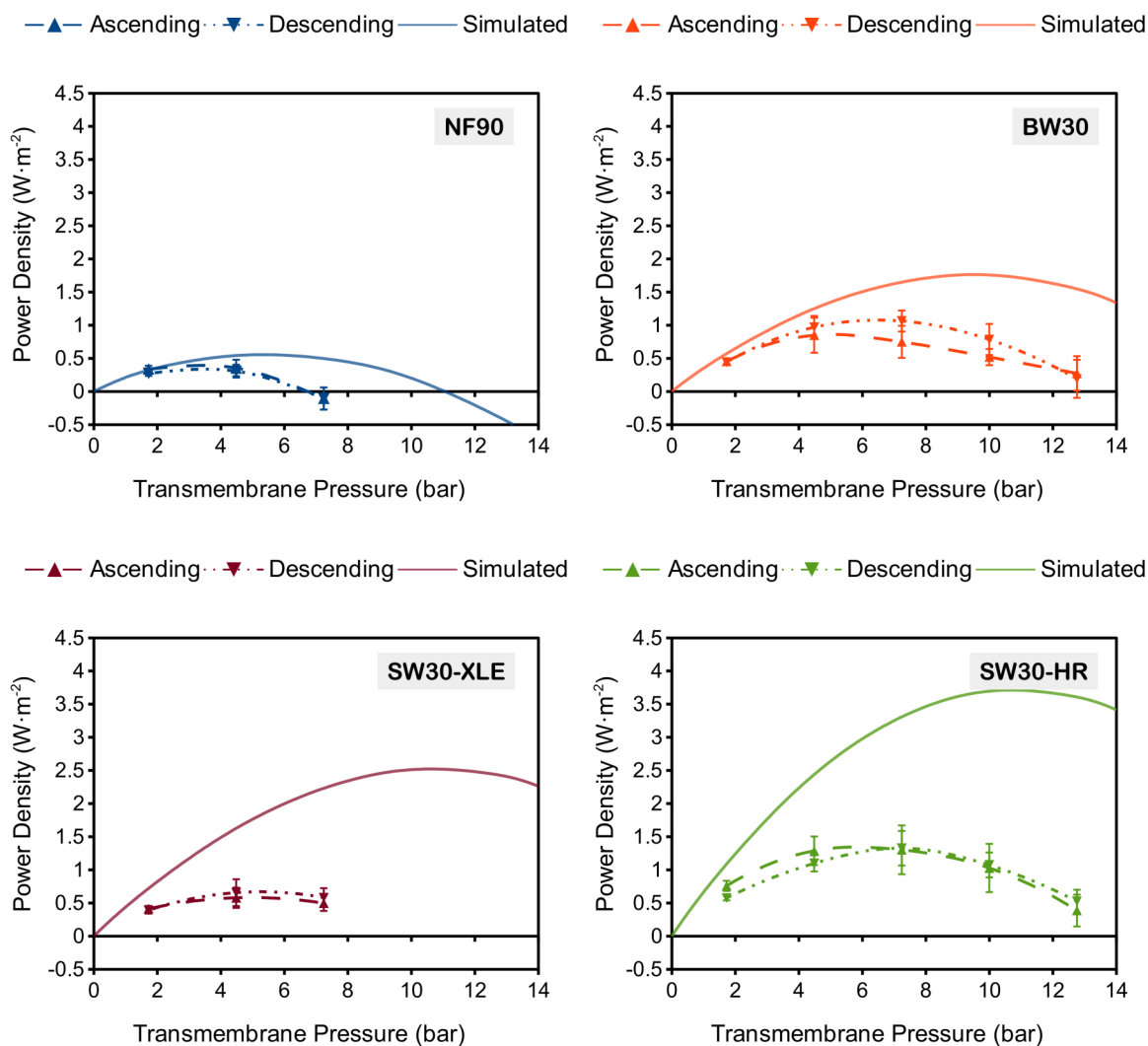


Fig. 4.10. Power Densities for PRO tests using PDA modified TFC membranes at 20°C, cross-flow velocities of 0.25 m·s⁻¹, and draw solution concentration of 0.5 M NaCl.

4.3.5.2. Effective structural parameters

Effective structural parameters across the studied transmembrane pressures can be seen in Fig. 4.11. The effective structural parameter for all membranes increased with increasing

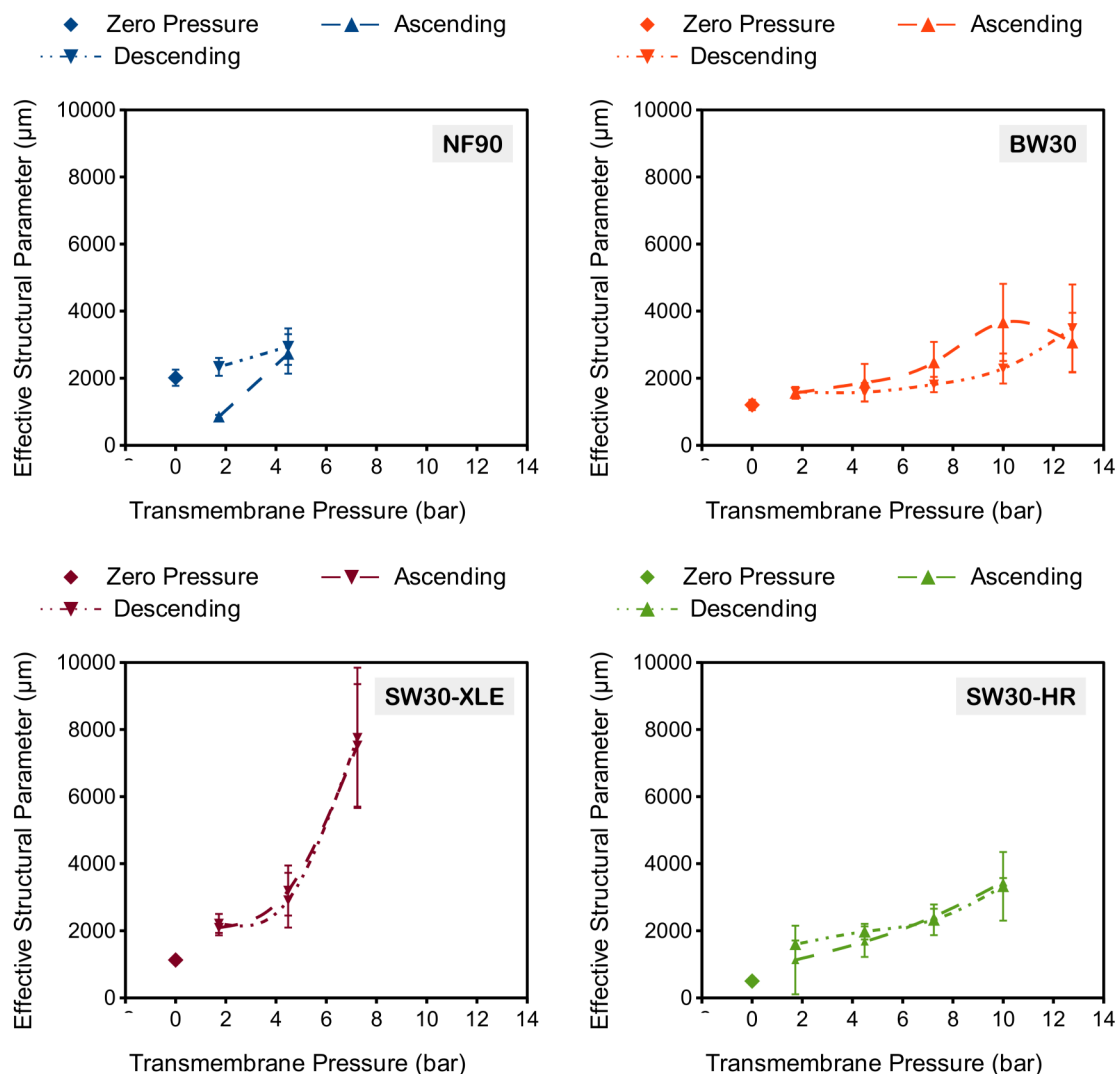


Fig. 4.11. Effective structural parameters calculated PRO tests using PDA modified TFC membranes at 20°C, cross-flow velocities of $0.25 \text{ m}\cdot\text{s}^{-1}$, and draw solution concentration of $0.5 \text{ mol}\cdot\text{L}^{-1}$ NaCl. The isolated data point not connected by dashed lines represents the value observed at zero transmembrane pressure (this data is also shown in Fig. 4.6).

transmembrane pressure. Compaction will decrease the thickness of the support layer from the collapse of pores within the membrane support layer. While the classical relationship, the Bruggemann relation,⁶⁰ between porosity and tortuosity is an empirical one it does provide some qualitative information in support of the quantitative data (Fig. 4.11) on the response of materials to compaction .

$$\tau = \gamma \epsilon^{1-\alpha} \quad (4.7)$$

The Bruggemann relation, shown in Eq. (4.7), contains two constants (γ and α) which relate to the morphology of a structure. While this study does not attempt to define the values of these constants, the values for both γ and α are typically greater than 1.⁶⁰ If the value for α in the Bruggemann relation for this membrane was assumed to be greater than 1, a drop in the porosity of the support layer, regardless of magnitude, will increase the tortuosity (since ϵ is always less than 1).

The steadily increasing effective structural parameters for all these membranes implies that the loss of porosity and corresponding increase in the tortuosity proves more detrimental than the reduction in thickness from compaction is beneficial. A reduction of the applied pressure mostly returns water flux to initially measured values. The recovery of water flux suggests that

compaction of the membrane support layer is reversible, under the range of applied transmembrane pressures studied. These significant changes in effective structural parameter with increasing hydrostatic pressures illustrates the need to build membrane structures robust enough to withstand compaction and characterized under process conditions appropriate for the desired final application.

4.3.5.3. Sodium chloride reverse solute flux

Reverse solute fluxes for membranes tested with non-zero transmembrane pressures can be seen in Fig. 4.12. The experimentally observed increase in reverse solute flux with applied transmembrane pressure may have contributed to the lower than expected observed water fluxes and power density. The increased reverse solute flux would substantially decrease the transmembrane osmotic pressure. A decrease in the transmembrane osmosis pressure will lower the applied transmembrane hydrostatic pressure where water flux across the membrane will be zero. Findings of this nature were reported in a study by She et al. who exclusively worked with the commercial cellulose acetate membrane platform made by HTITM.²⁵ More recent observations by Touati et al. also noted increases in reverse solute flux with increase transmembrane hydrostatic pressure.³¹

To understand the source of the increased reverse solute permeation a predicted reverse solute flux was generated using effective structural parameter data in Fig. 4.11 and Eq. (4.6).

This calculation accounts for variable effective structural parameters with pressure and like the

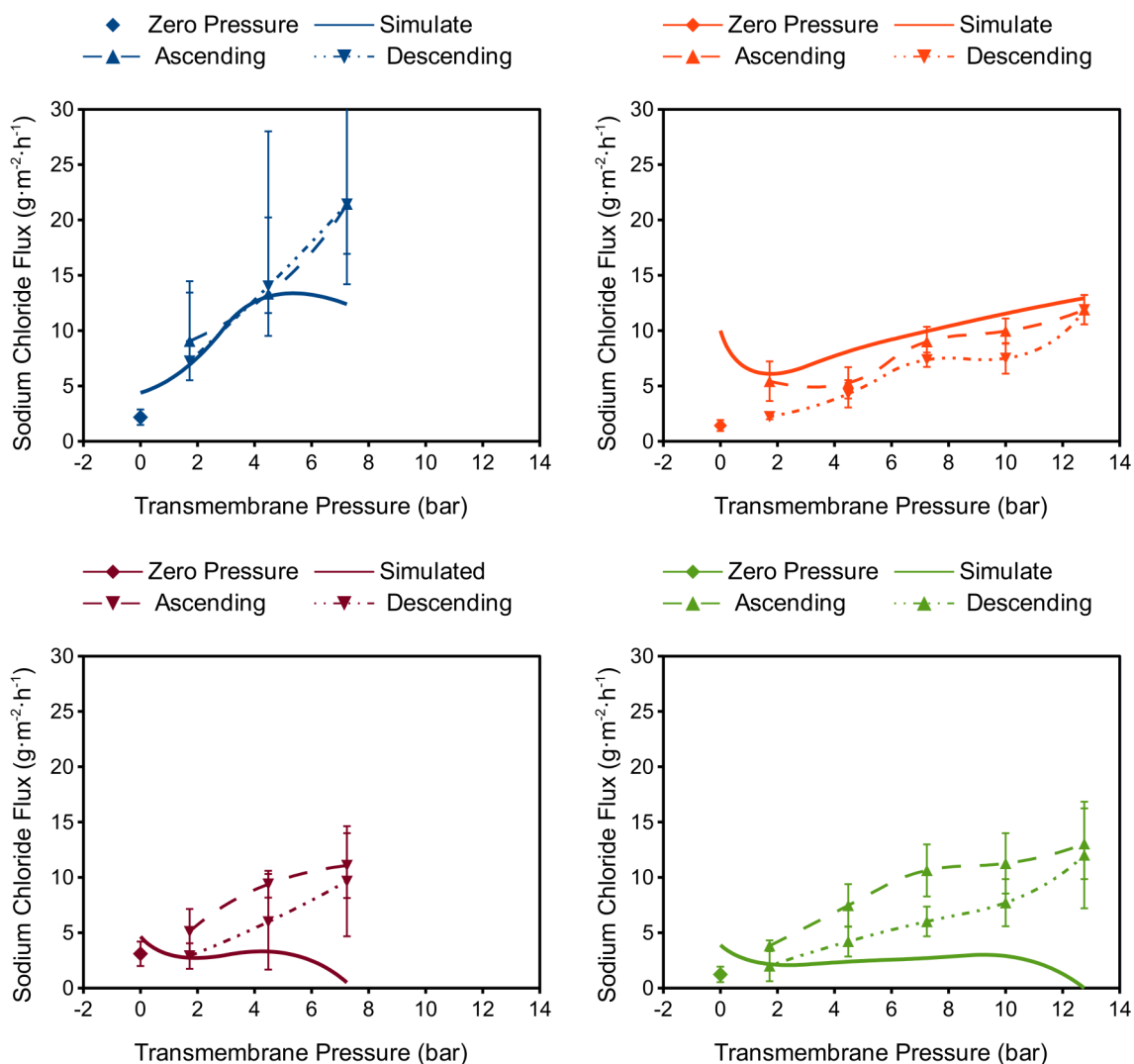


Fig. 4.12. Reverse solute flux for PRO tests using PDA modified TFC membranes at 20°C, cross-flow velocities of $0.25 \text{m} \cdot \text{s}^{-1}$, and draw solution concentration of $0.5 \text{mol} \cdot \text{L}^{-1}$ NaCl. The deviation from predicted behavior suggests selective layer damage from sample compression.

effective structural parameters presented, assumes constant solute permeability with constant external boundary layer thickness. These data indicate that the increased reverse solute permeation for the NF90 and BW30 membranes is a result of decreasing ECP from declining water flux. The similar trend demonstrated between the predicted and experimentally measured reverse solute fluxes would suggest that significant damage to the selective layers of the NF90 and BW30 has not occurred. Damage to the selective layer would alter membrane permselectivity, and likely present significantly higher reverse solute fluxes than those predicted from numerical simulation. Permanent selective layer damage would also result in deviations between ascending and descending pressure ramps for both water and reverse solute flux. This assumes that the membrane is adequately supported from the lowest starting pressure and no damage occurs on startup (i.e. at pressures below 1.7 bar).

Effects attributable to selective layer damage can be clearly seen for the SW30-XLE and SW30-HR membranes. This is shown in the deviation between predicted and observed solute fluxes (Fig. 4.12). The simulated solute flux predicts that a sharp increase in effective structural parameters (Fig. 4.11) would decrease the reverse solute flux from compaction of the membrane's support layer. The sharp disparity between simulated and experimentally

observed values suggests that the assumptions of constant solute permeability, constant water permeance, or both are not appropriate.

The split between adherence to and deviance from the predicted and experimental reverse solute flux can be traced to the different support layer structures (Fig 2). The division between structure and PRO performance has been discussed elsewhere but it has been suggested that low tortuosity support layers (i.e. the macrovoids present within the support layer of the SW30-XLE and SW30-HR) should offer better performance in FO are unsuitable for applied hydrostatic pressures due to easier deformation of these structures (i.e. collapse of the macrovoids).^{61,62} These studies instead offer membranes built upon a spongy pore structure (i.e. the NF90 and BW30) as optimal structures for PRO due to their resistance to compaction

4.4. Conclusions

PDA modified commercial TFC membranes showed improved water flux over unmodified variants. A numerical comparison of water flux for varying support and selective layer characteristics has shown that in the PRO mode water permeance becomes less significant compared to solute permeability as draw solute concentration increases. Testing of these membranes in bench scale PRO process conditions showed the experimental performance of

these membranes was found to be significantly lower than those predicted through numerical simulation. The lower than expected performance was attributed to reverse solute flux and support layer compaction.

List of symbols

A	water permeance of the membrane
B	solute permeability
$C_{d,b}$	bulk draw solute concentration
$C_{f,b}$	feed bulk concentration
$C_{f,i}$	inlet feed concentration
$D_{f,b}$	bulk diffusivity of the draw solute in the feed solution
i	dissociation constant (2 for sodium chloride)
J_s	reverse solute flux
J_w	water flux
k	external mass transfer coefficient
R_{const}	ideal gas constant
R	rejection

S	effective structural parameter
T	absolute temperature
W	power density of the membrane
ΔP	hydrostatic pressure difference between the draw and feed solutions
$\Delta \pi$	osmotic pressure difference between the draw and feed solutions
α	Bruggeman exponent
γ	Bruggeman scaling parameter
Y_i	element recovery

References

1. Cath, T. Y.; Childress, A. E.; Elimelech, M. Forward osmosis: Principles, applications, and recent developments. *J. Membr. Sci.* **2006**, *281*, 70-87.
2. Hoover, L. A.; Phillip, W. A.; Tiraferri, A. ; Yip, N. Y.; Elimelech, M. Forward with Osmosis: Emerging Applications for Greater Sustainability. *Environ. Sci. Technol.* **2011**, *45*, 9824–9830.
3. Chung, T.-S. ; Zhang, S. ; Wang, K. Y.; Su, J. ; Ling, M. M. Forward osmosis processes: Yesterday, today, and tomorrow. *Desalination* **2012**, *287*, 78-81.
4. McGinnis, R. L.; Elimelech, M. Global challenges in energy and water supply: the promise of engineered osmosis. *Environ. Sci. Technol.* **2008**, *42*, 8625-8629.
5. Lutchmiah, K. ; Verliefde, A. R. D.; Roest, K. ; Rietveld, L. C.; Cornelissen, E. R. Forward osmosis for application in wastewater treatment: A review. *Water Res.* **2014**, *58*, 179-197.

6. Phuntsho, S. ; Shon, H. K.; Majeed, T. ; Saliby, I. E.; Vigneswaran, S. ; Kandasamy, J. ; Hong, S. ; Lee, S. Blended Fertilizers as Draw Solutions for Fertilizer-Drawn Forward Osmosis Desalination. *Environ. Sci. Technol.* **2012**, *46*, 4567-4575.
7. Garcia-Castello, E. M.; McCutcheon, J. R.; Elimelech, M. Performance evaluation of sucrose concentration using forward osmosis. *J. Membr. Sci.* **2009**, *338*, 61-66.
8. Garcia-Castello, E. M.; McCutcheon, J. R. Dewatering press liquor derived from orange production by forward osmosis. *J. Membr. Sci.* **2011**, *372*, 97-101.
9. McCutcheon, J. R.; McGinnis, R. L.; Elimelech, M. A novel ammonia-carbon dioxide forward (direct) osmosis desalination process. *Desalination* **2005**, *174*, 1-11.
10. McCutcheon, J. R.; McGinnis, R. L.; Elimelech, M. Desalination by ammonia-carbon dioxide forward osmosis: Influence of draw and feed solution concentrations on process performance. *J. Membr. Sci.* **2006**, *278*, 114-123.
11. Arena, J. T.; Manickam, S. S.; Reimund, K. K.; Freeman, B. D.; McCutcheon, J. R. Solute and water transport in forward osmosis using polydopamine modified thin film composite membranes. *Desalination* **2014**, *343*, 8-16.
12. Lee, K. L.; Baker, R. W.; Lonsdale, H. K. Membranes for power generation by pressure-retarded osmosis. *J. Membr. Sci.* **1981**, *8*, 141-171.
13. Achilli, A. ; Cath, T. Y.; Childress, A. E. Power generation with pressure retarded osmosis: An experimental and theoretical investigation. *J. Membr. Sci.* **2009**, *343*, 42-52.
14. Anastasio, D. D.; Arena, J. T.; Cole, E. A.; McCutcheon, J. R. Impact of temperature on power density in closed-loop pressure retarded osmosis for grid storage. *J. Membr. Sci.* **2015**, *479*, 240-245.
15. Yip, N. Y.; Elimelech, M. Thermodynamic and Energy Efficiency Analysis of Power Generation from Natural Salinity Gradients by Pressure Retarded Osmosis. *Environ. Sci. Technol.* **2012**, *46*, 5230-5239.
16. Yip, N. Y.; Elimelech, M. Performance Limiting Effects in Power Generation from Salinity Gradients by Pressure Retarded Osmosis. *Environ. Sci. Technol.* **2011**, *45*, 10273-10282.
17. Bui, N. N.; McCutcheon, J. R. Nanofiber Supported Thin-Film Composite Membrane for Pressure-Retarded Osmosis. *Environ. Sci. Technol.* **2014**, *48*, 4129-4136.

18. She, Q. ; Jin, X. ; Tang, C. Y. Osmotic power production from salinity gradient resource by pressure retarded osmosis: Effects of operating conditions and reverse solute diffusion. *J. Membr. Sci.* **2012**, *401-402*, 262-273.
19. Achilli, A. ; Prante, J. L.; Hancock, N. T.; Maxwell, E. B.; Childress, A. E. Experimental Results from RO-PRO: A Next Generation System for Low-Energy Desalination. *Environ. Sci. Technol.* **2014**, *48*, 6437-6443.
20. Prante, J. L.; Ruskowitz, J. A.; Childress, A. E.; Achilli, A. RO-PRO desalination: An integrated low-energy approach to seawater desalination. *Appl. Energy* **2014**, *120*, 104-114.
21. McGinnis, R. L.; McCutcheon, J. R.; Elimelech, M. A novel ammonia–carbon dioxide osmotic heat engine for power generation. *J. Membr. Sci.* **2007**, *305*, 13-19.
22. McGinnis, R. L.; Elimelech, M. Energy requirements of ammonia–carbon dioxide forward. *Desalination* **2007**, *207*, 370-382.
23. Loeb, S. ; Titelman, L. ; Korngold, E. ; Freiman, J. Effect of porous support fabric on osmosis through a Loeb-Sourirajan type asymmetric membrane. *J. Membr. Sci.* **1997**, *129*, 243-249.
24. Yip, N. Y.; Tiraferri, A. ; Phillip, W. A.; Schiffman, J. D.; Elimelech, M. High Performance Thin Film Composite Forward Osmosis Membrane. *Environ. Sci. Technol.* **2010**, *44*, 3812-3818.
25. McCutcheon, J. R.; Elimelech, M. Influence of membrane support layer hydrophobicity on water flux in osmotically driven membrane processes. *J. Membr. Sci.* **2008**, *318*, 458-466.
26. Arena, J. T.; McCloskey, B. ; Freeman, B. D.; McCutcheon, J. R. Surface modification of thin film composite membrane support layers with polydopamine: Enabling use of reverse osmosis membranes in pressure retarded osmosis. *J. Membr. Sci.* **2011**, *375*, 55-62.
27. Cath, T. Y.; Gormly, S. ; Beaudry, E. G.; Flynn, M. T.; Adams, V. D.; Childress, A. E. Membrane contactor processes for wastewater reclamation in space Part I. Direct osmotic concentration as pretreatment for reverse osmosis. *J. Membr. Sci.* **2005**, *257*, 85-98.
28. Stone, M. L.; Rae, C. ; Stewart, F. F.; Wilson, A. D. Switchable polarity solvents as draw solutes for forward osmosis. *Desalination* **2013**, *312*, 124-129.

29. Cath, T. Y.; Elimelech, M.; McCutcheon, J. R.; McGinnis, R. L.; Achilli, A.; Anastasio, D.; Brady, A. R.; Childress, A. E.; Farr, I. V.; Hancock, N. T.; Lampi, J.; Nghiem, L. D.; Xie, M.; Yip, N. Y. Standard Methodology for Evaluating Membrane Performance in Osmotically Driven Membrane Processes. *Desalination* **2013**, *312*, 31-38.
30. Coday, B. D.; Heil, D. M.; Xu, P. ; Cath, T. Y. Effects of Transmembrane Hydraulic Pressure on Performance of Forward Osmosis Membranes. *Environ. Sci. Technol.* **2013**, *47*, 2386-2393.
31. Touati, K. ; Hänel, C. ; Tadeo, F. ; Schiestel, T. Effect of the feed and draw solution temperatures on PRO performance: Theoretical and experimental study. *Desalination* **2015**, *365*, 182-195.
32. Herron, J. Asymmetric forward osmosis membranes. United States Patent No. US 7,445,712, Nov. 4, 2008.
33. Baker, R. W. *Membrane Technology and Applications*, 2nd ed.; John Wiley & Sons Ltd: West Sussex, England, 2004.
34. Klaysom, C. ; Cath, T. Y.; Depuydt, T. ; Vankelecom, I. F. J. Forward and pressure retarded osmosis: potential solutions for global challenges in energy and water supply. *Chem. Soc. Rev.* **2013**, *42*, 6959-5989.
35. Petersen, R. J. Composite reverse osmosis and nanofiltration membranes. *J. Membr. Sci.* **1993**, *83*, 81-150.
36. Dow Water and Process Solutions. FILMTEC™ Reverse Osmosis Membranes Technical Manual, Form No. 609-00071-1009. http://msdssearch.dow.com/PublishedLiteratureDOWCOM/dh_08db/0901b803808db77d.pdf.
37. Cadotte, J. E.; Petersen, R. J.; Larson, R. E.; Erickson, E. E. A New Thin-Film Composite Seawater Reverse Osmosis Membrane. *Desalination* **1980**, *32*, 25-31.
38. Ren, J. ; McCutcheon, J. R. A new commercial thinfilm composite membrane for forward osmosis. *Desalination* **2014**, *343*, 187-193.
39. Bui, N. N.; Lind, M. L.; Hoek, E. M. V.; McCutcheon, J. R. Electrospun nanofiber supported thin film composite membranes for engineered osmosis. *J. Membr. Sci.* **2011**, *385-386*, 10-19.

40. Tiraferri, A. ; Yip, N. Y.; Phillip, W. A.; Schiffman, J. D.; Elimelech, M. Relating performance of thin-film composite forward osmosis membranes to support layer formation and structure. *J. Membr. Sci.* **2011**, *367*, 340-352.
41. Han, G. ; Zhang, S. ; Li, X. ; Widjojo, N. ; Chung, T. S. Thin film composite forward osmosis membranes based on polydopamine modified polysulfone substrates with enhancements in both water flux and salt rejection. *Chem. Eng. Sci.* **2012**, *80*, 219-231.
42. Tang, C. Y.; Kwon, Y.-N.; Leckie, J. O. Effect of membrane chemistry and coating layer on physiochemical properties of thin film composite polyamide RO and NF membranes I. FTIR and XPS characterization of polyamide and coating layer chemistry. *Desalination* **2009**, *242*, 149-167.
43. Dow Water and Process Solutions. DOW FILMTEC NF270-400 Nanofiltration Element, Form No. 609-00346-0911. http://msdssearch.dow.com/PublishedLiteratureDOWCOM/dh_0913/0901b80380913703.pdf.
44. Dow Water and Process Solutions. FILMTEC NF90-400/34i Nanofiltration Element, Form No. 609-00345-0413. http://msdssearch.dow.com/PublishedLiteratureDOWCOM/dh_08d7/0901b803808d71b7.pdf.
45. Dow Water and Process Solutions. DOW FILMTEC BW30-400 High Rejection, High Surface Area Brackish Water RO Element, Form No. 609-00091-0910. http://msdssearch.dow.com/PublishedLiteratureDOWCOM/dh_090d/0901b8038090d9a2.pdf.
46. Dow Water and Process Solutions. DOW™ FILMTEC SW30XLE-440i Seawater Reverse Osmosis Element with iLECInterlocking Endcaps, Form No. 609-03003-1109.
47. Dow Water and Process Solutions. FILMTEC SW30HR-380 High Rejection Seawater RO Element, Form No. 609-00390-1008. http://msdssearch.dow.com/PublishedLiteratureDOWCOM/dh_0183/0901b80380183ed6.pdf.
48. McCloskey, B. D.; Park, H. B.; Ju, H. ; Rowe, B. W.; Miller, D. J.; Chun, B. J.; Kin, K. ; Freeman, B. D. Influence of polydopamine deposition conditions on pure waterflux and foulant adhesion resistance of reverse osmosis, ultrafiltration, and microfiltration membranes. *Polymer* **2010**, *51*, 3472-3485.

49. McCloskey, B. D.; Park, H. B.; Ju, H. ; Rowe, B. W.; Miller, D. J.; Freeman, B. D. A bioinspired fouling-resistant surface modification for water purification membranes. *J. Membr. Sci.* **2012**, *413-414*, 82-90.
50. Kasemset, S. ; Lee, A. ; J, M. D.; Freeman, B. D.; Sharma, M. M. Effect of polydopamine deposition conditions on fouling resistance, physical properties, and permeation properties of reverse osmosis membranes in oil/water separation. *J. Membr. Sci.* **2013**, *425-426*, 208-216.
51. Arena, J. T.; Chwatko, M. ; Robillard, H. A.; McCutcheon, J. R. pH Sensitivity of Ion Exchange through a Thin Film Composite Membrane in Forward Osmosis. *Environ. Sci. Technol. Lett.* **2015**, *2*, 177-182.
52. McCabe, W. L.; Smith, J. C.; Harriot, P. *Unit Operations of Chemical Engineering*, 7th ed.; McGraw-Hill: New York, New York, 2005.
53. Lobo, V. M. M. Mutual Diffusion Coefficients in Aqueous Electrolyte Solutions. *Pure Appl. Chem.* **1993**, *65*, 2613-2640.
54. Comesana, J. F.; Otero, J. J.; Camesella, E. ; Correa, A. Densities and Viscosities of Ternary Systems of Water + Fructose + Sodium Chloride from 20 to 40 °C. *J. Chem. Eng. Data* **2001**, *46*, 1153-1155.
55. McCutcheon, J. R.; Elimelech, M. Influence of concentrative and dilutive internal concentration polarization on flux behavior in forward osmosis. *J. Membr. Sci.* **2006**, *284*, 237-247.
56. Manickam, S. S.; McCutcheon, J. R. Characterization of polymeric nonwovens using porosimetry, porometry and X-ray computed tomography. *J. Membr. Sci.* **2012**, *407-408*, 108-115.
57. Van Wagner, E. M.; Sagle, A. C.; Sharma, M. M.; Freeman, B. D. Effect of crossflow testing conditions, including feed pH and continuous feed filtration, on commercial reverse osmosis membrane performance. *J. Membr. Sci.* **2009**, *345*, 97-109.
58. Van Wagner, E. M.; Sagle, A. C.; Sharma, M. M.; La, Y.-H.; Freeman, B. D. Surface modification of commercial polyamide desalination membranes using poly(ethylene glycol) diglycidyl ether to enhance membrane fouling resistance. *J. Membr. Sci.* **2011**, *367*, 273-287.

59. Yip, N. Y.; Tiraferri, A. ; Phillip, W. A.; Schiffman, J. D.; Hoover, L. A.; Kim, Y. C.; Elimelech, M. Thin-Film Composite Pressure Retarded Osmosis Membranes for Sustainable Power Generation from Salinity Gradients. *Environ. Sci. Technol.* **2011**, *45*, 4360-4369.
60. Thorat, I. V.; Stephenson, D. E.; Zacharias, N. A.; Zaghbi, K. ; Harb, J. N.; Wheeler, D. R. Quantifying tortuosity in porous Li-ion battery materials. *J. Power Sources* **2009**, *188*, 592-600.
61. Han, G. ; Zhang, S. ; Li, X. ; Chung, T. S. High performance thinfilm composite pressure retarded osmosis (PRO) membranes for renewable salinity-gradient energy generation. *J. Membr. Sci.* **2013**, *440*, 108-121.
62. Widjojo, N. ; Chung, T. S.; Weber, M. ; Maletzko, C. ; Warzelhan, V. The role of sulphonated polymer and macrovoid-free structure in the support layer for thin-film composite (TFC) forward osmosis (FO) membranes. *J. Membr. Sci.* **2011**, *383*, 214-223.

Chapter 5

Solute and water transport in forward osmosis using polydopamine modified thin film composite membranes

Arena et al. *Desalination* **2015**, *343*, 8-16. doi:10.1016/j.desal.2014.01.009

5.1. Introduction

Forward Osmosis (FO) is an emerging process being considered for the desalination, purification, and treatment of water.¹⁻⁶ A functional FO process requires an easily recoverable draw solution capable of generating high osmotic pressures as well as a highly productive and selective membrane.^{1,4,7} Various draw solutes exist, but only the ammonia-carbon dioxide ($\text{NH}_3\text{-CO}_2$) draw solution has been demonstrated as both an effective and recyclable solute that may enable osmotically driven desalination.^{1,4,7-10} Amongst the most commonly studied membrane for forward osmosis is the asymmetric cellulose triacetate (CTA) manufactured by Hydration Technology Innovations (HTI).^{1,4,9-13} This membrane's morphology has been optimized for use in osmotically driven membrane processes¹². The CTA membrane while

offering acceptable permselectivity and desirable hydrophilicity has inherent chemical compatibility drawbacks, notably hydrolysis in alkaline conditions.¹⁴⁻¹⁶ Hydrolysis reduces salt rejection, which in FO translates to higher draw solute cross-over and a lower osmotic pressure difference across the membrane.^{15,16} The $\text{NH}_3\text{-CO}_2$ draw solution will hydrolyze CTA as this draw solution can be expected to have pHs above 7.7.^{13,17}

This leads to the consideration of alternative membrane chemistries for use with the $\text{NH}_3\text{-CO}_2$ draw solution. The commercial alternative to the CTA membranes is the thin film composite (TFC) membrane platform. These membranes, typically used in reverse osmosis, comprise an ultra-thin aromatic polyamide layer supported by a polysulfone (PSu) or polyethersulfone (PES) layer that has been cast onto a polyester (PET) nonwoven¹⁸. Each of these layers is capable of withstanding a broad range of pH and temperature conditions making them suitable for use with the $\text{NH}_3\text{-CO}_2$ draw solution. Despite these desirable characteristics for use FO processes early studies which attempted to use TFC membranes in FO found the performance of TFC RO membranes to be inferior to that of HTI's CA FO membrane^{1,2}. In later work, the lack of TFC support layer wetting was demonstrated as a hindrance to osmotic flux due to a reduced effective porosity and enhanced internal

concentration polarization (ICP).^{19,20} To address this problem the use of TFC membranes with an intrinsically hydrophilic support would be desirable. This would require a retuning of the delicate interfacial polymerization process, which can be impacted by the support layer properties.^{20,21} Furthermore, hydrophilic supports may plasticize in the presence of water and cause damage to the fragile selective layer. Ideally, one could start with a TFC membrane made from a non-swelling hydrophobic support that also exhibits good permselectivity; then modify that membrane's support layer to increase its hydrophilicity. Recently commercial TFC FO membranes have just begun to enter the market with limited availability, with only HTI providing theirs for sale at the time of writing.^{6,11,22,23}

A recently developed technique to impart a hydrophilic character onto microfiltration, ultrafiltration, and reverse osmosis membrane selective layers for enhanced fouling resistance to oil/water emulsions and protein mixtures was reported by McCloskey and co-workers using polydopamine (PDA).²⁴⁻²⁷ PDA is a polymer with a chemistry similar to the adhesive secretions of mussels.²⁸⁻³⁰ It is formed from the spontaneous polymerization of dopamine in an alkaline aqueous solution. A subsequent study by Arena et al. examined the first use of PDA modified membranes for osmotically driven membrane process. This was done through the application

of PDA to TFC membrane *support* layer(s). Significant improvements in the water flux of PDA modified TFC RO membranes was observed in the pressure retarded osmosis (PRO) orientation.³¹ Others, such as Han, adopted this technique prior to synthesis of the membrane.³²

With the improved performance of these membranes in the PRO mode, similar improvement should be possible in the FO mode as well. The excellent selectivity of these membranes as well as tolerance to the often used ammonia-carbon dioxide draw solution make such a platform appealing. These membranes were tested for desalination performance using this draw solution in hopes of demonstrating the promise of these modified membranes; however, rejection, especially for cations, was far lower than anticipated. This is attributable to an ion exchange phenomenon taking place across the polyamide selective layer.

5.2. Materials and methods

5.2.1. Selected membranes and chemicals

The membranes selected for this investigation are the Dow Water & Process Solutions™ BW30 and SW30-XLE. Both membranes' support layers are made of PSu supported by a PET nonwoven.³³ These membranes were chosen for their high permselectivity, use in earlier

Table 5.1. Varieties of BW30 and SW30-XLE examined in this study.

Name	Descriptions
Neat	Used as received
No PET	PET fabric backing layer removed
PDA 1h	PDA modified with 1h coating time
PDA 42h	PDA modified with 42h coating time

studies, and reported properties.³⁴ Membranes were characterized in each for four varieties described in Table. 5.1. Sodium chloride, tris-hydrochloride, sodium hydroxide, ammonium bicarbonate, and ammonium hydroxide were purchased from Fisher Scientific (Pittsburgh, PA). Dopamine-hydrochloride was purchased from Sigma-Aldrich (St. Louis, MO). Isopropanol, sodium tetraphenyl boron, potassium chromate, calcium nitrate, and silver nitrate were purchased from Acros Organics (Geel, Belgium). Water used in this study was ultrapure Milli-Q water produce by a Millipore Integral 10 water system, (Millipore Corporation, Billerica, MA).

5.2.2. Polydopamine modification of thin film composite membranes

The PDA modification followed the procedure set forth in previous work (Chapter 3).³¹ Since the PDA formation only occurs in the aqueous phase, it was necessary to prewet the support in isopropanol (IPA) prior to PDA modification. The support was soaked IPA for 1 hour

and then washed in a series of three deionized water baths for 45 minutes each. Following the IPA wetting and DI water rinsing, the membranes were stored in deionized water at 4°C before being modified with PDA. The dopamine polymerization took place within a custom built coating container where the membrane separates two reservoirs.³¹ This container ensures that nearly all of the PDA polymerizes within the PSu layer and not the selective layer (which would negatively impact permeability).^{24,26,27} Both sides of the membrane were placed in contact with a pH 8.8 Tris buffer solution. Dopamine-HCl was added to the solution in contact with membranes' PSu support layers to bring the support layer coating solution to a concentration of 2 g·L⁻¹ dopamine. Polymerization occurs at room temperature with non-agitated solutions exposed to the air. The PDA polymerization can be observed upon the addition of dopamine where the formation of PDA is indicated by the change in color of the polymerizing dopamine solution from clear to orange and finally to brown.

5.2.3. Mercury intrusion porosimetry

A mercury intrusion porosimeter (MIP) (AutoPoreIV, Micrometrics) was used to characterize the membranes for pore diameter and total pore volume. The Washburn equation was used to calculate the pore diameters from the intrusion pressure.

$$d = \frac{-4\gamma \cdot \cos(\theta)}{P} \quad (5.1)$$

In Eq. (5.1), P is the intrusion pressure (MPa), d is the pore diameter (μm), γ is the surface tension of mercury ($485 \text{ dynes}\cdot\text{cm}^{-1}$) and θ is the contact angle of mercury (a value of 130° was assumed) with the sample. The sample was tested in the pressure range of 1-720 bar. It is to be noted Eq. (5.1) assumes that measured pore diameters are cylindrical. While this assumption is idealized for the membrane supports tested in this study, the resulting values for d calculated in Eq. (5.1) represents the equivalent cylindrical pore diameters of the support. It is also to be noted that the intrusion technique can detect both through and blind pores but not closed pores.³³

5.2.4. Fourier transform infrared spectroscopy

The modified TFC RO membranes were tested in Fourier transform infrared (FTIR) spectroscopy to examine the surface functional groups of the membranes' selective layers. Membranes were tested, after drying, in a Thermo Scientific (Waltham, MA) Nicolet iS10 FTIR spectrophotometer with Smart iTR attachment was used to perform these measurements on a

dried membrane. Measurements were taken on the selective layer using 64 scans with a resolution of 4 cm⁻¹.

5.2.5. Osmotic flux testing of modified membranes

5.2.5.1. Sodium chloride as the draw solute

Both neat and modified TFC RO membranes were tested under osmotic flux conditions with the membrane oriented in the FO mode (with the support layer facing the draw solution)³⁵.

Both membranes were tested in each of the four following varieties neat described in Table

5.1. Membranes not modified with PDA were tested following storage in deionized water. Prior to testing no wetting technique was implemented. The membrane area exposed to the feed and draw solutions were approximately nineteen square centimeters (three square inches).

Sodium chloride (NaCl) was used as the draw solute at concentrations of 0.05 M, 0.1 M, 0.5 M, 1.0 M, and 1.5 M. The osmotic flux testing procedure has been described previously.^{11,20,31,36,37}

Temperature was maintained at 23±1°C. Flux was measured gravimetrically using a balance (Denver Instruments PI-4002, Denver Instruments Bohemia, NY) connected to a computer measuring the mass of the draw solution tank once per minute. The osmotic pressures produced by these draw solutions (as presented in the figures) were calculated using the van't

Hoff equation.³⁸ Tests were run in triplicate using fresh membrane samples. Reverse solute flux was monitored by measuring of the feed solution conductivity.

5.2.5.2. Determination of the effective structural parameter

The structural parameter is a measure of the effective diffusive distance of a solute through a porous media.^{5,11,35,36,39} Solutes and water can be assumed as only capable of diffusing only through a wetted pore, thus a lack of wetting can have a large impact on the effective structural parameter of a porous material.^{19,31} The importance of the structural parameter is shown in the governing equation for water flux in the FO orientation, which including feed solution external mass transfer limitations can be represented by the following equation.³⁶

$$J_w = A \left\{ \frac{\pi_{d,b} \exp\left(-\frac{J_w \cdot S}{D}\right) - \pi_{f,b} \exp\left(-\frac{J_w}{k}\right)}{1 + \frac{B}{J_w} \left[\exp\left(\frac{J_w}{k}\right) - \exp\left(-\frac{J_w \cdot S}{D}\right) \right]} \right\} \quad (5.2)$$

In Eq. (5.2), J_w is the water flux, A is the water permeance, $\pi_{d,b}$ is the osmotic pressure of the draw solution, S is the structural parameter, D is the solute diffusivity in water, $\pi_{f,b}$ is the osmotic pressure of the feed solution, k is the external mass transfer coefficient, and B is the solute permeability (Fig. 5.1). Osmotic pressures can be calculated using the van't Hoff

equation.³⁸ The water permeance

(A) and solute permeability (B) are

commonly determined using

reverse osmosis.^{11,31} The structural

parameter can be determined from

a numerical solution to Eq. (5.2)

from experimental data. The

structural parameter is often

defined as a function of support

layer thickness (t), porosity (ϵ), and

tortuosity (τ) ($S = t \cdot \tau \cdot \epsilon^{-1}$), and is representative of the effective diffusion distance through the

support; however, rather than measuring each of these values individually (which can be

difficult to do accurately), S can be fit to the Eq. (5.2) above using experimental data providing

an “effective structural parameter.” The approach accounts for poor wetting in the support

since unwetted pores not available for solute transport.^{19,31}

5.2.5.3. Ammonia-carbon dioxide draw solution

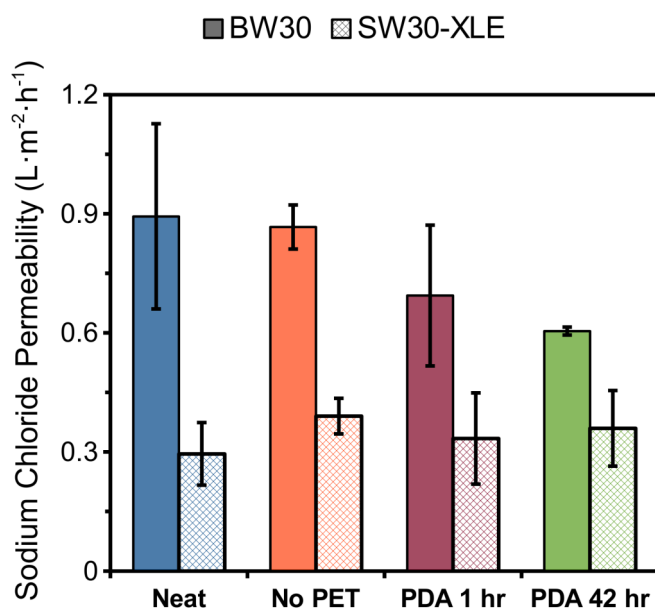


Fig. 5.1. Sodium chloride permeability of the BW30 (solid) and SW30-XLE (cross-hatched) membranes measured by at 15.5 bar by Arena et al.³¹ Descriptions of the membrane varieties in Table 5.1.

PDA modified TFC membranes were tested for NaCl rejection in forward osmosis using an $\text{NH}_3\text{-CO}_2$ based draw solution. These tests were performed in a laboratory scale osmosis test systems using a 2.0 M draw solution with an ammonia to carbon dioxide ratio of 1.2:1 on a molar basis and a feed solution of 0.25 M sodium chloride. These solutions were run counter-current with a cross flow velocity of $0.25 \text{ m}\cdot\text{s}^{-1}$ at $23\pm 1^\circ\text{C}$, matching the testing conditions using the NaCl draw solution. The membrane support layer was in contact with the $\text{NH}_3\text{-CO}_2$ draw solution (FO mode). Experiments were also run for a short time with the draw solution against a deionized water feed to measure the pure water flux for the $\text{NH}_3\text{-CO}_2$ draw solution.

Loss of draw solutes via permeation through the membrane negatively impacts the overall cost and efficiency of FO processes because draw solutes that are lost must be replaced after draw solution recovery.^{6,40,41} Toxic draw solutes that cannot be easily recovered may also contaminate the brine complicating its disposal.⁴² The flux of ammonia species (both as ammonia and ammonium) from the draw to the feed solution was measured gravimetrically using sodium tetraphenyl boron as a precipitating agent.^{43,44} A small sample of feed solution was removed from the feed tank and analyzed. When added to a solution containing ammonia species, ammonium tetraphenyl borate is formed and precipitates out of solution. This

precipitate was captured using fine porosity filter paper, washed with 1°C DI water, dried, and massed on an analytical balance (Denver Instruments PI-114, Denver Instruments Bohemia, NY). Following filtration of the ammonium tetraphenyl borate mixture a small amount of sodium tetraphenyl boron was added to the filtered solution to ensure that all of the ammonia species in solution were precipitated.

Sodium flux was determined from a mass balance based on the final concentration of sodium in the draw solution, analyzed via atomic absorption spectroscopy in a Perkin-Elmer 3100 AA (Perkin-Elmer, Waltham, MA) equipped with a sodium cathode lamp (Perkin-Elmer Intensitron Part# 303-6065, Perkin-Elmer, Waltham, MA). Solutions were analyzed using an air-acetylene flame with the detector set at 589 nm. Standard solutions were made with sodium chloride in diluted ammonium bicarbonate solution at concentrations ranging from 2 ppm to 12 ppm. The instrument was blanked against an ammonium bicarbonate draw solution with the same dilution factor as the sodium chloride-containing draw solution. Ammonium bicarbonate draw samples were diluted to give an absorbance in the range of the standard solutions.

Chloride flux was determined from a mass balance based on the final concentration of

chloride in the draw solution, which was determined using the Mohr titration.⁴³ In the Mohr titration chloride is titrated with silver nitrate in the presence of a potassium chromate indicator. At the end point of the titration excess silver ions form silver chromate producing a reddish brown color within the solution. Due to the presence of bicarbonate in the draw solution being analyzed the solution was boiled to dryness prior to the titration to volatilize all of the ammonia and carbon dioxide within the solution. Following drying, the residual solutes were rehydrated and the resulting solution was titrated. A complete validation of this technique is presented in Appendix 3.

5.3. Results and discussion

5.3.1. Porosimetry characterization

Mercury intrusion porosimetry (MIP) was performed on both modified and unmodified membranes to examine the effect of the PDA modification on membrane support layer pore diameters and porosity. As

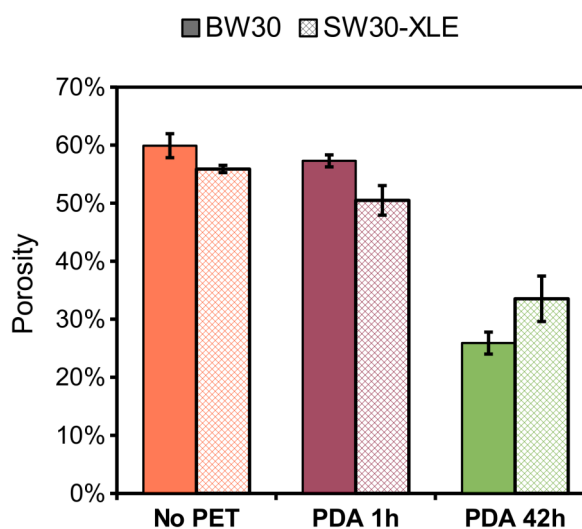


Fig. 5.2. Porosity data from MIP of BW30 (solid) and SW30-XLE (cross-hatched) membranes. Descriptions of the membrane varieties are in Table 5.1.

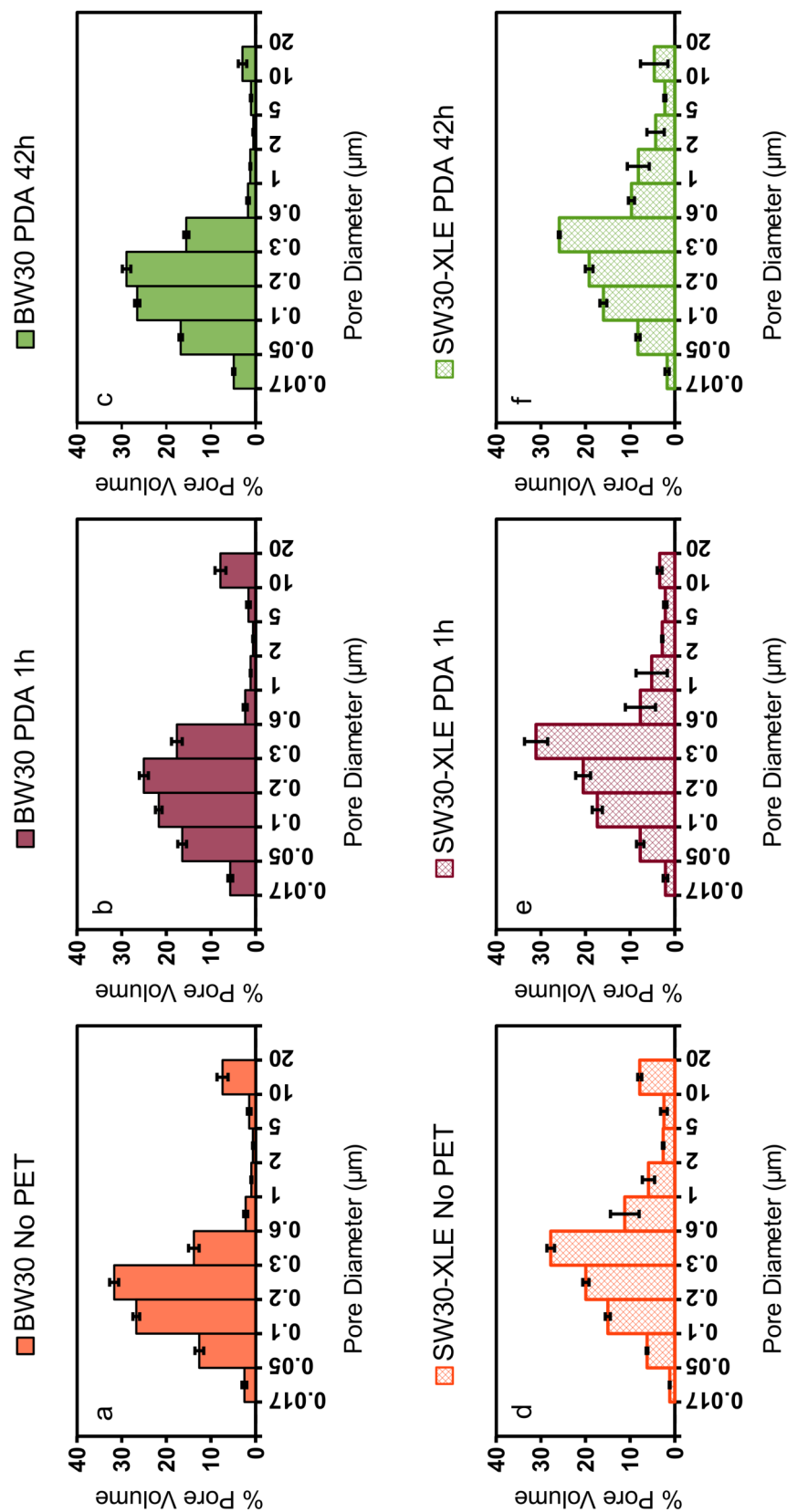


Fig. 5.3. Pore diameter histograms from mercury intrusion porosimetry for of BW30 No PET (a), BW30 PDA 1h (b), BW30 PDA 42h (c), SW30-XLE No PET (d), SW30-XLE PDA 1h (e), and SW30-XLE PDA 42h (f) membranes.

shown in Fig. 5.2, the porosity for both membrane types (i.e., BW30 and SW30-XLE) decreased as a result of polydopamine deposition, and the samples exposed to the dopamine coating solution for a longer time (i.e. 42h) had a lower porosity than those treated for only one hour. This decrease in porosity directly competes with the increased wettability as measured by contact angle goniometry as reported by Arena (Chapter 3).³¹

Fig. 5.3 presents the effective pore size distribution for the membranes considered in this study. There were minimal changes in the pore diameter distribution for membranes with higher coating times. These membranes exhibited a slight shift toward smaller pores, but given the thinness of PDA layers^{24,45} the pore diameter distributions do not change dramatically. Care should be taken when scrutinizing MIP data too closely as the high pressures employed by cause irreversible sample compression and skew results; however, for comparative purposes the unmodified and modified membranes would deform similarly and so this technique is reasonable for comparing porosity changes.

5.3.2. FTIR spectra

The FTIR spectra for these membranes, shown in Fig. 5.4, are characteristic for those membranes based upon a fully aromatic polyamide.⁴⁶ The strong similarities in the FTIR

spectra for the BW30 and SW30-XLE membranes is to be expected given their common lineage stemming from the FT30 membrane originally developed by Cadotte.^{34,48} Also, based upon the FTIR spectra PDA cannot be detected. This is unsurprising many of the functional groups characteristic of PDA are already present in an aromatic polyamide, which based upon the structure proposed by Dreyer consists of an indole or indoline like structure (containing a

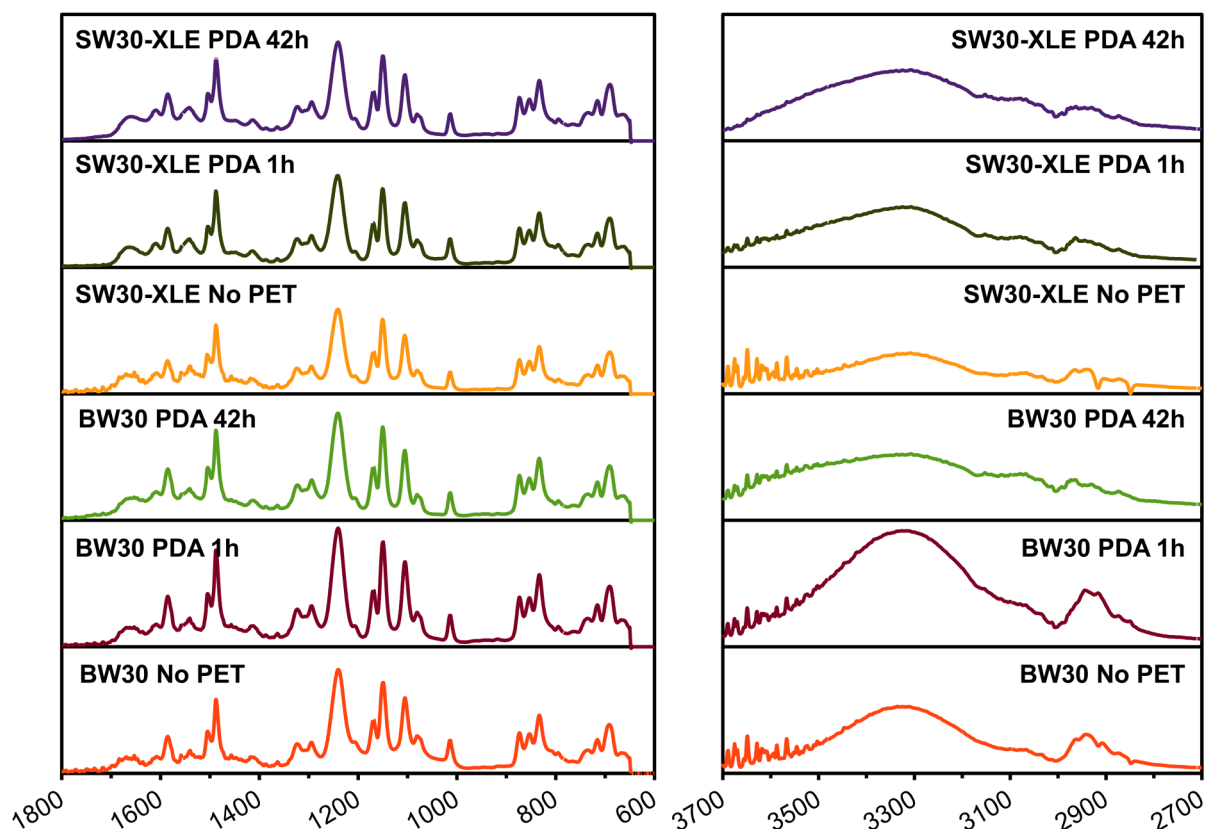


Fig. 5.4. FTIR spectra of the selective layer for PDA modified commercial TFC membranes at wave numbers from 1800 to 600 cm^{-1} and 3700 to 2700 cm^{-1} . The peaks are consistent with those typically found for a fully aromatic TFC.⁴⁶ The broad peak from 3000 to 2800 is likely attributed to solid state hydrogen bonded hydroxyl stretch in the polyamide layer's carboxylic acid moieties.⁴⁷

N-H), carbonyl and hydroxyl functional groups.⁴⁹ Overall the application of PDA to the membrane support layers does not appear to significantly alter the surface functional groups of the membranes selective layer.

An interesting peak of the spectra (found in Fig. 5.4) is the 3000-2800 cm⁻¹ peak. This peak can be only attributed to a hydrogen bonded hydroxyl stretch of a solid state carboxylic acid.⁴⁷ This peak implies incomplete cross-linking between the trimesoyl chloride and m-phenylene diamine monomers of the polyamide, producing a functional group that can be expected to deprotonate at elevated pHs. This deprotonation of the polyamide selective layer would give rise to negative surface charges of the membranes as detailed in the literature.^{50,51} Additionally, deprotonation of carboxylic acid groups of a polyamide can also be attributed to improved rejections of these membranes at slightly basic pHs.^{18,48,52} As will be discussed below, these charged groups may play a significant role in other transport processes during FO.

5.3.3. Osmotic flux performance

5.3.3.1. Water flux for a sodium chloride draw solution

Fig. 5.5 shows that osmotic water flux was increased significantly following modification of the BW30 and SW30-XLE membranes with PDA. PDA modification caused water flux to

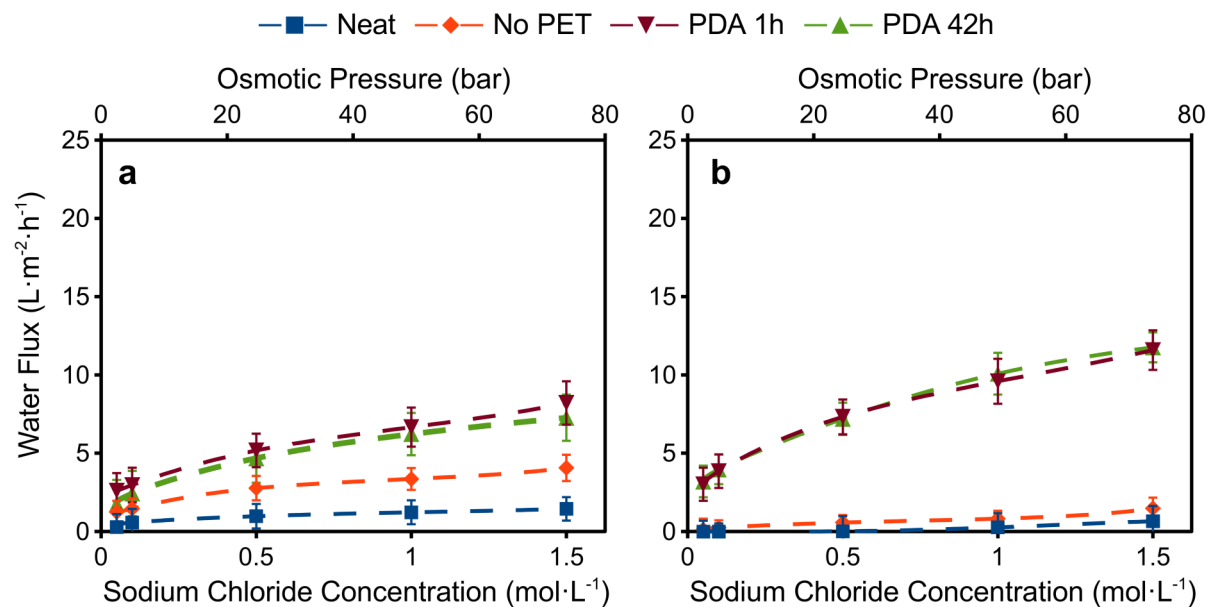


Fig. 5.5. Osmotic flux performance of BW30 (a) and SW30-XLE (b) membranes at $23 \pm 1^\circ\text{C}$, $0.25 \text{ m} \cdot \text{s}^{-1}$ feed and draw cross-flow velocity, and no transmembrane hydrostatic pressure. Descriptions of the membrane varieties are in Table 5.1.

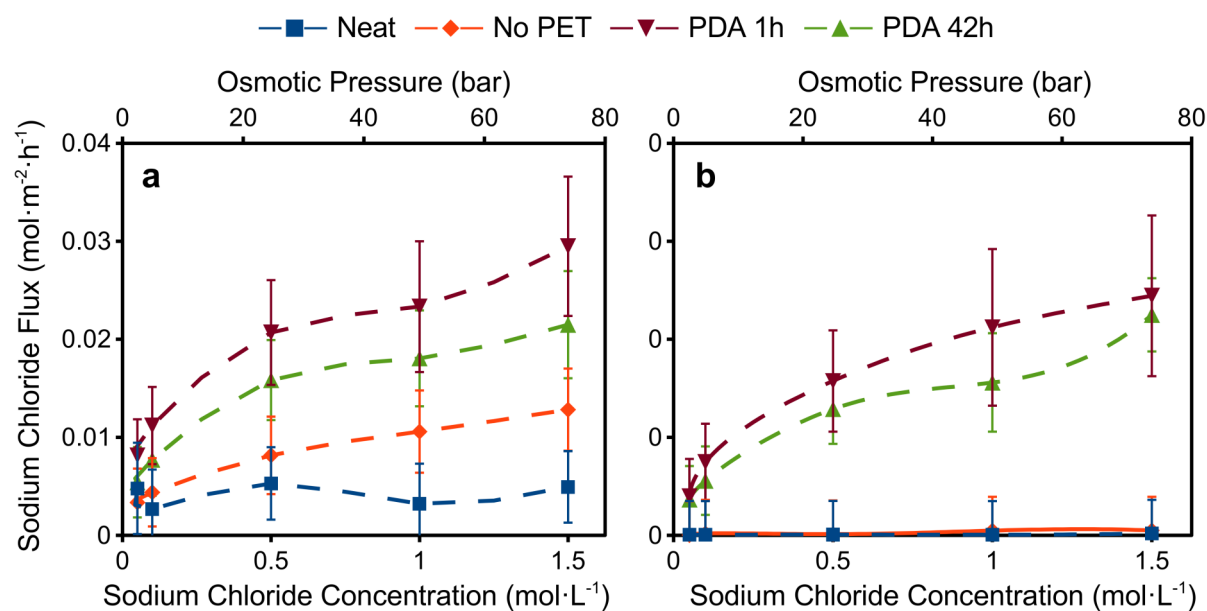


Fig. 5.6. Reverse solute (sodium chloride) flux across BW30 (a) and SW30-XLE (b) membranes at $23 \pm 1^\circ\text{C}$, $0.25 \text{ m} \cdot \text{s}^{-1}$ feed and draw cross-flow velocity, and no transmembrane hydrostatic pressure. Descriptions of the membrane varieties are in Table 5.1.

increase by up to a factor of 4 for the BW30 and up to a factor of 6 for the SW30-XLE membrane. This observation is similar to those reported previously, where the PDA modified BW30 and SW30-XLE membranes exhibited an 8 and 12 fold increase in flux, respectively.³¹ The PDA 42h membranes showed slightly decreased (but not statistically significant) water flux when compared to the PDA 1h membrane. This can be explained to be a result of decrease porosity within the membrane support layers as shown in Fig. 5.2. The increase water flux for the PDA modified membranes may be attributed to the increased wettability of membrane support layer increasing the rate of draw solutes transport through the membrane support layer. This will increase the concentration, and osmotic pressure, of the draw solution at the membrane interface.

5.3.3.2.Reverse solute flux for a sodium chloride draw solution

The salt flux increased (Fig. 5.6) after PDA modification for both the BW30 and SW30-XLE membranes as a result of the improved wettability of the membranes' support layer. As support layer wetting improves, solutes can more easily diffuse through a membrane's support layer. This increases the concentration of those solutes at the selective layer interface and results in increased solute flux.

5.3.3.3. Membrane structural parameters

Effective structural parameters for the membranes considered in this study were calculated using Eq. (5.2). Water permeance and sodium chloride permeability values reported in Arena et al.³¹ were used for this analysis. As shown in Fig. 5.7, removal of the PET backing layer resulted in a 70% reduction in the effective structural

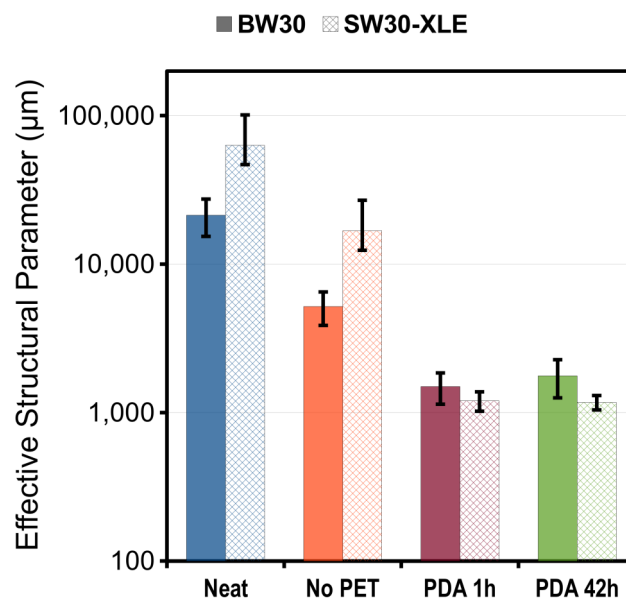


Fig. 5.7. Structural parameters of BW30 (solid bars) and SW30-XLE (cross-hatched bars) membranes calculated from RO data presented in Arena et al.³¹ Descriptions of the membrane varieties are in Table 5.1.

parameters for both the BW30 and SW30-XLE. Following removal of the PET layers these membranes still exhibit structural parameters orders of magnitude higher than their structure would suggest is possible based upon their thickness and porosity⁵³.

This finding suggests that the poor wetting of the PSu layer is the primary cause of the high effective structural parameters for both the BW30 and SW30-XLE; however, poor wetting of the PSu layer seems to be more severe for the SW30-XLE as shown by this membrane's

higher effective structural parameters. Modification of these membrane's PSu layer with PDA resulted in a near order of magnitude decrease in the effective structural parameter for both membranes. This result is particularly interesting given that membrane porosity is reduced by the PDA coating process, as shown in Fig. 5.2. The mass transfer resistance of the support has been reduced due to PDA coating despite the fact that the porosity of the support layer is decreased as a result of PDA coating.

5.3.4. Desalination performance of PDA modified TFC membranes

5.3.4.1. Water flux in forward osmosis desalination

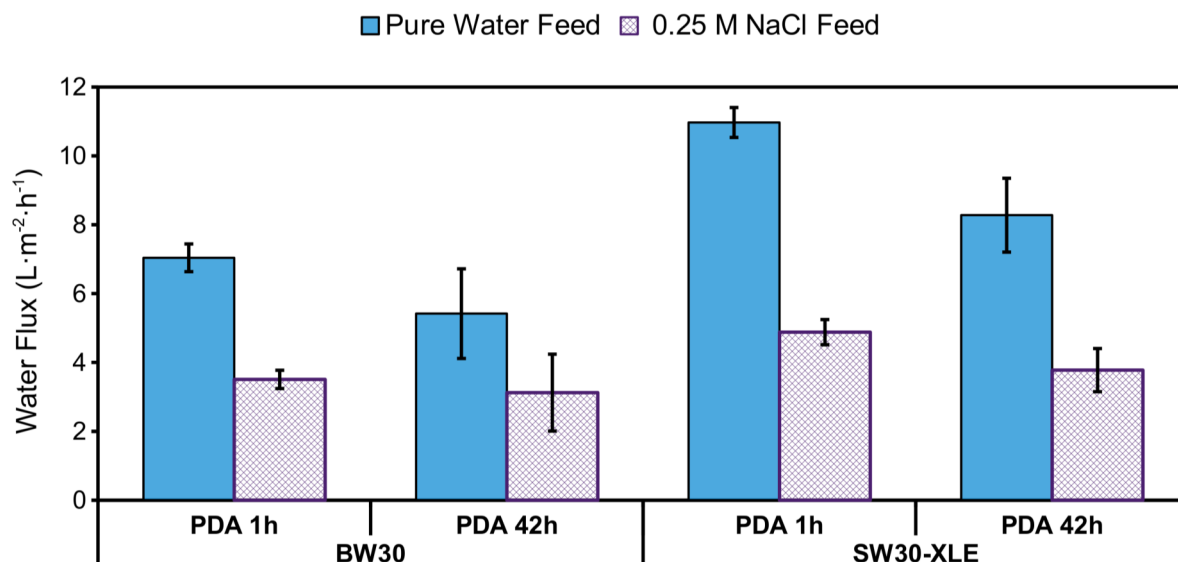


Fig. 5.8. Osmotic flux data for pure water (solid bars) and 0.25 M sodium chloride (cross-hatched bars) feed solutions against a 2.0 M $\text{NH}_3\text{-CO}_2$ solution at $23\pm 1^\circ\text{C}$, $0.25\text{ m}\cdot\text{s}^{-1}$ draw and feed cross-flow velocity, and no transmembrane hydrostatic pressure.

By comparing the pure water fluxes for the $\text{NH}_3\text{-CO}_2$ draw solution in Fig. 5.8 to water fluxes for a NaCl draw solution presented in Fig. 5.5 it becomes apparent that the $\text{NH}_3\text{-CO}_2$ draw solution produces similar water fluxes to a 1.0 M sodium chloride draw solution under these test conditions. Upon addition of sodium chloride water, fluxes decreased by more than 50%. This is likely due to external concentration polarization effects, increasing the osmotic pressure of the feed solution at the membrane selective layer interface.

5.3.4.2. Solute flux in forward osmosis desalination

Reverse solute flux was measured for the ammonia species permeating through the membrane in both the molecular and ionic forms (as ammonia and ammonium respectively) from the draw solution into the feed solution. The ammonia species crossover was measured between $0.75\text{-}0.9\text{ mol}\cdot\text{m}^{-2}\cdot\text{hr}^{-1}$. Ammonia being a polar molecule like water and of similar size to water with a more mobile hydration shell than ammonium⁵⁴ prevents the membrane from easily discriminating between water and ammonia molecules¹⁶.

Sodium and chloride ion fluxes are given in Fig. 5.9. As would be expected, the SW30-XLE exhibited significantly lower forward sodium flux (cross-hatched bars) than the BW30 due to its higher selectivity. On the other hand, chloride flux is dramatically lower for both membranes.

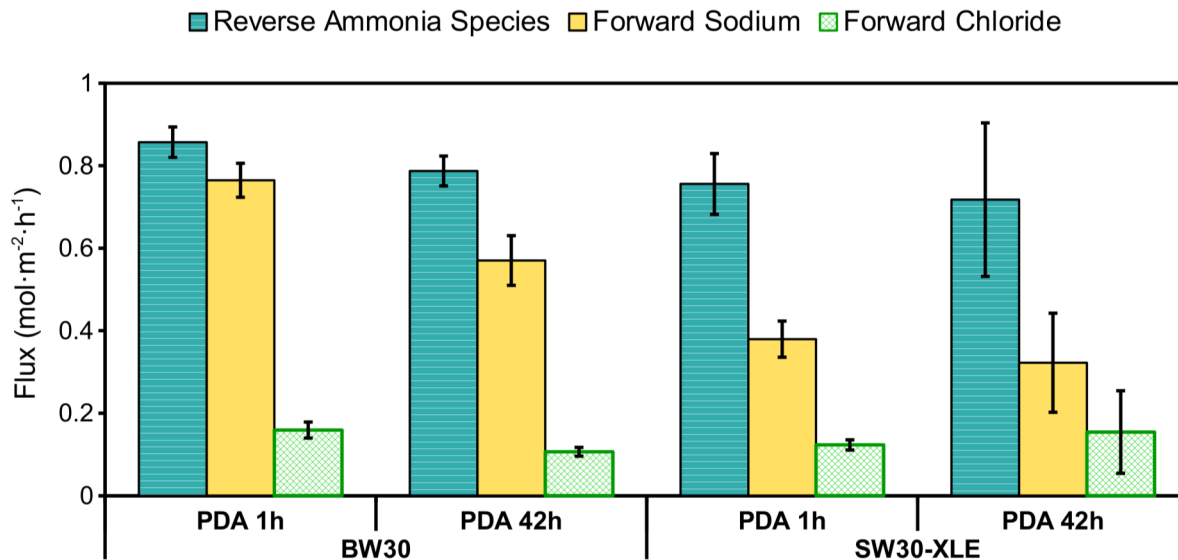


Fig. 5.9. Solute fluxes for osmotically driven sodium chloride rejection. The lined bar represents ammonia species reverse solute fluxes, the solid bar represents sodium ion forward solute fluxes, and the cross-hatched bar represents chloride ion forward solute fluxes at $23\pm1^\circ\text{C}$, $0.25\text{ m}\cdot\text{s}^{-1}$ draw and feed cross-flow velocity, and no transmembrane hydrostatic pressure.

This was an unanticipated finding since, in early studies on FO desalination using HTI's CTA membrane and this draw solute found high NaCl rejections.^{1,13}

The unequal sodium and chloride ion fluxes must mean that a cation from the draw solution is moving to the feed solution from the draw solution, since electroneutrality must be maintained. The only cation available in the draw solute is ammonium. It is interesting to note that in all instances the ammonia flux was greater than or equivalent to the sodium flux. This supports evidence of ion exchange since it would close the mass balance for both ammonia

and sodium moving between the two solutions.

The ion flux data is converted to rejection values in Fig. 5.10 (done by multiplying forward solute flux by water flux to determine the concentration of water passing through the membrane then dividing this by the concentration of the feed water). The SW30-XLE had better sodium and chloride rejection under these process conditions with around 65% rejection of sodium and 85-90% rejection of chloride for both the PDA 1h and PDA 42h membranes. The BW30 exhibited a large disparity in sodium and chloride rejections. The rejections of the sodium ion were 15-25% while the chloride ion rejections were 80-85%. The cation exchange

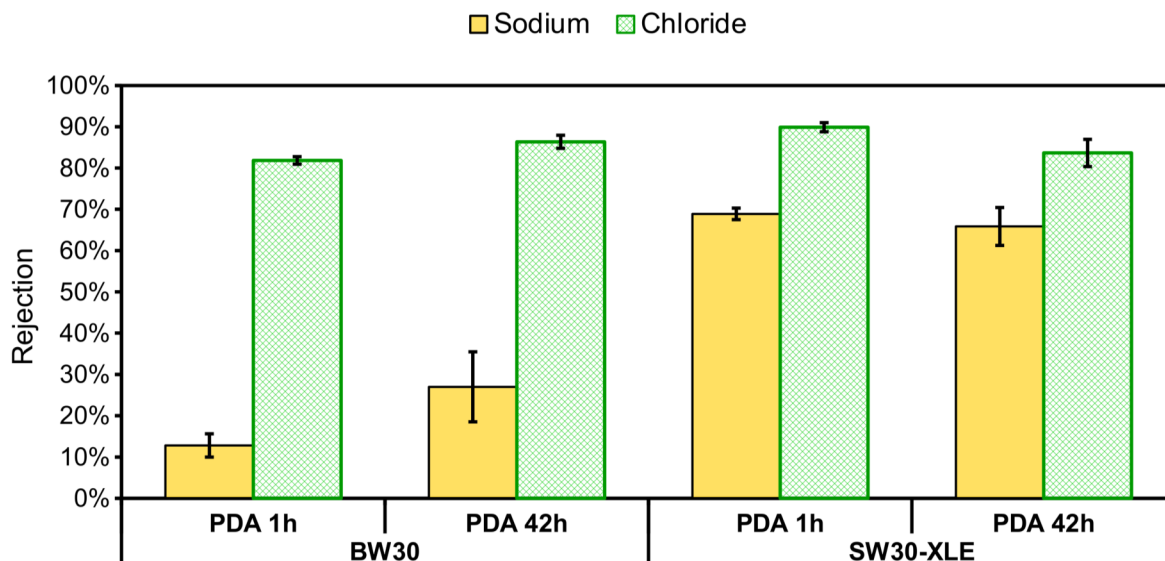


Fig. 5.10. Observed rejection for a 2.0 M $\text{NH}_3\text{-CO}_2$ draw solution versus 0.25 M sodium chloride feed. The solid bars represent sodium rejection and the cross-hatched bars represent chloride rejection at $23\pm 1^\circ\text{C}$, $0.25 \text{ m}\cdot\text{s}^{-1}$ draw and feed cross-flow velocity, and no transmembrane hydrostatic pressure.

occurring between the 0.25 M NaCl feed and the 2.0 M $\text{NH}_3\text{-CO}_2$ draw solutions present a phenomena never directly reported. These data could also explain low sodium chloride rejections⁵⁵ or uneven anion and cation rejections of various electrolytes²³ reported by others using TFC membranes.

5.3.4.3. Ion exchange mechanisms

There are two possible mechanisms for the ion exchange behavior exhibited between the NaCl feed and $\text{NH}_3\text{-CO}_2$ draw solutions. The first is reliant upon the equilibria amongst ammonia species within the draw solution (Chapter 2).¹⁷ Three nitrogen containing species are present within the draw solution solution: ammonia, ammonium, and carbamate. These species are in equilibrium, but ammonia is uncharged, has chemical interactions similar to water, and a less rigid hydration shell (in relation cation and anion species).⁵⁴ As such ammonia can easily diffuse through the membrane selective layer without affecting electroneutrality between the two solutions. Ammonia present within feed solution can now speciate into ammonium, causing an imbalance of charge. This charge imbalance drives a sodium ion (the only cation available on the feed side) to diffuse into the draw solution thus producing the unequal feed solution ion fluxes. The second mechanism for ion exchange is the

selective layer functioning as a cation exchanger where negatively charged functional groups of a membrane's selective layer allow for preferential transport of cations.

Similar ion exchange behavior to those illustrated in Fig. 5.9 (this being unequal anion to cation transport for electrolytes) was reported in a recent publication by Coday observed unequal feed solute ion transport using non-volatile solutes with commercial TFC FO membranes.²³ As these solutes do not exist in equilibrium between a charged and uncharged species this would imply that the membrane chemistry is the dominating factor in ion transport behavior. This is further reinforced by observations also by Coday et al. where HTI's CTA FO membrane was also tested displaying higher cation rejections than TFC FO membranes.²³ Additionally the high rejections of sodium chloride in studies using HTI's CA membrane with the $\text{NH}_3\text{-CO}_2$ draw solution further demonstrate the importance of membrane chemistry.^{1,13}

A classical cation exchange resin should be a cross-linked water insoluble structure with acidic functional groups (i.e. sulfonic, carboxylic, phenolic, etc.). These acid functional groups when deprotonated would have a negative charge allowing for ionic interactions with cations, specifically cations residing within the polymer structure and exchanging cations in solution. Cation exchangers with carboxylic acid functionality are pH sensitive only functioning as such

at pHs above 7.⁴³ The FTIR spectra for these membranes indicate carboxylic functional groups are part of the polyamide selective layers of these membranes (Fig. 5.4).⁴⁷ So the most likely reason for the ion exchange behavior is the deprotonation of carboxylic acids functional groups of polyamide making available cation exchange site within the polyamide layer.^{43,51,52} This allows for the movement of cations between the feed and draw solutions; therefore, in order to mitigate this behavior in polyamide based TFC membranes the pH would need to be below 7 (not possible with all draw solutions). Alternatively other selectively layer chemistries can be synthesized or revisited.

5.4. Conclusions

This study explored the impact on FO properties resulting from the application of a thin film of PDA on the PSu support structure of a commercial TFC RO membrane. A four and six fold enhancement in the FO mode osmotic flux of the BW30 and SW30-XLE membranes, respectively, were observed after modification with PDA. Overall, these membranes were shown to have modest flux under desalination conditions with a 2.0 M $\text{NH}_3\text{-CO}_2$ draw solution and a 0.25 M sodium chloride feed; however, low sodium rejections were observed due to cation exchange between the draw and feed solutions. Evidence for this ion exchange is

provided by the unequal fluxes between sodium and chloride. A tuning of process conditions or membrane chemistry may enable higher rejections for both ions within the feed solution.

References

1. McCutcheon, J. R.; McGinnis, R. L.; Elimelech, M. A novel ammonia-carbon dioxide forward (direct) osmosis desalination process. *Desalination* **2005**, *174*, 1-11.
2. Cath, T. Y.; Gormly, S.; Beaudry, E. G.; Flynn, M. T.; Adams, V. D.; Childress, A. E. Membrane contactor processes for wastewater reclamation in space Part I. Direct osmotic concentration as pretreatment for reverse osmosis. *J. Membr. Sci.* **2005**, *257*, 85-98.
3. Kravath, R. E.; Davis, J. A. Desalination of sea water by direct osmosis. *Desalination* **1975**, *16*, 151-155.
4. Achilli, A.; Cath, T. Y.; Childress, A. E. Selection of inorganic-based draw solutions for forward osmosis applications. *J. Membr. Sci.* **2010**, *364*, 233-241.
5. Cath, T. Y.; Childress, A. E.; Elimelech, M. Forward osmosis: Principles, applications, and recent developments. *J. Membr. Sci.* **2006**, *281*, 70-87.
6. McGinnis, R. L.; Hancock, N. T.; Nowosielski-Slepawron, M. S.; McGurgan, G. D. Pilot Demonstration of the NH_3/CO_2 forward osmosis desalination process on high salinity brines. *Desalination* **2013**, *312*, 67-74.
7. McGinnis, R. L.; Elimelech, M. Energy requirements of ammonia-carbon dioxide forward osmosis desalination. *Desalination* **2007**, *207*, 370-382.
8. Yen, S. K.; Mehnas Haja, F. N.; Su, M.; Wang, K. Y.; Chung, T. S. Study of draw solutes using 2-methylimidazole-based compounds in forward osmosis. *J. Membr. Sci.* **2010**, *364*, 242-252.
9. Ge, Q.; Su, J.; Chung, T.S.; Amy, G. Hydrophilic Superparamagnetic Nanoparticles: Synthesis, Characterization, and Performance in Forward Osmosis Processes. *Ind. Eng. Chem. Res.* **2011**, *50*, 382-288.

10. Ling, M. M.; Wang, K. Y.; Chung, T. S. Highly water-soluble magnetic nanoparticles as novel draw solutes in forward osmosis for water reuse. *Ind. Eng. Chem. Res.* **2010**, *49*, 5869-5876.
11. Cath, T. Y.; Elimelech, M.; McCutcheon, J. R.; McGinnis, R. L.; Achilli, A.; Anastasio, D.; Brady, A. R.; Childress, A. E.; Farr, I. V.; Hancock, N. T.; Lampi, J.; Nghiem, L. D.; Xie, M.; Yip, N. Y. Standard Methodology for Evaluating Membrane Performance in Osmotically Driven Membrane Processes. *Desalination* **2013**, *312*, 31-38.
12. Herron, J. Asymmetric forward osmosis membranes. United States Patent No. US 7,445,712, Nov. 4, 2008.
13. McCutcheon, J. R.; McGinnis, R. L.; Elimelech, M. Desalination by ammonia-carbon dioxide forward osmosis: Influence of draw and feed solution concentrations on process performance. *J. Membr. Sci.* **2006**, *278*, 114-123.
14. Vos, K. D.; Burris, F. O.; Riley, R. L. Kinetic Study of the Hydrolysis of Cellulose Acetate in the pH Range of 2-10. *J. Appl. Polym. Sci.* **1966**, *10*, 825-832.
15. Watters, J. C.; Klein, E.; Fleischman, M.; Roberts, J. S.; Hall, B. Rejection Spectra of Reverse Osmosis Membranes Degraded by Hydrolysis of Chlorine Attack. *Desalination* **1986**, *60*, 93-110.
16. Baker, R. W. *Membrane Technology and Applications*, 2nd ed.; John Wiley & Sons Ltd: West Sussex, England, 2004.
17. Mani, F.; Peruzzini, M.; Stoppioni, P. CO₂ absorption by aqueous NH₃ solutions: speciation of ammonium. *Green Chem.* **2006**, *8*, 995-1000.
18. Petersen, R. J. Composite reverse osmosis and nanofiltration membranes. *J. Membr. Sci.* **1993**, *83*, 81-150.
19. McCutcheon, J. R.; Elimelech, M. Influence of membrane support layer hydrophobicity on water flux in osmotically driven membrane processes. *J. Membr. Sci.* **2008**, *318*, 458-466.
20. Bui, N. N.; Lind, M. L.; Hoek, E. M. V.; McCutcheon, J. R. Electrospun nanofiber supported thin film composite membranes for engineered osmosis. *J. Membr. Sci.* **2011**, *385-386*, 10-19.

21. Ghosh, A. K.; Hoek, E. M. V. Impacts of support membrane structure and chemistry on polyamide–polysulfone interfacial composite membranes. *J. Membr. Sci.* **2009**, *336*, 140-148.
22. Hydration Technology Innovations™, HTI's New Thin Film Forward Osmosis Membrane in Production. <http://www.htiwater.com/news/press-room/content/2012/press-HTI-HTIThinFilmMembrane042512.pdf>.
23. Coday, B. D.; Heil, D. M.; Xu, P.; Cath, T. Y. Effects of Transmembrane Hydraulic Pressure on Performance of Forward Osmosis Membranes. *Environ. Sci. Technol.* **2013**, *47*, 2386-2393.
24. McCloskey, B. D.; Park, H. B.; Ju, H.; Rowe, B. W.; Miller, D. J.; Chun, B. J.; Kin, K.; Freeman, B. D. Influence of polydopamine deposition conditions on pure waterflux and foulant adhesion resistance of reverse osmosis, ultrafiltration, and microfiltration membranes. *Polymer* **2010**, *51*, 3472-3485.
25. McCloskey, B. D.; Park, H. B.; Ju, H.; Rowe, B. W.; Miller, D. J.; Freeman, B. D. A bioinspired fouling-resistant surface modification for water purification membranes. *J. Membr. Sci.* **2012**, *413-414*, 82-90.
26. Miller, D. J.; Araújo, P. A.; Correia, P. B.; Ramsey, M. M.; Kruithof, J. C.; van Loosdrecht, M. C. M.; Freeman, B. D.; Paul, D. R.; Whiteley, M.; Vrouwenvelder, J. S. Short-term adhesion and long-term biofouling testing of polydopamine and poly(ethylene glycol) surface modifications of membranes and feed spacers for biofouling control. *Water Res.* **2012**, *46*, 3737-3753.
27. Kasemset, S.; Lee, A.; J, M. D.; Freeman, B. D.; Sharma, M. M. Effect of polydopamine deposition conditions on fouling resistance, physical properties, and permeation properties of reverse osmosis membranes in oil/water separation. *J. Membr. Sci.* **2013**, *425-426*, 208-216.
28. Lee, H.; Lee, Y.; Scherer, N. F.; Messersmith, P. B. Single-molecule mechanics of mussel adhesion. *Proc. Natl. Acad. Sci. U.S.A.* **2006**, *103*, 12999-13003.
29. Lee, H.; Lee, Y.; Statz, A. R.; Rho, J.; Park, T. G.; Messersmith, P. B. Substrate-independent layer-by-layer assembly by using mussel-adhesive-inspired polymers. *Adv. Mater.* **2008**, *20*, 1619-1623.

30. Lee, H.; Dellatore, S. M.; M, M. W.; Messersmith, P. B. Mussel-inspired surface chemistry for multifunctional coating. *Science* **2007**, *318*, 426-430.
31. Arena, J. T.; McCloskey, B.; Freeman, B. D.; McCutcheon, J. R. Surface modification of thin film composite membrane support layers with polydopamine: Enabling use of reverse osmosis membranes in pressure retarded osmosis. *J. Membr. Sci.* **2011**, *375*, 55-62.
32. Han, G.; Zhang, S.; Li, X.; Widjojo, N.; Chung, T. S. Thin film composite forward osmosis membranes based on polydopamine modified polysulfone substrates with enhancements in both water flux and salt rejection. *Chem. Eng. Sci.* **2012**, *80*, 219-231.
33. Manickam, S. S.; McCutcheon, J. R. Characterization of polymeric nonwovens using porosimetry, porometry and X-ray computed tomography. *J. Membr. Sci.* **2012**, *407-408*, 108-115.
34. Dow Water and Process Solutions. FILMTEC™ Reverse Osmosis Membranes Technical Manual, Form No. 609-00071-1009. http://msdssearch.dow.com/PublishedLiteratureDOWCOM/dh_08db/0901b803808db77d.pdf.
35. McCutcheon, J. R.; Elimelech, M. Modeling Water Flux in Forward Osmosis: Implications for Improved Membrane Design. *AIChE J.* **2007**, *53*, 1736-1744.
36. Tiraferri, A.; Yip, N. Y.; Straub, A. P.; Castrillon, S. R.-V.; Elimelech, M. A method for the simultaneous determination of transport and structural parameters of forward osmosis membranes. *J. Membr. Sci.* **2013**, *444*, 523-538.
37. Phillip, W. A.; Yong, J. S.; Elimelech, M. Reverse draw solute permeation in forward osmosis: modeling and experiments. *Environ. Sci. Technol.* **2010**, *44*, 5170-5176.
38. Robinson, R. A.; Stokes, R. H. *Electrolyte Solutions*, 2nd ed.; Dover Publications: Mineola, 2002.
39. Yip, N. Y.; Elimelech, M. Performance Limiting Effects in Power Generation from Salinity Gradients by Pressure Retarded Osmosis. *Environ. Sci. Technol.* **2011**, *45*, 10273-10282.
40. Hancock, N. T.; Cath, T. Y. Solute Coupled Diffusion in Osmotically Driven Membrane Processes. *Environ. Sci. Technol.* **2009**, *43*, 6769-6775.

41. Hancock, N. T.; Phillip, W. A.; Elimelech, M.; Cath, T. Y. Bidirectional Permeation of Electrolytes in Osmotically Driven Membrane Processes. *Environ. Sci. Technol.* **2011**, *45*, 10462-10651.
42. Stone, M. L.; Rae, C.; Stewart, F. F.; Wilson, A. D. Switchable polarity solvents as draw solutes for forward osmosis. *Desalination* **2013**, *312*, 124-129.
43. Jeffrey, G. H.; Bassett, J.; Mendham, J.; Denny, R. C. *Vogel's Textbook of Quantitative Chemical Analysis*, 5th ed.; Longman Scientific & Technical: Essex, 1989.
44. Harris, D. C. *Quantitative Chemical Analysis*, 6th ed.; W.H. Freeman and Company: New York, 2003.
45. Pan, H.; Jia, H.; Qiao, S.; Jiang, Z.; Wang, J.; Wang, B.; Zhong, Y. Bioinspired fabrication of high performance composite membranes with ultrathin defect-free skin layer. *J. Membr. Sci.* **2009**, *341*, 279-285.
46. Tang, C. Y.; Kwon, Y.-N.; Leckie, J. O. Effect of membrane chemistry and coating layer on physiochemical properties of thin film composite polyamide RO and NF membranes I. FTIR and XPS characterization of polyamide and coating layer chemistry. *Desalination* **2009**, *242*, 149-167.
47. Lambert, J. B.; Shurvell, H. F.; Lightner, D. A.; Cooks, R. G. *Organic Structural Spectroscopy*; Prentice-Hall, Inc.: Upper Saddle River, NJ, 1998.
48. Cadotte, J. E.; Petersen, R. J.; Larson, R. E.; Erickson, E. E. A New Thin-Film Composite Seawater Reverse Osmosis Membrane. *Desalination* **1980**, *32*, 25-31.
49. Dreyer, D. R.; Miller, D. J.; Freeman, B. D.; Paul, D. R.; Bielawski, C. W. Elucidating the structure of poly(dopamine). *Langmuir* **2012**, *28*, 6428-6435.
50. Tang, C. Y.; Kwon, Y. N.; Leckie, J. O. Characterization of Humic Acid Characterization of Humic Acid Nanofiltration Membranes by Transmission Electron Microscopy and Streaming Potential Measurements. *Environ. Sci. Technol.* **2007**, *41*, 942-949.
51. Van Wagner, E. M.; Freeman, B. D.; Sharma, M. M.; Hickner, M. A.; Altman, S. J. *Polyamide Desalination Membrane Characterization and Surface Modification to Enhance Fouling Resistance*; Sandia National Laboratories: Albuquerque, 2010.

52. Van Wagner, E. M.; Sagle, A. C.; Sharma, M. M.; Freeman, B. D. Effect of crossflow testing conditions, including feed pH and continuous feed filtration, on commercial reverse osmosis membrane performance. *J. Membr. Sci.* **2009**, *345*, 97-109.
53. Manickam, S. S.; Gelb, J.; McCutcheon, J. R. Pore structure characterization of asymmetric membranes: Non-destructive characterization of porosity and tortuosity. *J. Membr. Sci.* **2014**, *454*, 549-554.
54. Hesske, H.; Gloe, K. Hydration Behavior of Alkyl Amines and Their Corresponding Protonated Forms. 1. Ammonia and Methylamine. *J. Phys. Chem.* **2007**, *111*, 9848-9853.
55. Low, S. C. Preliminary studies of seawater desalination using forward osmosis. *Desalin. Water Treat.* **2009**, *7*, 41-46.
56. McCutcheon, J. R.; Elimelech, M. Influence of concentrative and dilutive internal concentration polarization on flux behavior in forward osmosis. *J. Membr. Sci.* **2006**, *284*, 237-247.

Chapter 6

Comparison of polydopamine modified thin film composite reverse osmosis membranes to forward osmosis membranes available commercially

6.1. Introduction

Forward osmosis (FO) processes are an emerging membrane separation processes driven by a chemical potential difference.^{1,2} In FO processes, a dilute feed water and concentrated draw solution flows on the opposite sides of a semi-permeable membrane. Water permeates along the chemical potential/osmotic pressure/concentration difference across the membrane from the feed solution into the draw solution leaving solutes behind within a concentrated feed stream.³⁻⁶ This separation requires no energy input, as it is driven by the spontaneous thermodynamic tendency towards osmotic equilibrium. The earliest work in FO for water purification used concentrated sugar solutions to drive osmosis across a cellulose acetate

reverse osmosis (RO) membranes.^{3,4} These studies used a comestible draw solution unsuitable for a continuous FO process.

For a continuous desalination process the ideal draw solute is one which can be easily removed. The only significant energy input into the process is used for the separation of the draw solute and water. A variety of draw solutes have been proposed for FO desalination processes. Amongst these are surface modified nano-particles,⁷ switchable polarity solvents,⁸ polymers which display a thermal sensitivity to water solubility,⁹ and electrolytes.¹⁰⁻¹² Electrolyte draw solutes offer many advantages over alternatives being their generally lower viscosities and higher diffusivities. Sodium chloride (NaCl) is commonly used as draw solute for FO-RO processes where an FO is used to dilute a NaCl solution that is subsequently concentrated in a following RO step.^{13,14} Another branch of electrolyte draw solutions for consideration are those based upon thermolytic draw solutes, which consists of water soluble gases forming ionic species within solution.^{5,6,15} This allows for a sufficiently high concentration of draw solute to concentrate brines up to 180,000 mg·L⁻¹.¹⁶ One proposed thermolytic draw solute^{12,17} and proved for seawater desalination by McCutcheon is a mixture of ammonia (NH₃) and carbon dioxide (CO₂) gases.^{5,6} A detailed discussion of the ammonia-carbon dioxide (NH₃-CO₂)

draw solution can be found in Chapter 2.

FO processes require both an easily recovered draw solute and membrane capable of giving high water flux. The current most widely available FO membrane is produced by Hydration Technology Innovations (HTI). This membrane is made from cellulose triacetate, formed through a Loeb-Sourirajan type wet casting process.¹⁸ While this has produced a membrane with sufficient permeability, selectivity and chemical resilience to operate in a number of processes,^{1,5,7,13,19-23} cellulose acetates are vulnerable to hydrolysis which results in the replacement of acetyl groups with hydroxyl degrading membrane selectivity.^{24,25} Additionally, membranes made from cellulose acetates characteristically tend to have lower water permeance than a similar thin film composite membrane.²⁴

These limitations of CTA membranes have encouraged the development of alternative membrane chemistries for FO. Thin film composite (TFC) membranes have been considered as the logical replacement for cellulose derived membranes in FO; however, early studies observing commercial TFC reverse osmosis membranes in forward osmosis reported low water fluxes.^{5,21} TFC membranes typically employ a cross-linked polyamide selective layer that, while susceptible to degradation by hypochlorous acid and hypochlorite salts,²⁶ exhibits

stability over a broader pH range than cellulose acetate based membranes.²⁴

The advantages of TFC membranes have driven the development of new membranes adapted for the unique requirements of FO processes where the support layer has been designed to minimize solute diffusion limitations. This chapter will compare performance characteristics of an early generation TFC FO membrane from Oasys Water and HTI's CTA with polydopamine (PDA) modified RO membranes²⁷ in a bench scale FO process using the ammonia-carbon dioxide ($\text{NH}_3\text{-CO}_2$) to concentrate sodium chloride. The usage of the $\text{NH}_3\text{-CO}_2$ FO process is significant in its use with this membrane platform in Oasys Water's osmotic brine concentrator and showed high recovery of draw solute and rejection of feed solution component.¹⁶

6.2. Materials and methods

6.2.1. Selective membranes and chemicals

This study seeks to compare water and ion transport across FO membrane operating within an $\text{NH}_3\text{-CO}_2$ draw solution based desalination processes. Two commercial membranes were selected. The first is a proprietary TFC membrane, later referred to as the O-TFC, provided by Oasys Water (Boston, MA). The second is the asymmetric CTA FO membrane,

provided by Hydration Technology Innovations (Corvallis, OR). Compared to these will be the polydopamine (PDA) modified reverse osmosis (RO) membranes (BW30 and SW30-XLE), provided by Dow Water and Process Solution and modified by the method previously established in Arena et al.^{28,27} Sodium chloride, ammonium bicarbonate, and ammonium hydroxide were purchased from Fisher Scientific (Pittsburgh, PA). Sodium tetraphenyl boron, potassium chromate, and silver nitrate were purchased from Acros Organics (Geel, Belgium). Isopropanol was purchased from J.T. Baker (Center Valley, PA). Water used in this study was ultrapure Milli-Q (18.2 MΩ) water produced by a Millipore Integral 10 water system, (Millipore Corporation, Billerica, MA).

6.2.2. Membrane performance in forward osmosis desalination

6.2.2.1. Forward osmosis desalination testing

The O-TFC, CTA and PDA modified RO membranes were assessed for sodium chloride rejection in forward osmosis using the $\text{NH}_3\text{-CO}_2$ based draw solution. The $\text{NH}_3\text{-CO}_2$ desalination tests were performed in a laboratory scale osmosis test systems using a 2.0 M (carbon basis) draw solution. The ammonia to carbon dioxide ratio was varied for these tests to observe what effect if any this would have on desalination performance. A 1.2:1 $\text{NH}_3\text{:CO}_2$

(molar basis) draw solution was used with a feed solution of 0.25 M sodium chloride.²⁷ These solutions were circulated counter-current with a cross flow velocity of $0.25 \text{ m}\cdot\text{s}^{-1}$ at $23\pm 1^\circ\text{C}$. The membrane support layer was in contact with the $\text{NH}_3\text{-CO}_2$ draw solution (FO mode). Experiments were also run for a short time with the draw solution against a deionized water feed to measure the pure water flux for the $\text{NH}_3\text{-CO}_2$ draw solution.

6.2.2.2. Dissolved species quantification

The flux of ammonia species, sodium, and chloride were measured using techniques previously illustrated by Arena et al.²⁷ All fluxes were determined based on the change in concentration of the solute of interest (i.e. ammonia species present within the feed solution, sodium and chloride ions within the draw solution) over the duration of the test and the membrane surface area. The concentration of ammonium species was measured gravimetrically using sodium tetraphenyl boron to precipitate ammonia as ammonium tetraphenyl borate.^{29,30} The concentration of chloride was determined from the Mohr titration²⁹ on a sample of rehydrated draw solution from which the water, dissolved ammonia and dissolved carbon dioxide has been boiled off. The concentration of sodium was determined using a Perkin-Elmer 3100 Atomic Absorption Spectrometer (Perkin-Elmer, Waltham, MA)

equipped with a sodium hollow cathode lamp (Perkin-Elmer Intensitron Part# 303-6065, Perkin-Elmer Waltham, MA).

6.2.3. Calculation of theoretical rejections

Solute permeability and water flux influence the rejection of a membrane operating in reverse osmosis. Dense selective layer membranes like those used in RO and FO have their transport governed by solution-diffusion. In solution-diffusion solute rejection is driven by the solute permeability and water flux across a membrane. In studies of RO membrane performance the solute permeability is calculated from the observed or experimental rejection and water flux in an RO experiment using a saline feed.²⁰

$$B = \frac{(1-R) J_w}{R} \quad (6.1)$$

Eq. (6.2) is used in to calculate the solute permeability from rejection and water flux observed in a RO test. In Eq. (6.2) B is the solute permeability of the membrane, R is the solute rejection, and J_w is the water flux. Values used for the solute rejection can be intrinsic or observed. Intrinsic rejections are corrected for the accumulation of solutes at the membrane selective layer, or external concentration polarization (ECP). ECP is calculated using

established mass transfer correlations based on the hydrodynamics and solution properties.^{1,31}

Eq. (6.1) can be solved for rejection and from here the solute permeability and water flux can be used to approximate rejection using Eq. (6.2).

$$R = \frac{J_w}{B + J_w} \quad (6.2)$$

From Eq. (6.2) the water flux observed in the FO desalination experiments can be used to approximate the rejection that would be expected for the same flux in an RO type experiment.

Calculated the expected rejection this way calculates what can be called the theoretical rejection. The theoretical rejection would be representative of the solute rejection that would be observed if the membrane were operating in an RO experiment at the same water flux.

Calculating the theoretical rejection using water flux observed in the FO desalination tests approximates solute rejection of the membrane absent the interaction of cations or anions with the membrane selective layer. Theoretical rejection calculates the ideal rejection of solutes that, in the case of dissociating solutes, cross through the membrane as a cation or anion with any counterions needed to maintain electroneutrality.

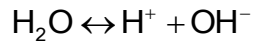
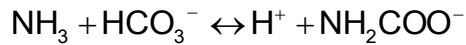
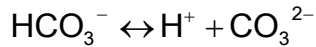
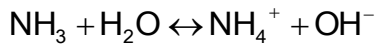
6.2.4. Speciation of the ammonia-carbon dioxide draw solution

The $\text{NH}_3\text{-CO}_2$ draw solution comprises a varied mixture of chemical species within solution.

Within the draw solution there are dissolved NH_3 and CO_2 gases in addition to ammonium (NH_4^+) cations and bicarbonate (HCO_3^-), carbonate (CO_3^{2-}), and carbamate (NH_2COO^-) anions.

Table 6.1. Relationships governing the speciation of $\text{NH}_3\text{-CO}_2$ draw solution

Chemical Equilibria



Mass Balances

$$m_{\text{total-N}} = m_{\text{NH}_3} + m_{\text{NH}_4^+} + m_{\text{NH}_2\text{COO}^-}$$

$$m_{\text{total-C}} = m_{\text{CO}_2} + m_{\text{HCO}_3^-} + m_{\text{CO}_3^{2-}} + m_{\text{NH}_2\text{COO}^-}$$

Electroneutrality

$$m_{\text{NH}_4^+} = m_{\text{HCO}_3^-} + 2m_{\text{CO}_3^{2-}} + m_{\text{NH}_2\text{COO}^-}$$

The solution is typically alkaline having

pHs > 7 .^{6,27} Many studies on the equilibrium

relationship between NH_3 and CO_2 gases

within solution have been performed.³²⁻³⁵

Draw solute speciation is affected by 5

chemical equilibria, mass balances upon the

nitrogen species, carbon species, and

solution electroneutrality.³³

The concentration of each species is

dependent on the concentration of aqueous

ammonia and carbon dioxide. Using the

relationships shown in Table 6.1 a numerical

determination for the concentration of ionic and neutral species within solution can be obtained. Draw solute speciation was determined numerically using Mathematica accounting for ion, and molecular interactions parameters given by Edwards et al.,³³ NH_3 and CO_2 equilibrium constants from Kawazuishi and Prausnitz,³² and water self-dissociation equilibrium constants from Robinson and Stokes.³⁶ The source code of this program is in Appendix 1. In solving for the speciation of the $\text{NH}_3\text{-CO}_2$ draw solution a direct calculation of the osmotic pressure of these solution can be obtain from the water activity in solution by Eq. (6.3).³⁶⁻³⁸

$$\pi = -\frac{1}{v_w} \ln(a_w)RT \quad (6.3)$$

Here π is the osmotic pressure of the solution in bar, R is the ideal gas constant ($0.08314 \text{ L}\cdot\text{bar}\cdot\text{mol}^{-1}\cdot\text{K}^{-1}$), T is the absolute temperature, v_w is the molar volume of water ($0.018018 \text{ L}\cdot\text{mol}^{-1}$) and a_w is the molal activity of water.

6.3. Results and discussion

6.3.1. Membrane transport properties

Reverse osmosis performance data for the PDA modified RO membranes are reported in Chapter 3²⁸ and effective structural parameters for these membrane are reported in

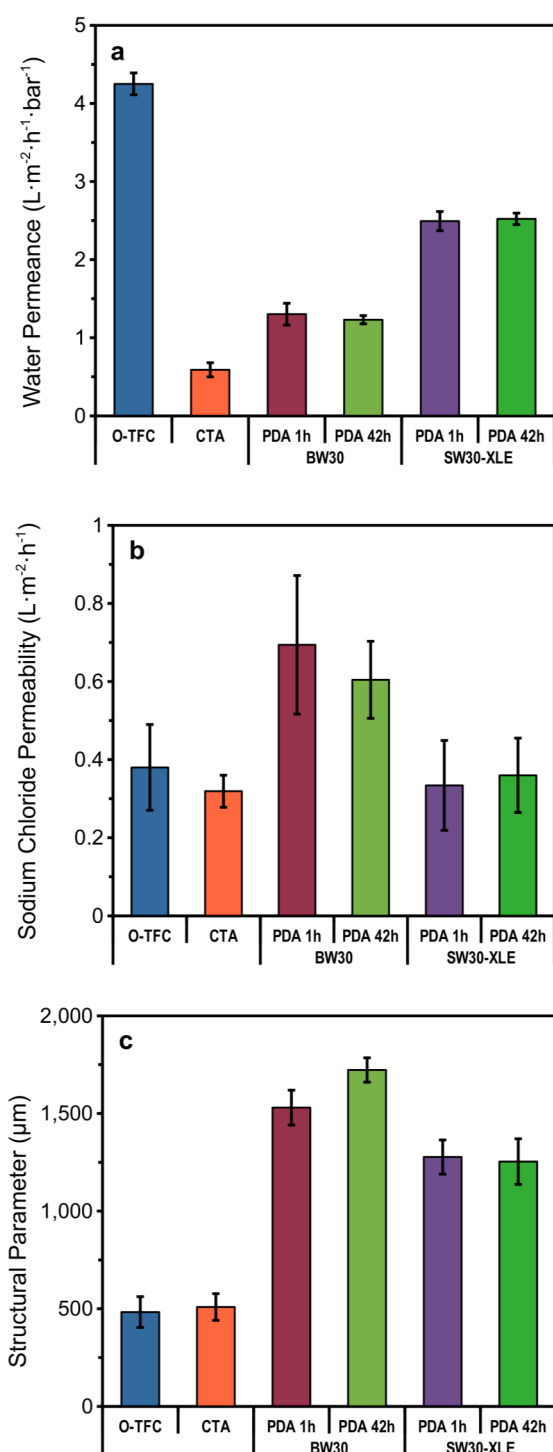


Fig. 6.1. Water permeance (A), solute permeability (B), and effective structural parameters (S) for commercial FO and PDA modified RO membranes.

Chapter 5.²⁷ A complete characterization of the O-TFC can be found in Appendix 2. The CTA membrane has been extensively characterized; the water permeance and solute permeability in this study were previously reported by Anastasio et al. and Bui et al.,^{39,40} and the effective structural parameters were reported by Cath et al.⁴¹ The membrane transport properties are shown in Fig. 6.1.

The water permeance of these membranes are shown in Fig. 6.1a. Most visible in these data are the higher water permeance that the TFC membrane chemistries have over the CTA membrane

shown here. The O-TFC membrane has

much higher water permeance than the other membranes in this study surpassing the PDA 1h and PDA 42h SW30-XLE by nearly a factor of two. This is while all of the observed membranes except for the PDA 1h and PDA 42h BW30 membranes have a solute permeability of approximately $0.3 \text{ L}\cdot\text{m}^{-2}\cdot\text{h}^{-1}$ (Fig. 6.2b). One last notable aspect in the transport properties of these membranes are significantly lower than effective structural parameters which membranes designed specifically for FO possess. This shows the advantages of a purpose built FO membrane support layers have over modification a pre-existing structure.

6.3.2. Membrane performance in forward osmosis desalination

Fig. 6.2 show water fluxes for the $\text{NH}_3\text{-CO}_2$ draw solution for both pure water and 0.25 M sodium chloride across commercial FO and PDA modified RO membranes. Upon addition of sodium chloride water, fluxes decreased by more than 50% for the TFC membranes (both the O-TFC and PDA modified RO membranes). The CTA membrane also showed a slight drop in water flux. The reduction in water flux from the addition of sodium chloride to the feed solution is likely due to osmotic pressure of the sodium chloride solution compounded by concentrative external polarization of the feed. The advantages of low structural parameters are shown here

where, with a 0.25 M sodium chloride feed solution, the commercial FO membranes show 2-4 times more water flux over their PDA modified RO counterparts.

Fig. 6.3 show reverse ammonia species flux and forward sodium and chloride flux. The reverse ammonia species flux represents the permeation of both the molecular and ionic forms of ammonia (i.e. ammonia, ammonium, and carbamate) from the draw solution into the feed solution. Ammonia being polar molecule like water and of similar size to water with a more mobile hydration shell than ammonium⁴² prevents the membrane from easily discriminating between water and aqueous ammonia.²⁴ This may in part contribute to the high observed

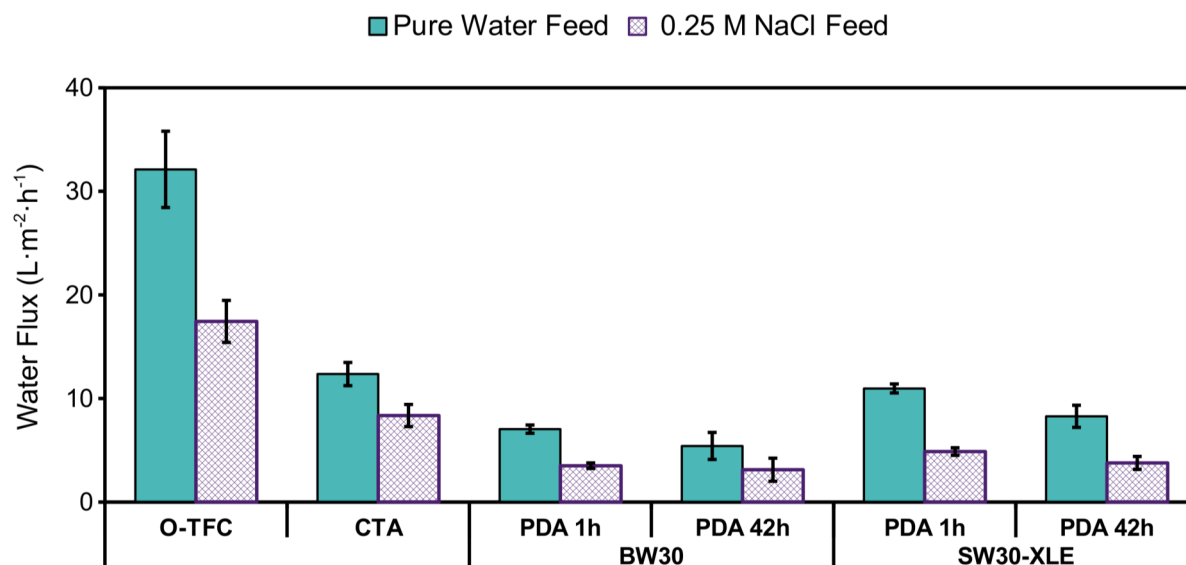


Fig. 6.2. Water flux across commercial FO and PDA modified RO membranes using a 2.0 M 1.2:1 NH₃-CO₂ draw solution with feed solutions of deionized water and 0.25 M sodium chloride at 23±1°C and 0.25 m·s⁻¹.

ammonia species flux; however, at this $\text{NH}_3:\text{CO}_2$ ratio there is little ammonia ($<0.1 \text{ mol}_{\text{NH}_3} \cdot \text{kg}^{-1}$) in solution (Table 6.1).

The forward solute flux is the flux of sodium and chloride ions. Large differences in the forward cation and anion fluxes are shown in Fig. 6.3. Sodium flux is an order of magnitude higher than the chloride flux for all of the $\text{NH}_3:\text{CO}_2$ ratios tested. The lower chloride flux suggests that anion transport is not necessary to maintain electroneutrality between the feed and draw solution. This suggests that sodium-ammonium cation exchange is occurring. Ion does not appear to occur across the CTA membrane, as shown in Fig. 6.3. The CTA

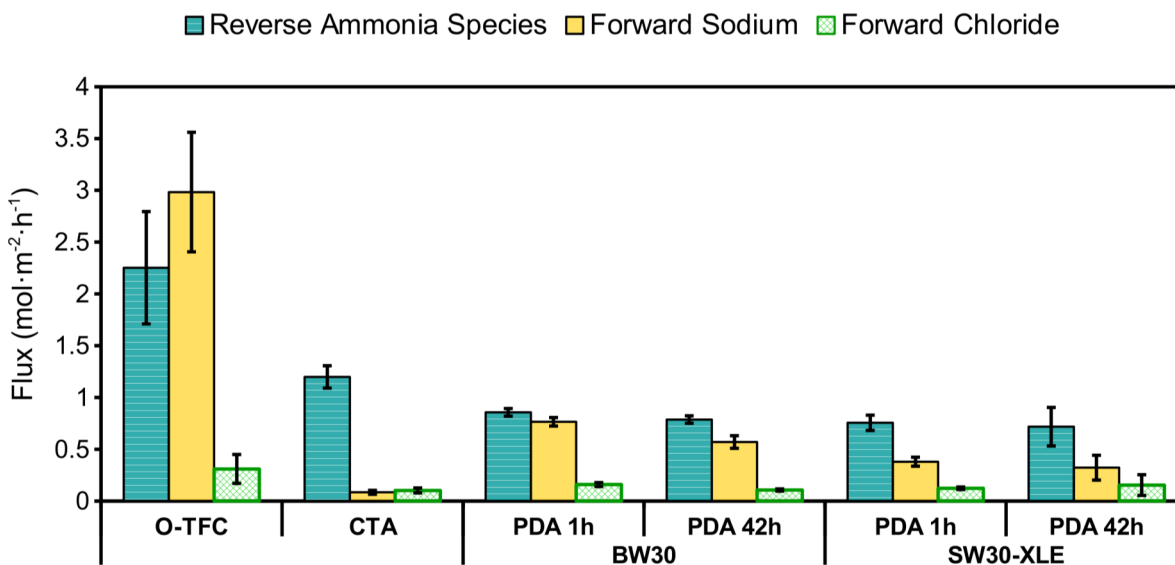


Fig. 6.3. Reverse ammonia species, forward sodium, and forward chloride fluxes across commercial FO and PDA modified RO membranes with a 2.0 M 1.2:1 $\text{NH}_3\text{-CO}_2$ draw solution at $23 \pm 1^\circ\text{C}$ and $0.25 \text{ m} \cdot \text{s}^{-1}$.

membrane, which chemically identical to those use in previous studies,^{5,6} show essentially equivalent fluxes of both the sodium and chloride ions. This suggests that the unequal forward ion flux (being between sodium and chloride) is impacted by the membrane chemistry.

The unequal sodium and chloride ion fluxes suggests that, as stated in Chapter 5,²⁷ a cation from the draw solution is

Table 6.2. Speciation of a 2.0M 1.2:1 NH₃-CO₂ draw solution at 23°C.

$m_{\text{total-N}}$ (mol/kg _{H₂O})	2.36
$m_{\text{total-C}}$ (mol/kg _{H₂O})	2.06
ρ_{solution} (kg/L)	1.058
m_{NH_3} (mol/kg _{H₂O})	0.0612
m_{CO_2} (mol/kg _{H₂O})	0.0632
$m_{\text{NH}_4^+}$ (mol/kg _{H₂O})	2.04
$m_{\text{HCO}_3^-}$ (mol/kg _{H₂O})	1.77
$m_{\text{CO}_3^{2-}}$ (mol/kg _{H₂O})	0.0113
$m_{\text{NH}_2\text{COO}^-}$ (mol/kg _{H₂O})	0.255
Ionic strength (mol/kg)	2.05
π (bar)	50.1

moving to the feed solution from the draw solution. Since electroneutrality must be maintained the only cation available in the draw solute is ammonium, and that in all instances the ammonia flux was greater than or equivalent to the sodium flux. Ammonia (as NH_{3(aq)}) transport through the selective layer may not be significant since the 1.2:1 NH₃:CO₂ draw solution has little dissolved ammonia (Table 6.2). The low dissolved ammonia concentration means that nearly all of ammonia species flux must occur from the exchange of ammonium with sodium.

6.3.3. Ion exchange and its effect on feed solute rejection

The effect of cation exchange in decreasing the sodium rejection of TFC membranes is clearly visible in Fig. 6.4. The CTA membrane, which does not appear to cation exchange under these test conditions, has a theoretical rejection similar to those experimentally observed for both sodium and chloride. This helps to illustrate the usefulness of theoretical rejection as a test for interactions between draw and feed solutes that would be detrimental to feed solute selectivity. In the specific context of a membrane cation exchanging would have a low rejection of cations.

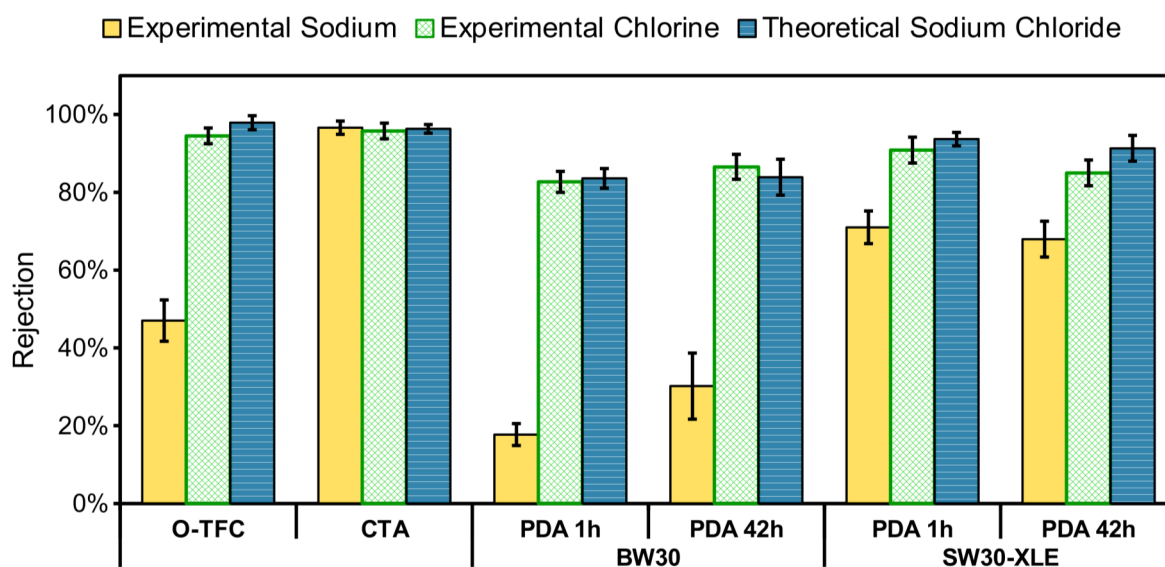


Fig. 6.4. Experimentally observed sodium and chloride rejections with theoretical sodium chloride rejection.

Low cation rejection can be seen for the TFC membranes shown in Fig. 6.4. Of the TFC membranes studied the PDA modified SW30-XLE membrane has the highest observed sodium rejection. The other TFC membranes had 20% (O-TFC), 30% (PDA 42h BW30), and 50% (PDA 1h BW30) lower sodium rejections than did the SW30-XLE membranes. The lower sodium rejections observed for the PDA modified BW30 as compared to the SW30-XLE is discussed in Chapter 5.²⁷ The higher sodium rejections for the PDA modified SW30-XLE membrane is interesting since this membrane has a similar solute permeability but lower water permeance and lower FO water flux. This suggests there may be a connection between rate of cation transport and water permeance. Where high water permeance allow for higher water flux at a certain transmembrane osmotic pressure difference these selective layers may also contain higher concentrations of functional groups which contribute cation exchange. This relationship would be specifically relevant to TFC membrane's synthesized from a diamine and triacyl chloride such as the TFC membranes studied here.^{43,44}

In contrast to the low sodium rejections observed for the TFC membranes the chloride rejections of all CTA and TFC membranes was in agreement with the theoretical rejections calculated. This helps to illustrate the usefulness of theoretical rejection in analyzing the impact

of ion exchange on decreasing feed solute rejection, since it can reasonably and easily predict the approximate rejection of a feed solute absent any interactions with draw solutes and/or the membrane.

6.4. Conclusions

Of two possible mechanisms hypothesized for the cation exchange between the sodium chloride feed and $\text{NH}_3\text{-CO}_2$ draw solutions. The first is reliant upon the existence of the chemical equilibrium amongst ammonia species within the draw solution²⁷. The equivalent ion fluxes of sodium and chloride when testing for the CTA membrane does imply that this phenomena is not likely the mechanism for the observed ion exchange; however, there should still be some uncertainty since the hydrolysis of CTA would produce acetate anions.²⁵ These anions could possibly balance the electroneutrality difference between the draw and feed solutions. The second mechanism for cation exchange would be the polyamide functioning as a cation exchanger from its carboxylic acid functional groups. Deprotonation of carboxylic acids functional groups of polyamide are available cation exchange sites within the polyamide layer. This functionality of the polyamide would permit the movement of cations between the feed and draw solutions.²⁷

Absent data for the forward flux of the feed solute anions the detrimental effects of cation exchange on feed solute rejection could also have been examined with a comparison of the theoretical sodium chloride rejection and those observed experimentally providing the ability to study cation transport when using a feed and draw solute having a common anion or cation.

References

1. Cath, T. Y.; Childress, A. E.; Elimelech, M. Forward osmosis: Principles, applications, and recent developments. *J. Membr. Sci.* **2006**, *281*, 70-87.
2. Hoover, L. A.; Phillip, W. A.; Tiraferri, A.; Yip, N. Y.; Elimelech, M. Forward with Osmosis: Emerging Applications for Greater Sustainability. *Environ. Sci. Technol.* **2011**, *45*, 9824-9830.
3. Kravath, R. E.; Davis, J. A. Desalination of sea water by direct osmosis. *Desalination* **1975**, *16*, 151-155.
4. Kessler, J.; Moody, C. Drinking water from sea water by forward osmosis. *Desalination* **1976**, *18*, 297-306.
5. McCutcheon, J. R.; McGinnis, R. L.; Elimelech, M. A novel ammonia-carbon dioxide forward (direct) osmosis desalination process. *Desalination* **2005**, *174*, 1-11.
6. McCutcheon, J. R.; McGinnis, R. L.; Elimelech, M. Desalination by ammonia-carbon dioxide forward osmosis: Influence of draw and feed solution concentrations on process performance. *J. Membr. Sci.* **2006**, *278*, 114-123.
7. Ling, M. M.; Chung, T.-S. Desalination process using super hydrophilic nanoparticles via forward osmosis. *Desalination* **2011**, *278*, 194-202.
8. Stone, M. L.; Rae, C.; Stewart, F. F.; Wilson, A. D. Switchable polarity solvents as draw solutes for forward osmosis. *Desalination* **2013**, *312*, 124-129.

9. Carmignani, G.; Sitkiewitz, S.; Webley, J. W. Recovery of retrograde soluble solute for forward osmosis water treatment. US 2012/0267308 A1, October 25, 2012.
10. Achilli, A.; Cath, T. Y.; Childress, A. E. Selection of inorganic-based draw solutions for forward osmosis applications. *J. Membr. Sci.* **2010**, *364*, 233-241.
11. McGinnis, R. L. Osmotic Desalinization Process. US 6,391,205 B1, May 21, 2002.
12. McGinnis, R. Osmotic Desalination Process. US 8,753,514 B2, June 17, 2014.
13. Cath, T. Y.; Hancock, N. T.; Lundin, C. D.; Hoppe-Jones, C.; Drewes, J. E. A multi-barrier osmotic dilution process for simultaneous desalination and purification of impaired water. *J. Membr. Sci.* **2010**, *362*, 417-436.
14. Hancock, N. T.; Black, N. D.; Cath, T. Y. A comparative life cycle assessment of hybrid osmotic dilution desalination and established seawater desalination and wastewater reclamation process. *Water Res.* **2012**, *46*, 1145-1154.
15. McGinnis, R. L.; Elimelech, M. Energy requirements of ammonia-carbon dioxide forward. *Desalination* **2007**, *207*, 370-382.
16. McGinnis, R. L.; Hancock, N. T.; Nowosielski-Slepowron, M. S.; McGurgan, G. D. Pilot Demonstration of the NH₃/CO₂ forward osmosis desalination process on high salinity brines. *Desalination* **2013**, *312*, 67-74.
17. Neff, R. A. Solvent extractor. US 3,130,156 A, April 21, 1964.
18. Herron, J. Asymmetric forward osmosis membranes. United States Patent No. US 7,445,712, Nov. 4, 2008.
19. Cath, T. Y.; Adams, D.; Childress, A. E. Membrane contactor processes for wastewater reclamation in space II. Combined direct osmosis, osmotic distillation, and membrane distillation for treatment of metabolic wastewater. *J. Membr. Sci.* **2005**, *257*, 111-119.
20. Chung, T.-S.; Zhang, S.; Wang, K. Y.; Su, J.; Ling, M. M. Forward osmosis processes: Yesterday, today, and tomorrow. *Desalination* **2012**, *287*, 78-81.
21. Cath, T. Y.; Gormly, S.; Beaudry, E. G.; Flynn, M. T.; Adams, V. D.; Childress, A. E. Membrane contactor processes for wastewater reclamation in space Part I. Direct osmotic concentration as pretreatment for reverse osmosis. *J. Membr. Sci.* **2005**, *257*, 85-98.

22. Ge, Q.; Su, J.; Chung, T.-S.; Amy, G. Hydrophilic Superparamagnetic Nanoparticles: Synthesis, Characterization, and Performance in Forward Osmosis Processes. *Ind. Eng. Chem. Res.* **2011**, *50*, 382-288.
23. She, Q.; Jin, X.; Tang, C. Y. Osmotic power production from salinity gradient resource by pressure retarded osmosis: Effects of operating conditions and reverse solute diffusion. *J. Membr. Sci.* **2012**, *401-402*, 262-273.
24. Baker, R. W. *Membrane Technology and Applications*, 2nd ed; John Wiley & Sons Ltd: West Sussex, England, 2004.
25. Vos, K. D.; Burris, F. O.; Riley, R. L. Kinetic Study of the Hydrolysis of Cellulose Acetate in the pH Range of 2-10. *J. Appl. Polym. Sci.* **1966**, *10*, 825-832.
26. Watters, J. C.; Klein, E.; Fleischman, M.; Roberts, J. S.; Hall, B. Rejection Spectra of Reverse Osmosis Membranes Degraded by Hydrolysis of Chlorine Attack. *Desalination* **1986**, *60*, 93-110.
27. Arena, J. T.; Manickam, S. S.; Reimund, K. K.; Freeman, B. D.; McCutcheon, J. R. Solute and water transport in forward osmosis using polydopamine modified thin film composite membranes. *Desalination* **2014**, *343*, 8-16.
28. Arena, J. T.; McCloskey, B.; Freeman, B. D.; McCutcheon, J. R. Surface modification of thin film composite membrane support layers with polydopamine: Enabling use of reverse osmosis membranes in pressure retarded osmosis. *J. Membr. Sci.* **2011**, *375*, 55-62.
29. Jeffrey, G. H.; Bassett, J.; Mendham, J.; Denny, R. C. *Vogel's Textbook of Quantitative Chemical Analysis*, 5th ed.; Longman Scientific & Technical: Essex, England, 1989.
30. Harris, D. C. *Quantitative Chemical Analysis*, 6th ed.; W.H. Freeman and Company: New York, 2003.
31. McCabe, W. L.; Smith, J. C.; Harriot, P. *Unit Operations of Chemical Engineering*, 7th Edition ed.; McGraw-Hill: New York, 2005.
32. Kawazuishi, K.; Prausnitz, J. M. Correlation of Vapor-Liquid Equilibria for the System of Ammonia-Carbon Dioxide-Water. *Ind. Eng. Chem. Res.* **1987**, *26*, 1482-1485.

33. Edwards, T. J.; Maurer, G.; Newman, J.; Prausnitz, J. M. Vapor-Liquid Equilibria in Multicomponent Aqueous Solutions of Volatile Weak Electrolytes. *AIChE J.* **1978**, *24*, 966-976.
34. Pawlikowski, E. M.; Newman, J.; Prausnitz, J. M. Phase Equilibria for Aqueous Systems of Ammonia and Carbon Dioxide. *Ind. Eng. Chem. Proc. Des. Dev.* **1982**, *21*, 764-770.
35. Buetler, D.; Renon, H. Representation of $\text{NH}_3\text{-H}_2\text{S-H}_2\text{O}$, $\text{NH}_3\text{-CO}_2\text{-H}_2\text{O}$, and $\text{NH}_3\text{-SO}_2\text{-H}_2\text{O}$ Vapor-Liquid Equilibria. *Ind. Eng. Chem. Proc. Des. Dev.* **1978**, *17*, 220-230.
36. Robinson, R. A.; Stokes, R. H. *Electrolyte Solutions*, 2nd ed.; Dover Publications: Mineola, 2002.
37. Prausnitz, J. M.; Lichtenthaler, R. N.; de Azevedo, E. G. *Molecular Thermodynamics of Fluid-Phase Equilibria*, 3rd ed.; Prentice-Hall, Inc.: Upper Saddle River, 1999.
38. Grattoni, A.; Merlo, M. Osmotic Pressure beyond Concentration Restrictions. *J. Phys. Chem. Part B* **2007**, *111*, 11770-11775.
39. Anastasio, D. D.; Arena, J. T.; Cole, E. A.; McCutcheon, J. R. Impact of temperature on power density in closed-loop pressure retarded osmosis for grid storage. *J. Membr. Sci.* **2015**, *479*, 240-245.
40. Bui, N. N.; Arena, J. T.; McCutcheon, J. R. Proper accounting of mass transfer Resistances in forward osmosis: Improving the Accuracy of model Predictions of structural parameter. *J. Membr. Sci.* **2015**, *492*, 289-302.
41. Cath, T. Y.; Elimelech, M.; McCutcheon, J. R.; McGinnis, R. L.; Achilli, A.; Anastasio, D.; Brady, A. R.; Childress, A. E.; Farr, I. V.; Hancock, N. T.; Lampi, J.; Nghiem, L. D.; Xie, M.; Yip, N. Y. Standard Methodology for Evaluating Membrane Performance in Osmotically Driven Membrane Processes. *Desalination* **2013**, *312*, 31-38.
42. Hesske, H.; Gloe, K. Hydration Behavior of Alkyl Amines and Their Corresponding Protonated Forms. 1. Ammonia and Methylamine. *J. Phys. Chem.* **2007**, *111*, 9848-9853.
43. Dow Water and Process Solutions. FILMTEC™ Reverse Osmosis Membranes Technical Manual, Form No. 609-00071-1009. http://msdssearch.dow.com/PublishedLiteratureDOWCOM/dh_08db/0901b803808db77d.pdf.

44. McGinnis, R.; McGurgan, G. Forward osmosis membranes. United States Patent No. US 8,181,794, May 22, 2012.
45. McGinnis, R. L.; Elimelech, M. Global challenges in energy and water supply: the promise of engineered osmosis. *Environ. Sci. Technol.* **2008**, *42*, 8625-8629.
46. Klaysom, C.; Cath, T. Y.; Depuydt, T.; Vankelecom, I. F. J. Forward and pressure retarded osmosis: potential solutions for global challenges in energy and water supply. *Chem. Soc. Rev.* **2013**, *42*, 6959-5989.
47. Garcia-Castello, E. M.; McCutcheon, J. R. Dewatering press liquor derived from orange production by forward osmosis. *J. Membr. Sci.* **2011**, *372*, 97-101.
48. McGinnis, R. L.; McCutcheon, J. R.; Elimelech, M. A novel ammonia-carbon dioxide osmotic heat engine for power generation. *J. Membr. Sci.* **2007**, *305*, 13-19.
49. Straub, A. P.; Yip, N. Y.; Elimelech, M. Raising the Bar: Increased Hydraulic Pressure Allows Unprecedented High Power Densities in Pressure-Retarded Osmosis. *Environ. Sci. Technol. Lett.* **2014**, *1*, 55-59.
50. Bui, N. N.; Lind, M. L.; Hoek, E. M. V.; McCutcheon, J. R. Electrospun nanofiber supported thin film composite membranes for engineered osmosis. *J. Membr. Sci.* **2011**, *385-386*, 10-19.
51. Bui, N. N.; McCutcheon, J. R. Hydrophilic Nanofibers as New Supports for Thin Film Composite Membranes for Engineered Osmosis. *Environ. Sci. Technol.* **2013**, *47*, 1761-1769.
52. Ren, J.; McCutcheon, J. R. A new commercial thinfilm composite membrane for forward osmosis. *Desalination* **2014**, *343*, 187-193.
53. Wang, R.; Shi, L.; Tang, C. Y.; Chou, S.; Qui, C.; Fane, A. G. Characterization of novel forward osmosis hollow fiber membranes. *J. Membr. Sci.* **2010**, *355*, 158-167.
54. Yip, N. Y.; Tiraferri, A.; Phillip, W. A.; Schiffman, J. D.; Elimelech, M. High Performance Thin Film Composite Forward Osmosis Membrane. *Environ. Sci. Technol.* **2010**, *44*, 3812-3818.

55. Song, X.; Lui, Z.; Sun, D. D. Nano Gives the Answer: Breaking the Bottleneck of Internal Concentration Polarization with a Nanofiber Composite Forward Osmosis Membrane for a High Water Production Rate. *Adv. Mater.* **2011**, *23*, 3256-3260.
56. Huang, L.; McCutcheon, J. R. Hydrophilic nylon 6,6 nanofibers supported thin film composite membranes for engineered osmosis. *J. Membr. Sci.* **2014**, *457*, 162-169.
57. Hoover, L. A.; Schiffman, J. D.; Elimelech, M. Nanofibers in thin-film composite membrane support layers: Enabling expanded application of forward and pressure retarded osmosis. *Desalination* **2013**, *308*, 73-81.
58. Coday, B. D.; Heil, D. M.; Xu, P.; Cath, T. Y. Effects of Transmembrane Hydraulic Pressure on Performance of Forward Osmosis Membranes. *Environ. Sci. Technol.* **2013**, *47*, 2386-2393.
59. Bui, N. N.; McCutcheon, J. R. Nanofiber Supported Thin-Film Composite Membrane for Pressure-Retarded Osmosis. *Environ. Sci. Technol.* **2014**, *48*, 4129-4136.
60. Achilli, A.; Cath, T. Y.; Childress, A. E. Power generation with pressure retarded osmosis: An experimental and theoretical investigation. *J. Membr. Sci.* **2009**, *343*, 42-52.
61. Han, G.; Zhang, S.; Li, X.; Chung, T. S. High performance thinfilm composite pressure retarded osmosis (PRO) membranes for renewable salinity-gradient energy generation. *J. Membr. Sci.* **2013**, *440*, 108-121.
62. Song, X.; Lui, Z.; Sun, D. D. Energy recovery from concentrated seawater brine by thin-film nanofiber composite pressure retarded osmosis membranes with high power density. *Energy Environ. Sci.* **2013**, *6*, 1199-1210.

Chapter 7

pH sensitivity of ion exchange through a commercial thin film composite membrane in forward osmosis

Arena et al. *Environ. Sci. Technol. Lett.* **2015**, *2*, 177-182. doi:10.1021/acs.estlett.5b00138

7.1. Introduction

Forward osmosis (FO) processes use an osmotic pressure gradient to drive water flux across a semipermeable membrane.¹⁻³ A critical part of FO process design is draw solute selection.⁴⁻¹¹ In a FO process, suitable draw solutes need both high solubility and diffusivity to effectively exert osmotic pressure across asymmetric semipermeable membranes. Electrolyte draw solutes have become common in many large-scale applications of FO processes.²⁻¹⁴ Opposite draw solute selection in FO process design is membrane selection. Membranes tailored for FO need to have high permselectivity and a low structural parameter to allow for efficient water transport across an asymmetric membrane.^{15,16} Cellulose triacetate (CTA) was used to form the first membrane designed specifically for FO.^{4,17,18} In an effort to improve

performance, thin film composite (TFC) membranes have been introduced as a new platform for FO membrane design.^{2,19,20} Among the advantages of TFC membranes is the higher water permeance at similar selectivities and hydrolytic stabilities.^{21,22}

The polyamide selective layer of a TFC membrane is commonly made from the reaction of trimesoyl chloride (TMC) and m-phenylenediamine (MPD).²³ The reaction yields a partially cross-linked structure with the TMC monomer forming two or three amide bonds.²⁴ TMC monomers that form only two amide bonds have a third acyl chloride that does not form an amide bond.^{24,25} This remaining acyl chloride group later hydrolyzes to a carboxylic acid. Carboxylic acid functional groups deprotonate at alkaline pH, imparting a negative charge that may facilitate the transport of cations through the polyamide.^{26,27} In reverse osmosis (RO) membranes using this chemistry, the charge aids in salt rejection because the negative charge repels anions (like chloride). Charge neutrality requires that the membrane need reject only one ion because cations cannot cross without their counterion. In FO processes that employ an electrolyte draw solution, cations from the feed solution may move across the negatively charged polyamide without their counterion, maintaining electroneutrality by exchanging with cations within the draw solution.^{18,26,28}

Evidence of cation exchange is observed as disparate forward cation and anion fluxes or high forward and reverse flux of a single ionic species. This behavior has been observed under neutral and alkaline conditions between monovalent cations.^{18,26,28} A similar ion exchange behavior has been observed for the CTA membrane with anions when the draw or feed solution contains nitrate.^{29,30} One notable study by Lu et al. found some of the sensitivity of these functional groups to pH differences across a thin film composite membrane using ammonium chloride as a draw solute and a feed solution of sodium chloride at pH 3 and 6. Ammonium chloride in solution has a pH of 4.5. Ion exchange observed occurring across the commercial FO membrane did so with a pH gradient across the membrane. This caused the draw solution to have a pH below and the feed solutions to have a pH above the pKa of the carboxylic acid functional groups.²⁸ Elsewhere, pH gradients across the cellulose triacetate FO membrane have been seen to influence the transport of propanoic acid into a feed solution of deionized water with the sharpest difference in propionic acid transport occurring over a narrow pH range (i.e. $\text{pH} = \text{pKa} \pm 2$).³¹ This means that a pH gradient present across the membrane's selective layer with a weak electrolyte may influence cation transport through its permeation of the selective layer as a neutral species (i.e. as ammonia) and with the pH

gradient causing speciation back to ammonium and forcing the transport of sodium in a mechanism hypothesized by Arena et al.²⁶

To date, no study has included a systematic observation of forward and reverse cation transport in the absence of a pH gradient across the membrane using strong acid/strong base electrolytes. The choice of strong acid/strong base electrolytes eliminates the existence of neutral species and allows for pH control by buffering the feed and draw solutions to influence membrane properties. The objective of this study is to concretely show that cation/membrane interactions are the driving force of cation exchange in forward osmosis.

7.2. Materials and Methods

7.2.1. Materials

The membrane used in this study is a commercial TFC FO membrane from Hydration Technology Innovations (HTI). This membrane is later termed TFC. The feed and draw solutes used in this study were sodium chloride and potassium chloride (Fisher Scientific, Pittsburgh, PA). The draw and feed solutions were buffered using Bistris and CAPS buffer purchased from Fisher Scientific, citric acid monohydrate purchased from Acros Organics (Geel, Belgium), and Tris buffer purchased from Sigma-Aldrich (St. Louis, MO). The pH was adjusted using

hydrochloric acid (Sigma-Aldrich), potassium hydroxide (Acros Organics), and sodium hydroxide (Fisher Scientific). Water used in this study was ultrapure Milli-Q (18.2 MΩ) water produced by a Millipore Integral 10 water system (Millipore Corp., Billerica, MA).

7.2.3. Evaluation of membrane physicochemical properties

7.2.3.1. Scanning electron microscopy

The top and cross-section images of the TFC membrane, coated with a thin layer of gold, were obtained using a JEOL 6335F field emission scanning electron microscope (JEOL USA, Inc., Peabody, MA). To obtain cross sectional images, the membrane was soaked in ethanol, followed by hexane, and immersed in liquid nitrogen. While frozen, the membrane was fractured, and the woven mesh was cut closely to the fractured edge.

7.2.3.2. Fourier transform infrared spectroscopy

The TFC membrane was evaluated using FTIR to identify key functional groups of the membrane's selective layer and verify the presence of a polyamide selective layer. The FTIR analysis was performed on a dried membrane sample using A Thermo Scientific (Waltham, MA) Nicolet iS10 FTIR spectrometer with a Smart iTR attachment. Measurements were taken of the membrane's selective layer using 64 scans with a resolution of 4 cm⁻¹.

Table 7.1. Conditions of the varying draw and feed solutions used in this study.

Solution pH	1.0 M KCl draw solution		Buffer only feed solution		0.1 M NaCl feed solution	
	Buffer	pH Adjustor	Buffer	pH Adjustor	Buffer	pH Adjustor
2	0.1 M CA	HCl	0.1 M CitA	HCl	0.1 M CA	HCl
4	0.1 M CA	KOH	0.1 M CA	KOH	0.1 M CA	NaOH
6	0.1 M Bistris	HCl	0.1 M Bistris	HCl	0.1 M Bistris	HCl
8	0.1 M Tris	HCl	0.1 M Tris	HCl	0.1 M Tris	HCl
10	0.1 M CAPS	KOH	0.1 M CAPS	KOH	0.1 M CAPS	NaOH

7.2.4. Testing of ion transport in forward osmosis

7.2.4.1. Draw and feed solution preparation

Conditions for the draw and feed solutions are a reflection the test methodology used within this study. pH across the membrane was controlled by the buffering of the draw and feed solutions. To cover the range of pH desired for study four different buffers were selected: citric acid (CA), Bis(2-hydroxyethyl)iminotris(hydroxymethyl)methane (Bistris), Tris(hydroxymethyl)aminomethane (Tris), and 3-Cyclohexylamino-1-propanesulfonic acid (CAPS). CA was used to buffer the pH 2 and pH 4 test and has a pK_1 and pK_2 of 3.13 and 4.76 respectively.³⁴ Bistris was used to buffer the pH 6 test and has a pK_1 of 6.46. Tris was used to buffer the pH 8 test and has a pK_1 of 8.08. CAPS was used to buffer the pH 10 test

and has a pK_1 of 10.40.⁵¹ For tests performed at a pH 2, 6, and 8 hydrochloric acid (HCl) was added to the feed and draw solutions to lower the pH to their desired values.

Test performed at pH 4 and 10 required a strong base be added to the buffer to increase the pH to desired values. Potassium hydroxide (KOH) was selected to adjust the pH of the 1.0 M potassium chloride (KCl) draw solution and a feed solution consisting of only buffer. While the addition of KOH to the feed solution required measurement of the initial potassium concentration, only this selection would ensure that only a concentration gradient of common cations existed between the draw and feed solutions. The use of a strong base containing other cations may influence the observed reverse flux of potassium occurring at the beginning of FO tests. For the part of the FO tests where the feed solution had a concentration of 0.1 M sodium chloride (NaCl), sodium hydroxide (NaOH) was the strong base added to increase the pH of the feed solution. The concentration of NaCl within the feed solution was increased by the addition of a 0.5 M NaCl solution having a buffer concentration of 0.01 M. Adjusting the pH of the buffered NaCl stock solution with NaOH as opposed to KOH was done to simplify bookkeeping by not altering the potassium concentration within the feed during the addition of NaCl to increase the feed NaCl concentration. A summary of the buffer, pH adjustor, draw, and

feed solution concentrations is shown in Table 7.1.

7.2.4.1. Forward osmosis testing

The feed and draw solutions were buffered at identical pH values of 2, 4, 6, 8, and 10. Potassium chloride was selected as a model draw solute to serve as an analogue for draw solutions proposed for forward osmosis processes.^{4,7,15,26,32} Using potassium chloride eliminates a draw solute which contains a weak acid or weak base and ensures easy quantification using atomic absorption spectroscopy.^{33,34}

Forward osmosis tests were performed on a laboratory-scale FO system using a buffered draw solution of 1.0 M potassium chloride with feed solutions of only buffer and buffered 0.1 M sodium chloride. These solutions were circulated counter-current in bench-scale forward osmosis test systems with a cross-flow velocity of $0.25 \text{ m}\cdot\text{s}^{-1}$ at $20\pm0.5 \text{ }^{\circ}\text{C}$. For these tests, the membrane support layer was in contact with the potassium chloride draw solution (FO mode).³² Water flux and reverse potassium flux were observed sequentially for feed solutions consisting of only buffer and 0.1 M buffered sodium chloride. Forward sodium flux was observed when the feed solution was buffered 0.1 M sodium chloride. FO experiments were begun by

monitoring water flux across the membrane using a feed solution of buffer only. After the first hour, the feed solution was adjusted to a sodium chloride concentration of 0.1 M. Water flux was monitored for at least an additional 2 h using the buffered 0.1 M sodium chloride feed solution.

7.2.4.2. Measurement of ion concentrations

The feed and draw solutions were analyzed for potassium and sodium concentration, respectively. Samples were extracted prior to the addition of sodium chloride to the feed solution and at the end of the test. Initial samples of the feed solution were taken when potassium hydroxide was needed to adjust the pH (i.e., the pH 4 and 10 tests). Potassium and sodium concentrations were measured by direct aspiration atomic absorption (AA) spectrophotometry on a Thermo Scientific ICE 3000 atomic absorption spectrometer (Thermo Scientific, Nashua, NH) equipped with a combination potassium/sodium hollow cathode lamp. The solutions were analyzed according to U.S. Environmental Protection Agency method 700B, which has lower detection limits of 0.01 and 0.002 mg·L⁻¹ and sensitivities of 0.04 and 0.015 mg·L⁻¹ for potassium and sodium, respectively.³⁵ Some samples required significant dilution so that they were in the measurable range of the instrument. The measured

concentrations of sodium and potassium within these solutions were used to determine the total mass of potassium within the feed and sodium within the draw. The change in mass was divided by the time interval between sample extraction, molar mass, and membrane surface area to calculate the forward (in the direction of water flux) sodium and reverse (opposite the direction of water flux) potassium molar fluxes.

7.3. Results and Discussions

7.3.1. Membrane physicochemical properties

Fig 7.1 shows the chemical and morphological characteristics of the membrane used in this study. The TFC membrane's selective layer has an FTIR spectrum that has been characteristically attributable to a fully aromatic polyamide.^{38,39} This membrane shares peaks that have been noted previously by Ren and McCutcheon at 1655, 1610, and 1545 cm^{-1} (Fig. 7.1b) for an earlier iteration of this TFC FO membrane.¹⁹ Additionally, the available patent literature states that the polymerized selective layer consisted of m-phenylenediamine (MPD) and trimesoyl chloride (TMC),³⁶ further suggesting the presence of carboxylic acid functional groups characteristically present within the partially cross-linked structure of a TFC membrane's polyamide.³⁷ The carboxylic acid functional group would give this membrane an isoelectric

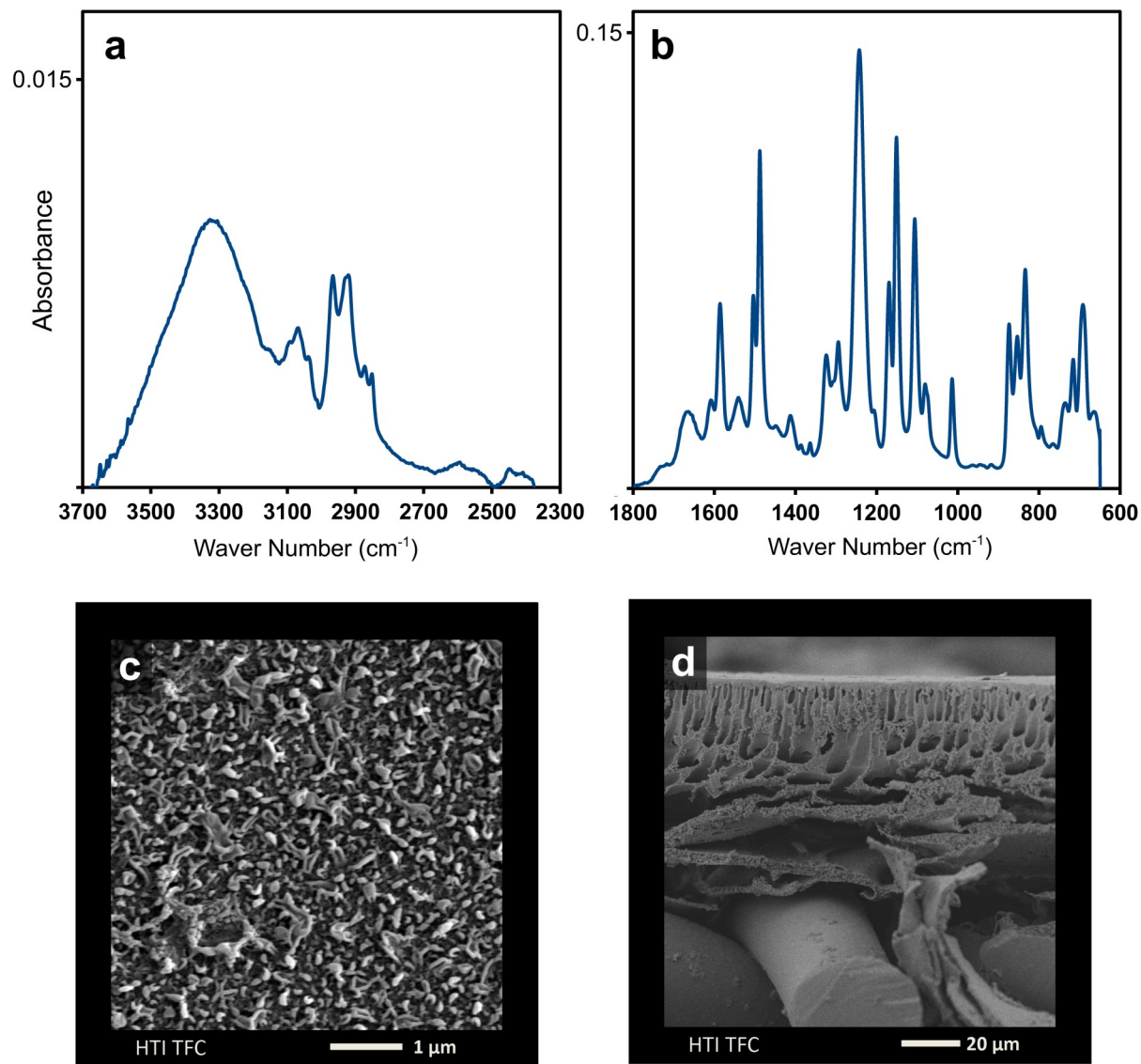


Fig. 7.1. FTIR spectra of HTI's TFC FO membrane at wave numbers of 2300-3700 cm^{-1} (a) and 600-1800 cm^{-1} (b). SEM images of the structure of the HTI TFC membrane's selective layer (c), support layers (d).

point around pH 5 that has been observed by Tang et al., who characterized different permselective RO membranes in streaming potential.³⁸ In addition to the FTIR spectra, the TFC also possesses the rough surface morphology that has been noted in other studies characterizing the polyamide selective layers of TFC membranes for both forward and reverse osmosis (Fig. 7.1c).^{19,40} In addition to the selective layer structure, the cross section of this membrane shows a fingerlike pore morphology shown to be desirable in FO membrane structure (Fig. 7.1d).⁴¹⁻⁴³

7.3.1.2 Comparison of gen 1 and gen 2 TFC FTIR spectra

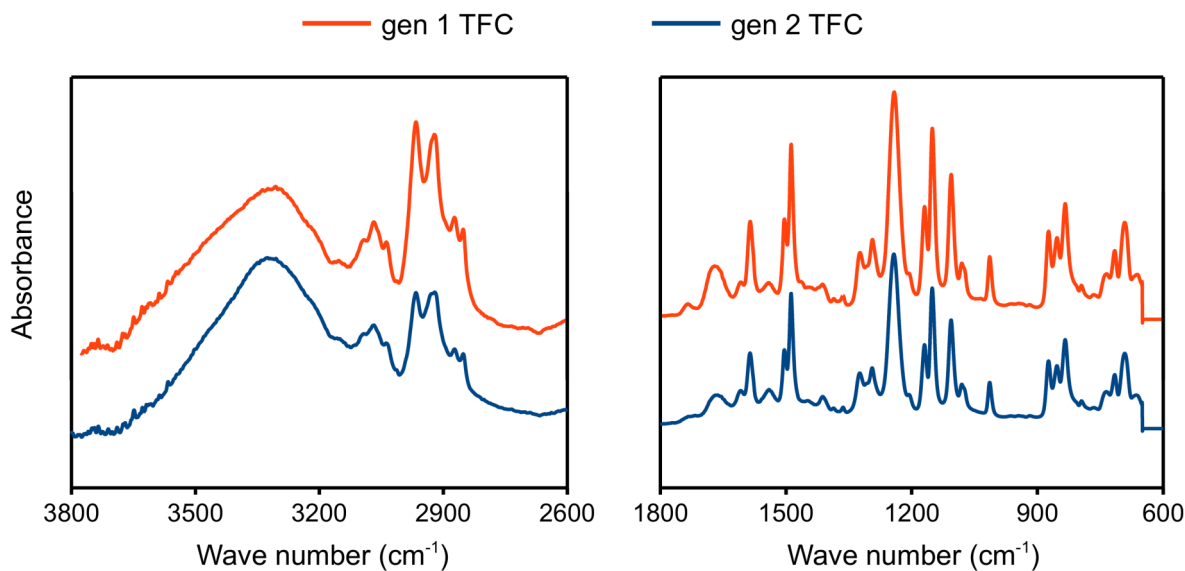


Fig. 7.2. FTIR spectra comparing HTI's gen TFC¹⁹ to the gen 2 TFC.

Fig. 7.2. Shows the nearly identical spectra of HTI's 2nd generation (gen 2 TFC) thin film composite (TFC) membrane used in this study under FTIR with the 1st generation of HTI's TFC membrane (gen 1 TFC) previously studied by Ren and McCutcheon.¹⁹ This shows the common chemistry lineage of these two membrane structures and as mentioned by Ren and McCutcheon¹⁹ and Coday et al.¹⁸ this membrane is a polyamide thin film composite, which according to available patent literature³⁶ is prepared from the interfacial polymerization of the conventional TFC reverse osmosis membrane monomers those being m-phenylenediamine (MPD) and trimesoylchloride (TMC).^{23,37} The usage of the MPD-TMC chemistry in the selective layer preparation means that the selective layer of these membranes will possess some carboxylic acid functionality.

7.3.2. pH dependence of water and ion flux in forward osmosis

The water and solute fluxes across the TFC as affected by draw and feed solution pH are shown in Fig. 7.3 and Fig. 7.4. These data encompass a number of interesting findings in both contradiction and agreement with those previously reported. Water flux did not change significantly with pH, coinciding with behavior that has been observed for polyamide TFC membranes in RO.^{37,44} These same studies noted an increase in the level of sodium chloride

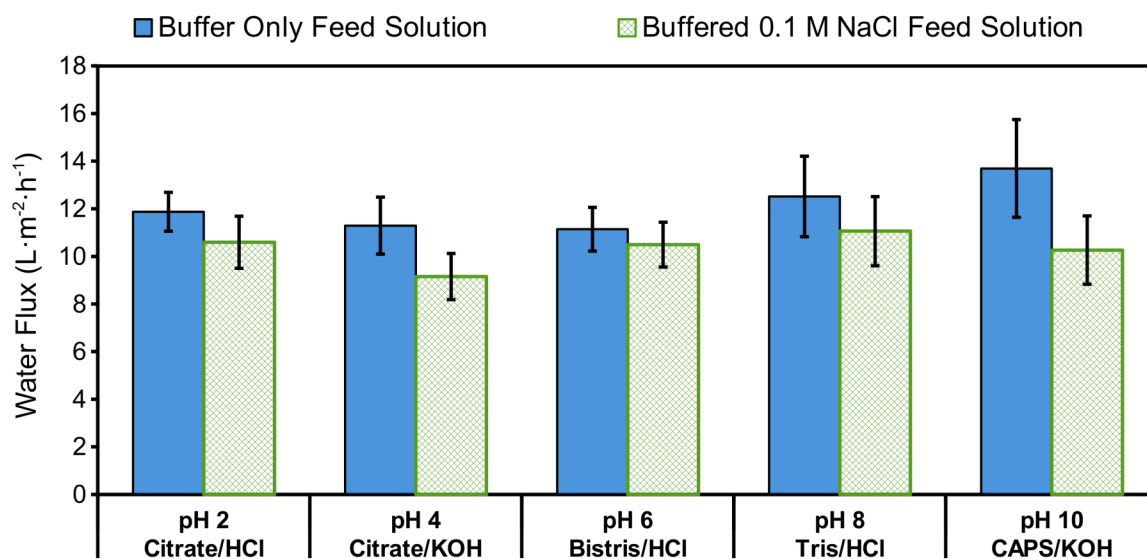


Fig. 7.3. Observed water flux for a 1.0 M potassium chloride draw solution using feed solution of only buffer and buffered 0.1 M sodium chloride at a pH of 2-10 (a). Temperature 20°C and 0.25 m·s⁻¹ cross-flow velocity.

rejection (decreased solute permeability) at more alkaline pH values.^{37,44} When this is translated to FO, a decrease in solute permeability would also decrease the reverse solute flux.⁴⁵ Potassium reverse flux for a feed solution of only buffer appears to follow no clear trend with respect to pH (Fig. 7.4a). It remains statistically flat from pH 2 to 8, only showing a significant increase at pH 10. This contradicts any premise that the solute permeability of this membrane should decrease with an increase in pH, as a decrease in solute permeability should also decrease the reverse solute flux of potassium. The potassium reverse flux represents potassium chloride flux when the feed solution contains only buffer. There is no

buffer concentration difference between the feed and draw solutions, so potassium that crosses the membrane selective layer must carry chloride with it to maintain electroneutrality between the feed and draw solution.^{18,29,46,47}

There is only a slight decrease in water flux upon addition of sodium chloride to the feed solution. This parallels more significant drops in water flux noted upon comparison of water flux observed with a feed solution of deionized water to water flux observed with a 0.25 M sodium chloride using the ammonia/carbon dioxide draw solution.²⁶ The lack of a substantial drop in water flux upon addition of sodium chloride to the feed is likely due to the buffer within the feed

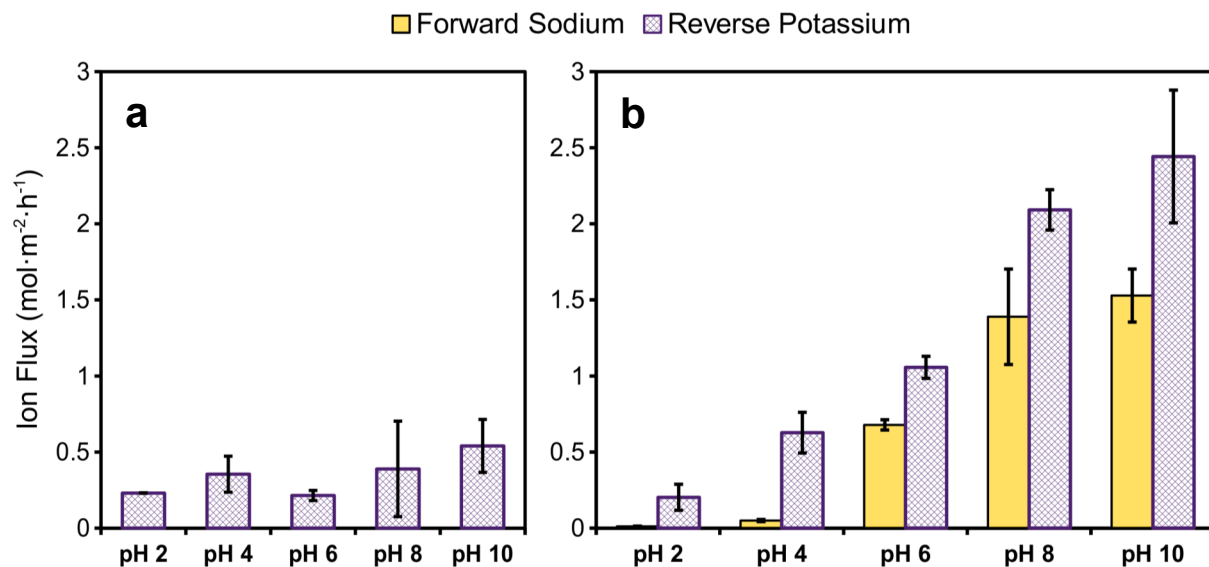


Fig. 7.4. Observed ion flux for a 1.0 M potassium chloride draw solution using a feed solution of only buffer (a) and buffered 0.1 M sodium chloride (b). Temperature 20°C and $0.25 \text{ m} \cdot \text{s}^{-1}$ cross-flow velocity.

solution. Although the bulk buffer concentrations are equivalent, they do exert osmotic pressure and more importantly are impacted by external concentration polarization (ECP). ECP will reduce flux by increasing the buffer selective layer concentration, reducing the osmotic pressure difference across the membrane. This makes for a less noticeable drop in water flux when the feed solution is changed from only buffer to a buffered 0.1 M sodium chloride solution.

Large differences can be observed in the forward solute flux of sodium and reverse solute flux of potassium with increasing pH. Sodium flux at pH 2 and 4 is 2 orders of magnitude lower than sodium fluxes are at pH 10. This change must be strongly influenced by carboxylic acid functional groups within the selective layer. Polyamide selective layers that have been analyzed by ζ potential show neutral charges between pH 4 and 6.^{27,28,48,49} Similar results have been noted by contact angle titration, which measures the contact angle of a buffered solution dropped onto a polyamide.^{48,50} As the pH increases, carboxylic acid functional groups become deprotonated ($-\text{COOH}$ becomes $-\text{COO}^-$), increasing negative charges on the membrane's surface. If homogeneity within the polyamide is assumed, increasing negative charges on the selective layer surface would correspond to increasing negative charges within the

membrane's selective layer, because the pH is constant on both sides of the selective layer.

The increasing number of negative charges will increase the extent of cation transport across

the polyamide. This is demonstrated in Fig. 7.4b where a sharp increase in forward and

reverse cation flux is observed at higher pH. Cation transport will be limited by the available

negative charges within the polyamide (to maintain local electroneutrality). The physical

structure of the polyamide will impose a limit on the rate of cation exchange across the

polyamide (by the number of carboxylic acid functional groups in the polyamide structure).

Such a maximum may occur at $\text{pH} > 8$, as forward and reverse cation flux are statistically

similar between $\text{pH} 8$ and 10 (Fig. 7.4b).

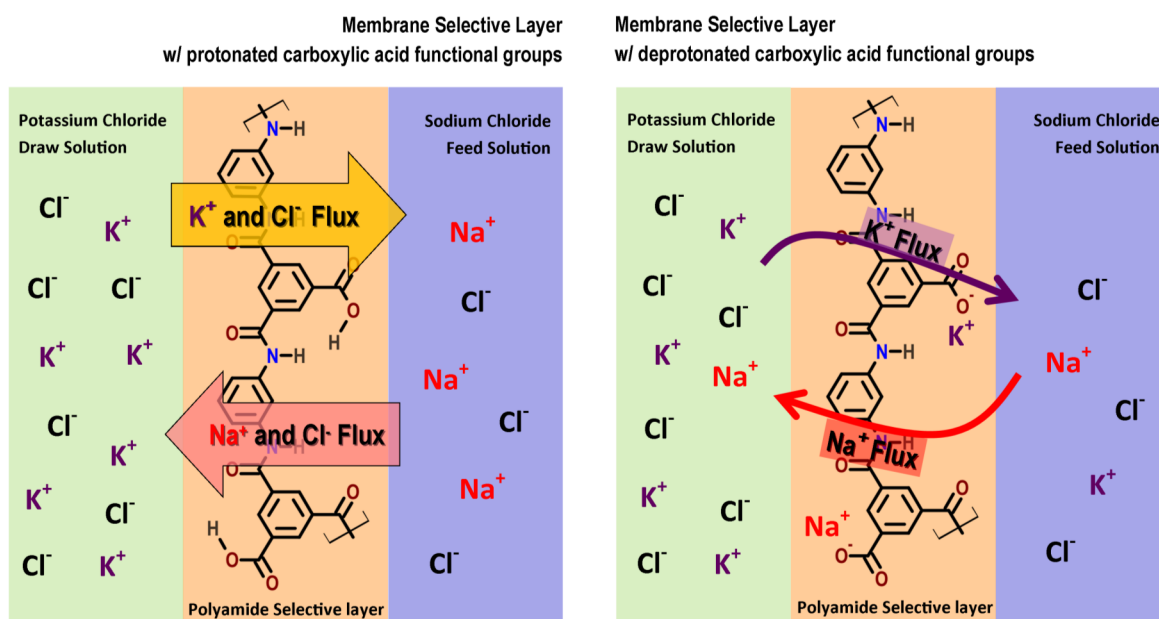


Fig. 7.5. Representation of reverse solute transport vial cation/anion diffusion and cation exchange through a polyamide selective layer.

Potassium flux was higher than the sodium flux across the studied pH range. The difference between the forward sodium flux and reverse potassium flux (Fig. 7.4b) is approximately equivalent to the reverse potassium flux where the feed solution is only buffer (Fig. 7.4a). This indicates that the reverse potassium flux using a buffered 0.1 M sodium chloride feed solution encompasses both Fickian diffusion and facilitated transport between the feed and draw solutions. Dual paths for solute transport create a complicated design challenge in FO membrane selective layer development. Low solute permeabilities (to anion/cation pairs) are needed as well as the development of selective layer chemistries lacking charged functional groups that contribute to ion transport under process conditions.

References

1. Hoover, L. A.; Phillip, W. A.; Tiraferri, A.; Yip, N. Y.; Elimelech, M. Forward with Osmosis: Emerging Applications for Greater Sustainability. *Environ. Sci. Technol.* **2011**, *45*, 9824-9830.
2. Cath, T. Y.; Childress, A. E.; Elimelech, M. Forward osmosis: Principles, applications, and recent developments. *J. Membr. Sci.* **2006**, *281*, 70-87.
3. Chung, T.-S.; Zhang, S.; Wang, K. Y.; Su, J.; Ling, M. M. Forward osmosis processes: Yesterday, today, and tomorrow. *Desalination* **2012**, *287*, 78-81.
4. McCutcheon, J. R.; McGinnis, R. L.; Elimelech, M. A novel ammonia-carbon dioxide forward (direct) osmosis desalination process. *Desalination* **2005**, *174*, 1-11.

5. Achilli, A.; Cath, T. Y.; Childress, A. E. Selection of inorganic-based draw solutions for forward osmosis applications. *J. Membr. Sci.* **2010**, *364*, 233-241.
6. Carmignani, G.; Sitkiewitz, S.; Webley, J. W. Recovery of retrograde soluble solute for forward osmosis water treatment. U.S. Patent 0267308 A1, October 25, 2012.
7. Stone, M. L.; Rae, C.; Stewart, F. F.; Wilson, A. D. Switchable polarity solvents as draw solutes for forward osmosis. *Desalination* **2013**, *312*, 124-129.
8. Ling, M. M.; Chung, T.-S. Desalination process using super hydrophilic nanoparticles via forward osmosis. *Desalination* **2011**, *278*, 194-202.
9. Phuntsho, S.; Shon, H. K.; Majeed, T.; El Saliby, I.; Vigneswaran, S.; Kandasamy, J.; Hong, S.; Lee, S. Blended Fertilizers as Draw Solutions for Fertilizer-Drawn Forward Osmosis Desalination. *Environ. Sci. Technol.* **2012**, *46*, 4567-4575.
10. Kim, T. W.; Kim, Y.; Yun, C.; Jang, H.; Kim, W.; Park, S. Systematic approach for draw solute selection and optimal system design for forward osmosis desalination. *Desalination* **2012**, *284*, 253-260.
11. Kim, T. W.; Park, S.; Yeh, K. Cost-effective design of a draw solution recovery process for forward osmosis desalination. *Desalination* **2013**, *327*, 46-51.
12. Cath, T. Y.; Hancock, N. T.; Lundin, C. D.; Hoppe-Jones, C.; Drewes, J. E. A multi-barrier osmotic dilution process for simultaneous desalination and purification of impaired water. *J. Membr. Sci.* **2010**, *362*, 417-436.
13. Hickenbottom, K. L.; Hancock, N. T.; Hutchings, N. R.; Appleton, E. W.; Beaudry, E. G.; Xu, P.; Cath, T. Y. Forward osmosis treatment of drilling mud and fracturing wastewater from oil and gas operations. *Desalination* **2013**, *312*, 60-66.
14. McGinnis, R. L.; Hancock, N. T.; Nowosielski-Slepowron, M. S.; McGurgan, G. D. Pilot Demonstration of the NH₃/CO₂ forward osmosis desalination process on high salinity brines. *Desalination* **2013**, *312*, 67-74.
15. McCutcheon, J. R.; Elimelech, M. Modeling Water Flux in Forward Osmosis: Implications for Improved Membrane Design. *AIChE J.* **2007**, *53*, 1736-1744.

16. Bui, N. N.; Lind, M. L.; Hoek, E. M. V.; McCutcheon, J. R. Electrospun nanofiber supported thin film composite membranes for engineered osmosis. *J. Membr. Sci.* **2011**, *385-386*, 10-19.
17. Herron, J. Asymmetric forward osmosis membranes. U.S. Patent 7,445,712, November 4, 2008.
18. Coday, B. D.; Heil, D. M.; Xu, P.; Cath, T. Y. Effects of Transmembrane Hydraulic Pressure on Performance of Forward Osmosis Membranes. *Environ. Sci. Technol.* **2013**, *47*, 2386-2393.
19. Ren, J.; McCutcheon, J. R. A new commercial thinfilm composite membrane for forward osmosis. *Desalination* **2014**, *343*, 187-193.
20. Straub, A. P.; Yip, N. Y.; Elimelech, M. Raising the Bar: Increased Hydraulic Pressure Allows Unprecedented High Power Densities in Pressure-Retarded Osmosis. *Environ. Sci. Technol. Lett.* **2014**, *1*, 55-59.
21. Klaysom, C.; Cath, T. Y.; Depuydt, T.; Vankelecom, I. F. J. Forward and pressure retarded osmosis: potential solutions for global challenges in energy and water supply. *Chem. Soc. Rev.* **2013**, *42*, 6959-5989.
22. Lutchmiah, K.; Verliefde, A. R. D.; Roest, K.; Rietveld, L. C.; Cornelissen, E. R. Forward osmosis for application in wastewater treatment: A review. *Water Res.* **2014**, *58*, 179-197.
23. Cadotte, J. E.; Petersen, R. J.; Larson, R. E.; Erickson, E. E. A New Thin-Film Composite Seawater Reverse Osmosis Membrane. *Desalination* **1980**, *32*, 25-31.
24. Kwak, S. Y.; Jung, S. G.; Kim, S. H. Structure-Motion-Performance Relationship of Flux-Enhanced Reverse Osmosis (RO) Membranes Composed of Aromatic Polyamide Thin Film. *Environ. Sci. Technol.* **2001**, *35*, 4334-4340.
25. Cadotte, J. E.; King, R. S.; Majerle, R. J.; Petersen, R. J. Interfacial Synthesis in the Preparation of Reverse Osmosis Membranes. *J. Macromol. Sci. Chem.* **1981**, *15*, 727-755.
26. Arena, J. T.; Manickam, S. S.; Reimund, K. K.; Freeman, B. D.; McCutcheon, J. R. Solute and water transport in forward osmosis using polydopamine modified thin film composite membranes. *Desalination* **2014**, *343*, 8-16.

27. Tang, C. Y.; Kwon, Y. N.; Leckie, J. O. Characterization of Humic Acid Characterization of Humic Acid Nanofiltration Membranes by Transmission Electron Microscopy and Streaming Potential Measurements. *Environ. Sci. Technol.* **2007**, *41*, 942-949.
28. Lu, X.; Boo, C.; Ma, J.; Elimelech, M. Bidirectional Diffusion of Ammonium and Sodium Cations in Forward Osmosis: Role of Membrane Active Layer Surface Chemistry and Charge. *Environ. Sci. Technol.* **2014**, *48*, 14369-14376.
29. Hancock, N. T.; Phillip, W. A.; Elimelech, M.; Cath, T. Y. Bidirectional Permeation of Electrolytes in Osmotically Driven Membrane Processes. *Environ. Sci. Technol.* **2011**, *45*, 10642-10651.
30. Irvine, G. J.; Rajesh, S.; Georgiadis, M.; Phillip, W. A. Ion Selective Permeation Through Cellulose Acetate Membranes in Forward Osmosis. *Environ. Sci. Technol.* **2013**, *47*, 13745-13753.
31. Yong, J. S.; Phillip, W. A.; Elimelech, M. Reverse Permeation of Weak Electrolyte Draw Solutes in Forward Osmosis. *Ind. Eng. Chem. Res.* **2012**, *51*, 13463-13472.
32. McCutcheon, J. R.; McGinnis, R. L.; Elimelech, M. Desalination by ammonia-carbon dioxide forward osmosis: Influence of draw and feed solution concentrations on process performance. *J. Membr. Sci.* **2006**, *278*, 114-123.
33. Skoog, D. A.; Holler, F. J.; Crouch, S. R. *Principles of instrumental analysis*, 5th ed.; Harcourt Brace College Publishers: Orlando, FL, 2007.
34. Harris, D. C. *Quantitative Chemical Analysis*, 6th ed.; W. H. Freeman and Co.: New York, 2003.
35. Method 700B Flame Atomic Absorption Spectrophotometry. U.S. Environmental Protection Agency: Washington, DC, 2007, (<http://www.epa.gov/epawaste/hazard/testmethods/sw846/pdfs/7000b.pdf>).
36. Farr, I. V.; Bharwada, U. J.; Gullinkala, T. Method to Improve Forward Osmosis Membrane Performance. U.S. Patent 0026091 A1, January 31, 2013.
37. Petersen, R. J. Composite reverse osmosis and nanofiltration membranes. *J. Membr. Sci.* **1993**, *83*, 81-150.

38. Tang, C. Y.; Kwon, Y. N.; Leckie, J. O. Probing the nano- and micro-scales of reverse osmosis membranes—A comprehensive characterization of physiochemical properties of uncoated and coated membranes by XPS, TEM, ATR-FTIR, and streaming potential measurements. *J. Membr. Sci.* **2007**, *287*, 146-156.
39. Lambert, J. B.; Shurvell, H. F.; Lightner, D. A.; Cooks, R. G. *Organic Structural Spectroscopy*; Prentice-Hall, Inc.: Upper Saddle River, NJ, 1998.
40. Kwak, S. Y.; Jung, S. G.; Yoon, Y. S.; Ihm, D. W. Details of Surface Features in Aromatic Polyamide Reverse Osmosis Membranes Characterized by Scanning Electron and Atomic Force Microscopy. *J. Polym. Sci. Part B Polym. Phys.* **1999**, *37*, 1429-1440.
41. Yip, N. Y.; Tiraferri, A.; Phillip, W. A.; Schiffman, J. D.; Elimelech, M. High Performance Thin Film Composite Forward Osmosis Membrane. *Environ. Sci. Technol.* **2010**, *44*, 3812-3818.
42. Tiraferri, A.; Yip, N. Y.; Phillip, W. A.; Schiffman, J. D.; Elimelech, M. Relating performance of thin-film composite forward osmosis membranes to support layer formation and structure. *J. Membr. Sci.* **2011**, *367*, 340-352.
43. Hoover, L. A.; Schiffman, J. D.; Elimelech, M. Nanofibers in thin-film composite membrane support layers: Enabling expanded application of forward and pressure retarded osmosis. *Desalination* **2013**, *308*, 73-81.
44. Van Wagner, E. M.; Sagle, A. C.; Sharma, M. M.; Freeman, B. D. Effect of crossflow testing conditions, including feed pH and continuous feed filtration, on commercial reverse osmosis membrane performance. *J. Membr. Sci.* **2009**, *345*, 97-109.
45. Tiraferri, A.; Yip, N. Y.; Straub, A. P.; Romero-Vargas Castrillon, S.; Elimelech, M. A method for the simultaneous determination of transport and structural parameters of forward osmosis membranes. *J. Membr. Sci.* **2013**, *444*, 523-538.
46. Donnan, F. G. The theory of membrane equilibria. *Chem. Rev.* **1924**, *1*, 73-90.
47. Phillip, W. A.; Yong, J. S.; Elimelech, M. Reverse draw solute permeation in forward osmosis: modeling and experiments. *Environ. Sci. Technol.* **2010**, *44*, 5170-5176.

48. Hurwitz, G.; Guillen, G. R.; Hoek, E. M. V. Probing polyamide membrane surface charge, zeta potential, wettability, and hydrophilicity with contact angle measurements. *J. Membr. Sci.* **2010**, *349*, 349-357.
49. Childress, A. E.; Elimelech, M. Effect of solution chemistry on the surface charge of polymeric reverse osmosis and nanofiltration membranes. *J. Membr. Sci.* **1996**, *119*, 253-268.
50. Wamser, C. C.; Gilbert, M. I. Detection of Surface Functional Group Asymmetry in Interfacially-Polymerized Films by Contact Angle Titrations. *Langmuir* **1992**, *8*, 1608-1614.
51. Speight, J. G. Lange's *Handbook of Chemistry*, 16th ed.; McGraw Hill: New York, 2005.

Chapter 8

Alternative and post-treated polyamide chemistries for the mitigation of ion exchange in forward osmosis

8.1. Introduction

Reverse osmosis (RO) has arisen to become the dominate means of desalination worldwide. While RO is an energy intensive process, the efficiency of RO processes has been continuously improving, approaching the minimum theoretical energy needed to desalinate.¹ Despite the significant improvements in the energy efficiency of RO, there are still significant electrical energy requirements for seawater desalination compared to treatment and distribution of conventional freshwater sources.² Tangential to the electrical energy costs of desalination there are also water demands on electrical energy production.^{2,3} The link existing between water consumed in energy production and energy needed for water desalination (and treatment) has become known as the water-energy nexus.^{4,5}

Ultimately, electrical energy consumption for desalination generates additional water needs for electrical energy production.² One way to contend with this interdependency is to co-generate water and power by using the waste heat of a power plant to drive a desalination or water reuse process. This would allow power plants to make their own water from unconventional water sources, lessening their requirements on high demand freshwater sources. Forward osmosis (FO) has been identified as one technology that could feasibly use this waste heat to drive reuse and desalination.^{6,7} In a FO process, low temperature heat sources would be used for the recovery of draw solutes.⁸⁻¹⁰

One specific FO process examined by McGinnis, McCutcheon, and Elimelech used a draw solution of dissolved ammonia and carbon dioxide gases.^{6,11-13} These gases in solution form a mixture of highly soluble ammonium bicarbonate, ammonium carbonate, and ammonium carbamate salts.^{6,14,15} This draw solution has demonstrated the capability of desalinating seawater at elevated temperature in prior studies using a cellulose triacetate (CTA) membrane, designed specifically for FO processes;^{11,12} however, the ammonia-carbon dioxide draw solution is alkaline, introducing a long term incompatibility with the CTA membrane due to hydrolysis.^{16,17} This has necessitated the development of membranes tolerant to alkaline

conditions. Mirroring RO membrane development, the thin film composite (TFC) membrane chemistry has been viewed as the logical successor to CTA, offering superior tolerance to alkaline conditions at the expense of bleach tolerance.¹⁸ While many academic and commercial TFC membranes have become available specifically for FO processes,¹⁹⁻²¹ more recent studies have identified cation exchange will occur across TFC membranes because of chemical interactions between carboxylic acid functional groups present within the chemical structural of a TFC membrane's polyamide selective layer and monovalent cations.²²⁻²⁴

The interconnectedness between draw solutes, feed solutes, and membrane chemistry have been observed in a number of studies where a draw solution offering good water flux and feed solute rejection are often initially characterized with membranes that do not have long term stability to the draw solution.^{11,12,25} Opposite these studies are draw solutions to which the membrane has long term stability and good water flux, but offers poor rejection of one or more components of the feed solution.^{20,22,23}

This study seeks to overcome these deficiencies by using modified and alternative polyamides for improved feed solute rejection. These new polyamides will be formed upon hydrophobic low structural parameter support layers and the newly synthesized TFC

membranes will be modified with polydopamine (PDA) for FO. These membranes will be characterized in FO, first using a sodium chloride draw solution to benchmark basic FO performance. These tests will be followed by tests to assess membranes ion transport properties using a buffered pH 8 potassium chloride draw solution against a buffered pH 8 sodium chloride feed solution.

8.2. Materials and methods

8.2.1. Materials

polymers used in this study were Udel P-1700 polysulfone and Solef L3 polyvinylidene fluoride, generously provided by Solvay Specialty Polymers. Sodium chloride, potassium chloride, sodium hydroxide, 1-methyl-2-pyrrolidinone, 2-propanol, and Tris HCl buffer were purchased from Fisher Scientific (Pittsburgh, PA). Tris(hydroxymethyl)aminomethane, dopamine hydrochloride, acetone, dimethyl formamide, hexane, m-phenylenediamine, and 1,3,5-benzenetricarbonyl trichloride, were purchased from Sigma Aldrich (St. Louis, MO). Ethylene diamine was purchased from Acros Organics (Geel, Belgium). Isopar-G was purchased from Univar (Redmond, WA). Water used in this study was ultrapure Milli-Q

(18.2 MΩ) water produced by a Millipore Integral 10 water system, (Millipore Corporation, Billerica, MA).

8.2.2. TFC membrane preparation

The study uses lab made TFC FO membranes whose polyamides were formed upon a hydrophobic support layer.³⁷ The support layer used was a composite of polyvinylidene fluoride (PVDF) nanofibers with a film of polysulfone (PSu) cast over it, mirroring the approach previously demonstrated by Hoover et al.³⁴ Three different selective layers were formed in this study; a control membrane formed from MPD and TMC (MPD-TFC), a membrane formed from ED and TMC (ED-TFC), and a membrane formed from MPD and TMC post-treated with ED after polyamide formation (MPD-TFC/ED). This modification was performed in an attempt prevent the formation of carboxylic functional groups by reacting the unreacted acyl chloride functional groups before hydrolysis in the presence of water. Each of these polyamides were synthesized on PVDF-PSu composite support layers. Following the membrane's polyamide selective layer formation, the all the membrane support layers were modified, for improved hydrophilicity, with polydopamine (PDA).^{22,38,39}

8.2.2.1. Electrospinning of polyvinylidene fluoride fibers

Electrospinning is the controlled deposition of polymer fibers using an electric field. In an electrospinning process, a filament of polymer solution is drawn out by a voltage potential existing across an air gap between the polymer solution and a grounded collector.²⁶⁻³⁰

Electrospun fibers produced in this study were made from a polymer solution of 11.1% PVDF (1:8 polymer:solvent ratio) dissolved in a blend of dimethylformamide (DMF) and acetone at a ratio of 4:1 DMF:acetone. The electrospun fibers were collected upon a rotating drum³¹ wrapped with a polypropylene nonwoven from Freudenberg Nonwovens (Los Angeles, CA). The PVDF solution was dispensed through a 20 gauge blunt needle at $5 \text{ mL}\cdot\text{h}^{-1}$. An 18 kV potential was placed upon a needle 26 cm from a grounded rotating drum. The PVDF fiber mats were prepared at room temperature and 65-75% relative humidity.

8.2.2.2. Casting of polysulfone support layer

Phase inverted PSu supports have represented the overwhelming majority of substrates used for the interfacial synthesis of polyamide selective layers for both RO and FO TFC membranes.^{18,19,32-34} While electrospun fibers have been used as standalone substrates for polyamide synthesis,^{26,27,30,31} the mechanical stability of these membranes is problematic, as

the electrospun fibers poorly adhere to polyethylene terephthalate (PET) nonwovens. There has been some reported success in the integration of electrospun fibers with cast PSu. This earlier study used electrospun fibers made from PET in lieu of the conventional PET nonwovens as the base layer of TFC membrane for FO.³⁴ Here a similar approach was used: instead of PET electrospun, PVDF fibers were the base layer of the membrane's support. To make the PSu support, a polymer solution of 11.8% PSu in NMP (2:15 polymer:solvent ratio) was prepared and stirred for 2 hours at 35°C. After mixing, the solution was allowed to cool overnight while stirring continued. The following morning the solution was heated to 40°C and transferred to warmed glass vials which were then tightly sealed. The vials of PSu solution were sonicated for 45 minutes. In preparation for casting, the PVDF fibers were removed from the polypropylene substrate, laid upon a glass plate, and secured with tape. The PSu solution was cast upon the PVDF fibers at a height of 100 µm. After casting, the glass plate was immediately immersed in an ice water bath causing the phase inversion of the PSu solution. The prepared PVDF-PSu composite support layer was then directly used as a substrate for the interfacial polymerization of a polyamide selective layer.

8.2.2.3. Polyamide formation by interfacial polymerization

Interfacial polymerization (IP) is the formation of a polymer film at the interface between two immiscible solvents. In membrane applications, polyamides compose the overwhelming majority of selective layers prepared by IP.^{35,36} These polyamides are formed from the reaction of an acyl chloride within a nonpolar organic solvent and an aqueous diamine or polyamine.³⁵ The most common polyamide in both FO and RO applications is synthesized from *m*-phenylenediamine (MPD) in water and 1,3,5-benzenetricarbonyl trichloride (alternatively called trimesoylchloride or TMC) in an alkane.^{18,26,32-34} The use of these monomers in interfacially polymerized TFC membrane was first reported by Cadotte et al.¹⁸, preceded by many years of study in the preparation of synthesized films for the separation of dissolved solids and water.³⁵ An early polyamide chemistry used for TFC membrane selective layers used ethylene diamine (ED) instead of MPD in aqueous phase and TMC within the organic phase, and was observed having 95-97% sodium chloride rejection at 13.8 bar (200 psi).³⁵

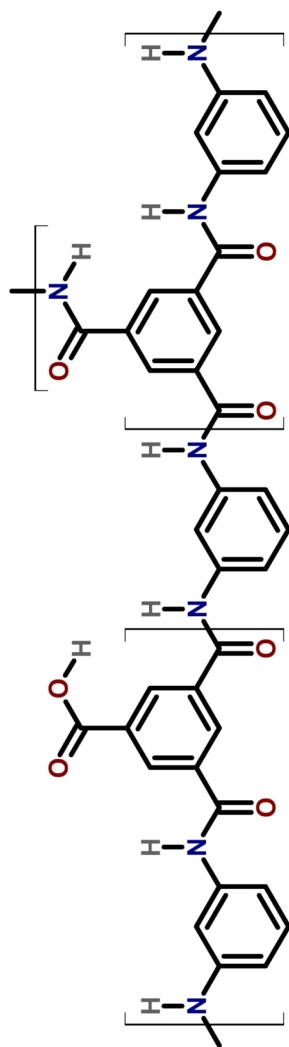
Three different selective layers were formed in this study; a control membrane formed from MPD and TMC (MPD-TFC), a membrane formed from ED and TMC (ED-TFC), and a membrane formed from MPD and TMC, post-treated with ED after polyamide formation

(MPD-TFC/ED). In this study, the selective layers were formed using solutions of 0.28 molal aqueous diamine (3% MPD or 1.1% ED by weight) and 0.15% (by weight) TMC in the organic solvent Isopar-G. The first step in IP was taping the PSu-PVDF composite support to a glass plate and clamping over it an EPDM (ethylene propylene diene monomer) rubber gasket and UHMW PE (ultra-high molecular weight polyethylene) frame, similar to the frames demonstrated in the formation of TFC membranes by Xie et al.³⁷ This creates a shallow reservoir above the top of the PSu-PVDF support layer. The aqueous diamine is then poured over the support layer. The amine solution is left in contact with the support layer for 4 minutes and poured off. Excess droplets of diamine solution were removed with an air knife (Exair Corporation, Cincinnati, OH).²⁷ After the excess diamine was removed, a fresh gasket and frame were clamped onto the PSu-PVDF layer. TMC solution was poured onto the top surface of the PSu-PVDF layer and remained in contact for 4 minutes.

Membranes post-treated by ED, were rinsed with Isopar to remove residual TMC from the selective layer surface. ED was then poured over the polyamide selective layer. After 4 minutes, the ED was removed and the resulting MPD-TFC/ED membrane was rinsed with and stored in deionized water. Membranes not treated with ED following polyamide synthesis were

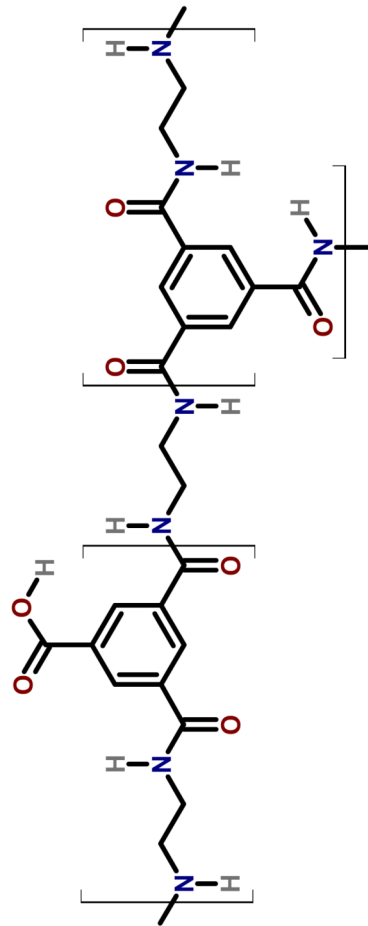
m-phenylenediamine
& trimesoyl chloride

MPD-TFC



ethylene diamine
& trimesoyl chloride

ED-TFC



m-phenylenediamine
& trimesoyl chloride
w/ ethylene diamine
post-treatment

MPD-TFC/ED

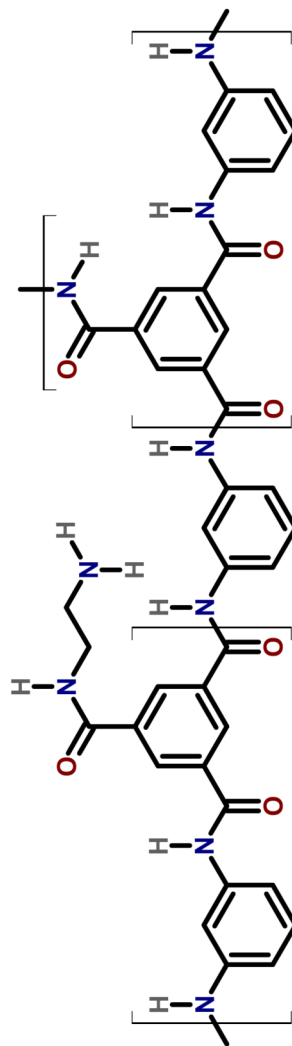


Fig. 8.1. Idealized structures of the polyamide selective layers prepared in this study following hydrolysis of unreacted acyl chloride functional groups.

rinsed with hexane after the removal of the TMC solution and the gasket and frame. The hexane rinsed polyamide was allowed to air dry and was rinsed a second time with hexane. After a second air dry the MPD-TFC and ED-TFC membranes were stored in deionized water. Following the membrane's polyamide selective layer formation, the membrane support layer was modified, for improved hydrophilicity, by the application polydopamine (PDA). Fig. 8.1 shows the hypothesized structures of the polyamides formed in this study.

8.2.2.4. Polydopamine modification

Upon the synthesis of the MPD-TFC, ED-TFC, and MPD-TFC/ED the membranes were modified with polydopamine (PDA).^{22,38,39} This modification followed previously established approaches^{22,38} with slight changes in the procedure used to prewet and wash the support. The TFC membranes were prewetted with a 50% isopropyl alcohol (IPA) solution for 15 minutes. To remove remaining IPA within the membrane's support layer, the membranes were soaked in three successive water baths each for thirty minutes. The polydopamine modification was done within a specially designed coating box where the membrane separates two reservoirs. The formation of polydopamine was done in 450 mL of pH 8.8 Tris-HCl buffer solution with 0.90 g added dopamine-HCl in contact with the support layers of the TFC membrane.

Modification of TFC membranes occurred at room temperature within a stirred cell for 1h. The Tris/dopamine solution was then poured off the membrane. After PDA modification, the membranes rinsed with deionized water and stored at 4°C in deionized water.

8.2.3. Evaluation of membrane morphology with scanning electron microscopy

The TFC membranes were imaged on JEOL 6335F Field Emission SEM (JEOL USA, Inc. Peabody, MA). Top down images of the membrane selective layer and side view images of the membranes support layer were captured. To obtain images of the support layer cross-section, a freeze fracturing technique was used to prepare the samples by soaking the membrane in ethanol followed by hexane and immersed into liquid nitrogen. While frozen the polymer support layer was fractured and the newly fractured membrane was mounted on a 90° aluminum stub with carbon tape. .

8.2.4. Benchmarking membrane performance in forward osmosis

The new TFC FO membranes were tested to observe water flux and reverse solute flux. Tests were initiated with deionized water circulating counter-current on both sides of the membrane at a cross flow velocity of $0.25 \text{ m}\cdot\text{s}^{-1}$ and a temperature of $20\pm 0.5 \text{ }^{\circ}\text{C}$ with a slightly ($\sim 0.01 \text{ bar}$) higher hydrostatic pressure against the membrane's selective layer. The support

layer side of the membrane was further supported with a custom designed 3d printed spacer. A slight pressure differential was used to detect defects within the polyamide. If minimal flux was observed ($<1 \text{ L}\cdot\text{m}^{-2}\cdot\text{h}^{-1}$) sodium chloride was added to the selective layer solution, increasing its concentration to 0.1 M. The membrane is now operating in the PRO mode with a 0.1 M sodium chloride draw solution and a deionized water feed solution. Water and sodium chloride flux were observed with the latter being tracked using a conductivity probe.

After the observation of PRO mode water and salt flux, sodium chloride was added to the solution contacting the membrane's support layer, making the formerly deionized water a solution of 0.5 M sodium chloride. The membrane is now operating in the FO mode with a 0.5M sodium chloride draw solution and a 0.1 M sodium chloride feed solution. The draw solution of the FO system was subsequently increased to 1.0 M and 1.5 M sodium chloride while the feed solution was kept at a concentration to 0.1 M sodium chloride. Benchmarking FO analyses of the MPD-TFC, ED-TFC, and MPD-TFC/ED membranes were performed a minimum of three times and the data later presented are averages and standard deviations of these tests.

8.2.4.1. 3d printed support

To support the membrane under the slight applied pressure in forward osmosis membrane testing a support spacer was designed to support the membrane within the membrane cell. The spacer was designed to fit the contours of the

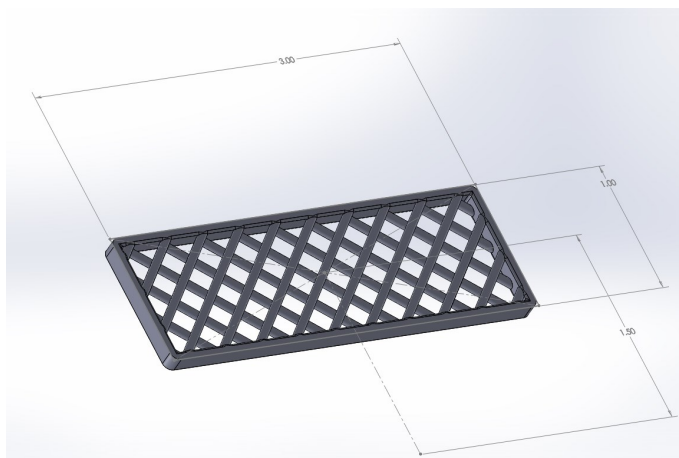


Fig. 8.2. Mesh spacer used to support the thin film composite membrane within the FO test cell. Note that the dimensions are in inches.

designed to fit the contours of the membrane cell and prepared in SolidWorks. The 3d sketch was saved as an STL file and printed on a FormLabs Form1 3d printer. An image of the spacer is shown in Fig. 8.2.

8.2.5. Calculation of membrane transport properties

While water flux is a useful in the evaluation of membrane performance water permeance (A), solute permeability (B), and effective structural parameter (S) are needed for projecting membrane performance to conditions which may not be easily reproduced experimentally.^{40,41} New membranes being assessed for FO processes are commonly characterized in reverse osmosis to measure A and B. These values for A and B are then used to calculate S from

experimental osmotic flux data.^{21,22,33,42,43} One alternative approach reported by Tiraferri et al. used data exclusively from FO tests to determine A, B, and S.⁴² In this study, A, B, and S of the MPD-TFC, ED-TFC, and MPD-TFC/ED were calculated from data collected in the FO benchmarking tests of these membranes using a Mathematica program created by the authors. Calculation of membrane transport properties was initiated by solving the governing equation for water flux assuming a perfectly selective membrane Eq. (8.1)⁴⁰ for A and S using the average water flux observed in the FO mode at draw solution concentrations of 0.5 M, 1.0 M, and 1.5 M sodium chloride with a feed solution of 0.1 M sodium chloride. To approximate the external mass transfer coefficient, k was calculated using established empirical correlations.^{8,40,44}

$$J_w = A \left\{ c_{d,b} \exp \left(- \frac{J_w S}{D_{d,b}} \right) i R_{\text{const}} T - c_{f,b} \exp \left(\frac{J_w}{k} \right) i R_{\text{const}} T \right\} \quad (8.1)$$

From calculated A and S values from Eq. (8.1), the value for S was used to solve for B using Eq. (8.2).⁴²

$$J_s = B \left\{ \frac{c_{d,b} \exp\left(-\frac{J_w S}{D_{d,b}}\right) - c_{f,b} \exp\left(\frac{J_w}{k}\right)}{1 + \frac{B}{J_w} \left[\exp\left(\frac{J_w}{k}\right) - \exp\left(-\frac{J_w S}{D_{d,b}}\right) \right]} \right\} \quad (8.2)$$

Using the value for B calculated from Eq. (8.2), A and S can then be calculated using a more rigorous form of the governing equation for water flux which does not assume a perfectly selective membrane, Eq. (8.3).

$$J_w = A \left\{ \frac{c_{d,b} \exp\left(-\frac{J_w S}{D_{d,b}}\right) iR_{\text{const}} T - c_{f,b} \exp\left(\frac{J_w}{k}\right) iR_{\text{const}} T}{1 + \frac{B}{J_w} \left[\exp\left(\frac{J_w}{k}\right) - \exp\left(-\frac{J_w S}{D_{d,b}}\right) \right]} \right\} \quad (8.3)$$

The value for S calculated from Eq. (8.3) can then be used in Eq. (8.2) to solve for B. This creates an iterative loop where values for A, B, and S can be cycled between Eq. (8.2) and Eq. (8.3). The true values for A, B, and S can be found by comparing the calculated values of A, B, and S of each iteration with the previous looking for convergence between calculated values of A, B, and S. After values for A, B, and S were calculated, small variations in water and solute flux were introduced by adding or subtracting a fraction of the aggregated error from the averaged values. The adjusted water and solute flux were then used to perform additional

calculations of A, B, and S. This adjustment of water and solute flux and calculation of A, B, and S was performed 1000 times. The values for A, B, and S shown later represent averages and standard deviations for these 1000 replicates of the A, B, and S calculation.

8.2.6. Testing of ion transport in forward osmosis

To observe the effect of alternative chemistries, the forward flux of sodium ions and reverse flux of potassium ions in FO was observed using a feed and draw solution buffered at pH 8 with Tris and hydrochloric acid. A recent study by Arena et al. cited the significance of pH in cation exchange in FO and observed this behavior occurring at pH 8.²⁴ The ion transport tests were initiated by circulating solutions of 0.01 M Tris on both sides of the membrane at a cross flow velocity of $0.25 \text{ m}\cdot\text{s}^{-1}$ and a temperature of $20\pm 0.5 \text{ }^{\circ}\text{C}$. A slightly ($\sim 0.01 \text{ bar}$) higher hydrostatic pressure was applied to the membrane's selective layer with the same custom designed 3d printed spacer supporting the membrane used in the FO benchmarking tests. After membrane stabilization, the solution contacting the membrane's selective layer is increased in concentration to 0.1M by adding a concentrated NaCl solution containing 0.01 M buffer. Water flux and reverse solute flux across with the membrane was observed for the PRO mode with a 0.1 M NaCl draw solution and a feed solution of only buffer. After which 50 mL of

the support layer (feed) solution was removed to analyze its sodium concentration. The support layer solution was made into the draw solution by increasing its concentration to 1.0 M KCl through the addition of a concentrated buffered KCl solution. The membrane is operating in the FO mode with a buffered 0.1 M NaCl feed solution and 1.0 M KCl draw solution. Water flux was observed, followed by the removal of 50mL of both the support (draw) and selective (feed) layer solutions to analyze their sodium and potassium concentrations, respectively.

8.2.7. Analysis of draw and feed solution cations

As in prior study,²⁴ potassium and sodium concentrations were measured by direct aspiration atomic absorption (AA) spectrophotometry on a Thermo Scientific ICE 3000 AA spectrometer (Thermo Scientific, Nashua, New Hampshire) equipped with a combination potassium/sodium hollow cathode lamp. This analysis was done according to US EPA method 700B which has a lower detection limit of 0.01 mg·L⁻¹ and 0.002 mg·L⁻¹ and a sensitivity of 0.04 mg·L⁻¹ and 0.015 mg·L⁻¹ for potassium and sodium respectively.⁴⁵ The measured concentrations of sodium and potassium within these solutions helped to determine the total mass of potassium and sodium within the analyzed solutions. The change in mass was divided by the time interval between sample extraction, molar mass, and membrane surface area to

calculate the sodium and potassium flux.

Going from the PRO to FO membrane orientations by the shift in water flux direction means that the NaCl concentration at the selective layer may change significantly since ECP transitions from dilutive to concentrative. To aid in the analysis of the of sodium flux, the interface concentration of sodium chloride was calculated using Eq. (8.4) and Eq. (8.5) for the PRO and FO modes respectively. The mass transfer coefficient (k) was calculated using established correlations.^{40,44,46}

$$C_{NaCl,m} = C_{NaCl,b} \exp\left(-\frac{J_w}{k}\right) \quad (8.4)$$

$$C_{NaCl,m} = C_{NaCl,b} \exp\left(\frac{J_w}{k}\right) \quad (8.5)$$

8.2.4.5. Theoretical rejections

The rejection of a membrane from water flux can be calculated using Eq. (8.6).⁴⁷ Eq. (8.6) is a solution to the equation that calculates solute permeability from rejections measured in reverse osmosis.⁸

$$R = \frac{J_w}{B + J_w} \quad (8.6)$$

Eq. (8.6) can be used to calculate rejection from water flux observed across a membrane in a FO desalination experiment. The calculated rejection is a theoretical prediction of rejection across a membrane or theoretical rejection. Theoretical rejection represents solute rejection as it would occur in a reverse osmosis style experiment where the driver of water flux is hydrostatic pressure, ion transport across the membrane only occurs with their counterion, and the membrane transport is driven by solution-diffusion.⁴⁷ In this study, Eq. (8.6) was used to calculate this ideal rejection across these membranes using water flux measured in the FO ion transport tests. This helps to identify the presence of ion exchange in reducing membrane rejection, represented by significant disparity between the experimental and theoretical rejections.

To predict the theoretical rejection for these FO tests the solute permeability of the membrane was calculated at pH 8 using Eq. (8.2) from the reverse sodium flux data observed in the FO ion transport tests for a draw solution of buffered 0.1 M NaCl and a feed solution of only buffer in the PRO mode and S values calculated iteratively from the FO benchmarking tests. Similar to the calculation for A, B, and S from the FO benchmarking tests, solute permeability was initially calculated using the averaged reverse sodium flux data. Additional

calculations of the solute permeability were performed by adding or subtracting a fraction of the aggregated error from the averaged values for the reverse sodium. The solute permeabilities presented here are averages and standard deviations of this calculation performed 1000 times. This calculated solute permeability and water flux observed for the FO ion transport tests were used in Eq. (8.6) to calculate the theoretical rejection for the MPD-TFC, ED-TFC, and MPD-TFC/ED membranes and used to compare the impact of ion exchange on these membranes' sodium rejection.

8.3. Results and discussion

8.3.1. Membrane morphology

Fig. 8.3 shows the SEM images of these membrane cross-sections and selective layer surfaces. The different membranes all have similar support layer morphologies showing that none of the selective layer synthesis techniques appear to influence support layer morphology. The support layers of these membranes are 70 μm thick and have long finger-like pores which have been previously sought after in the engineering of optimized support layers in membranes tailored for FO.^{34,57} One notable absence is the presence of fibers at the bottom of the support layer. Instead of the fibers there is a spongy pore structure at the bottom of these

membranes' supports. This implies that, upon casting of the PSu solution, the PVDF fibers may slightly dissolve and undergo phase inversion with the PSu when immersed in the water bath. The dissolution of the fibers must occur very quickly within the ~10s from the casting of the PSu solution to phase inversion in the water bath.

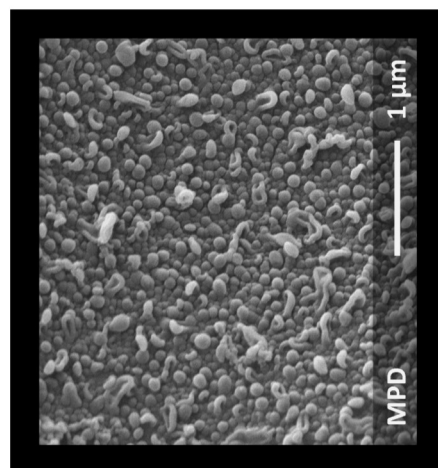
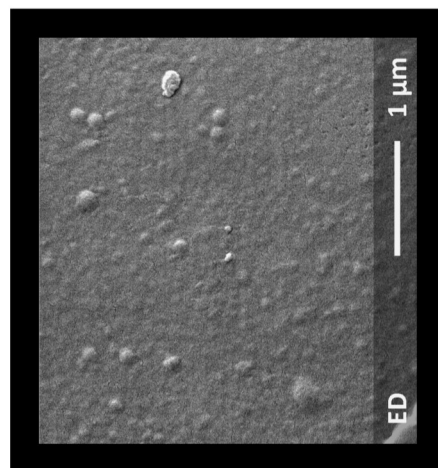
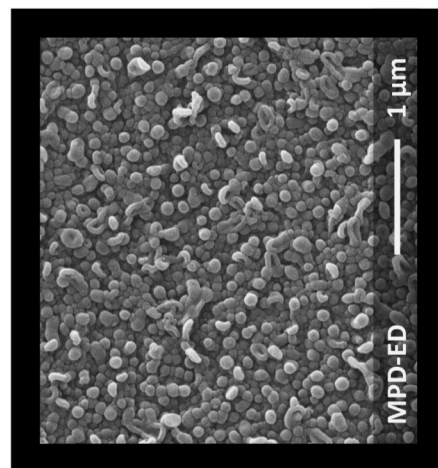
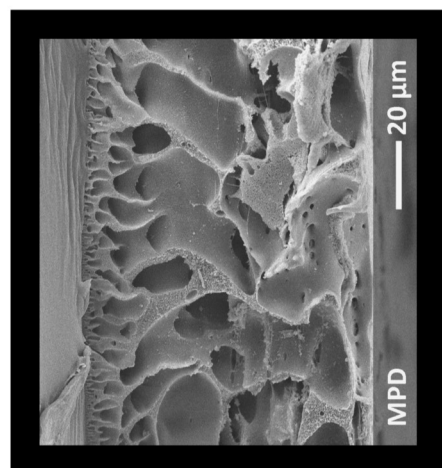
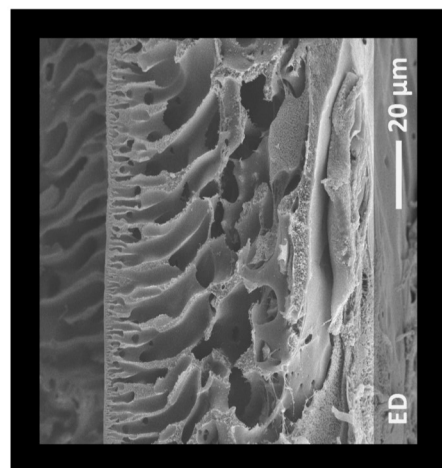
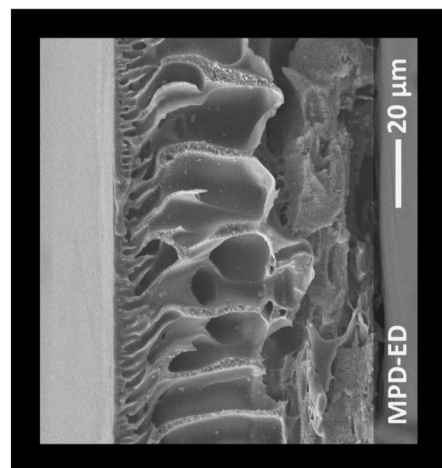
The selective layer morphologies show two things. Most notable are the similarity between the aqueous MPD based selective layers (MPD-TFC and MPD-TFC/ED) and the differences between these and membranes prepared from aqueous ED (ED-TFC). The similarity of the aqueous MPD based selective layers (MPD-TFC and MPD-TFC/ED) is their shared rough morphology. This rough morphology has also been observed in conventional TFC RO and FO membranes.^{19,36,48,58,59}

The ED-TFC possesses a smooth selective layer differentiating it from the characteristically rough selective layers observed in polyamides prepared from aqueous MPD. It instead shares a smooth surface morphology previously observed for selective layer synthesized from polyethylenimine.^{36,48} The smooth selective layer may be the result of a rapid selective layer formation and termination of the IP reaction.³⁶ This may be due to the lower molecular weight of ED giving it a faster diffusivity within both the organic phase and the forming polyamide film.

MPD-TFC/ED

ED-TFC

MPD-TFC



Side

Top

Fig. 8.3. Structure of the membranes' selective and support layers

Rapid motion of ED would cause a rapid and complete reaction of TMC incorporated into the forming selective layer. This would be a beneficial behavior since the acyl chloride functional groups would form amide bonds rather than hydrolyze to carboxylic acid functional groups. A quick reaction of acyl chloride functional groups in polyamide formation inhibits further diffusion and reaction of diamine and acyl chloride growing the polyamide after the initial formation of the dense film. Cadotte et al. suggested this behavior gives rise to the rough surface morphology created from the IP of MPD and TMC.³⁶

8.3.2. Membrane performance in forward osmosis

8.3.2.1. Performance using a model draw solute

Water and solute flux for the TFC membranes made in this study are shown in Fig. 8.5, while the fitted A, B, and S values are shown in Table 8.1. Water fluxes across these membranes were modest with the lowest performing TFC membrane showing $5\text{--}12\text{ L}\cdot\text{m}^{-2}\cdot\text{h}^{-1}$ in the FO mode with a 0.1 M NaCl feed solution. The closeness of the observed water flux between the MPD-TFC and ED-TFC membranes is interesting as these membranes have statistically insignificant differences between these membranes' solute permeability and structural parameters but significant differences in water permeance. The small differences

between the observed water flux for these membranes is the result of differing water permeance (Fig. 8.4a and Table 8.1). Parallel to the observed water flux is the closeness of the experimentally observed reversed sodium flux for a 0.1 M NaCl draw solution in the PRO mode (Fig. 8.4b). The small differences in reverse solute flux of the MPD-TFC vs. ED-TFC are due the slight difference in selective layer interface draw solute concentrations from external concentration polarization (ECP).

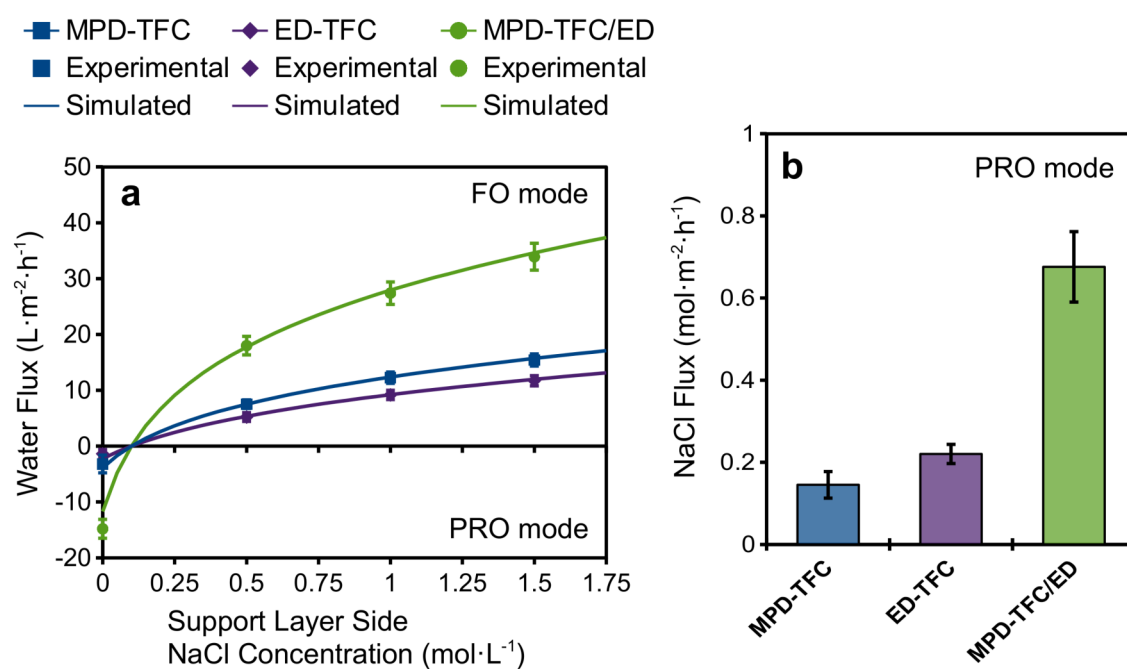


Fig. 8.4. Water flux across the TFC membranes used in this study (a). Selective layer side solution is 0.1 M NaCl. Positive water flux represents FO mode water flux and negative water flux represents PRO mode water flux (i.e. support layer solution is deionized water). Simulated flux data represents water flux calculate base on transport properties in Table 8.1. PRO mode reverse solute flux for a draw solution of 0.1M NaCl and feed solution of deionized water (b). Test performed with a cross-flow velocity of 0.25 m·s⁻¹ and a temperature of 20°C.

Table 8.1. Transport properties of the TFC membranes used in this study.

	A ($\text{L}\cdot\text{m}^{-2}\cdot\text{h}^{-1}\cdot\text{bar}^{-1}$)	B ($\text{L}\cdot\text{m}^{-2}\cdot\text{h}^{-1}$)	S (μm)
MPD-TFC	1.00 \pm 0.17	1.82 \pm 0.33	344 \pm 10
ED-TFC	0.58 \pm 0.11	2.05 \pm 0.20	365 \pm 25
MPD-TFC/ED	5.07 \pm 0.89	11.90 \pm 1.96	193 \pm 20

While the MPD-TFC and ED-TFC performed similarly, higher water flux and reverse solute flux was observed for the MPD-TFC/ED membrane (Fig. 8.4a). The higher fluxes translate to increased water permeance (A) and solute permeability (B) by a factor of five and six, respectively, when compared to the MPD-TFC membrane from which it was derived (Table 8.1). This contrasts an earlier study by Boo et al. who observed no significant change in water permeance or solute permeability upon the surface modification of a commercial TFC membrane surface modified to form reactive esters which were further treated with aqueous ED.²³ Other studies which have examined the water permeance of FO and RO membranes following attachment of surface modifying compounds noted no significant change or a slight decrease in water permeance.⁴⁹⁻⁵¹ The ED post-treatment employed here appears to have a similar effect to membrane performance as a sodium hypochlorite degradation⁴¹ or organic solvent activation.^{52,53} Both of these approaches remove loosely reacted polyamide from the

surface of the selective layer and further degrade⁴¹ or swell the polyamide⁵² increasing permeance at the cost of increasing solute permeability.^{41,53} A further point is the 100 μm drop in the effective structural parameter of the MPD-TFC/ED compared to that of the MPD-TFC. While the decrease in the effective structural parameter is not the result of any visible morphology changes in the membrane support layer, the ED post-treatment may be affecting the PSu/polyamide interface; however, this change is more likely due to inaccuracies in the structural parameter model which uses assumptions that may not be applicable to lower selectivity membranes.⁵⁴

8.3.3. Ion transport

Water flux and solute flux across these membrane in FO using pH 8 buffered solutions are shown in Fig. 8.5 and Fig. 8.6 respectively. The observed water flux for these membranes mirrored those observed in PRO mode (0.1 M draw and deionized water feed) and FO mode (1.0 M draw and 0.1 M feed) conditions at ambient pH (Fig. 8.4a). Reverse sodium flux across these membranes for a 0.1M sodium chloride draw solution at pH 8 is also similar to reverse solute flux observed at ambient pH (Fig. 8.4b). Upon addition of potassium chloride, sodium chloride transport across these membranes changes significantly for the MPD-TFC and

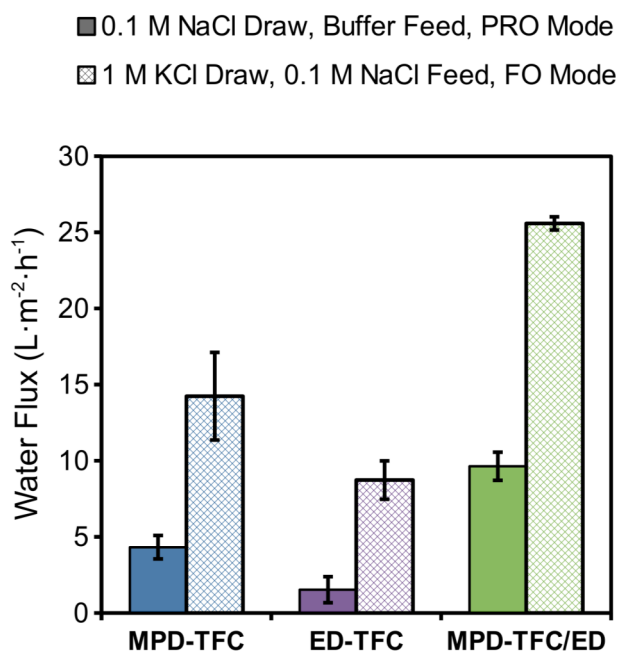


Fig. 8.5. Observed water flux for a blue solution of pH 8 buffer 0.1 M sodium chloride solution opposing red solution of only pH 8 buffer and a buffered 1.0 M potassium chloride solution.

MPD-TFC/ED (Fig. 8.6a and Fig. 8.6b).

The shift from PRO mode to FO mode (by the addition of KCl to the support layer solution) changes the ECP effect on the selective layer solution from dilutive (CP modulus<1) to concentrative (CP modulus>1). As

shown in Table 2, this change is most significant for the MPD-TFC/ED due to the higher water flux. Increased NaCl

concentration at the membrane would also increase the forward sodium flux absent any ion exchange effects. This may in part explain why the forward sodium flux is higher than the reverse sodium flux for the MPD-TFC/ED. The high reverse potassium flux is itself not indicative of cation exchange. Other membranes which have not shown cation exchange as disparate forward cation and anion flux have shown significantly higher reverse solute flux than forward solute flux.^{23,24}

The lower water flux across the MPD-TFC and ED-TFC membranes, means ECP is less significant. A smaller change in ECP means that changing ECP would not so significantly contribute to the observed increase in forward sodium flux across the MPD-TFC. The increase in reverse sodium flux (Fig. 8.6a) compared to forward sodium flux (Fig. 8.6b) for the MPD-TFC is influenced by cation exchange between potassium and sodium ions across the MPD based polyamide. Similar potassium/sodium exchange has been observed across a commercial TFC FO membrane made by Hydration Technology Innovations at pH 8.²⁴ This behavior is expected since the MPD-TFC membrane's selective layer employs the same

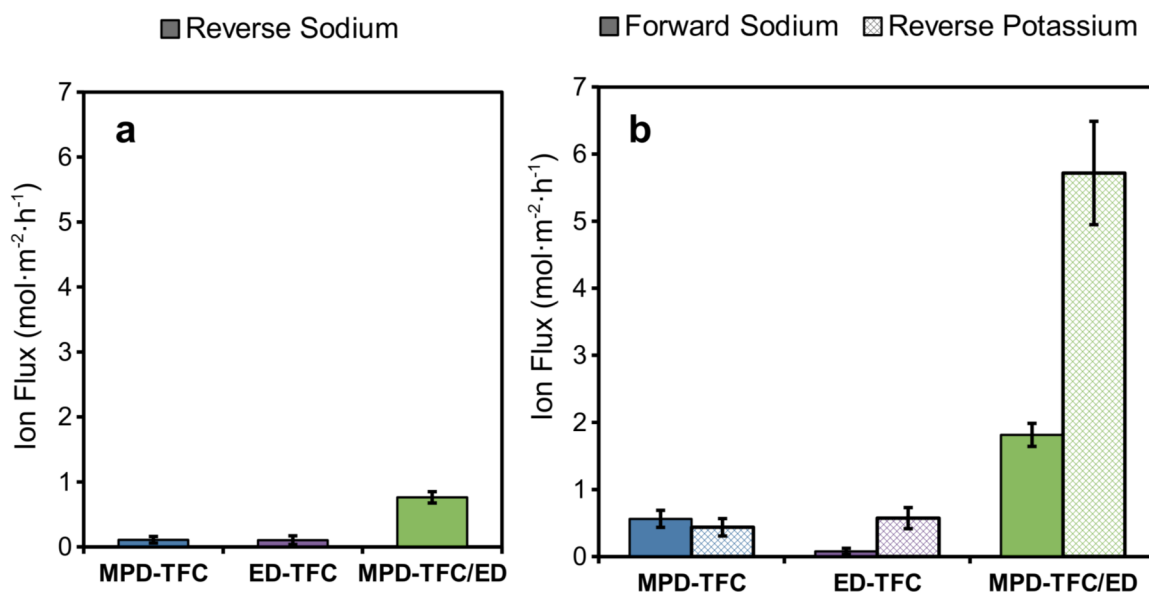


Fig. 8.7. Observed reverse sodium flux for a pH 8 buffered 0.1 M sodium chloride draw solution and a feed solution of pH 8 buffer in the PRO mode (a). Observed forward sodium and reverse potassium flux for a red solution of pH 8 buffered 1.0 M potassium chloride solution and a blue solution of pH 8 buffered 0.1 M sodium chloride (b).

chemistry as most other TFC membranes used in FO.^{22,24,26,27,34,55-57} While, membrane permselectively appears to affect the rate of cation exchange and not its occurrence,^{20,22} ion exchange is more restricted to the chemistry of a membrane's selective layer.^{20,23}

Forward and reverse cation flux for the ED-TFC membrane shows behavior similar to those observed for the MPD-TFC/ED membrane, only to a lower magnitude. Like the MPD-TFC membrane, the lower water flux across the ED-TFC would also not significantly change ECP. This can be seen in the insignificant changes in the forward sodium flux (Fig. 8.6b) compared to the reverse sodium flux (Fig. 8.6a). Also parallel to the potassium flux observed for the MPD-TFC/ED membrane, the ED-TFC also had significantly higher reverse potassium flux over forward flux.

Due to the same anions being present within the draw and feed solution, the sodium rejection of these membranes represents a direct route for identifying the significant changes to sodium selectivity influenced by the presence or absence of cation exchange. The sodium rejection of these membranes was calculated using the sodium concentration of water permeating through the selective layer (J_s/J_w) and the sodium chloride concentration at the membrane's selective layer. For calculation of the theoretical rejection, the solute permeability

Table 8.2. Solute permeability and sodium chloride concentrations at the membrane selective layer for the ion transport study.

Membrane	B ($\text{L}\cdot\text{m}^{-2}\cdot\text{h}^{-1}$) pH 8	$C_{\text{NaCl},m}$ ($\text{mol}\cdot\text{L}^{-1}$) PRO mode pH 8	$C_{\text{NaCl},m}$ ($\text{mol}\cdot\text{L}^{-1}$) FO Mode pH 8
MPD-TFC	1.34 \pm 0.43	0.0940 \pm 0.0004	0.123 \pm 0.005
ED-TFC	1.19 \pm 0.50	0.0978 \pm 0.0009	0.113 \pm 0.002
MPD-TFC/ED	21.5 \pm 4.2	0.0871 \pm 0.0010	0.144 \pm 0.001

for these membranes is needed. The calculated solute permeabilities are shown in Table 8.2.

These solute permeabilities and water fluxes for a 1.0 M pH 8 potassium chloride draw and 0.1 M pH 8 sodium chloride feed were used in the calculation of the theoretical rejections using Eq. (8.5).

Comparisons of theoretical and experimental rejections illustrate cation exchange suppression. For example the MPD-TFC, which displays an expected cation exchange behavior, has a 20% lower experimental rejection compared to its theoretical rejection, meaning that sodium is exchanging with potassium, and the increased sodium flux reduces the rejection of sodium below what is expected. Opposite these results are the MPD-TFC/ED and ED-TFC membrane which have experimental rejections statistically similar to their theoretical rejections. This shows that the ED-TFC and MPD-TFC/ED selective layers do not exhibit

cation exchange with solutes in the draw

and feed solutions. The ED-TFC

selective layer gave the highest sodium

rejection observed experimentally using

a monovalent electrolyte draw solute at

alkaline pH with a rejection of 91.6%.

Although the MPD-TFC/ED membrane

only had an experimentally observed

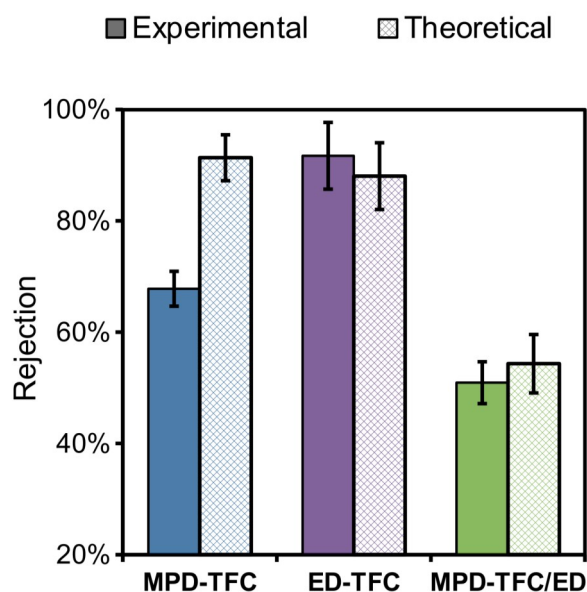


Fig. 8.8. Intrinsic and theoretical rejections of sodium chloride at pH 8.

rejection of 50.9%, this occurred due to damage incurred during the ED post-treatment and not

cation exchange. This is supported by the similarity between the theoretical and experimental

rejections.

The demonstrated efficacy of ED as either a base monomer in polyamide formation or as a

modifier for existing polyamides to mitigate cation exchange is significant in opening

opportunities for alternative amine/acyl chloride polyamide chemistries that, may be viable in

FO for applications where cation exchange is problematic.³⁵ Care should be taken; however,

not to use harsh reaction conditions which may significantly degrade the membranes selectivity.

List of Symbols

A	water permeance of the membrane
B	solute permeability
$C_{d,b}$	bulk draw solute concentration
$C_{f,b}$	feed bulk concentration
$D_{d,b}$	bulk diffusivity of the draw solute in the feed solution
i	dissociation constant (2 for sodium chloride)
J_s	reverse solute flux
J_w	water flux
k	external mass transfer coefficient
R_{const}	ideal gas constant
R	rejection
S	effective structural parameter
T	absolute temperature

References

1. Elimelech, M.; Phillip, W. A. The Future of Seawater Desalination: Energy, Technology, and the Environment. *Science* **2011**, *333*, 712-717.
2. Hall, M. R.; West, J.; Sherman, B.; Lane, J.; de Haas, D. Long-Term Trends and Opportunities for Managing Regional Water Supply and Wastewater Greenhouse Gas Emissions. *Environ. Sci. Technol.* **2011**, *45*, 5434-5440.
3. Blackhurst, M.; Hendrickson, C.; Vidal, J. S. I. Direct and Indirect Water Withdrawals for U.S. Industrial Sectors. *Environ. Sci. Technol.* **2011**, *44*, 2126-2130.
4. Schnoor, J. L. Water-Energy Nexus. *Environ. Sci. Technol.* **2011**, *45*, 5065-5065.
5. Scott, C. A.; Pierce, S. A.; Pasqualetti, M. J.; Jones, A. L.; Montz, B. E.; Hoover, J. H. Policy and institutional dimensions of the water–energy nexus. *Energy Policy* **2011**, *39*, 6622-6630.
6. McGinnis, R. L.; Elimelech, M. Energy requirements of ammonia–carbon dioxide forward. *Desalination* **2007**, *207*, 370-382.
7. Zhou, X.; Gingerich, D. B.; Mauter, M. S. Water Treatment Capacity of Forward-Osmosis Systems Utilizing Power-Plant Waste Heat. *Ind. Eng. Chem. Res.* **2015**, *54*, 6378-6389.
8. Cath, T. Y.; Childress, A. E.; Elimelech, M. Forward osmosis: Principles, applications, and recent developments. *J. Membr. Sci.* **2006**, *281*, 70-87.
9. Hoover, L. A.; Phillip, W. A.; Tiraferri, A.; Yip, N. Y.; Elimelech, M. Forward with Osmosis: Emerging Applications for Greater Sustainability. *Environ. Sci. Technol.* **2011**, *45*, 9824–9830.
10. Chung, T.-S.; Zhang, S.; Wang, K. Y.; Su, J.; Ling, M. M. Forward osmosis processes: Yesterday, today, and tomorrow. *Desalination* **2012**, *287*, 78-81.
11. McCutcheon, J. R.; McGinnis, R. L.; Elimelech, M. A novel ammonia-carbon dioxide forward (direct) osmosis desalination process. *Desalination* **2005**, *174*, 1-11.

12. McCutcheon, J. R.; McGinnis, R. L.; Elimelech, M. Desalination by ammonia-carbon dioxide forward osmosis: Influence of draw and feed solution concentrations on process performance. *J. Membr. Sci.* **2006**, *278*, 114-123.
13. McGinnis, R. Osmotic Desalination Process. US 2005/0145568 A1, July 7, 2005.
14. Mani, F.; Peruzzini, M.; Stoppioni, P. CO₂ absorption by aqueous NH₃ solutions: speciation of ammonium. *Green Chem.* **2006**, *8*, 995-1000.
15. Edwards, T. J.; Maurer, G.; Newman, J.; Prausnitz, J. M. Vapor-Liquid Equilibria in Multicomponent Aqueous Solutions of Volatile Weak Electrolytes. *AIChE J.* **1978**, *24*, 966-976.
16. Vos, K. D.; Burris, F. O.; Riley, R. L. Kinetic Study of the Hydrolysis of Cellulose Acetate in the pH Range of 2-10. *J. Appl. Polym. Sci.* **1966**, *10*, 825-832.
17. Watters, J. C.; Klein, E.; Fleischman, M.; Roberts, J. S.; Hall, B. Rejection Spectra of Reverse Osmosis Membranes Degraded by Hydrolysis of Chlorine Attack. *Desalination* **1986**, *60*, 93-110.
18. Cadotte, J. E.; Petersen, R. J.; Larson, R. E.; Erickson, E. E. A New Thin-Film Composite Seawater Reverse Osmosis Membrane. *Desalination* **1980**, *32*, 25-31.
19. Ren, J.; McCutcheon, J. R. A new commercial thinfilm composite membrane for forward osmosis. *Desalination* **2014**, *343*, 187-193.
20. Coday, B. D.; Heil, D. M.; Xu, P.; Cath, T. Y. Effects of Transmembrane Hydraulic Pressure on Performance of Forward Osmosis Membranes. *Environ. Sci. Technol.* **2013**, *47*, 2386-2393.
21. Cath, T. Y.; Elimelech, M.; McCutcheon, J. R.; McGinnis, R. L.; Achilli, A.; Anastasio, D.; Brady, A. R.; Childress, A. E.; Farr, I. V.; Hancock, N. T.; Lampi, J.; Nghiem, L. D.; Xie, M.; Yip, N. Y. Standard Methodology for Evaluating Membrane Performance in Osmotically Driven Membrane Processes. *Desalination* **2013**, *312*, 31-38.
22. Arena, J. T.; Manickam, S. S.; Reimund, K. K.; Freeman, B. D.; McCutcheon, J. R. Solute and water transport in forward osmosis using polydopamine modified thin film composite membranes. *Desalination* **2014**, *343*, 8-16.

23. Lu, X.; Boo, C.; Ma, J.; Elimelech, M. Bidirectional Diffusion of Ammonium and Sodium Cations in Forward Osmosis: Role of Membrane Active Layer Surface Chemistry and Charge. *Environ. Sci. Technol.* **2014**, *48*, 14369-14376.
24. Arena, J. T.; Chwatko, M.; Robillard, H. A.; McCutcheon, J. R. pH Sensitivity of Ion Exchange through a Thin Film Composite Membrane in Forward Osmosis. *Environ. Sci. Technol. Lett.* **2015**, *2*, 177-182.
25. Stone, M. L.; Rae, C.; Stewart, F. F.; Wilson, A. D. Switchable polarity solvents as draw solutes for forward osmosis. *Desalination* **2013**, *312*, 124-129.
26. Bui, N. N.; McCutcheon, J. R. Hydrophilic Nanofibers as New Supports for Thin Film Composite Membranes for Engineered Osmosis. *Environ. Sci. Technol.* **2013**, *47*, 1761-1769.
27. Bui, N. N.; Lind, M. L.; Hoek, E. M. V.; McCutcheon, J. R. Electrospun nanofiber supported thin film composite membranes for engineered osmosis. *J. Membr. Sci.* **2011**, *385-386*, 10-19.
28. Doshi, J.; Reneker, D. H. Electrospinning process and applications of electrospun fibers. *J. Electrostat.* **1995**, *35*, 151-160.
29. Goh, Y.; Shakir, I.; Hussain, R. Electrospun fibers for tissue engineering, drug delivery, and wound dressing. *J. Mater. Sci.* **2013**, *48*, 3027-3054.
30. Tian, M.; Qui, C.; Liao, Y.; Chou, S.; Wang, R. Preparation of polyamide thin film composite forward osmosis membrane using electrospun polyvinylidene fluoride (pvdf) nanofibers as substrates. *Sep. Purif. Technol.* **2013**, *118*, 727-736.
31. Huang, L.; McCutcheon, J. R. Hydrophilic nylon 6,6 nanofibers supported thin film composite membranes for engineered osmosis. *J. Membr. Sci.* **2014**, *457*, 162-169.
32. Tiraferri, A.; Yip, N. Y.; Phillip, W. A.; Schiffman, J. D.; Elimelech, M. Relating performance of thin-film composite forward osmosis membranes to support layer formation and structure. *J. Membr. Sci.* **2011**, *367*, 340-352.
33. Yip, N. Y.; Tiraferri, A.; Phillip, W. A.; Schiffman, J. D.; Elimelech, M. High Performance Thin Film Composite Forward Osmosis Membrane. *Environ. Sci. Technol.* **2010**, *44*, 3812-3818.

34. Hoover, L. A.; Schiffman, J. D.; Elimelech, M. Nanofibers in thin-film composite membrane support layers: Enabling expanded application of forward and pressure retarded osmosis. *Desalination* **2013**, *308*, 73-81.
35. Petersen, R. J. Composite reverse osmosis and nanofiltration membranes. *J. Membr. Sci.* **1993**, *83*, 81-150.
36. Cadotte, J. E.; King, R. S.; Majerle, R. J.; Petersen, R. J. Interfacial Synthesis in the Preparation of Reverse Osmosis Membranes. *J. Macromol. Sci. Chem.* **1981**, *15*, 727-755.
37. Xie, W.; Geise, G. M.; Freeman, B. D.; Lee, H. S.; Byun, G.; McGrath, J. E. Polyamide interfacial composite membranes prepared from m-phenylene diamine, trimesoyl chloride and a new disulfonated diamine. *J. Membr. Sci.* **2012**, *403-404*, 152-161.
38. Arena, J. T.; McCloskey, B.; Freeman, B. D.; McCutcheon, J. R. Surface modification of thin film composite membrane support layers with polydopamine: Enabling use of reverse osmosis membranes in pressure retarded osmosis. *J. Membr. Sci.* **2011**, *375*, 55-62.
39. Han, G.; Zhang, S.; Li, X.; Widjojo, N.; Chung, T. S. Thin film composite forward osmosis membranes based on polydopamine modified polysulfone substrates with enhancements in both water flux and salt rejection. *Chem. Eng. Sci.* **2012**, *80*, 219-231.
40. McCutcheon, J. R.; Elimelech, M. Modeling Water Flux in Forward Osmosis: Implications for Improved Membrane Design. *AIChE J.* **2007**, *53*, 1736-1744.
41. Yip, N. Y.; Tiraferri, A.; Phillip, W. A.; Schiffman, J. D.; Hoover, L. A.; Kim, Y. C.; Elimelech, M. Thin-Film Composite Pressure Retarded Osmosis Membranes for Sustainable Power Generation from Salinity Gradients. *Environ. Sci. Technol.* **2011**, *45*, 4360-4369.
42. Tiraferri, A.; Yip, N. Y.; Straub, A. P.; Castrillon, S. R.-V.; Elimelech, M. A method for the simultaneous determination of transport and structural parameters of forward osmosis membranes. *J. Membr. Sci.* **2013**, *444*, 523-538.
43. Bui, N. N.; Arena, J. T.; McCutcheon, J. R. Proper accounting of mass transfer Resistances in forward osmosis: Improving the Accuracy of model Predictions of structural parameter. *J. Membr. Sci.* **2015**, *492*, 289-302.
44. McCabe, W. L.; Smith, J. C.; Harriot, P. *Unit Operations of Chemical Engineering*, 7th ed.; McGraw-Hill: New York, New York, 2005.

45. United States EPA. Method 700B Flame Atomic Absorption Spectrophotometry, 2007.
<http://www.epa.gov/epawaste/hazard/testmethods/sw846/pdfs/7000b.pdf>.
46. Cath, T. Y.; Childress, A. E.; Elimelech, M. Forward osmosis: Principles, applications, and recent developments. *J. Membr. Sci.* **2006**, *281*, 70-87.
47. Tang, C. Y.; She, Q.; Lay, W. C. L.; Wang, R.; Fane, A. G. Coupled effects of internal concentration polarization and fouling on flux behavior of forward osmosis membranes during humic acid filtration. *J. Membr. Sci.* **2010**, *354*, 123-133.
48. Bui, N. N.; McCutcheon, J. R. Nanofiber Supported Thin-Film Composite Membrane for Pressure-Retarded Osmosis. *Environ. Sci. Technol.* **2014**, *48*, 4129-4136.
49. Lu, X.; Boo, C.; Ma, J. E. M. In Situ Surface Chemical Modification of Thin-Film Composite Forward Osmosis Membranes for Enhanced Organic Fouling Resistance. *Environ. Sci. Technol.* **2013**, *47*, 12219-12228.
50. Castrillón, S. R. V.; Lu, X.; Shaffer, D. L.; Elimelech, M. Amine enrichment and poly (ethylene glycol) (PEG) surface modification of thin-film composite forward osmosis membranes for organic fouling control. *J. Membr. Sci.* **2014**, *450*, 331-339.
51. Sagle, A. C.; Van Wagner, E. M.; Ju, H.; McCloskey, B. D.; Freeman, B. D.; Sharma, M. M. PEG-coated reverse osmosis membranes: Desalination properties and fouling resistance. *J. Membr. Sci.* **2009**, *340*, 92-108.
52. Solomon, M. F. J.; Bhole, Y.; Livingston, A. G. High flux membranes for organic solvent nanofiltration (OSN)—Interfacial. *J. Membr. Sci.* **2012**, *423-424*, 371-382.
53. Cui, Y.; Lui, X. Y.; Chung, T. S. Enhanced osmotic energy generation from salinity gradients by modifying thin film composite membranes. *Chem. Eng. J.* **2014**, *242*, 195-203.
54. Manickam, S. S.; McCutcheon, J. R. Model thin film composite membranes for forward osmosis: Demonstrating the inaccuracy of existing structural parameter models. *J. Membr. Sci.* **2015**, *483*, 70-74.
55. Coday, B. D.; Heil, D. M.; Xu, P.; Cath, T. Y. Effects of Transmembrane Hydraulic Pressure on Performance of Forward Osmosis Membranes. *Environ. Sci. Technol.* **2013**, *47*, 2386-2393.

56. Farr, I. V.; Bharwada, U. J.; Gullinkala, T. Method to Improve Forward Osmosis Membrane Performance. US 2013/0026091 A1, Jan. 31, 2013.
57. Yip, N. Y.; Tiraferri, A.; Phillip, W. A.; Schiffman, J. D.; Elimelech, M. High Performance Thin Film Composite Forward Osmosis Membrane. *Environ. Sci. Technol.* **2010**, *44*, 3812-3818.
58. Kwak, S. Y.; Jung, S. G.; Yoon, Y. S.; Ihm, D. W. Details of Surface Features in Aromatic Polyamide Reverse Osmosis Membranes Characterized by Scanning Electron and Atomic Force Microscopy. *J. Polym. Sci. Part B Polym. Phys.* **1999**, *37*, 1429-1440.
59. Tang, C. Y.; Kwon, Y. N.; Leckie, J. O. Probing the nano- and micro-scales of reverse osmosis membranes—A comprehensive characterization of physiochemical properties of uncoated and coated membranes by XPS, TEM, ATR-FTIR, and streaming potential measurements. *J. Membr. Sci.* **2007**, *287*, 146-156.

Concluding remarks

Overall, the final studies of this dissertation feel more like a beginning than a end. The limitations of membrane selective layers open a new area of investigation for research in forward osmosis. With the problem of support layers preparation for reduced diffusion limitations largely solved, the development of thin film composite polyamides for forward osmosis will likely mirror the rapid expansion of interfacially synthesized polyamides for reverse osmosis that happened three decades earlier. There are many polyamines which may produce selective layers superior to the ethylenediamine/trimesoylchloride selective layers presented in Chapter 8. Alternative selective layer chemistries will hopefully prove fruitful and viable long-term draw solute/membrane combinations will come to the fore and introduce new low energy water purification, desalination, and reclamation processes. While the

competitiveness and viability of these processes still remains in question as there are many unknowns in the mechanics of draw solute recovery and suitable means of low energy draw solute/solution separation/concentration still require perfecting. While, there are still many more papers to write in the realm of forward osmosis processes and membranes, I hope that my work had made valuable contributions to further the study of forward osmosis, membrane science, and chemical engineering.

Appendix 1

Speciation of the ammonia-carbon dioxide draw solution

The follow code draws upon the methodology established in
Edwards, T.J.; et al. *AIChE J.* **1978**, 24, 966-976.

Equilibrium constants (except water) from
Kawazuishi, K.; Prausnitz, J.M. *Ind. Eng. Chem. Res.* **1987**, 26, 1485-1488.

Debye-Huckel Parameters from
Lewis, et al. *Thermodynamics*, McGraw-Hill, New York, 1961.

Water equilibrium constants from
Robinson, R. A.; Stokes, R. H. *Electrolyte Solutions*, Mineola, 2002.

Constraints

total carbon molality, total nitrogen molality, and solution temperature

Valid Temperature range 20-100 C

```
carbonTotal = 2.061360914;  
nitrogenTotal = 2.359054333;  
solTemp = 23;
```

Calculation of interaction parameters

```
b0NH3NH3[temp_] := (-0.0260) + (12.29/(temp + 273.15));  
b0NH3CO2[temp_] := 0;  
b0NH3NH4[temp_] := 0;  
b0NH3HCO3[temp_] := 0.135 - (1.165*10^(-3)*(temp + 273.15)) + (2.05*10^(-6)*(temp + 273.15)^2);  
b0NH3CO3[temp_] := 0.06;  
b0NH3NH2COO[temp_] := 0;  
b0NH3H[temp_] := 0.015;  
b0NH3OH[temp_] := 0.227 - (1.147*10^(-3)*(temp + 273.15)) + (2.6*10^(-6)*(temp + 273.15)^2);  
  
b0NH4HCO3[temp_] := (-0.028) + (-0.049);
```

```

b0NH4CO3[temp_] := (-0.028) + (-0.034);
b0NH4CO2[temp_] := 0.037 - (2.38*10^(-4))*(temp + 273.15)) + (3.83*10^(-7))*(temp + 273.15)^2);
b0NH4NH2COO[temp_] := (-0.028) + 0.078;
b0NH4OH[temp_] := 0.088 + (-0.028);

b0CO2CO2[temp_] := (-0.4922) + (149.2/(temp + 273.15));
b0CO2HCO3[temp_] := 0;
b0CO2CO3[temp_] := 0;
b0CO2NH2COO[temp_] := 0.017;
b0CO2H[temp_] := 0.033;
b0CO2OH[temp_] := 0.26 - (1.62*10^(-3))*(temp + 273.15)) + (2.89*10^(-6))*(temp + 273.15));

b0HCO3H[temp_] := 0.120 + (-0.049);
b0CO3H[temp_] := 0.120 + (-0.034);
b0HNNH2COO[temp_] := 0.120 + 0.078;
b0HOH[temp_] := 0.120 + 0.088;

b1NH4HCO3[temp_] := 0.018 + 3.06*b0NH4HCO3[temp];
b1NH4CO3[temp_] := 0.018 + 3.06*b0NH4CO3[temp];
b1NH4OH[temp_] := 0.018 + 3.06*b0NH4OH[temp];
b1NH4NH2COO[temp_] := 0.018 + 3.06*b0NH4NH2COO[temp];

b1HCO3H[temp_] := 0.018 + 3.06*b0HCO3H[temp];

b1CO3H[temp_] := 0.018 + 3.06*b0CO3H[temp];

b1HNNH2COO[temp_] := 0.018 + 3.06*b0HNNH2COO[temp];
b1HOH[temp_] := 0.018 + 3.06*b0HOH[temp];

b0Values[temp_] := {{0, "NH3", "CO2", "NH4", "HCO3", "CO3", "NH2COO", "H", "OH"},
    {"NH3", b0NH3NH3[temp], b0NH3CO2[temp], b0NH3NH4[temp],
    b0NH3HCO3[temp], b0NH3CO3[temp], b0NH3NH2COO[temp], b0NH3H[temp], b0NH3OH[temp]},
    {"CO2", b0NH3CO2[temp], b0CO2CO2[temp], b0NH4CO2[temp], b0CO2HCO3[temp],
    b0CO2CO3[temp], b0CO2NH2COO[temp], b0CO2H[temp], b0CO2OH[temp]},
    {"NH4", b0NH3NH4[temp], b0NH4CO2[temp], 0, b0NH4HCO3[temp],
    b0NH4CO3[temp], b0NH4NH2COO[temp], 0, b0NH4OH[temp]},
    {"HCO3", b0NH3HCO3[temp], b0CO2HCO3[temp], b0NH4HCO3[temp], 0, 0, 0, b0HCO3H[temp], 0},
    {"CO3", b0NH3CO3[temp], b0CO2CO3[temp], b0NH4CO3[temp], 0, 0, 0, b0CO3H[temp], 0},
    {"NH2COO", b0NH3NH2COO[temp],
    b0CO2NH2COO[temp], b0NH4NH2COO[temp], 0, 0, 0, b0HNNH2COO[temp], 0},
    {"H", b0NH3H[temp], b0CO2H[temp], 0, b0HCO3H[temp],
    b0CO3H[temp], b0HNNH2COO[temp], 0, b0HOH[temp]},
    {"OH", b0NH3OH[temp], b0CO2H[temp], b0NH4OH[temp], 0, 0, 0, b0HOH[temp], 0}}

b1Values[temp_] := {{0, "NH3", "CO2", "NH4", "HCO3", "CO3", "NH2COO", "H", "OH"},
    {"NH3", 0, 0, 0, 0, 0, 0, 0, 0}, {"CO2", 0, 0, 0, 0, 0, 0, 0, 0},
    {"NH4", 0, 0, 0, b1NH4HCO3[temp], b1NH4CO3[temp], b1NH4NH2COO[temp], 0, b1NH4OH[temp]},

```

```

    {"HCO3", 0, 0, b1NH4HCO3[temp], 0, 0, 0, b1HCO3H[temp], 0},
    {"CO3", 0, 0, b1NH4CO3[temp], 0, 0, 0, b1CO3H[temp], 0},
    {"NH2COO", 0, 0, b1NH4NH2COO[temp], 0, 0, 0, b1HNNH2COO[temp], 0},
    {"H", 0, 0, 0, b1HCO3H[temp], b1CO3H[temp], b1HNNH2COO[temp], 0, b1HOH[temp]},
    {"OH", 0, 0, b1NH4OH[temp], 0, 0, 0, b1HOH[temp], 0}}

b0Values[solTemp]
b1Values[solTemp]

{{0, NH3, CO2, NH4, HCO3, CO3, NH2COO, H, OH},
 {NH3, 0.0154992, 0, 0, -0.0302199, 0.06, 0, 0.015, 0.115348},
 {CO2, 0, 0.0115988, 0.000107247, 0, 0, 0.017, 0.033, -0.218907},
 {NH4, 0, 0.000107247, 0, -0.077, -0.062, 0.05, 0, 0.06},
 {HCO3, -0.0302199, 0, -0.077, 0, 0, 0, 0.071, 0},
 {CO3, 0.06, 0, -0.062, 0, 0, 0, 0.086, 0}, {NH2COO, 0, 0.017, 0.05, 0, 0, 0, 0.198, 0},
 {H, 0.015, 0.033, 0, 0.071, 0.086, 0.198, 0, 0.208},
 {OH, 0.115348, 0.033, 0.06, 0, 0, 0, 0.208, 0}}

{{0, NH3, CO2, NH4, HCO3, CO3, NH2COO, H, OH}, {NH3, 0, 0, 0, 0, 0, 0, 0, 0},
 {CO2, 0, 0, 0, 0, 0, 0, 0, 0}, {NH4, 0, 0, 0, -0.21762, -0.17172, 0.171, 0, 0.2016},
 {HCO3, 0, 0, -0.21762, 0, 0, 0, 0.23526, 0},
 {CO3, 0, 0, -0.17172, 0, 0, 0, 0.28116, 0}, {NH2COO, 0, 0, 0.171, 0, 0, 0, 0.62388, 0},
 {H, 0, 0, 0, 0.23526, 0.28116, 0.62388, 0, 0.65448}, {OH, 0, 0, 0.2016, 0, 0, 0, 0.65448, 0}}

```

Equilibrium equation

```

equilibria[absTemp_, a1_, a2_, a3_, a4_] := Exp[(a1/absTemp) + (a2*Log[absTemp]) + (a3*absTemp) + (a4)]

equilibria[T, a1, a2, a3, a4]

```

$$e^{a_4 + \frac{a_1}{T} + a_3 T + a_2 \log[T]}$$

Ion activity

```

activityion[aPhi_, z_, ionic_, mjb0ij_, mjb1ij_, mjmkbjk_] :=
  Exp[-aPhi*z^2 ((Sqrt[ionic])/(1 + 1.2*Sqrt[ionic]) + (2*Log[1 + 1.2*Sqrt[ionic]])/(1.2)) +
    2*(mjb0ij + ((mjb1ij/(2*ionic))*(1 - (1 + 2*Sqrt[ionic])*Exp[(-2)*Sqrt[ionic]]))) -
    (z^2/(4*ionic^2))*(1 - (1 + 2*Sqrt[ionic] + 2*ionic)*Exp[-2*Sqrt[ionic]])]

activityion[aPhi, z, ionic, mib0ij, mib1ij, mjmkbjk];

```


Debye-Huckel Parameter

```
aPhiDebye[temp_] := Module[{tempXaGamma, aGamma},
  tempXaGamma = {{0, 0.492}, {10, 0.499}, {20, 0.507}, {25, 0.511}, {30, 0.517},
    {40, 0.524}, {50, 0.534}, {60, 0.545}, {70, 0.556}, {80, 0.569}, {90, 0.582}, {100, 0.596}};
  aGamma = Interpolation[tempXaGamma, temp];
  (2.303*aGamma)/3]

aPhiDebye[solTemp]
```

0.39093

Ionic strength of solution

```
ionicStr[nh4_, hco3_, co3_, nh2coo_, oh_, h_] := 0.5 ((1^2*Abs[nh4]) + ((-1)^2*Abs[hco3]) +
  ((-2)^2*Abs[co3]) + ((-1)^2*Abs[nh2coo]) + ((-1)^2*Abs[oh]) + (1^2*Abs[h]))

ionicStr[nh4, hco3, co3, nh2coo, oh, h]
```

0.5 (4 Abs[co3] + Abs[h] + Abs[hco3] + Abs[nh2coo] + Abs[nh4] + Abs[oh])

Summation of interaction parameters times molality for each component

```
mjbij[temp_, ionic_, nh3_, co2_, nh4_, hco3_, co3_, nh2coo_, h_, oh_] := Module[{b0, b1, mb = Array[0 &, {8, 3}],
  mol = {nh3, co2, nh4, hco3, co3, nh2coo, h, oh}},
  b0 = b0Values[temp];
  b1 = b1Values[temp];
  Print[mb];
  Print[mol];
  For[i = 1, i ≤ 8, i++, mb[[i, 1]] = b0[[i + 1, 1]];
  For[j = 1, j ≤ 8, j++, mb[[i, 2]] += (b0[[i + 1, j + 1]]*mol[[j]])];
  For[j = 1, j ≤ 8, j++, mb[[i, 3]] += (b1[[i + 1, j + 1]]*mol[[j]])];
  Print[mb]]
```

```
mNH3bNH3j0[temp_, nh3_, co2_, nh4_, hco3_, co3_, nh2coo_, h_, oh_] :=
  b0Values[temp][[2, 2]]*nh3 + b0Values[temp][[2, 3]]*co2 +
  b0Values[temp][[2, 4]]*nh4 + b0Values[temp][[2, 5]]*hco3 + b0Values[temp][[2, 6]]*co3 +
  b0Values[temp][[2, 7]]*nh2coo + b0Values[temp][[2, 8]]*h + b0Values[temp][[2, 9]]*oh
mNH3bNH3j1[temp_, nh3_, co2_, nh4_, hco3_, co3_, nh2coo_, h_, oh_] :=
  (b1Values[temp][[2, 2]]*nh3 + b1Values[temp][[2, 3]]*co2 +
  b1Values[temp][[2, 4]]*nh4 + b1Values[temp][[2, 5]]*hco3 + b1Values[temp][[2, 6]]*co3 +
  b1Values[temp][[2, 7]]*nh2coo + b1Values[temp][[2, 8]]*h + b1Values[temp][[2, 9]]*oh)

mCO2bCO2j0[temp_, nh3_, co2_, nh4_, hco3_, co3_, nh2coo_, h_, oh_] :=
  b0Values[temp][[3, 2]]*nh3 + b0Values[temp][[3, 3]]*co2 +
  b0Values[temp][[3, 4]]*nh4 + b0Values[temp][[3, 5]]*hco3 + b0Values[temp][[3, 6]]*co3 +
  b0Values[temp][[3, 7]]*nh2coo + b0Values[temp][[3, 8]]*h + b0Values[temp][[3, 9]]*oh
mCO2bCO2j1[temp_, nh3_, co2_, nh4_, hco3_, co3_, nh2coo_, h_, oh_] :=
```

```

(b1Values[temp][[3, 2]]*nh3 + b1Values[temp][[3, 3]]*co2 +
  b1Values[temp][[3, 4]]*nh4 + b1Values[temp][[3, 5]]*hco3 + b1Values[temp][[3, 6]]*co3 +
  b1Values[temp][[3, 7]]*nh2coo + b1Values[temp][[3, 8]]*h + b1Values[temp][[3, 9]]*oh)

mNH4bNH4j0[temp_, nh3_, co2_, nh4_, hco3_, co3_, nh2coo_, h_, oh_] :=
  b0Values[temp][[4, 2]]*nh3 + b0Values[temp][[4, 3]]*co2 +
  b0Values[temp][[4, 4]]*nh4 + b0Values[temp][[4, 5]]*hco3 + b0Values[temp][[4, 6]]*co3 +
  b0Values[temp][[4, 7]]*nh2coo + b0Values[temp][[4, 8]]*h + b0Values[temp][[4, 9]]*oh
mNH4bNH4j1[temp_, nh3_, co2_, nh4_, hco3_, co3_, nh2coo_, h_, oh_] :=
  (b1Values[temp][[4, 2]]*nh3 + b1Values[temp][[4, 3]]*co2 +
    b1Values[temp][[4, 4]]*nh4 + b1Values[temp][[4, 5]]*hco3 + b1Values[temp][[4, 6]]*co3 +
    b1Values[temp][[4, 7]]*nh2coo + b1Values[temp][[4, 8]]*h + b1Values[temp][[4, 9]]*oh)

mHCO3bHCO3j0[temp_, nh3_, co2_, nh4_, hco3_, co3_, nh2coo_, h_, oh_] :=
  b0Values[temp][[5, 2]]*nh3 + b0Values[temp][[5, 3]]*co2 +
  b0Values[temp][[5, 4]]*nh4 + b0Values[temp][[5, 5]]*hco3 + b0Values[temp][[5, 6]]*co3 +
  b0Values[temp][[5, 7]]*nh2coo + b0Values[temp][[5, 8]]*h + b0Values[temp][[5, 9]]*oh
mHCO3bHCO3j1[temp_, nh3_, co2_, nh4_, hco3_, co3_, nh2coo_, h_, oh_] :=
  (b1Values[temp][[5, 2]]*nh3 + b1Values[temp][[5, 3]]*co2 +
    b1Values[temp][[5, 4]]*nh4 + b1Values[temp][[5, 5]]*hco3 + b1Values[temp][[5, 6]]*co3 +
    b1Values[temp][[5, 7]]*nh2coo + b1Values[temp][[5, 8]]*h + b1Values[temp][[5, 9]]*oh)

mCO3bCO3j0[temp_, nh3_, co2_, nh4_, hco3_, co3_, nh2coo_, h_, oh_] :=
  b0Values[temp][[6, 2]]*nh3 + b0Values[temp][[6, 3]]*co2 +
  b0Values[temp][[6, 4]]*nh4 + b0Values[temp][[6, 5]]*hco3 + b0Values[temp][[6, 6]]*co3 +
  b0Values[temp][[6, 7]]*nh2coo + b0Values[temp][[6, 8]]*h + b0Values[temp][[6, 9]]*oh
mCO3bCO3j1[temp_, nh3_, co2_, nh4_, hco3_, co3_, nh2coo_, h_, oh_] :=
  (b1Values[temp][[6, 2]]*nh3 + b1Values[temp][[6, 3]]*co2 +
    b1Values[temp][[6, 4]]*nh4 + b1Values[temp][[6, 5]]*hco3 + b1Values[temp][[6, 6]]*co3 +
    b1Values[temp][[6, 7]]*nh2coo + b1Values[temp][[6, 8]]*h + b1Values[temp][[6, 9]]*oh)

mNH2COObNH2COOj0[temp_, nh3_, co2_, nh4_, hco3_, co3_, nh2coo_, h_, oh_] :=
  b0Values[temp][[7, 2]]*nh3 + b0Values[temp][[7, 3]]*co2 +
  b0Values[temp][[7, 4]]*nh4 + b0Values[temp][[7, 5]]*hco3 + b0Values[temp][[7, 6]]*co3 +
  b0Values[temp][[7, 7]]*nh2coo + b0Values[temp][[7, 8]]*h + b0Values[temp][[7, 9]]*oh
mNH2COObNH2COOj1[temp_, nh3_, co2_, nh4_, hco3_, co3_, nh2coo_, h_, oh_] :=
  (b1Values[temp][[7, 2]]*nh3 + b1Values[temp][[7, 3]]*co2 +
    b1Values[temp][[7, 4]]*nh4 + b1Values[temp][[7, 5]]*hco3 + b1Values[temp][[7, 6]]*co3 +
    b1Values[temp][[7, 7]]*nh2coo + b1Values[temp][[7, 8]]*h + b1Values[temp][[7, 9]]*oh)

mHbHj0[temp_, nh3_, co2_, nh4_, hco3_, co3_, nh2coo_, h_, oh_] :=
  b0Values[temp][[8, 2]]*nh3 + b0Values[temp][[8, 3]]*co2 +
  b0Values[temp][[8, 4]]*nh4 + b0Values[temp][[8, 5]]*hco3 + b0Values[temp][[8, 6]]*co3 +
  b0Values[temp][[8, 7]]*nh2coo + b0Values[temp][[8, 8]]*h + b0Values[temp][[8, 9]]*oh
mHbHj1[temp_, nh3_, co2_, nh4_, hco3_, co3_, nh2coo_, h_, oh_] :=
  (b1Values[temp][[8, 2]]*nh3 + b1Values[temp][[8, 3]]*co2 +
    b1Values[temp][[8, 4]]*nh4 + b1Values[temp][[8, 5]]*hco3 + b1Values[temp][[8, 6]]*co3 +

```

```

b1Values[temp][[8, 7]]*nh2coo + b1Values[temp][[8, 8]]*h + b1Values[temp][[8, 9]]*oh)

mOHbOHj0[temp_, nh3_, co2_, nh4_, hco3_, co3_, nh2coo_, h_, oh_] :=
b0Values[temp][[9, 2]]*nh3 + b0Values[temp][[9, 3]]*co2 +
b0Values[temp][[9, 4]]*nh4 + b0Values[temp][[9, 5]]*hco3 + b0Values[temp][[9, 6]]*co3 +
b0Values[temp][[9, 7]]*nh2coo + b0Values[temp][[9, 8]]*h + b0Values[temp][[9, 9]]*oh
mOHbOHj1[temp_, nh3_, co2_, nh4_, hco3_, co3_, nh2coo_, h_, oh_] :=
(b1Values[temp][[9, 2]]*nh3 + b1Values[temp][[9, 3]]*co2 +
b1Values[temp][[9, 4]]*nh4 + b1Values[temp][[9, 5]]*hco3 + b1Values[temp][[9, 6]]*co3 +
b1Values[temp][[9, 7]]*nh2coo + b1Values[temp][[9, 8]]*h + b1Values[temp][[9, 9]]*oh)

b0Values[solTemp][[1, 2]]
mNH3bNH3j0[solTemp, nh3, co2, nh4, hco3, co3, nh2coo, h, oh]
mNH3bNH3j1[solTemp, nh3, co2, nh4, hco3, co3, nh2coo, h, oh]
b0Values[solTemp][[1, 3]]
mCO2bCO2j0[solTemp, nh3, co2, nh4, hco3, co3, nh2coo, h, oh]
mCO2bCO2j1[solTemp, nh3, co2, nh4, hco3, co3, nh2coo, h, oh]
b0Values[solTemp][[1, 4]]
mNH4bNH4j0[solTemp, nh3, co2, nh4, hco3, co3, nh2coo, h, oh]
mNH4bNH4j1[solTemp, nh3, co2, nh4, hco3, co3, nh2coo, h, oh]
b0Values[solTemp][[1, 5]]
mHCO3bHCO3j0[solTemp, nh3, co2, nh4, hco3, co3, nh2coo, h, oh]
mHCO3bHCO3j1[solTemp, nh3, co2, nh4, hco3, co3, nh2coo, h, oh]
b0Values[solTemp][[1, 6]]
mCO3bCO3j0[solTemp, nh3, co2, nh4, hco3, co3, nh2coo, h, oh]
mCO3bCO3j1[solTemp, nh3, co2, nh4, hco3, co3, nh2coo, h, oh]
b0Values[solTemp][[1, 7]]
mNH2COObNH2COOj0[solTemp, nh3, co2, nh4, hco3, co3, nh2coo, h, oh]
mNH2COObNH2COOj1[solTemp, nh3, co2, nh4, hco3, co3, nh2coo, h, oh]
b0Values[solTemp][[1, 8]]
mHbHj0[solTemp, nh3, co2, nh4, hco3, co3, nh2coo, h, oh]
mHbHj1[solTemp, nh3, co2, nh4, hco3, co3, nh2coo, h, oh]
b0Values[solTemp][[1, 9]]
mOHbOHj0[solTemp, nh3, co2, nh4, hco3, co3, nh2coo, h, oh]
mOHbOHj1[solTemp, nh3, co2, nh4, hco3, co3, nh2coo, h, oh]

```

NH3

0.06 co3 + 0.015 h - 0.0302199 hco3 + 0.0154992 nh3 + 0.115348 oh

0

CO2

0.0115988 co2 + 0.033 h + 0.017 nh2coo + 0.000107247 nh4 - 0.218907 oh

0

NH4

$$0.000107247 \text{ co}_2 - 0.062 \text{ co}_3 - 0.077 \text{ hco}_3 + 0.05 \text{ nh}_2\text{coo} + 0.06 \text{ oh}$$

$$-0.17172 \text{ co}_3 - 0.21762 \text{ hco}_3 + 0.171 \text{ nh}_2\text{coo} + 0.2016 \text{ oh}$$

HC03

$$0.071 \text{ h} - 0.0302199 \text{ nh}_3 - 0.077 \text{ nh}_4$$

$$0.23526 \text{ h} - 0.21762 \text{ nh}_4$$

C03

$$0.086 \text{ h} + 0.06 \text{ nh}_3 - 0.062 \text{ nh}_4$$

$$0.28116 \text{ h} - 0.17172 \text{ nh}_4$$

NH2C00

$$0.017 \text{ co}_2 + 0.198 \text{ h} + 0.05 \text{ nh}_4$$

$$0.62388 \text{ h} + 0.171 \text{ nh}_4$$

H

$$0.033 \text{ co}_2 + 0.086 \text{ co}_3 + 0.071 \text{ hco}_3 + 0.198 \text{ nh}_2\text{coo} + 0.015 \text{ nh}_3 + 0.208 \text{ oh}$$

$$0.28116 \text{ co}_3 + 0.23526 \text{ hco}_3 + 0.62388 \text{ nh}_2\text{coo} + 0.65448 \text{ oh}$$

OH

$$0.033 \text{ co}_2 + 0.208 \text{ h} + 0.115348 \text{ nh}_3 + 0.06 \text{ nh}_4$$

$$0.65448 \text{ h} + 0.2016 \text{ nh}_4$$

Water activity

```
activitywater[mWater_, aPhi_, ionic_, mimjb0ij_, mimjb1ij_, mi_] :=  
  Exp[mWater*((2*aPhi*ionic^(3/2))/(1 + 1.2*Sqrt[ionic]) - (mimjb0ij + mimjb1ij)) - mWater*mi]
```

```
mimjb0ij[temp_, nh3_, co2_, nh4_, hco3_, co3_, nh2coo_, h_, oh_] :=  
  mNH3bNH3j0[temp, nh3, co2, nh4, hco3, co3, nh2coo, h, oh] +  
  mCO2bCO2j0[temp, nh3, co2, nh4, hco3, co3, nh2coo, h, oh] + mNH4bNH4j0[temp, nh3, co2,  
    nh4, hco3, co3, nh2coo, h, oh] + mCO3bCO3j0[temp, nh3, co2, nh4, hco3, co3, nh2coo, h, oh] +  
  mNH2COObNH2COOj0[temp, nh3, co2, nh4, hco3, co3, nh2coo, h, oh] +  
  mHbHj0[solTemp, nh3, co2, nh4, hco3, co3, nh2coo, h, oh] +  
  mOHbOHj0[solTemp, nh3, co2, nh4, hco3, co3, nh2coo, h, oh]
```

```
mimjb0ij[solTemp, nh3, co2, nh4, hco3, co3, nh2coo, h, oh]
```

$$0.094706 \text{ co}_2 + 0.084 \text{ co}_3 + 0.54 \text{ h} - 0.0362199 \text{ hco}_3 +$$

$$0.265 \text{ nh}_2\text{coo} + 0.205848 \text{ nh}_3 + 0.0481072 \text{ nh}_4 + 0.164441 \text{ oh}$$

```

mjmbjk[temp_, nh3_, co2_, nh4_, hco3_, co3_, nh2coo_, h_, oh_] :=
  (nh3*nh3)*b1Values[temp][[2, 2]] + (nh3*co2)*b1Values[temp][[2, 3]] +
  (nh3*nh4)*b1Values[temp][[2, 4]] + (nh3*hco3)*b1Values[temp][[2, 5]] + (nh3*co3)*b1Values[temp][[2, 6]] +
  (nh3*nh2coo)*b1Values[temp][[2, 7]] + (nh3*h)*b1Values[temp][[2, 8]] + (nh3*oh)*b1Values[temp][[2, 9]] +
  (co2*nh3)*b1Values[temp][[3, 2]] + (co2*co2)*b1Values[temp][[3, 3]] +
  (co2*nh4)*b1Values[temp][[3, 4]] + (co2*hco3)*b1Values[temp][[3, 5]] + (co2*co3)*b1Values[temp][[3, 6]] +
  (co2*nh2coo)*b1Values[temp][[3, 7]] + (co2*h)*b1Values[temp][[3, 8]] + (co2*oh)*b1Values[temp][[3, 9]] +
  (nh4*nh3)*b1Values[temp][[4, 2]] + (nh4*co2)*b1Values[temp][[4, 3]] +
  (nh4*nh4)*b1Values[temp][[4, 4]] + (nh4*hco3)*b1Values[temp][[4, 5]] + (nh4*co3)*b1Values[temp][[4, 6]] +
  (nh4*nh2coo)*b1Values[temp][[4, 7]] + (nh4*h)*b1Values[temp][[4, 8]] + (nh4*oh)*b1Values[temp][[4, 9]] +
  (hco3*nh3)*b1Values[temp][[5, 2]] + (hco3*co2)*b1Values[temp][[5, 3]] +
  (hco3*nh4)*b1Values[temp][[5, 4]] + (hco3*hco3)*b1Values[temp][[5, 5]] +
  (hco3*co3)*b1Values[temp][[5, 6]] + (hco3*nh2coo)*b1Values[temp][[5, 7]] +
  (hco3*h)*b1Values[temp][[5, 8]] + (hco3*oh)*b1Values[temp][[5, 9]] +
  (co3*nh3)*b1Values[temp][[6, 2]] + (co3*co2)*b1Values[temp][[6, 3]] +
  (co3*nh4)*b1Values[temp][[6, 4]] + (co3*hco3)*b1Values[temp][[6, 5]] + (co3*co3)*b1Values[temp][[6, 6]] +
  (co3*nh2coo)*b1Values[temp][[6, 7]] + (co3*h)*b1Values[temp][[6, 8]] + (co3*oh)*b1Values[temp][[6, 9]] +
  (nh2coo*nh3)*b1Values[temp][[7, 2]] + (nh2coo*co2)*b1Values[temp][[7, 3]] +
  (nh2coo*nh4)*b1Values[temp][[7, 4]] + (nh2coo*hco3)*b1Values[temp][[7, 5]] +
  (nh2coo*co3)*b1Values[temp][[7, 6]] + (nh2coo*nh2coo)*b1Values[temp][[7, 7]] +
  (nh2coo*h)*b1Values[temp][[7, 8]] + (nh2coo*oh)*b1Values[temp][[7, 9]] +
  (h*nh3)*b1Values[temp][[8, 2]] + (h*co2)*b1Values[temp][[8, 3]] +
  (h*nh4)*b1Values[temp][[8, 4]] + (h*hco3)*b1Values[temp][[8, 5]] + (h*co3)*b1Values[temp][[8, 6]] +
  (h*nh2coo)*b1Values[temp][[8, 7]] + (h*h)*b1Values[temp][[8, 8]] + (h*oh)*b1Values[temp][[8, 9]] +
  (oh*nh3)*b1Values[temp][[9, 2]] + (oh*co2)*b1Values[temp][[9, 3]] +
  (oh*nh4)*b1Values[temp][[9, 4]] + (oh*hco3)*b1Values[temp][[9, 5]] + (oh*co3)*b1Values[temp][[9, 6]] +
  (oh*nh2coo)*b1Values[temp][[9, 7]] + (oh*h)*b1Values[temp][[9, 8]] + (oh*oh)*b1Values[temp][[9, 9]]

mjmbjk[solTemp, nh3, co2, nh4, hco3, co3, nh2coo, h, oh]

```

0.56232 co3 h + 0.47052 h hco3 + 1.24776 h nh2coo - 0.34344 co3 nh4 -
 0.43524 hco3 nh4 + 0.342 nh2coo nh4 + 1.30896 h oh + 0.4032 nh4 oh

```

mi[nh3_, co2_, nh4_, hco3_, co3_, nh2coo_, h_, oh_] := nh3 + co2 + nh4 + hco3 + co3 + nh2coo + h + oh

activitywater[0.018, aPhiDebye[solTemp], ionic, mimjb0ij[solTemp, ionic, nh3, co2, nh4, hco3, co3, nh2coo, h, oh],
  mjmbjk[solTemp, nh3, co2, nh4, hco3, co3, nh2coo, h, oh], mi[nh3, co2, nh4, hco3, co3, nh2coo, h, oh]];

```

Equilibrium constants

```
ammonium[temp_, nh3_, h2o_, nh4_, oh_, acNH4_, acOH_, acNH3_] := Module[{K, absTemp},
  absTemp = temp + 273.15;
  K = equilibria[absTemp, -5914.082, -15.06399, -0.01100801, 97.97152];
  K == (nh4*oh)/(nh3*h2o)*(acNH4*acOH)/(acNH3)]

ammonium[solTemp, nh3, h2o, nh4, oh, 1, 1, 1]
```

$$0.000016945 = \frac{\text{nh4 oh}}{\text{h2o nh3}}$$

```
bicarbonate[temp_, co2_, h2o_, hco3_, h_, acCO2_, acHCO3_, acH_] := Module[{K, absTemp},
  absTemp = temp + 273.15;
  K = equilibria[absTemp, -7726.010, -14.50613, -0.02798420, 102.2755];
  K == (hco3*h)/(co2*h2o)]

bicarbonate[solTemp, co2, h2o, hco3, h, 1, 1, 1]
```

$$4.32956 \times 10^{-7} = \frac{\text{h hco3}}{\text{co2 h2o}}$$

```
carbonate[temp_, hco3_, co3_, h_, acHCO3_, acCO3_, acH_] := Module[{K, absTemp},
  absTemp = temp + 273.15;
  K = equilibria[absTemp, -9137.258, -18.11192, -0.02245619, 116.7371];
  K == (co3*h)/(hco3)]

carbonate[solTemp, hco3, co3, h, 1, 1, 1]
```

$$4.4333 \times 10^{-11} = \frac{\text{co3 h}}{\text{hco3}}$$

```
carbamate[temp_, nh3_, hco3_, nh2coo_, h2o_, acNH3_, acHCO3_, acNH2COO_] := Module[{K, absTemp},
  absTemp = temp + 273.15;
  K = equilibria[absTemp, 604.1164, -4.017263, 0.005030950, 20.15214];
  K == (nh2coo*h2o)/(nh3*hco3)]

carbamate[solTemp, nh3, hco3, nh2coo, h2o, 1, 1, 1]
```

$$2.27107 = \frac{\text{h2o nh2coo}}{\text{hco3 nh3}}$$

```

water[temp_, h_, oh_, h2o_, acH_, acOH_] := Module[{K, absTemp},
  absTemp = temp + 273.15;
  K = 10^(-(4471.33/absTemp - 6.0846 + 0.017053*absTemp));
  K == (oh*h)/h2o]

```

```
water[solTemp, h, oh, h2o, 1, 1]
```

$$8.63298 \times 10^{-15} = \frac{h \text{ oh}}{h2o}$$

Non-equilibrium system constraints

```

totalcarbon[carbontotal_, co2_, co3_, hco3_, nh2coo_] :=
  carbontotal == Abs[co2] + Abs[co3] + Abs[nh2coo] + Abs[hco3]
totalnitrogen[nitrogentotal_, nh3_, nh4_, nh2coo_] :=
  nitrogentotal == Abs[nh3] + Abs[nh4] + Abs[nh2coo]
electroneutrality[co3_, nh2coo_, hco3_, nh4_] :=
  2*Abs[co3] + Abs[nh2coo] + Abs[hco3] == Abs[nh4]

```

Activity of each species

```

activitywater[0.018, aPhiDebye[solTemp], ionic, mimjb0ij[solTemp, nh3, co2, nh4, hco3, co3, nh2coo, h, oh],
  mjmbjk[solTemp, nh3, co2, nh4, hco3, co3, nh2coo, h, oh], mi[nh3, co2, nh4, hco3, co3, nh2coo, h, oh]];
activityion[aPhiDebye[solTemp], 1, ionic, mHbHj0[solTemp, nh3, co2, nh4, hco3, co3, nh2coo, h, oh],
  mHbHj1[solTemp, nh3, co2, nh4, hco3, co3, nh2coo, h, oh],
  mjmbjk[solTemp, nh3, co2, nh4, hco3, co3, nh2coo, 0, oh]];
activityion[aPhiDebye[solTemp], -1, ionic, mOHbOHj0[solTemp, nh3, co2, nh4, hco3, co3, nh2coo, h, oh],
  mOHbOHj1[solTemp, nh3, co2, nh4, hco3, co3, nh2coo, h, oh],
  mjmbjk[solTemp, nh3, co2, nh4, hco3, co3, nh2coo, h, 0]];
activityion[aPhiDebye[solTemp], 0, ionic, mNH3bNH3j0[solTemp, nh3, co2, nh4, hco3, co3, nh2coo, h, oh],
  mNH3bNH3j1[solTemp, nh3, co2, nh4, hco3, co3, nh2coo, h, oh],
  mjmbjk[solTemp, 0, co2, nh4, hco3, co3, nh2coo, h, oh]];
activityion[aPhiDebye[solTemp], 1, ionic, mNH4bNH4j0[solTemp, nh3, co2, nh4, hco3, co3, nh2coo, h, oh],
  mNH4bNH4j1[solTemp, nh3, co2, nh4, hco3, co3, nh2coo, h, oh],
  mjmbjk[solTemp, nh3, co2, 0, hco3, co3, nh2coo, h, oh]];
activityion[aPhiDebye[solTemp], 0, ionic, mCO2bCO2j0[solTemp, nh3, co2, nh4, hco3, co3, nh2coo, h, oh],
  mCO2bCO2j1[solTemp, nh3, co2, nh4, hco3, co3, nh2coo, h, oh],
  mjmbjk[solTemp, nh3, 0, nh4, hco3, co3, nh2coo, h, oh]];
activityion[aPhiDebye[solTemp], -1, ionic, mHCO3bHCO3j0[solTemp, nh3, co2, nh4, hco3, co3, nh2coo, h, oh],
  mHCO3bHCO3j1[solTemp, nh3, co2, nh4, hco3, co3, nh2coo, h, oh],
  mjmbjk[solTemp, nh3, co2, nh4, 0, co3, nh2coo, h, oh]];
activityion[aPhiDebye[solTemp], -1, ionic, mNH2COObNH2COOj0[solTemp, nh3, co2, nh4, hco3, co3, nh2coo, h, oh],
  mNH2COObNH2COOj1[solTemp, nh3, co2, nh4, hco3, co3, nh2coo, h, oh],
  mjmbjk[solTemp, nh3, co2, nh4, hco3, co3, 0, h, oh]];
activityion[aPhiDebye[solTemp], -2, ionic, mCO3bCO3j0[solTemp, nh3, co2, nh4, hco3, co3, nh2coo, h, oh],
  mCO3bCO3j1[solTemp, nh3, co2, nh4, hco3, co3, nh2coo, h, oh],
  mjmbjk[solTemp, nh3, co2, nh4, hco3, 0, nh2coo, h, oh]];

```

Speciation for ideality

all interaction parameters = 0
 activity coefficients = 1
 water activity = mol fraction

```
molWater = ((carbonTotal + nitrogenTotal) * 18.02 / 1000) ^ (-1) * (carbonTotal + nitrogenTotal)
waterMolFrac = molWater / (carbonTotal + nitrogenTotal + molWater)

idealSpecies = Quiet[NSolve[{
  water[solTemp, h, oh, h2o, 1, 1],
  ammonium[solTemp, nh3, h2o, nh4, oh, 1, 1, 1],
  bicarbonate[solTemp, co2, h2o, hco3, h, 1, 1, 1],
  carbonate[solTemp, hco3, co3, h, 1, 1, 1],
  carbamate[solTemp, nh3, hco3, nh2coo, h2o, 1, 1, 1],
  totalcarbon[carbonTotal, co2, co3, hco3, nh2coo],
  totalnitrogen[nitrogenTotal, nh3, nh4, nh2coo],
  electroneutrality[co3, nh2coo, hco3, nh4],
  hco3 > 0,
  co3 > 0,
  nh3 > 0,
  nh4 > 0,
  co2 > 0,
  nh2coo > 0,
  oh > 0,
  h > 0,
  h2o == waterMolFrac},
  {hco3, co3, nh3, nh4, co2, nh2coo, oh, h, h2o}, Reals]]

hco3conc = hco3 /. idealSpecies[[1]];
co3conc = co3 /. idealSpecies[[1]];
nh4conc = nh4 /. idealSpecies[[1]];
nh2cooconc = nh2coo /. idealSpecies[[1]];
nh3conc = nh3 /. idealSpecies[[1]];
ohconc = oh /. idealSpecies[[1]];
hconc = h /. idealSpecies[[1]];
co2conc = co2 /. idealSpecies[[1]];
idealOsmoticPressure =
  (hco3conc + co3conc + nh4conc + nh2cooconc + nh3conc) * 8.314 * 10^-2 * (273.15 + solTemp)
```

55.4939

0.926221

```
{ { hco3 -> 1.70586, co3 -> 0.00508766, nh3 -> 0.0686585, nh4 -> 2.00322, co2 -> 0.0632322,
  nh2coo -> 0.287179, oh -> 5.37925 * 10^-7, h -> 1.48646 * 10^-8, h2o -> 0.926221 } }
```

100.211


```

ionicIdealVal = ionicStr[nh4conc, hco3conc, co3conc, nh2cooconc, ohconc, hconc]
aH2OidealVal = activitywater[0.018, aPhiDebye[solTemp], ionicIdealVal,
    mimjb0ij[solTemp, nh3conc, co2conc, nh4conc, hco3conc, co3conc, nh2cooconc, hco3conc, ohconc],
    mjmbjk[solTemp, nh3conc, co2conc, nh4conc, hco3conc, co3conc, nh2cooconc, hconc, ohconc],
    mi[nh3conc, co2conc, nh4conc, hco3conc, co3conc, nh2cooconc, hconc, ohconc]]
acHidealVal = activityion[aPhiDebye[solTemp], 1, ionicIdealVal,
    mHbHj0[solTemp, nh3conc, co2conc, nh4conc, hco3conc, co3conc, nh2cooconc, hconc, ohconc],
    mHbHj1[solTemp, nh3conc, co2conc, nh4conc, hco3conc, co3conc, nh2cooconc, hconc, ohconc],
    mjmbjk[solTemp, nh3conc, co2conc, nh4conc, hco3conc, co3conc, nh2cooconc, 0, ohconc]]
acOHidealVal = activityion[aPhiDebye[solTemp], -1, ionicIdealVal,
    mOHbOHj0[solTemp, nh3conc, co2conc, nh4conc, hco3conc, co3conc, nh2cooconc, hconc, ohconc],
    mOHbOHj1[solTemp, nh3conc, co2conc, nh4conc, hco3conc, co3conc, nh2cooconc, hconc, ohconc],
    mjmbjk[solTemp, nh3conc, co2conc, nh4conc, hco3conc, co3conc, nh2cooconc, hconc, 0]]
acNH3idealVal = activityion[aPhiDebye[solTemp], 0, ionicIdealVal,
    mNH3bNH3j0[solTemp, nh3conc, co2conc, nh4conc, hco3conc, co3conc, nh2cooconc, hconc, ohconc],
    mNH3bNH3j1[solTemp, nh3conc, co2conc, nh4conc, hco3conc, co3conc, nh2cooconc, hconc, ohconc],
    mjmbjk[solTemp, 0, co2conc, nh4conc, hco3conc, co3conc, nh2cooconc, hconc, ohconc]]
acNH4idealVal = activityion[aPhiDebye[solTemp], 1, ionicIdealVal,
    mNH4bNH4j0[solTemp, nh3conc, co2conc, nh4conc, hco3conc, co3conc, nh2cooconc, hconc, ohconc],
    mNH4bNH4j1[solTemp, nh3conc, co2conc, nh4conc, hco3conc, co3conc, nh2cooconc, hconc, ohconc],
    mjmbjk[solTemp, nh3conc, co2conc, 0, hco3conc, co3conc, nh2cooconc, hconc, ohconc]]
acCO2idealVal = activityion[aPhiDebye[solTemp], 0, ionicIdealVal,
    mCO2bCO2j0[solTemp, nh3conc, co2conc, nh4conc, hco3conc, co3conc, nh2cooconc, hconc, ohconc],
    mCO2bCO2j1[solTemp, nh3conc, co2conc, nh4conc, hco3conc, co3conc, nh2cooconc, hconc, ohconc],
    mjmbjk[solTemp, nh3conc, 0, nh4conc, hco3conc, co3conc, nh2cooconc, hconc, ohconc]]
acHCO3idealVal = activityion[aPhiDebye[solTemp], -1, ionicIdealVal,
    mHCO3bHCO3j0[solTemp, nh3conc, co2conc, nh4conc, hco3conc, co3conc, nh2cooconc, hconc, ohconc],
    mHCO3bHCO3j1[solTemp, nh3conc, co2conc, nh4conc, hco3conc, co3conc, nh2cooconc, hconc, ohconc],
    mjmbjk[solTemp, nh3conc, co2conc, nh4conc, 0, co3conc, nh2cooconc, hconc, ohconc]]
acNH2COOidealVal = activityion[aPhiDebye[solTemp], -1, ionicIdealVal,
    mNH2COObNH2COOj0[solTemp, nh3conc, co2conc, nh4conc, hco3conc, co3conc, nh2cooconc, hconc, ohconc],
    mNH2COObNH2COOj1[solTemp, nh3conc, co2conc, nh4conc, hco3conc, co3conc, nh2cooconc, hconc, ohconc],
    mjmbjk[solTemp, nh3conc, co2conc, nh4conc, hco3conc, co3conc, 0, hconc, ohconc]]
acCO3idealVal = activityion[aPhiDebye[solTemp], -2, ionicIdealVal,
    mCO3bCO3j0[solTemp, nh3conc, co2conc, nh4conc, hco3conc, co3conc, nh2cooconc, hconc, ohconc],
    mCO3bCO3j1[solTemp, nh3conc, co2conc, nh4conc, hco3conc, co3conc, nh2cooconc, hconc, ohconc],
    mjmbjk[solTemp, nh3conc, co2conc, nh4conc, hco3conc, 0, nh2cooconc, hconc, ohconc]]

```

2.0083

0.94628

0.742088

0.625226

0.904509

0.287935

1.01173

0.254964

0.576249

0.0199176

Solution for non-ideal case

```

nonidealSpecies = FindRoot[{
  water[solTemp, h, oh, aH2O, acH, acOH],
  ammonium[solTemp, nh3, aH2O, nh4, oh, acNH3, acNH4, acOH],
  bicarbonate[solTemp, co2, aH2O, hco3, h, acCO2, acHCO3, acH],
  carbonate[solTemp, hco3, co3, h, acHCO3, acCO3, acH],
  carbamate[solTemp, nh3, hco3, nh2coo, aH2O, acNH3, acHCO3, acNH2COO],
  totalcarbon[carbonTotal, co2, co3, hco3, nh2coo],
  totalnitrogen[nitrogenTotal, nh3, nh4, nh2coo],
  electroneutrality[co3, nh2coo, hco3, nh4],
  ionic == ionicStr[nh4, hco3, co3, nh2coo, oh, h],
  aH2O ==
  activitywater[0.018, aPhiDebye[solTemp], ionic, mimjb0ij[solTemp, nh3, co2, nh4, hco3, co3, nh2coo, h, oh],
    mjmbjk[solTemp, nh3, co2, nh4, hco3, co3, nh2coo, h, oh], mi[nh3, co2, nh4, hco3, co3, nh2coo, h, oh]],
  acH == activityion[aPhiDebye[solTemp], 1, ionic, mHbHj0[solTemp, nh3, co2, nh4, hco3, co3, nh2coo, h, oh],
    mHbHj1[solTemp, nh3, co2, nh4, hco3, co3, nh2coo, h, oh],
    mjmbjk[solTemp, nh3, co2, nh4, hco3, co3, nh2coo, 0, oh]],
  acOH == activityion[aPhiDebye[solTemp], -1, ionic, mOHbOHj0[solTemp, nh3, co2, nh4, hco3,
    co3, nh2coo, h, oh], mOHbOHj1[solTemp, nh3, co2, nh4, hco3, co3, nh2coo, h, oh],
    mjmbjk[solTemp, nh3, co2, nh4, hco3, co3, nh2coo, h, 0]],
  acNH3 == activityion[aPhiDebye[solTemp], 0, ionic, mNH3bNH3j0[solTemp, nh3, co2, nh4, hco3,
    co3, nh2coo, h, oh], mNH3bNH3j1[solTemp, nh3, co2, nh4, hco3, co3, nh2coo, h, oh],
    mjmbjk[solTemp, 0, co2, nh4, hco3, co3, nh2coo, h, oh]],
  acNH4 == activityion[aPhiDebye[solTemp], 1, ionic, mNH4bNH4j0[solTemp, nh3, co2, nh4, hco3,
    co3, nh2coo, h, oh], mNH4bNH4j1[solTemp, nh3, co2, nh4, hco3, co3, nh2coo, h, oh],
    mjmbjk[solTemp, nh3, co2, 0, hco3, co3, nh2coo, h, oh]],
  acCO2 == activityion[aPhiDebye[solTemp], 0, ionic, mCO2bCO2j0[solTemp, nh3, co2, nh4, hco3,
    co3, nh2coo, h, oh], mCO2bCO2j1[solTemp, nh3, co2, nh4, hco3, co3, nh2coo, h, oh],
    mjmbjk[solTemp, nh3, 0, nh4, hco3, co3, nh2coo, h, oh]],
  acHCO3 == activityion[aPhiDebye[solTemp], -1, ionic, mHCO3bHCO3j0[solTemp, nh3, co2, nh4,
    hco3, co3, nh2coo, h, oh], mHCO3bHCO3j1[solTemp, nh3, co2, nh4, hco3, co3, nh2coo, h, oh],
    mjmbjk[solTemp, nh3, co2, nh4, 0, co3, nh2coo, h, oh]],
  acNH2COO == activityion[aPhiDebye[solTemp], -1, ionic, mNH2COObNH2COOj0[solTemp, nh3, co2, nh4,
    hco3, co3, nh2coo, h, oh], mNH2COObNH2COOj1[solTemp, nh3, co2, nh4, hco3, co3, nh2coo, h, oh],
    mjmbjk[solTemp, nh3, co2, nh4, hco3, co3, 0, h, oh]],
  acCO3 == activityion[aPhiDebye[solTemp], -2, ionic, mCO3bCO3j0[solTemp, nh3, co2, nh4,
    hco3, co3, nh2coo, h, oh], mCO3bCO3j1[solTemp, nh3, co2, nh4, hco3, co3, nh2coo, h, oh],
    mjmbjk[solTemp, nh3, co2, nh4, hco3, 0, nh2coo, h, oh]]],
  {{nh3, nh3conc}, {co2, co2conc}, {nh4, nh4conc}, {hco3, hco3conc}, {co3, co3conc},
  {nh2coo, nh2cooconc}, {h, hconc}, {oh, ohconc},
  {ionic, ionicIdealVal}, {aH2O, waterMolFrac},
  {acH, 1}, {acOH, 1}, {acNH3, 1}, {acNH4, 1}, {acCO2, 1}, {acHCO3, 1}, {acNH2COO, 1}, {acCO3, 1}},
  {MaxIterations -> 100000, AccuracyGoal -> 5, PrecisionGoal -> 6}]

```

```
{nh3 → 0.0611685, co2 → 0.0293044, nh4 → 2.04336, hco3 → 1.76623, co3 → 0.0113074,
nh2coo → 0.254522, h → 6.92485 × 10-9, oh → 1.20179 × 10-6, ionic → 2.05467,
aH2O → 0.964006, acH → 0.730673, acOH → 0.623316, acNH3 → 0.901679, acNH4 → 0.281274,
acCO2 → 1.00982, acHCO3 → 0.252198, acNH2COO → 0.575592, acCO3 → 0.019436}
```

Extraction of values and osmotic pressure calculation

```
nh3conc = nh3 /. nonidealSpecies;
nh4conc = nh4 /. nonidealSpecies;
hco3conc = hco3 /. nonidealSpecies;
co3conc = co3 /. nonidealSpecies;
nh2cooconc = nh2coo /. nonidealSpecies;
hconc = h /. nonidealSpecies;
ohconc = oh /. nonidealSpecies;
actCoNH3 = acNH3 /. nonidealSpecies;
actCoNH4 = acNH4 /. nonidealSpecies;
actCoHCO3 = acHCO3 /. nonidealSpecies;
actCoCO3 = acCO3 /. nonidealSpecies;
actCoNH2COO = acNH2COO /. nonidealSpecies;

osmoticPressure = -(1000/18.02)*8.314*10-2*(273.15 + solTemp) (Log[aH2O /. nonidealSpecies])

waterActivity = aH2O /. nonidealSpecies;
ionicStrength = ionic /. nonidealSpecies;
```

50.0883

Export of data

Exports molal concentrations of each component, osmotic pressure, water activity, and ionic strength
Default export location is to "My Documents" folder

```
exportMat = {"mTotalNH3", nitrogenTotal}, {"mTotalCO2", carbonTotal}, {"mNH3", nh3conc}, {"mCO2", co2conc},
{"mNH4", nh4conc}, {"mHCO3", hco3conc}, {"mCO3", co3conc}, {"mNH2COO", nh2cooconc}, {"mH", hconc},
{"mOH", ohconc}, {"piW", osmoticPressure}, {"waterActivity", waterActivity}, {"ionicStrength", ionicStrength}}

Export["nh3-co2_spec.xls", {"data" → exportMat}]
```

```
{ {mTotalNH3, 2.35905}, {mTotalCO2, 2.06136}, {mNH3, 0.0611685},
{mCO2, 0.0632322}, {mNH4, 2.04336}, {mHCO3, 1.76623}, {mCO3, 0.0113074},
{mNH2COO, 0.254522}, {mH, 6.92485 × 10-9}, {mOH, 1.20179 × 10-6},
{piW, 50.0883}, {waterActivity, 0.964006}, {ionicStrength, 2.05467} }
```

nh3-co2_spec.xls

Appendix 2

Design and iteration of the dopamine coating containers

A2.1 The original

The earliest origins of the dopamine coating container (DCC) arose in the early fall of 2009 with the objective of constructing an inexpensive container from readily available materials that could be sealed in such a way that only a single side of an asymmetric membrane could be coated by dopamine. Additionally, the materials of construction had to be resilient to the mildly alkaline aqueous conditions under which the dopamine polymerization occurs. Acrylonitrile butadiene styrene (ABS) plastic was selected as base material for what would become the first generation of the coating containers.

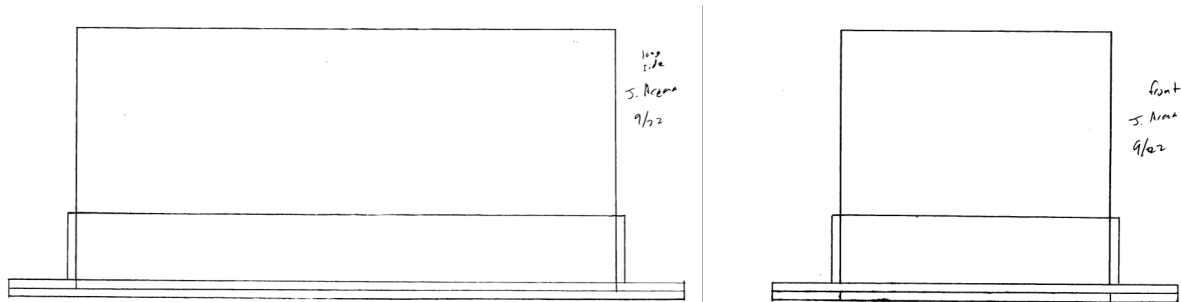


Fig. A2.1. Sketch of the first generation DCC from September 2009.

The first generation of the coating box was assembled from ABS plastic sheet with a thickness of 1/16 in that was cut into manageable widths (0.5 to 5 in) by the machine shop. Conventional plastic cement was used to glue together the first generation of the DCC.

Author's note: Retrospectively ABS pipe primer and pipe cement would have probably produced better results in the construction of the first generation DCC.

The container was design to have a separate base and top. The original sketch of the first generation DCC is shown in Fig. A2.1. The base top half of the DCC was assemble from two overlapping layers of 1/2 in ABS. This served as a framing to support the walls that were glued to this outer frame. The top half of this initial version of the DCC was not completely leak proof. The corners and any seems in the top half of the container were filled plastic repair epoxy putty. The gaps filled by the repair putty can be seen in Fig. A2.2.

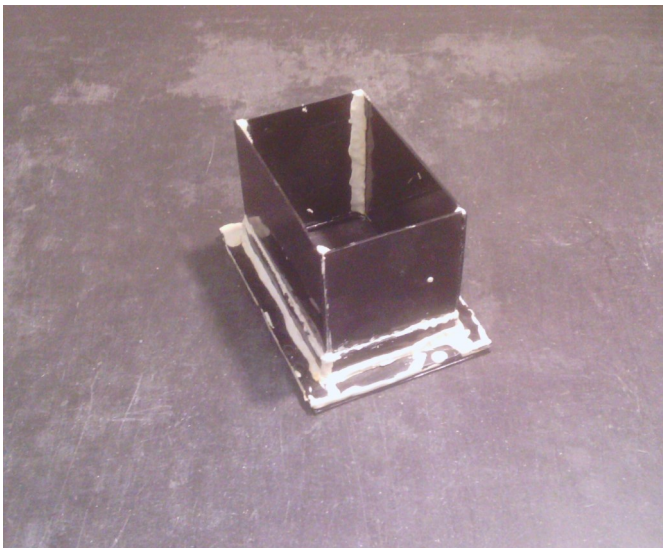


Fig. A2.2. The first generation DCC. Note the white epoxy used to seal the joints between ABS sheets.

To seal between the base top of the DCC a rubber gasket made from neoprene was used. Gaskets were cut by hand to the dimensions of the coating containers. In the use of the DCC this gasket would be placed between the top and base. The DCC was held together by eight medium

size binder clips. Neoprene was also used as a construction material to form a reservoir at the bottom of the base of the coating container. The base was assembled by gluing two gaskets to the ABS plastic bottom. This creates a $\sim 1/8$ in reservoir that during dopamine modification of a membrane could be filled with water or buffer solution to keep the polyamide hydrated and prevent it from sticking to the bottom of the DCC. Since plastic cement did not stick to the neoprene a food grade epoxy glue was use instead.

A2.2. The next generation

The first generation of the DCC was only made as a single unit. The second generation

was more widely produced and used in the earliest studies on the efficacy of the dopamine modification. These followed a similar construction to the first generation DCC. Three major

differences exist between the first and second generation DCC. The



Fig. A2.3. The top and bottom of the second generation DCC. The bottom of the second generation was used for subsequent iterations of the DCC.

second generation DCC is slightly shorter, it was assembled completely using food grade epoxy, and the top half was built upon neoprene gasket. To which the overlapping layers of the ABS strips were glued. Like the first generation the top walls of the DCC were ABS.

A2.3. Mass production

The second generation of the DCC was an effective tool in developing the methodology of the dopamine modification; however, the relatively slow curing time of the epoxy (~1 hour) and the need for precise sizing of the ABS sheets caused the construction of more DCCs to be a timely proposition. The third generation sought to overcome this limitation. The solid ABS walls

of the top half of the DCC were replaced by an ABS frame. On the inside of the ABS frame neoprene was used to create the walls. To aid in the sealing of the third generation DCC room temperature vulcanizing (RTV) silicon was used. This greatly shortened the time needed to cut the 1/2 in ABS strips and neoprene rubber to assemble new DCCs. In addition to sealing the third generation DCC the RTV silicon was also used for repairs of second generation DCCs where the walls separated at the corners. A comparison image of the second and third generation DCCs is shown in Fig. A2.4. One additional improvement made during this time

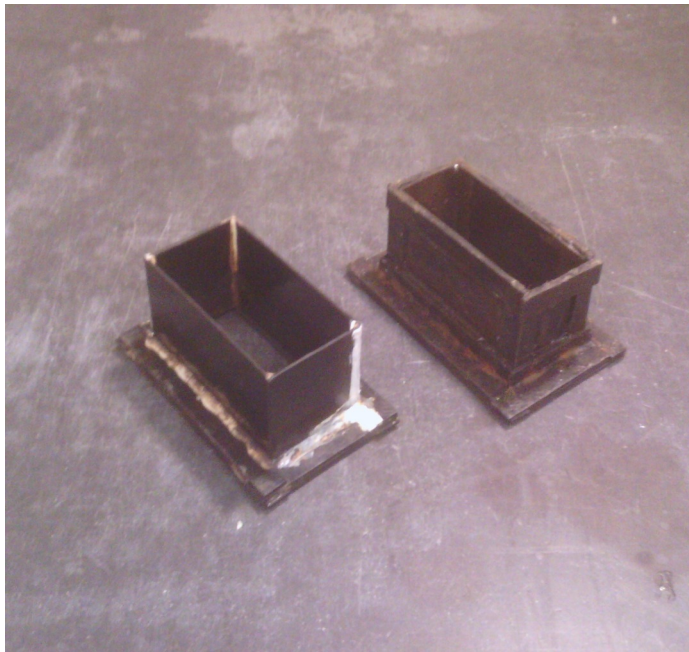


Fig. A2.4. The second and third generation DCCs. The second generation DCC has gaps sealed with white RTV silicon and the third generation DCC is sealed with black RTV silicon.

was the replacement of the neoprene rubber gasket with a closed cell foam one. This create a much better seal between the top and bottom of the DCC greatly reducing leakage.

A2.4. The rise of 3d printing

In the summer of 2013 a FormLabs Form 1 3d printer was purchased. This tool helped to pilot and construct the fourth and fifth generations of the DCCs. This printer uses a photosensitive resin of acrylic oligomers cured by an ultraviolet laser to produce high resolution objects. The fourth generation DCC was design as one solid piece to be printed by the Form 1. In actual use the Form 1 prove to be fairly disappointing. Many of the prints

typically failed require multiple attempt to get successful print. The quality of the prints improve with newer version of the printer firmware and usage of different print settings.

Eventually the fourth generation DCC was successfully printed; however, it has thick walls and used a substantial amount of resin to produce it. In the printed part there was a slight warp (more significant in the base of the DCC) and it was never used to dopamine modify a

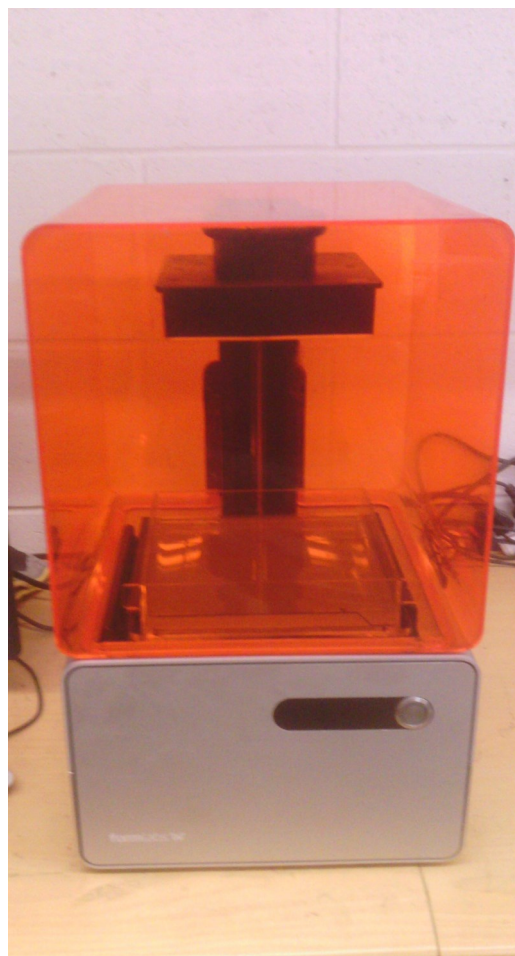


Fig. A2.5. FormLabs Form 1 3d printer.

membrane. The cost of the Form 1's resin (\$149 per liter) was the primary deterrent to a complete redesign rather than a tweaking of fourth generation DCCs.

A2.5. The fifth and final

The fifth generation of the DCC was an improvement on the forth to reduce the costs of resin and bet less sensitive to the quirks of the Form 1 printer. The initial iteration of the fifth generation DCC was also substantially larger than earlier generations. This was to accommodate the sample of membrane being made in the lab.



Fig. A2.6. The fourth generation DCC. The rough surface facing forward are the remnants of the supports needed to by the Form 1.

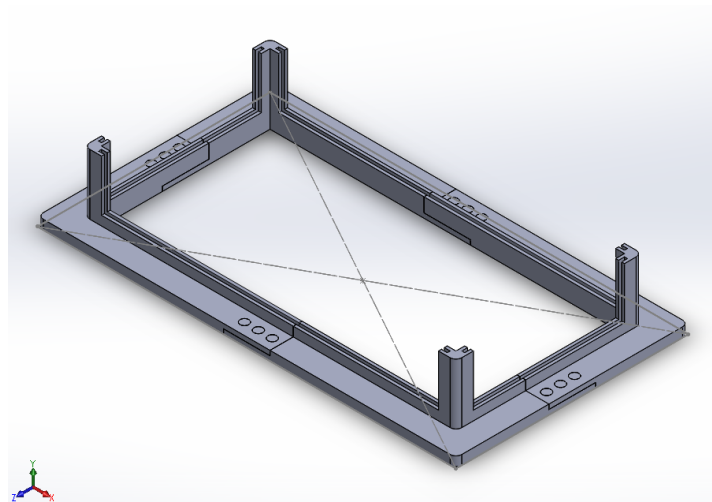


Fig. A2.7. The fifth generation DCC showing the four parts that lock together to make the larger top piece.

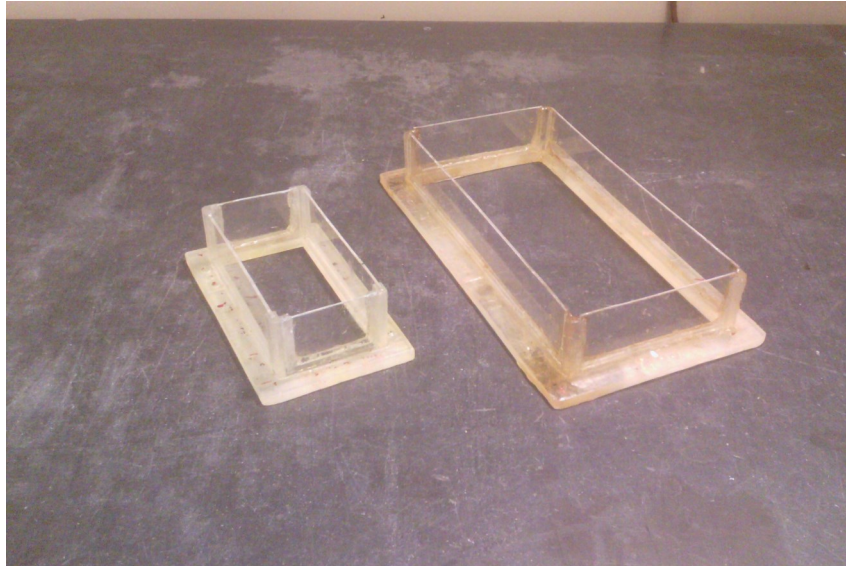


Fig. A2.8. The standard size and larger fifth generation DCCs.

It consisted of four pieces that would be fitted together to make a frame. These pieces consisted of the bottom edge of the top and the corners of the DCC. In the base and corners there was a 1/16 in groove where a piece of acrylic could be seated. Since only the base and corners needed to be 3d printed (the base was revert back to the first through third generation style of neoprene glued to a piece of ABS or acrylic) substantially less resin was need to produce a fifth generation DCC when compared to the fourth. Acrylic was selected as a wall material instead of ABS because initially the DCC was assembled by using the Form 1's resin to fuse the pieces together and there were concerns that the resin would not stick to ABS.

Author's note: Retrospectively the food grade epoxy could have been used far more simply than fusing the parts with the Form 1's resin turned out to be.

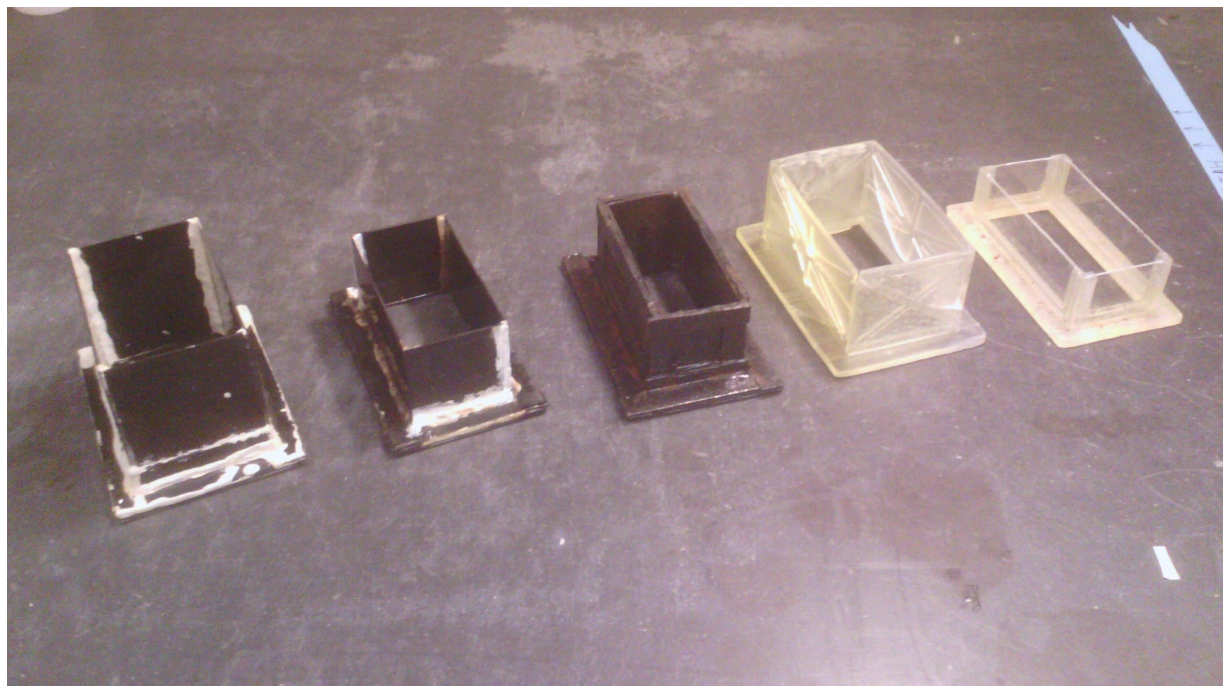


Fig. A2.9. The first through fifth generation of the DCC.

Appendix 3

Titration of chloride within the ammonia-carbon dioxide draw solution

A3.1 Method development

Chloride concentrations within samples of the ammonia-carbon dioxide ($\text{NH}_3\text{-CO}_2$) draw solution collected from desalination tests were determined using a modified Mohr titration. In the Mohr titration silver nitrate (AgNO_3) is titrated into a solution dosed with potassium chromate (KCrO_4). When the titration reaches the endpoint the solution's color will change from yellow to reddish-brown.¹ This titration was performed on the $\text{NH}_3\text{-CO}_2$ draw solution, which contains a mixture of ammonium, bicarbonate, carbonate, and carbamate ions. The high concentrations of these background ions interfered with the endpoint. Subtle modifications the established technique were tried to address this shortcoming. Initially, precipitation of the majority of the carbonates with calcium nitrate ($\text{Ca}(\text{NO}_3)_2$) was attempted as a way to eliminate

their interference with the titration. Despite $\text{Ca}(\text{NO}_3)_2$ blanking in the same way as water (having no titratable chloride) attempts to titrate solutions of a known chloride concentration in $\text{NH}_3\text{-CO}_2$ with added $\text{Ca}(\text{NO}_3)_2$ failed to produce accurate titres.

Another attempt to address the carbonates interference on the titration involved volatilization of the carbonates rather than precipitating them. For this approach, the solution to be titrated was boiled to dryness, and after cooling, the solution was rehydrated. The solutions were boiled in 125 mL Erlenmeyer flasks, and to prevent spattering and as a consequence a loss of some ions a perforated aluminum disk was placed over the mouth of the flask and rinsed during the rehydration. For these experiments 25 mL of solution was evaporated and rehydrated with 25 mL of deionized water.

The titration was performed in the same flask as the evaporation using a initial indicator concentration of $3.7 \text{ g}\cdot\text{L}^{-1} \text{ KCrO}_4$. To test this titration know solutions were prepared with concentrations of 0.00200 M, 0.00500 M, 0.0100 M, and 0.00150 M NaCl in 2.0 M $\text{NH}_3\text{-CO}_2$ draw solution. The solutions were all titred with a 0.01 M AgNO_3

solution. Upon reaching the endpoint 5.00 mL of 0.01001 M NaCl solution was added to the solution and re-titrated. This sequence of steps was performed three times per sample.

A3.2. Accuracy of titration on samples of known concentration

As these data indicate (Fig. A3.1) there is near perfect agreement between the known and titred concentrations for 0.00200 M and 0.00500 M. Close agreement was observed for 0.0100 and 0.0150 M solutions. The percent agreement between the actual and titred concentrations was calculated by Eq. (A3.1).

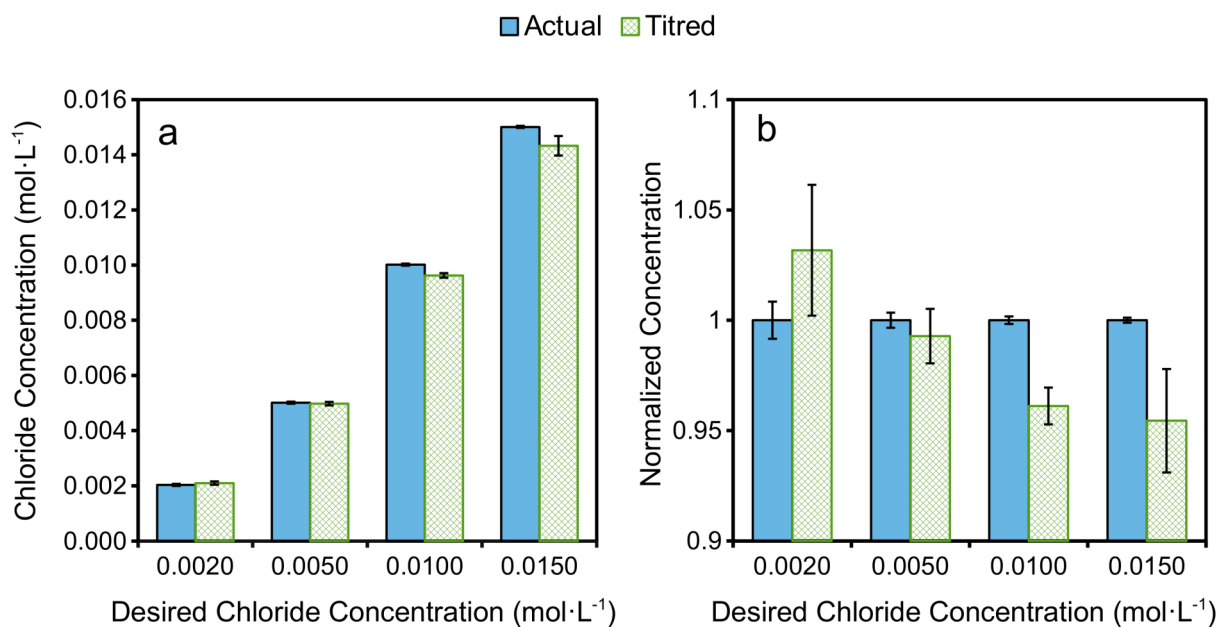


Fig. A3.1. Actual vs. titred concentrations of chloride from added sodium chloride within a 2.0 M NH₃-CO₂ draw solutions (a). Titled concentration of chloride normalized to the actual concentration within solution (b).

$$\% \text{Agreement} = 1 - \frac{|c_{\text{actual}} - c_{\text{titred}}|}{c_{\text{actual}}} \quad (\text{A3.1})$$

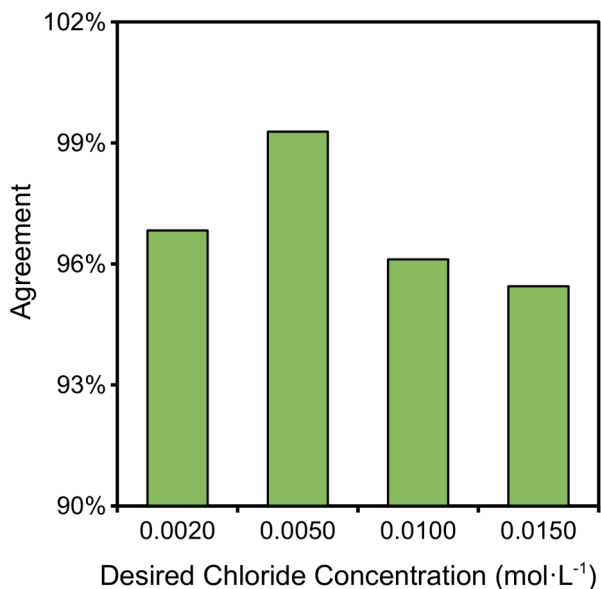


Fig. A3.2. Agreement between actual and titred chloride concentration for samples of 2.0 M NH₃-CO₂ draw solution having a known concentration of added sodium chloride.

In Eq. (A3.1) c_{actual} is the chloride concentration and c_{titred} is the is the titred chloride concentration. As shown in Fig. A3.2 all titrations measured a chloride concentration within 95.5% of the known concentration. The good agreement at low concentrations (within the ranges of the actual draw solutions described earlier) shows this to be a reasonably (>95%)

accurate for chloride determination in the presence of a much larger concentration of ammonium, bicarbonate, carbonate, and carbamate ions.

References

1. Jeffrey, G. H.; Bassett, J.; Mendham, J.; Denny R. C. *Vogel's Textbook of Quantitative Chemical Analysis*, Fifth ed.; Longman Scientific & Technical Essex, 1989.

Appendix 4

Numerical simulation of membrane performance and calculation of effective structural parameter

Initial Values and Solution options

To prevent errors restart the kernel with each calculation

Solution Types

- 1) Structural Parameter for Variable Concentration Range (assumes 0 TMP)
- 2) Structural Parameter for Variable Transmembrane Pressure (assumes PRO, negative TMP for AFO)
- 3) Water Flux for Variable Concentration Range (assumes 0 TMP)
- 4) Water Flux for Variable Pressure Range (assumes PRO, negative TMP for AFO)
- 5) Water Flux for Variable Pressure Range and Variable Structural Parameter
- 6) Solute Permeability and Effective Structural Parameter for Variable Concentration Range (needs water and salt flux from FO test)

```
solType = 3
externalPolarization = True
FO = True
temperature = 20 (*degrees C*)
flowrate = 1 (*LPM*)
```

3

True

True

20

1

Cell Dimensions

```
width = 1.0200  
height = 0.0980  
length = 3.150
```

1.02

0.098

3.15

Membrane Properties

User inputted membrane data

```
membr = "My membrane has a first name";  
waterPerm = (2.49331628365258 + 2.52225164962164)/2; (*in LMH/bar*)  
saltPerm = 0; (*in LMH*)  
structPara = {70}; (*in microns*)  
waterFlux = {1, 2, 10, 20, 30}; (*in LMH*)  
fluxErr = {1, 1, 1, 1, 1}; (*in LMH*)  
variablePressureConcentration = {0.5}; (*in mol/L NaCl*)  
variablePressureRange = {0, 1.7, 4.5, 7.3, 10.1, 12.9, 15.6, 18.4, 21.2, 24.0, 26.8}; (*in bar*)  
variableConcentrationRange = {0.05, 0.1, 0.5, 1.0, 1.5, 2.0}; (*in mol/L NaCl*)  
feedConcentration = {0};
```

x=0 to use membrane properties from the box above

```
x = 0;  
If[x ≠ 0, ClearAll[waterPerm, saltPerm, structPara, waterFlux, fluxErr,  
    variablePressureConcentration, variablePressureRange, variableConcentrationRange, feedConcentration]]
```

Data for analyzed membranes

Not all membranes were analyzed in all of the test regimes

Commercial Membranes

```

If[x == 1, membr = "Oasys TFC"];
If[x == 1, saltPerm = 0.3878];
If[x == 1, waterPerm = 4.248];
If[x == 1, structPara = {480}];
If[x == 1, variablePressureConcentration = {0.5}];
If[x == 1, variablePressureRange = {0, 1.7, 4.5, 7.3, 10.1, 12.9, 15.6, 18.4, 21.2, 24.0, 26.8}];
If[x == 1, variableConcentrationRange = {0.05, 0.1, 0.5, 1.0, 1.5}];
If[x == 1, feedConcentration = {0}];
If[x == 1, structParaRange = {495, 705, 1035, 1925, 2573 665}];
If[x == 1, structPressureRange = {1.72, 4.48, 7.24, 10.00, 12.76}];
If[x == 1, waterFlux = {-2.0602, 7.9468, 15.7625, 22.7438, 30.3983}];
If[x == 1, fluxErr = {2.6953, 2.0219, 2.1252, 2.5426, 2.3299}];

```

PDA modified Membranes

```

If[x == 18, membr = "PDA 1 hr SW30-HR"];
If[x == 18, variablePressureConcentration = {0.5}];
If[x == 18, variablePressureRange = {12.7553, 9.9974, 7.2395, 4.4816, 1.7237}];
If[x == 18, saltPerm = 0.1970];
If[x == 18, waterPerm = 1.7806];
If[x == 18, waterFlux = {1.48245, 3.8654, 6.5948, 8.8172, 12.0235}];
If[x == 18, fluxErr = {1.9631, 1.3479, 1.2960, 0.9742, 0.7455}];
If[x == 18, feedConcentration = {0}];
If[x == 18, structPara = 500];

If[x == 15, membr = "PDA 1 hr SW30-XLE"];
If[x == 15, variablePressureConcentration = {0.5}];
If[x == 15, variablePressureRange = {7.2395, 4.4816, 1.7237}];
If[x == 15, saltPerm = 0.4338];
If[x == 15, waterPerm = 2.4960];
If[x == 15, waterFlux = {2.8978, 5.2707, 8.1542}];
If[x == 15, fluxErr = {2.8002, 1.6252, 1.0224}];
If[x == 15, feedConcentration = {0}];
If[x == 15, structPara = 1130];

If[x == 14, membr = "PDA 1 hr BW30"];
If[x == 14, variablePressureConcentration = {0.5}];
If[x == 14, variablePressureRange = {12.7553, 9.9974, 7.2395, 4.4816, 1.7237}];
If[x == 14, saltPerm = 0.8032];
If[x == 14, waterPerm = 2.2213];
If[x == 14, waterFlux = {0.5372, 2.8250, 5.2892, 7.7922, 9.2462}];
If[x == 14, fluxErr = {0.8095, 0.8428, 0.7881, 1.3745, 0.7921}];
If[x == 14, feedConcentration = {0}];
If[x == 14, structPara = 1200];

If[x == 13, membr = "PDA 1 hr NF90"];

```

```

If[x == 13, variablePressureConcentration = {0.5}];
If[x == 13, variablePressureRange = {7.2395, 4.4816, 1.7237}];
If[x == 13, saltPerm = 2.1624];
If[x == 13, waterPerm = 7.2133];
If[x == 13, waterFlux = {-0.5261, 2.4632, 5.7192}];
If[x == 13, fluxErr = {0.8271, 0.7775, 0.7866}];
If[x == 13, feedConcentration = {0}];
If[x == 13, structPara = 2015];

If[x == 8, membr = "PDA 1 hr SW30-HR"];
If[x == 8, variablePressureConcentration = {0.5}];
If[x == 8, variablePressureRange = {1.7237, 4.48160, 7.2395, 9.9974, 12.7553}];
If[x == 8, saltPerm = 0.1970];
If[x == 8, waterPerm = 1.7806];
If[x == 8, waterFlux = {15.8324, 10.3389, 6.4776, 3.7005, 1.0915}];
If[x == 8, fluxErr = {1.6018, 1.74178, 1.8278, 1.3129, 1.3547}];
If[x == 8, feedConcentration = {0}];
If[x == 8, structPara = 500];

If[x == 5, membr = "PDA 1 hr SW30-XLE"];
If[x == 5, variablePressureConcentration = {0.5}];
If[x == 5, variablePressureRange = {1.7237, 4.4816, 7.2395}];
If[x == 5, saltPerm = 0.4338];
If[x == 5, waterPerm = 2.4960];
If[x == 5, waterFlux = {8.6100, 4.6468, 2.4718}];
If[x == 5, fluxErr = {0.9119, 1.2308, 2.3231}];
If[x == 5, feedConcentration = {0}];
If[x == 5, structPara = 1130];

If[x == 4, membr = "PDA 1 hr BW30"];
If[x == 4, variablePressureConcentration = {0.5}];
If[x == 4, variablePressureRange = {1.7237, 4.48160, 7.2395, 9.9974, 12.7553}];
If[x == 4, saltPerm = 0.8032];
If[x == 4, waterPerm = 2.2213];
If[x == 4, waterFlux = {9.4691, 6.8149, 3.7262, 1.8701, 0.7721}];
If[x == 4, fluxErr = {0.9856, 2.1223, 1.2026, 1.7708, 0.7331}];
If[x == 4, structParaRange = {1560, 1863, 2466, 3663, 3062}];
If[x == 4, feedConcentration = {0}];
If[x == 4, structPara = 1200];

If[x == 3, membr = "PDA 1 hr NF90"];
If[x == 3, variablePressureConcentration = {0.5}];
If[x == 3, variablePressureRange = {1.7237, 4.4816, 7.2395}];
If[x == 3, saltPerm = 2.1624];
If[x == 3, waterPerm = 7.2133];
If[x == 3, waterFlux = {17.0494, 2.8505, -0.5261}];
If[x == 3, fluxErr = {1.05176, 1.0000, 0.8271}];

```

```

If[x == 3, structParaRange = {853, 2724, 3 454 636}];
If[x == 3, feedConcentration = {0}];
If[x == 3, structPara = 2015];

```

Liwei's Membranes

```

If[x == 90, membr = "PVDF FO"];
If[x == 90, waterPerm = 1.4];
If[x == 90, variableConcentrationRange = {0.5, 1, 1.5, 2}];
If[x == 90, feedConcentration = {0}];
If[x == 90, waterFlux = {3.0, 4.9, 6.9, 8.4}];
If[x == 90, fluxErr = {0.31, 0.17, 0.14, 0.18}];
If[x == 90, soluteFlux = {0.30, 0.38, 0.51, 0.98}];
If[x == 90, soluteErr = {0.06, 0.06, 0.03, 0.36}];

If[x == 91, membr = "PVDF Pre-wetted FO"];
If[x == 91, waterPerm = 1.4];
If[x == 91, variableConcentrationRange = {0.5, 1, 1.5, 2}];
If[x == 91, feedConcentration = {0}];
If[x == 91, waterFlux = {17.1, 27.8, 33.1, 38.6}];
If[x == 91, fluxErr = {1.68, 4.03, 3.63, 2.30}];
If[x == 91, soluteFlux = {2.12, 5.51, 7.33, 12.53}];
If[x == 91, soluteErr = {0.85, 2.29, 0.97, 5.38}];

If[x == 92, membr = "Nylon coated PVDF FO"];
If[x == 92, waterPerm = 1.3];
If[x == 92, variableConcentrationRange = {0.5, 1, 1.5, 2}];
If[x == 92, feedConcentration = {0}];
If[x == 92, waterFlux = {16.1, 22.0, 29.5, 35.7}];
If[x == 92, fluxErr = {0.86, 1.01, 2.60, 3.01}];
If[x == 92, soluteFlux = {2.21, 3.63, 8.39, 12.63}];
If[x == 92, soluteErr = {1.38, 2.54, 8.43, 10.30}];

If[x == 93, membr = "PVDF PRO"];
If[x == 93, waterPerm = 1.4];
If[x == 93, variableConcentrationRange = {0.5, 1, 1.5, 2}];
If[x == 93, feedConcentration = {0}];
If[x == 93, waterFlux = {10.5, 20.4, 28.5, 37.6}];
If[x == 93, fluxErr = {1.46, 0.26, 3.64, 1.78}];
If[x == 93, soluteFlux = {3.99, 7.56, 11.87, 16.20}];
If[x == 93, soluteErr = {2.64, 3.98, 5.63, 8.32}];

If[x == 94, membr = "PVDF Pre-wetted PRO"];
If[x == 94, waterPerm = 1.4];
If[x == 94, variableConcentrationRange = {0.5, 1, 1.5, 2}];
If[x == 94, feedConcentration = {0}];
If[x == 94, waterFlux = {20.4, 33.5, 44.8, 55.2}];
If[x == 94, fluxErr = {2.67, 2.03, 2.35, 4.74}];

```

```

If[x == 94, soluteFlux = {6.03, 13.75, 16.17, 17.95}];
If[x == 94, soluteErr = {3.87, 5.19, 7.76, 5.68}];

If[x == 95, membr = "Nylon coated PVDF PRO"];
If[x == 95, waterPerm = 1.3];
If[x == 95, variableConcentrationRange = {0.5, 1, 1.5, 2}];
If[x == 95, feedConcentration = {0}];
If[x == 95, waterFlux = {20.2, 30.9, 40.8, 52.6}];
If[x == 95, fluxErr = {3.75, 2.55, 2.10, 3.96}];
If[x == 95, soluteFlux = {6.04, 13.23, 19.09, 27.95}];
If[x == 95, soluteErr = {0.89, 0.84, 7.23, 9.95}];

If[x ≥ 90 && x ≤ 95, soluteFlux = soluteFlux/58.45;
  soluteErr = soluteErr/58.45];

```

Dimensionless Values and Governing Equations

Reynolds Number

```

NRe[density_, velocity_, hydroDiam_, viscosity_] := Module[{eqn},
  eqn = (density*velocity*hydroDiam)/viscosity;
  eqn]
NRe[rho, v, d, mu]

```

$$\frac{d \rho v}{\mu}$$

Schmidt Number

```

NSc[viscosity_, density_, diffusivity_] := Module[{eqn},
  eqn = viscosity/(density*diffusivity);
  eqn]
NSc[mu, d, D]

```

$$\frac{\mu}{d D}$$

Sherwood Correlation

```

NSh[vNRe_, vNSc_, hydroDiam_, length_] := Module[{eqn},
  eqn = (1.85*(vNRe*vNSc*hydroDiam/length)^0.33);
  eqn]
NSh[Re, Sc, d, l]

```

$$1.85 \left(\frac{d Re Sc}{l} \right)^{0.33}$$

External Boundary Layer Thickness

```

boundaryThick[hydroDiam_, vNSh_] := Module[{eqn},
  eqn = hydroDiam/vNSh;
  eqn]
boundaryThick[d, Sh]

```

$\frac{d}{Sh}$

Governing Equation for Water Flux

```

fluxEqn[FOMode_, phiFunc_, wFlux_, wPerm_, sPerm_, struct_, delta_, pressureDiff_, temp_,
  concD_, concF_, diffD_, diffF_] := Module[{eqn, idGas, absTemp, dilCP, concCP, piDM, piFM},
  idGas = 8.3144621*10^(-2);
  absTemp = (temp + 273.15);
  If[FOMode, dilCP = Exp[-(wFlux*struct)/(diffD*3600*1000)],
  dilCP = Exp[-(wFlux*delta)/(diffD*3600*1000)]];
  If[FOMode, concCP = Exp[(wFlux*delta)/(diffF*3600*1000)],
  concCP = Exp[(wFlux*struct)/(diffF*3600*1000)]];
  piDM = 2*concD*idGas*absTemp*dilCP;
  piFM = 2*concF*idGas*absTemp*concCP;
  eqn = wPerm*((piDM - piFM)/(1 + (sPerm/wFlux)*(concCP - dilCP)) - pressureDiff) - wFlux;
  eqn]
fluxEqn[True, phi, jW, a, b, s, d, p, t, cD, cF, dD, dF]
fluxEqn[False, phi, jW, a, b, s, d, p, t, cD, cF, dD, dF]

```

$$\begin{aligned}
 & -jW + a \left(-p + \left(-0.166289 \, cF \, e^{\frac{d \, jW}{3600000 \, dF}} (273.15 + t) + 0.166289 \, cD \, e^{-\frac{jW \, s}{3600000 \, dD}} (273.15 + t) \right) \right) / \\
 & \left(1 + \frac{b \left(e^{\frac{d \, jW}{3600000 \, dF}} - e^{-\frac{jW \, s}{3600000 \, dD}} \right)}{jW} \right) \Bigg) \\
 & -jW + a \left(-p + \left(0.166289 \, cD \, e^{-\frac{d \, jW}{3600000 \, dD}} (273.15 + t) - 0.166289 \, cF \, e^{\frac{jW \, s}{3600000 \, dF}} (273.15 + t) \right) \right) / \\
 & \left(1 + \frac{b \left(-e^{-\frac{d \, jW}{3600000 \, dD}} + e^{\frac{jW \, s}{3600000 \, dF}} \right)}{jW} \right) \Bigg)
 \end{aligned}$$

Governing Equation for Salt Flux


```

saltFlux[FOMode_, wFlux_, sFlux_, wPerm_, sPerm_, struct_, delta_, temp_, concD_, concF_, diffD_, diffF_] :=
Module[{eqn, dilCP, concCP, concDM, concFM},
  If[FOMode, dilCP = Exp[-(wFlux * struct) / (diffD * 3600 * 1000)],
  dilCP = Exp[-(wFlux * delta) / (diffD * 3600 * 1000)];
  If[FOMode, concCP = Exp[(wFlux * delta) / (diffF * 3600 * 1000)],
  concCP = Exp[(wFlux * struct) / (diffF * 3600 * 1000)];
  concDM = concD * dilCP;
  concFM = concF * concCP;
  eqn = sPerm * ((concDM - concFM) / (1 + (sPerm / wFlux) * (concCP - dilCP))) - sFlux;
  eqn]
saltFlux[True, jW, jS, a, b, s, d, t, cD, cF, dD, dF]
saltFlux[False, jW, jS, a, b, s, d, t, cD, cF, dD, dF]

```

$$\begin{aligned}
& -jS + \frac{b \left(-cF e^{\frac{d jW}{3600000 dF}} + cD e^{-\frac{jW s}{3600000 dD}} \right)}{1 + \frac{b \left(e^{\frac{d jW}{3600000 dF}} - e^{-\frac{jW s}{3600000 dD}} \right)}{jW}} \\
& -jS + \frac{b \left(cD e^{-\frac{d jW}{3600000 dD}} - cF e^{\frac{jW s}{3600000 dF}} \right)}{1 + \frac{b \left(-e^{-\frac{d jW}{3600000 dD}} + e^{\frac{jW s}{3600000 dF}} \right)}{jW}}
\end{aligned}$$

Solution Physical Properties

Sodium Chloride Solution Density as a Function of Temperature and Concentration

```

denseCFunc[conc_, temp_] := Module[{eqn, densityData20, densityData30, densityData40},
  densityData20 = {998.2, 1018.5, 1037.8, 1056.4, 1074.15, 1091.3, 1107.95, 1123.8, 1139.4};
  densityData30 = {995.7, 1015.5, 1034.5, 1052.6, 1070.2, 1087.2, 1103.5, 1119.2, 1134.6};
  densityData40 = {992.2, 1011.8, 1030.4, 1048.4, 1065.8, 1082.5, 1098.7, 1114.3, 1129.6};

  eqn = ListInterpolation[{Interpolation[densityData20, {conc * 2.} + 1], Interpolation[densityData30, {conc * 2.} + 1],
    Interpolation[densityData40, {conc * 2.} + 1]}, {20, 30, 40}, InterpolationOrder -> 2];
  eqn[temp]]

denseCFunc[1, 20]

```

1037.8

Mutual Diffusion Coefficients for a Sodium Chloride Solution as a Function of Temperature and Concentration

```

diffFunc[conc_, temp_] := Module[{eqn, diffusivity18, diffusivity25, diffusivity35,
  concentration18, concentration25, concentration35, diffFunc18, diffFunc25, diffFunc35},
  diffusivity18 = {1.26, 1.24, 1.22, 1.2, 1.21, 1.22, 1.23, 1.26, 1.29, 1.33, 1.36, 1.43}/10^9;
  diffusivity25 = {1.547, 1.503, 1.484, 1.476, 1.474, 1.476,
    1.477, 1.478, 1.483, 1.485, 1.498, 1.507, 1.517, 1.541, 1.559, 1.584, 1.591}/10^9;
  diffusivity35 = {1.882, 1.884, 1.872, 1.863, 1.857, 1.867, 1.856, 1.858,
    1.86, 1.87, 1.891, 1.958, 1.976, 1.992, 1.999}/10^9;
  concentration18 = {0.05, 0.1, 0.2, 0.4, 0.6, 0.8, 1., 1.5, 2., 2.5, 3., 4};
  concentration25 = {0.01, 0.05, 0.1, 0.2, 0.5, 0.7, 0.8, 0.9, 1., 1.2, 1.6, 1.8, 2., 2.5, 3., 3.5, 4.};
  concentration35 = {0.0792, 0.0991, 0.1476, 0.1869, 0.1977,
    0.2965, 0.3946, 0.4933, 0.5942, 0.9752, 0.14483, 2.8099, 3.2452, 3.6785, 4.0859};
  Off[InterpolatingFunction::dmval];
  diffFunc18 = ListInterpolation[diffusivity18, concentration18];
  diffFunc25 = ListInterpolation[diffusivity25, concentration25];
  diffFunc35 = ListInterpolation[diffusivity35, concentration35];
  eqn =
  ListInterpolation[{diffFunc18[conc], diffFunc25[conc], diffFunc35[conc]}, {18, 25, 35}, InterpolationOrder → 2];
  On[InterpolatingFunction::dmval];
  eqn[temp]]

diffFunc[0, 20]

```

1.2301×10^{-9}

Sodium Chloride Solution Viscosity as a Function of Temperature and Concentration

```

viscosityFunc[conc_, temp_] := Module[{eqn, viscosity20, viscosity30, viscosity40},
  viscosity20 = {1.002, 1.047, 1.092, 1.144, 1.203, 1.272, 1.346, 1.42, 1.502}/10^3;
  viscosity30 = {0.7975, 0.834, 0.873, 0.917, 0.964, 1.015, 1.072, 1.133, 1.199}/10^3;
  viscosity40 = {0.653, 0.682, 0.716, 0.753, 0.793, 0.836, 0.836, 0.934, 0.989}/10^3;
  Off[InterpolatingFunction::dmval];

  eqn = ListInterpolation[{Interpolation[viscosity20, (conc*2.) + 1.], Interpolation[viscosity30, (conc*2.) + 1.],
    Interpolation[viscosity40, (conc*2.) + 1.]}, {20, 30, 40}, InterpolationOrder → 2];
  On[InterpolatingFunction::dmval];
  eqn[temp]]

viscosityFunc[1, 20]

```

0.001092

van't Hoff Coefficients for a Sodium Chloride Solution
value should only be used near 25C

```

phiFunc[conc_, temp_] := Module[{eqn, weightPercent, weightPer100,
  densityData10, densityData25, denseFunc10, denseFunc25, denseWFunc, phiConc, phiArr, i},
  weightPercent = {0, 1, 2, 4, 8, 12, 16, 20, 24, 26};
  densityData10 =
{0.999647, 1.00707, 1.01442, 1.02920, 1.05907, 1.08946, 1.12056, 1.15254, 1.18557, 1.20254}*1000;
  densityData25 = {0.997002, 1.00409, 1.01112, 1.02530, 1.05412,
    1.08365, 1.11401, 1.14522, 1.17776, 1.19443}*1000;
  denseFunc10 = ListInterpolation[densityData10, weightPercent, InterpolationOrder → 1];
  denseFunc25 = ListInterpolation[densityData25, weightPercent, InterpolationOrder → 1];
  denseWFunc = ListInterpolation[
    {denseFunc10[weightPer100], denseFunc25[weightPer100]}, {10, 25}, InterpolationOrder → 1];
  phiConc = {0.1, 0.2, 0.3, 0.4, 0.5, 0.6, 0.7, 0.8, 0.9, 1, 1.2, 1.4, 1.6, 1.8, 2, 2.2, 2.4,
    2.6, 2.8, 3, 3.2, 3.4, 3.6, 3.8, 4, 4.2, 4.4, 4.6, 4.8, 5, 5.2, 5.4, 5.6, 5.8, 6};
  Off[InterpolatingFunction::dmval]
  For[i = 1, i <= Length[phiConc], i++, weightPer100 = phiConc[[i]]*58.45/10;
    phiConc[[i]] = phiConc[[i]]*(1000/(1000 + phiConc[[i]]*58.45))*denseWFunc[temp]/1000];
  phiArr = {0.9324, 0.9245, 0.9215, 0.9203, 0.9209, 0.9230, 0.9257, 0.9288, 0.9320, 0.9355, 0.9428,
    0.9513, 0.9616, 0.9723, 0.9833, 0.9948, 1.0068, 1.0192, 1.0321, 1.0453, 1.0587, 1.0725, 1.0867,
    1.1013, 1.1158, 1.1306, 1.1456, 1.1608, 1.1761, 1.1916, 1.2072, 1.2229, 1.2389, 1.2548, 1.2706};
  On[InterpolatingFunction::dmval];
  eqn = ListInterpolation[phiArr, phiConc];
  eqn[conc]]

```

```
phiFunc[1, 20]
```

0.936131

Program Main Body

```

width = width*2.54/100;
height = height*2.54/100;
length = length*2.54/100;
hydroD = 4*(width*height)/(2*width + 2*height);
flowrate = flowrate/(1000*60);
veloc = flowrate/(width*height);
If[structPara[[1]] ≠ 0 || structPara[[1]] == 0, structPara = structPara*10−6];
If[structParaRange[[1]] ≠ 0 || structParaRange[[1]] == 0, structParaRange = structParaRange*10−6];

```

```

If[solType == 1, sVal = variableConcentrationRange*0];
If[solType == 2, sVal = variablePressureRange*0];
If[solType == 3, wFlux = variableConcentrationRange*0];
If[solType == 4, wFlux = variablePressureRange*0];
If[solType == 5, wFlux = structParaRange*0];
If[solType == 6,
  wFlux = variableConcentrationRange*0;
  sFlux = variableConcentrationRange*0;
  sPermRange = variableConcentrationRange*0;

```

```

    structRange = variableConcentrationRange*0;
    answer = variableConcentrationRange*0];

If[solType == 1 || solType == 3 || solType == 6, pressureRange = {0}];
If[solType == 2 || solType == 4, pressureRange = variablePressureRange];
If[solType == 5, pressureRange = structPressureRange];

Print[pressureRange]

If[solType == 1 || solType == 3 || solType == 6, drawConc = variableConcentrationRange]
If[solType == 2 || solType == 4 || solType == 5, drawConc = variablePressureConcentration];
diffDraw = drawConc*0;
viscDraw = drawConc*0;
denseDraw = drawConc*0;
For[i = 1, i ≤ Length[drawConc], i++,
    diffDraw[[i]] = diffFunc[drawConc[[i]], temperature];
    viscDraw[[i]] = viscosityFunc[drawConc[[i]], temperature];
    denseDraw[[i]] = denseCFunc[drawConc[[i]], temperature]]
Print[drawConc]
Print[diffDraw]
Print[viscDraw]
Print[denseDraw]

diffFeed = {diffFunc[feedConcentration[[1]], temperature]}
viscFeed = {viscosityFunc[feedConcentration[[1]], temperature]}
denseFeed = {denseCFunc[feedConcentration[[1]], temperature]}

If[FO == False, vNRe = drawConc*0];
If[FO == True, vNRe = feedConcentration*0];
vNSc = vNRe;
vNSh = vNRe;
If[FO == False, For[i = 1, i ≤ Length[drawConc], i++,
    Print[i];
    vNRe[[i]] = NRe[denseDraw[[i]], veloc, hydroD, viscDraw[[i]]];
    vNSc[[i]] = NSc[viscDraw[[i]], denseDraw[[i]], diffDraw[[i]]];
    vNSh[[i]] = NSh[vNRe[[i]], vNSc[[i]], hydroD, length]]
If[FO == True,
    vNRe[[1]] = NRe[denseFeed[[1]], veloc, hydroD, viscFeed[[1]]];
    vNSc[[1]] = NSc[viscFeed[[1]], denseFeed[[1]], diffFeed[[1]]];
    vNSh[[1]] = NSh[vNRe[[1]], vNSc[[1]], hydroD, length]]
Print[vNRe]
Print[vNSc]
Print[vNSh]
externalBoundThick = vNSh*0;
If[externalPolarization == True,
    For[i = 1, i ≤ Length[vNSh], i++, externalBoundThick[[i]] = boundaryThick[hydroD, vNSh[[i]]]]
Print[externalBoundThick]

```

```

{0}
{0.05, 0.1, 0.5, 1., 1.5, 2.}
{0.05, 0.1, 0.5, 1., 1.5, 2.}
{1.31066 × 10-9, 1.30658 × 10-9, 1.28068 × 10-9,
 1.30073 × 10-9, 1.32312 × 10-9, 1.35043 × 10-9}
{0.0010067, 0.00101134, 0.001047, 0.001092, 0.001144, 0.001203}
{1000.28, 1002.35, 1018.5, 1037.8, 1056.4, 1074.15}
{1.2301 × 10-9}
{0.001002}
{998.2}
67.5017
{1169.37}
{816.038}
{67.5017}
{0.0000672873}

```

```

If[solType == 3, For[i = 1, i ≤ Length[variableConcentrationRange], i++,
  wFlux[[i]] = FindRoot[fluxEqn[FO, 1, flux, waterPerm, saltPerm, structPara[[1]], externalBoundThick[[1]], 0,
    temperature, drawConc[[i]], feedConcentration[[1]], diffDraw[[i]], diffFeed[[1]]] == 0, {flux, 1}]]]

If[solType == 4, For[i = 1, i ≤ Length[pressureRange], i++,
  wFlux[[i]] = FindRoot[fluxEqn[FO, phiFunc[drawConc[[1]], temperature], flux, waterPerm,
    saltPerm, structPara[[1]], externalBoundThick[[1]], pressureRange[[i]], temperature,
    drawConc[[1]], feedConcentration[[1]], diffDraw[[1]], diffFeed[[1]]] == 0, {flux, 1}]]]

If[solType == 5, For[i = 1, i ≤ Length[pressureRange], i++,
  wFlux[[i]] = FindRoot[fluxEqn[FO, phiFunc[drawConc[[1]], temperature], flux, waterPerm,
    saltPerm, structParaRange[[i]], externalBoundThick[[1]], pressureRange[[i]], temperature,
    drawConc[[1]], feedConcentration[[1]], diffDraw[[1]], diffFeed[[1]]] == 0, {flux, 1}]]]

If[solType == 6,
  For[i = 1, i ≤ Length[drawConc], i++,
    answer[[i]] = FindRoot[{
      fluxEqn[FO, phiFunc[drawConc[[i]], temperature],
      waterFlux[[i]], waterPerm, b, s, externalBoundThick[[1]], pressureRange[[1]],
      temperature, drawConc[[i]], feedConcentration[[1]], diffDraw[[i]], diffFeed[[1]]] == 0,
      saltFlux[FO, waterFlux[[i]], soluteFlux[[i]], waterPerm, b, s, externalBoundThick[[1]],
      temperature, drawConc[[i]], feedConcentration[[1]], diffDraw[[i]], diffFeed[[1]]] == 0,
      {{b, 0}, {s, 0}}];
    sPermRange[[i]] = b /. answer[[i, 1]];
    structRange[[i]] = s /. answer[[i, 2]]];

```

```

avgSPerm = 0;
avgStruct = 0;

For[i = 1, i ≤ Length[sPermRange], i ++,
    avgSPerm = avgSPerm + sPermRange[[i]];
    avgStruct = avgStruct + structRange[[i]];
avgSPerm = avgSPerm / 4;
avgStruct = avgStruct / 4;

For[i = 1, i ≤ Length[drawConc], i ++,

    wFlux[[i]] = FindRoot[fluxEqn[FO, phiFunc[drawConc[[i]], temperature], flux, waterPerm, avgSPerm,
        avgStruct, externalBoundThick[[1]], pressureRange[[1]], temperature,
        drawConc[[i]], feedConcentration[[1]], diffDraw[[i]], diffFeed[[1]] == 0, {flux, 1}];
    fluxVal = flux /. wFlux;
    For[j = 1, j ≤ Length[fluxVal], j ++,

        sFlux[[j]] = FindRoot[saltFlux[FO, fluxVal[[j]], fluxSalt, waterPerm, avgSPerm, avgStruct, externalBoundThick[[1]],
            temperature, drawConc[[i]], feedConcentration[[1]], diffDraw[[j]], diffFeed[[1]], {fluxSalt, 0}]]

    If[solType == 6, saltVal = fluxSalt /. sFlux]

    If[solType == 3 || solType == 4 || solType == 5, fluxVal = flux /. wFlux]

    If[solType ≠ 6,
        Export["d:data.xls", {"Membrane" -> membr, "Re" -> vNRe,
            "Sc" -> vNSc, "Sh" -> vNSh, "externalThickness" -> externalBoundThick,
            "densityDraw" -> denseDraw, "viscosityDraw" -> viscDraw, "diffusivityDraw" -> diffDraw,
            "densityFeed" -> denseFeed, "viscosityFeed" -> viscFeed, "diffusivityFeed" -> diffFeed,
            "drawConcentrations" -> drawConc, "TMP" -> pressureRange, "waterFlux" -> fluxVal}],
        Export["d:data.xls", {"Membrane" -> membr, "FO Mode" -> FO, "Re" -> vNRe,
            "Sc" -> vNSc, "Sh" -> vNSh, "externalThickness" -> externalBoundThick,
            "densityDraw" -> denseDraw, "viscosityDraw" -> viscDraw, "diffusivityDraw" -> diffDraw,
            "densityFeed" -> denseFeed, "viscosityFeed" -> viscFeed, "diffusivityFeed" -> diffFeed,
            "drawConcentrations" -> drawConc, "solutePermeabilityRange" -> sPermRange,
            "structuralParameterRange" -> structRange, "solutePermability" -> avgSPerm,
            "structuralParameter" -> avgStruct, "calculatedWaterFlux" -> fluxVal, "calculatedSaltFlux" -> saltVal}]]

{5.6232, 10.4622, 35.6012, 54.2943, 67.7516, 78.714}

d:data.xls

```

Appendix 5

Character and performance relationships for a high water flux commercial thin film composite membrane in forward osmosis desalination and pressure retarded osmosis

A5.1. Introduction

This objective of this paper is to characterize an early generation TFC FO membrane from Oasys Water. Tests will be performed to examine the membrane's surface and pore structure. Additionally, the membranes will be tested to measure its intrinsic transport properties in reverse osmosis and forward osmosis using sodium chloride. Finally the membrane will be characterized under conditions inspired by FO processes specifically seawater-river water PRO process and FO desalination using the ammonia-carbon dioxide ($\text{NH}_3\text{-CO}_2$) draw solution. The usage of the $\text{NH}_3\text{-CO}_2$ FO process is significant in both its previously demonstrated capacity for desalination using HTI's CTA membrane ^{1,2} and its use in Oasys Water's osmotic brine concentrator.³

A5.2. Materials and Methods

A5.2.1. Materials

A proprietary TFC membrane, later referred to as the O-TFC, was provided by Oasys Water (Boston, MA) in July 2012. The continuous rapid evolution of TFC FO membranes means this particular membrane has since been superseded. Based on available patent literature the membrane is likely a polyamide TFC built upon a polysulfone (PSu)/ polyethylene terephthalate (PET) supporting layer.⁴ Sodium chloride, ammonium bicarbonate, and ammonium hydroxide were purchased from Fisher Scientific (Pittsburgh, PA). Sodium tetraphenyl boron, potassium chromate, and silver nitrate were purchased from Acros Organics (Geel, Belgium). Isopropanol was purchased from J.T. Baker (Center Valley, PA). Water used in this study was ultrapure Milli-Q (18.2 M Ω) water produced by a Millipore Integral 10 water system, (Millipore Corporation, Billerica, MA).

A5.2.2. Reverse osmosis characterization

The water permeance was measured in a lab scale reverse osmosis testing system at pressures between 8.6 bar and 29.3 bar at a temperature of 20°C. Rejection tests were carried

out following the measurement of water permeance at 15.5 bar with a 2000 ppm sodium chloride feed at 20°C with a cross flow velocity of 0.25 m·s⁻¹. Sodium chloride rejection was measured using conductivity. Based upon hydrodynamic conditions of the system and empirical data^{5,6} intrinsic rejections were determined from a Sherwood number correlation.^{7,8} Intrinsic rejection was used to determine the sodium chloride permeability for this membrane and calculated from Eqn. (A5.1).⁷

$$B = \frac{(1-R)}{R} A (\Delta P - \Delta \pi) = \frac{(1-R)}{R} J_w \quad (\text{A5.1})$$

Here B is the solute permeability (L·m⁻²·hr⁻¹), R is the rejection, A is the water permeance of the membrane (L·m⁻²·hr⁻¹·bar⁻¹), ΔP is the transmembrane hydrostatic pressure (bar), Δπ is the transmembrane osmotic pressure (bar), and J_w is the water flux of the rejection measurement (L·m⁻²·hr⁻¹).

A5.2.3. Membrane structure evaluation

A5.2.3.1 Scanning electron microscopy

The TFC membrane PSu layer pore structures were imaged with a FEI Phenom scanning electron microscope (SEM) (FEI Company Hillsboro, OR). These samples were prepared

using a freeze fracturing technique immersing the membrane liquid nitrogen after removal of the PET support layer and snapping the membrane in half. This technique has been used elsewhere to image the cross-sections of membranes and allows for a clean, straight break preserving the internal pore structure for observation.⁹ The TFC membrane's polyamide selective layer was imaged with a JEOL 6335F Field Emission SEM. The surface of the selective layer was imaged to observe morphology of the membrane selective layer.

A5.2.3.2. Mercury intrusion porosimetry

An AutoPoreIV mercury intrusion porosimeter (Micromeritics Instrument Corporation, Norcross, GA) was used to characterize the membranes for pore diameter and total pore volume. In mercury intrusion porosimetry (MIP), a sample chamber containing dried membrane samples is vacuum evacuated and mercury is intruded into the membrane pores. Intrusion pressures ranging from 0.14 to 1380 bar (2 to 20,000 psi) were used for the pore diameter measurements, measuring pores with diameters of 90 μm to 20 nm. This technique can detect both through and blind pores but not closed pores.^{10,11}

A5.2.3.3. Structural parameter calculation

A membranes structural parameter most defines the difference between membranes developed for hydrostatic pressure driven processes when compared to those developed for osmotic pressure driven membrane separations. The structural parameter is represented within the governing equations for water fluxes in both of the commonly referenced membrane orientations the PRO mode (draw solution in contact with the membrane selective layer) and the FO mode (draw solution in contact with the membrane support layer). Eq. (A5.2) and Eq. (A5.3) show one the more rigorous forms of the governing equation for water flux in both the PRO mode (Eq. (A5.2))¹² and FO mode (Eq. (A5.3)).¹³

$$J_w = A \left(\frac{\pi_{d,b} e^{\left(\frac{J_w}{k}\right)} + \pi_{f,b} e^{\left(\frac{J_w \cdot S}{D_{f,b}}\right)}}{1 + \frac{B}{J_w} \left(e^{\left(\frac{J_w \cdot S}{D_{f,b}}\right)} - e^{\left(\frac{J_w}{k}\right)} \right)} - \Delta P \right) \quad (A5.2)$$

$$J_w = A \left(\frac{\pi_{d,b} e^{\left(\frac{J_w \cdot S}{D_{d,b}} \right)} + \pi_{f,b} e^{\left(\frac{J_w}{k} \right)}}{1 + \frac{B}{J_w} \left(e^{\left(\frac{J_w}{k} \right)} - e^{\left(\frac{J_w \cdot S}{D_{d,b}} \right)} \right)} \right) \quad (A5.3)$$

In these equations J_w is water flux, A is water permeance, $\pi_{d,b}$ is the bulk draw osmotic pressure, k is the external boundary layer mass transfer coefficient, $\pi_{f,b}$ is the bulk feed osmotic pressure, S is the structural parameter for the membrane, $D_{f,b}$ is the bulk feed diffusivity, B is the solute permeability, ΔP is the transmembrane pressure, and $D_{d,b}$ is the bulk draw diffusivity.

The structural parameter of a membrane describes the effective diffusion limited distance with the membrane support structure and ideally relates to the morphology of the membrane's support structure, and this relationship is commonly expressed by Eq. (A5.4).^{7,14,15}

$$S = \frac{t \cdot \tau}{\epsilon} \quad (A5.4)$$

In Eqn. (A5.4), t is the thickness of the membrane support layer, τ is the tortuosity of the support layer, and ϵ is the porosity of the support layer. Despite this relationship the structural

parameter of a membrane is most commonly calculated from Eq. (A5.2) and Eq. (A5.3) by a numerical solution for S with specified experimental conditions (temperature, flow channel, cross-flow velocity, draw and feed solutions), measured water flux, and membrane selective layer properties (water permeance and solute permeability). In addition Eq. (A5.2) can be used to simulate membrane performance in a PRO process and various derivations of this equation have served as the standard benchmark for experimental membrane performance in PRO.¹⁶⁻¹⁹

A5.2.4. Membrane surface properties

A5.2.4.1. Fourier transform infrared spectroscopy

The O-TFC membrane was tested in Fourier transform infrared (FTIR) spectroscopy to examine the surface functional groups of the membranes' selective layers. A Thermo Scientific (Waltham, MA) Nicolet iS10 FTIR spectrophotometer with Smart iTR attachment was used to perform these measurements on a dried membrane. Measurements were taken on the selective layer using 64 scans with a resolution of 4 cm^{-1} .

A5.2.4.2. Surface hydrophilicity by contact angle goniometry

The support layer contact angles of a neat membrane and a membrane with the PET removed were measured using the sessile drop method,⁹ with air as the light phase and deionized water as the heavy phase, on a CAM 101 series contact angle goniometer (KSV Company Linthicum Heights, MD). The values were taken as an average of at least four points with a volume of $7 \pm 1 \mu\text{L}$.

A5.2.5. Osmotically driven membrane process performance

A5.2.5.1. Pressure retarded osmosis testing

Membranes were tested in triplicate using fresh membrane samples, following a short soak in a 50% 2-propanol/water solution (i.e. <1min), on a bench scale pressure retarded osmosis test system at an operating temperature of 20°C. The configuration of this system has been described in prior study.^{20,21} A draw solute concentration 0.5 M NaCl was used. The draw solution was circulated co-currently against a deionized water feed with cross-flow velocities of $0.25 \text{ m}\cdot\text{s}^{-1}$ for both the draw and feed solutions. A tricot RO permeate spacer was used to support the membrane in the PRO system cell. Pressure gauges located on the inlet and outlet

of the PRO cell served to measure the pressure drop through the cell so transmembrane pressure could be accurately determined. For the tightly packed feed spacer a pressure drop of 1.7 bar (24 psi) was observed with an inlet pressure of 1.9 bar (27 psi) and an outlet pressure of 0.2 bar (3 psi). For the purposes of this study an average feed pressure of 1bar was assumed for transmembrane pressure determination, making the transmembrane pressure equal to the draw solution pressure minus 1 bar. No noticeable pressure drop was observed within the draw solution channel.

The maximum hydrostatic pressure tested was statistically near the flux reversal point (i.e. the error bars overlap 0 L·m⁻²·h⁻¹ water flux). The flux reversal point can be defined as the hydrostatic pressure at which water flux is zero. Tests were started with a draw solution hydrostatic pressure of 2.8 bar (40 psi) and increased in 2.8 bar (40 psi) increments until the flux reversal point. After data was collected near the flux reversal point, pressures were decreased back to 2.8 bar again in 2.8 bar (40 psi) increments. The sequence of pressure increases and pressure decreases are later referenced as the ascending pressure ramp and descending pressure ramp, respectively. Running a PRO test in both ascending and descending pressure ramps allows for the detection of permanent damage to the membrane

selective layer, which would result in an increase in reverse solute flux during the descending pressure ramp due to loss of selectivity from selective layer damage.

Following collection of experimental data (water and solute flux) membrane structural parameter, theoretical water flux, and power density were calculated. Structural parameters were calculated using Eq. (A5.2) with PRO experimental data and assuming constant selective layer properties (i.e. no selective layer damage). This calculation seeks to illustrate how mass transport through the selective layer is impacted by membrane compaction from the increasing applied hydrostatic pressure.

Theoretical water fluxes as a function of changing draw solution hydrostatic pressure were calculated from Eq. (A5.2). These calculations were performed using three differing sets of assumptions, with considerations towards both external and internal concentration polarization. The water fluxes were calculated without either ECP or ICP, with ECP and without ICP, and without ECP with variable ECP. The assumptions and additional details included within the calculation of these theoretical water fluxes are in Table A5.1.

Table A5.1. Assumptions for the numerical simulation of membrane PRO performance with a 0.5M NaCl draw solution at 20°C and 0.25m/s.

Descriptor	Assumptions	Notes
Simulated	Constant A Constant B Constant S Negligible ECP	A and B values calculated from RO S value calculated from zero transmembrane pressure tests by Eqn. 2.
Simulated w/ compaction	Constant A Constant B Variable S w/ pressure Negligible ECP	A and B values calculated from RO Uses S values assumed to be variable with pressure and calculated from experimental data and finding numerical solutions for S using Eqn. 2.
Simulated w/ ECP	Constant A Constant B Constant S ECP w/ constant k	A and B values calculated from RO k calculated from Sherwood correlation based upon system hydrodynamic conditions. S value calculated from zero transmembrane pressure tests by Eqn. 2.

The theoretical power density can be calculated from a known transmembrane pressure and water flux using Eq. (A5.5).¹⁷

$$W = \eta \cdot J_w \cdot \Delta P \quad (\text{A5.5})$$

In Eq. (A5.5), W is the power density of the membrane, η is the turbine efficiency (for the

purpose of this study assumed to be 1), J_w is the water flux and ΔP is the transmembrane pressure.

A5.2.5.2. Forward osmosis desalination testing

The O-TFC membrane was assessed for NaCl rejection in forward osmosis by using the $\text{NH}_3\text{-CO}_2$ based draw solution. The salts formed from NH_3 and CO_2 gases in solution are highly soluble, and some formulations of the $\text{NH}_3\text{-CO}_2$ have sufficient osmotic pressure to dewater feeds solutions which possess a high concentration of dissolve solids. Its viability has been demonstrated in its use in Oasys Water's produced water brine concentrator which has been shown concentrating brines up to $180,000 \text{ mg}\cdot\text{L}^{-1}$ TDS.³ The $\text{NH}_3\text{-CO}_2$ desalination tests were performed in a laboratory scale osmosis test systems using a 2.0 M (carbon basis) draw solution. The ammonia to carbon dioxide ratio was varied for these tests to observe what effect if any this would have on desalination performance. The ratios used for this study were 1.2:1, 1.5:1 and 2:1 $\text{NH}_3\text{:CO}_2$ on a molar basis. A feed solution of 0.25 M sodium chloride was used for all draw solution compositions. These solutions were circulated counter-current with a cross flow velocity of $0.25 \text{ m}\cdot\text{s}^{-1}$ at $23\pm 1^\circ\text{C}$. The membrane support layer was in contact with the $\text{NH}_3\text{-CO}_2$ draw solution (FO mode). Experiments were also run for a short time with the draw

solution against a deionized water feed to measure the pure water flux for the $\text{NH}_3\text{-CO}_2$ draw solution.

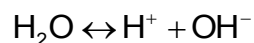
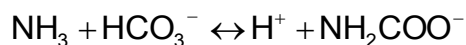
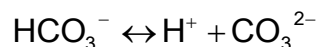
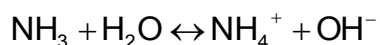
A5.2.5.4. Draw solution speciation

The $\text{NH}_3\text{-CO}_2$ draw solution comprises a varied mixture of chemical species within solution.

Within the draw solution there are dissolved NH_3 and CO_2 gases in addition to ammonium

Table A5.2. Relationships governing the speciation of $\text{NH}_3\text{-CO}_2$ draw solution

Chemical Equilibria



Mass Balances

$$m_{\text{total-N}} = m_{\text{NH}_3} + m_{\text{NH}_4^+} + m_{\text{NH}_2\text{COO}^-}$$

$$m_{\text{total-C}} = m_{\text{CO}_2} + m_{\text{HCO}_3^-} + m_{\text{CO}_3^{2-}} + m_{\text{NH}_2\text{COO}^-}$$

Electroneutrality

$$m_{\text{NH}_4^+} = m_{\text{HCO}_3^-} + 2m_{\text{CO}_3^{2-}} + m_{\text{NH}_2\text{COO}^-}$$

(NH_4^+) cations and bicarbonate (HCO_3^-), carbonate (CO_3^{2-}), and carbamate (NH_2COO^-)

) anions. The solution is typically alkaline

having pHs > 7 .^{2,11} Many studies on the

equilibrium relationship between NH_3 and

CO_2 gases within solution have been

performed.²²⁻²⁵ Draw solute speciation is

affected by 5 chemical equilibria, mass

balances upon the nitrogen species, carbon

species, and solution electroneutrality.²³

The concentration of each species is

dependent on the concentration of aqueous ammonia and carbon dioxide. Using the relationships shown in Table A5.2 a numerical determination for the concentration of ionic and neutral species within solution can be obtained. Draw solute speciation was determined numerical using Mathematica accounting for ion, and molecular interactions parameters given by Edwards et al.,²³ NH_3 and CO_2 equilibrium constants from Kawazuishi and Prausnitz,²² and water self-dissociation equilibrium constants from Robinson and Stokes.²⁶ The source code of this program can be found in Appendix 1. In solving for the speciation of the $\text{NH}_3\text{-CO}_2$ draw solution a direct calculation of the osmotic pressure of these solution can be obtain from the water activity in solution by Eq. (A5.6).²⁶⁻²⁸

$$\pi = -\frac{1}{v_w} \ln(a_w) RT \quad (\text{A5.6})$$

Here π is the osmotic pressure of the solution in bar, R is the ideal gas constant ($0.08314 \text{ L}\cdot\text{bar}\cdot\text{mol}^{-1}\cdot\text{K}^{-1}$), T is the absolute temperature, v_w is the molar volume of water ($0.018018 \text{ L}\cdot\text{mol}^{-1}$) and a_w is the molal activity of water.

A5.2.5.4. Dissolved species quantification

The flux of ammonia species, sodium, and chloride were measured using techniques

previously illustrated by Arena et al.¹¹ All fluxes were determined based on the change in concentration of the solute of interest (i.e. ammonia species present within the feed solution, sodium and chloride ions within the draw solution) over the duration of the test and the membrane surface area. The concentration of ammonium species was measured gravimetrically using sodium tetraphenyl boron to precipitate ammonia as ammonium tetraphenyl borate.^{29,30} The concentration of chloride was determined from the Mohr titration²⁹ on a sample of rehydrated draw solution from which the water, dissolved ammonia and dissolved carbon dioxide has been boiled off. The concentration of sodium was determined using a Perkin-Elmer 3100 Atomic Absorption Spectrometer (Perkin-Elmer, Waltham, MA) equipped with a sodium hollow cathode lamp (Perkin-Elmer Intensitron Part# 303-6065, Perkin-Elmer Waltham, MA).

A5.3. Results and discussion

A5.3.1 Membrane performance

Basic benchmark values for this membrane are shown in Table A5.3. Water permeance, sodium chloride rejection, and sodium chloride permeability were measured directly using reverse osmosis. The membrane's effective structural parameter was calculated based on the

Table A5.3. Experimentally determined transport properties for the O-TFC FO membrane.

Water Permeance	$4.25 \pm 0.04 \text{ L}\cdot\text{m}^{-2}\cdot\text{hr}^{-1}\cdot\text{bar}^{-1}$
2000 ppm Intrinsic Sodium Chloride Rejection (%)	$99.2 \pm 0.2 \%$
Sodium Chloride Permeability	$0.38 \pm 0.11 \text{ L}\cdot\text{m}^{-2}\cdot\text{hr}^{-1}$
Effective Structural Parameter	$483 \pm 79 \text{ }\mu\text{m}$

observed osmotic water fluxes in both the PRO and FO membrane orientations using Eq. (A5.2) and Eq. (A5.3) respectively. Comparing these to published values for other TFC membranes, the O-TFC membrane was observed having a higher water permeance compared to literature values for other TFC FO membranes' that were shown having a solute permeability less than $0.5 \text{ L}\cdot\text{m}^{-2}\cdot\text{hr}^{-1}$ when tested in reverse osmosis between 20-25°C.^{9,32,32}

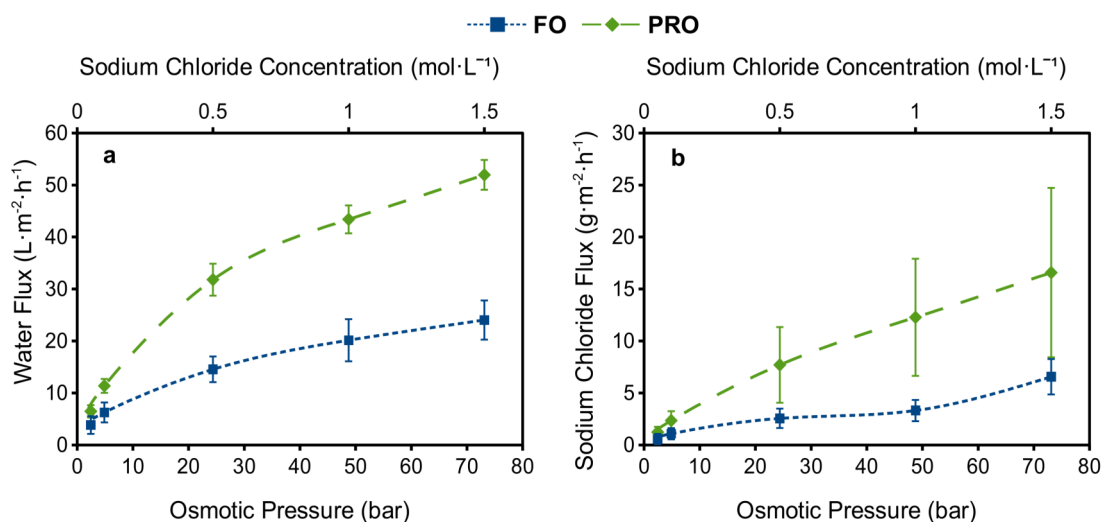


Fig. A5.1. Water flux (a) and sodium chloride reverse flux (b). NaCl draw, DI feed, $0.25 \text{ m}\cdot\text{s}^{-1}$, and 20°C.

This membrane presents comparatively high observed water flux greater than $50 \text{ L}\cdot\text{m}^{-2}\cdot\text{hr}^{-1}$ and $20 \text{ L}\cdot\text{m}^{-2}\cdot\text{hr}^{-1}$ in the PRO and FO orientations as shown in Fig. A5.1a.

A5.3.2. Membrane structural properties

A5.3.2.1. SEM images

SEMs of the O-TFC membrane, shown in Fig. A5.2, show the selective layer morphology and internal structure of this membrane. The selective layer morphology resembles the commonly noted ridge and valley structure consistent with an aromatic polyamide.^{33,34} The PSu support of this membrane is thin, having a thickness of around $35 \mu\text{m}$. The bottom $15\text{--}20 \mu\text{m}$ of the membrane support's pore structure has macrovoids with a spongy pore structure consisting of most of the

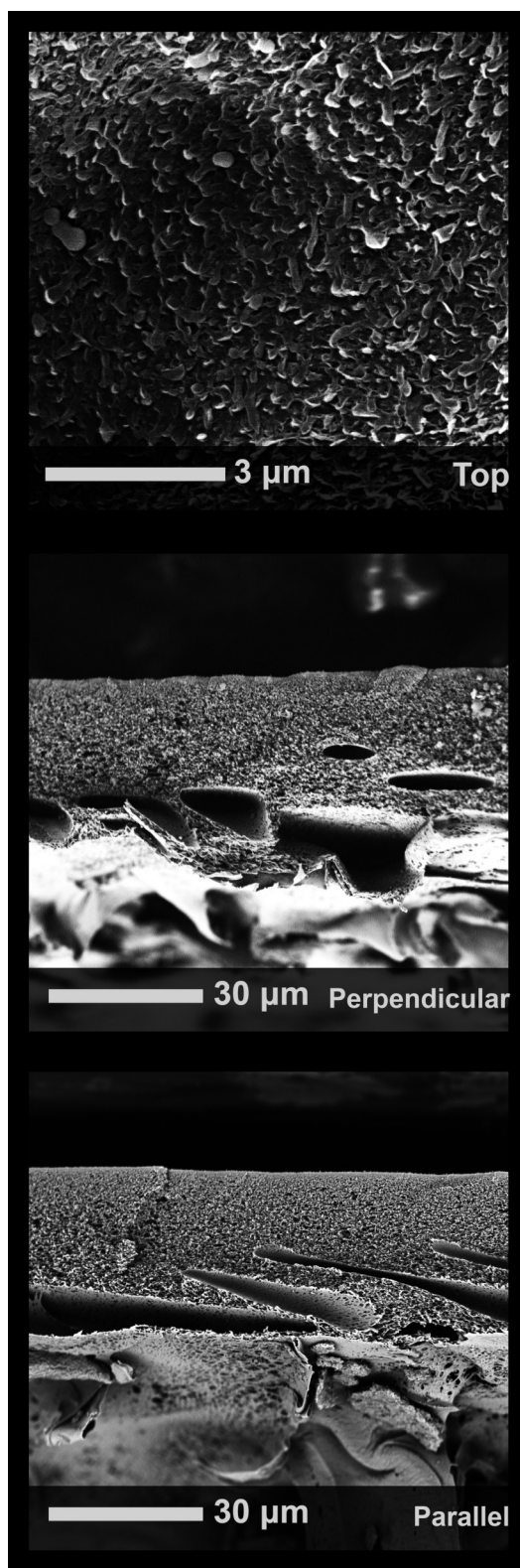


Fig. A5.2. Scanning electron microscope images of the O-TFC.

upper half of the support layer. The porous polymer support layer for this membrane is noticeably thinner than other flat sheet TFC membranes engineered for FO typically encountered in literature.^{14,32} Thin support layers are important factor in minimizing membrane structural parameter, which limits water flux in engineered osmosis processes from increased severity of ICP. Only TFC membranes which built upon nanofibrous supports have been shown with thinner porous mid-layers.^{15,20,35}

A5.3.2.2. Membrane support porosity and pore diameters

Support layer porosity, measured using mercury MIP, is shown in Fig. A5.3a. The measured porosity of complete support layer of the O-TFC membrane is approximately 65%. For comparison, the porosity of the O-TFC's support layer was also measured, using samples, following removal of the PET layer, and the porosity of just the PET was measured, coinciding with the porosity measured for the complete membrane structure. This is an interesting finding as it suggests that the porosity of the PET is dominant in the porosity of the complete structure. It necessary to note that this method may have an inherent bias toward lower porosities given that the high pressures can cause compaction of soft materials and the throttling of intruded mercury whereby larger pores are registered as smaller pores by the ink-bottle effect.¹⁰

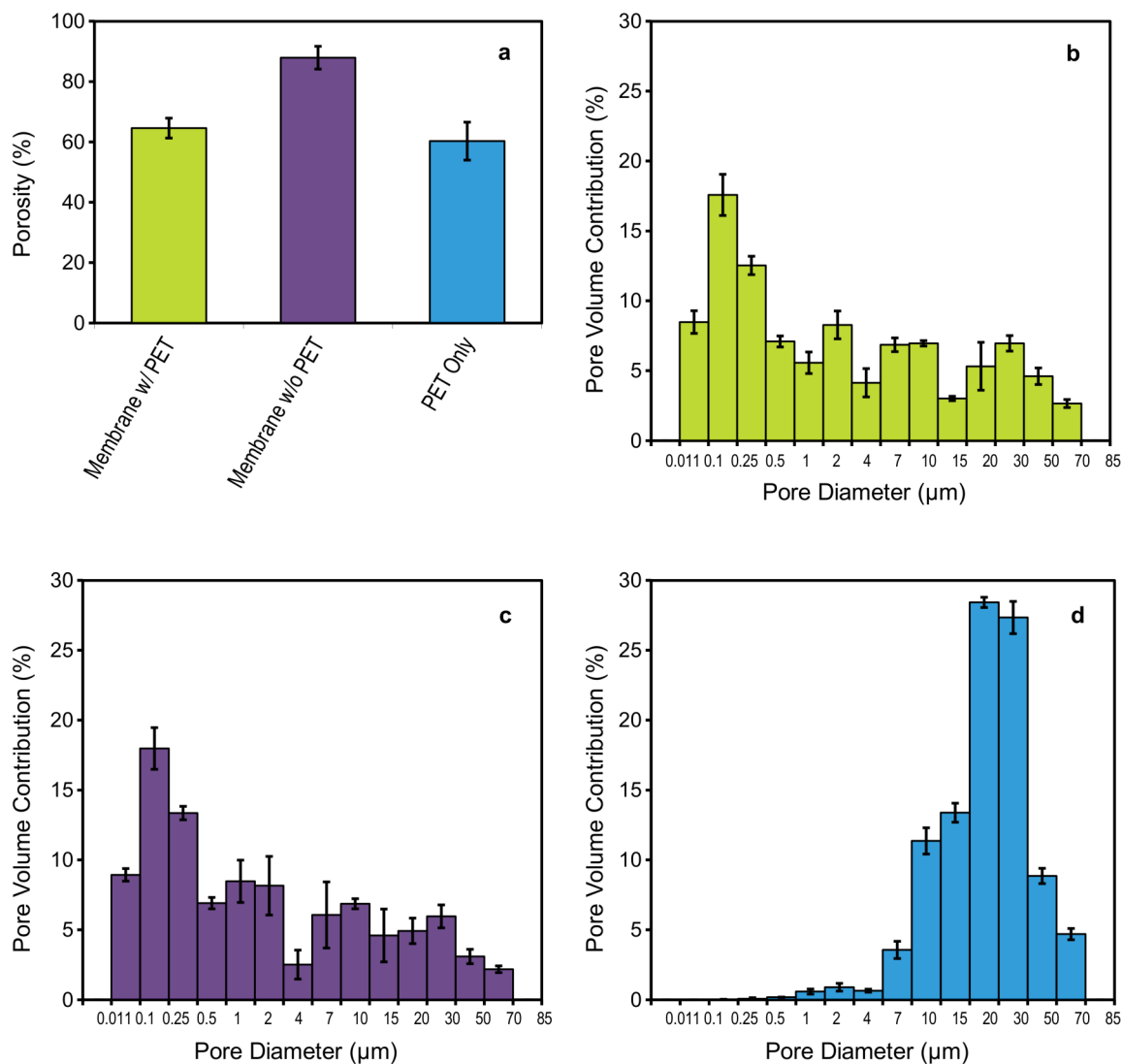


Fig. A5.3. MIP data for the O-TFC membrane's support layer (a) shows the porosity of the support layer with the PET fabric layer, without the PET fabric layer, and of only the PET fabric layer. (b), (c), and (d) show the pore diameter distributions for this membrane's support layer with the PET fabric layer, without the PET fabric layer, and of only the PET fabric layer respectively.

Fig. A5.3b, Fig. A5.3c, and Fig. A5.3d illustrate pore volume contributions to pore diameter for this membrane's support layers. It is noteworthy that upon removal of the PET layer the membranes pore diameter distribution fails to change significantly, except for a slight increase in pore volume contribution for pore diameters from 1-2 μm . This would suggest that the PET layer does not significantly enhance the porosity of the O-TFC membrane. Such a contribution would be presented as a spike to the pore volume contributions for pore diameters of 20-50 μm for the complete membrane structure (Fig. A5.3b) when compared to the membrane with the PET removed (Fig. A5.3c). The opposite behavior can be observed in Fig. A5.3a. The porosity of the PET appears to decrease or at least have a dominant contribution to the porosity of the complete support layer.

A5.3.3. Membrane surface properties and chemistry

A5.3.3.1. Membrane surface contact angles

Contact angles for the membrane surfaces are shown in Fig. A5.6. The selective layer of this membrane is the most hydrophilic surface in the structure. This is to be expected as a result of hydrogen bonding sites for water from carboxylic acid functional groups and the amide bonds within the chemical structure of the selective layer.³⁶ The support layers both with and

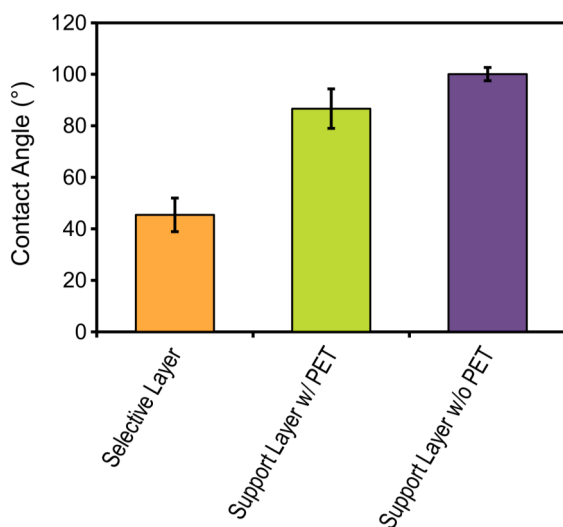


Fig. A5.4. Contact angle of differing membrane layer's using the sessile drop method with deionized water and a droplet size of $7 \pm 1 \mu\text{L}$.

without the PET layer are more hydrophobic.

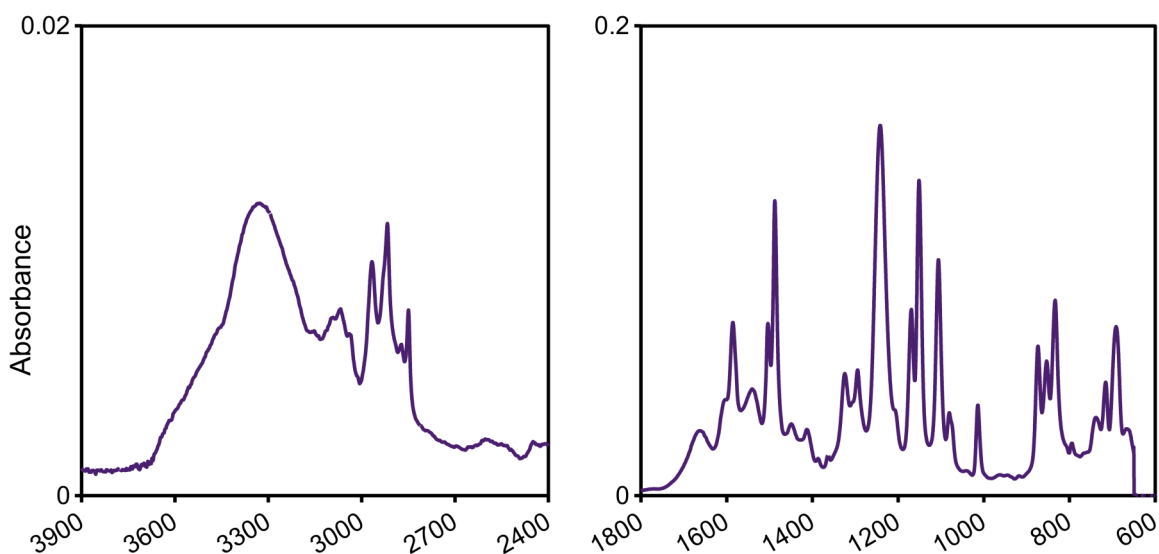
A lower contact angle for the membrane with the PET layer attached is likely the result of some wicking into the large pores of the PET layer. The PSu layer displays the hydrophobic character reported by others⁹

for TFC membranes. This inherent hydrophobicity explains the need for pre-

wetting the membrane with an alcohol prior to FO and PRO testing as illustrated in this study and others who have worked with varying iterations of this structure.^{37,38}

A5.3.3.2. FTIR spectra

The membranes selective layer has a FTIR spectrum attributable to aromatic polyamide. The peaks visible from $1700\text{--}1500 \text{ cm}^{-1}$ capture stretching vibrations attributable to C=O, C-N, and -CO-NH- bonds existing within the polyamide.^{39,40} Also notable are the peaks occurring between $3000\text{--}2500 \text{ cm}^{-1}$ which can be attributed to -OH stretching amongst carboxylic acid functional groups;^{11,40,41} however, the peak at 2900 cm^{-1} peaks can also be attributed to the -



A5.5. FTIR spectra of the membrane's selective layer from 3900 to 2400 cm^{-1} and 1800 to 600 cm^{-1} .

CH_3CCH_3- groups within polysulfone.³⁹ Carboxylic acid functionality within the polyamide would be significant as prior work by Arena et al. hypothesized the contribution of this functional group to a cation exchange behavior observed for membrane containing a polyamide selective layer when using electrolyte draw solutions.⁶ The peak at 2900 cm^{-1} that can be attributed to the $-\text{CH}_3\text{CCH}_3-$ and peaks within this spectra attributable to the $-\text{SO}_2-$ of a sulfone at ~ 1120 and ~ 1340 suggest that the membrane is built upon a polysulfone support layer.^{39,40}

A5.3.4. Osmotic performance

A5.3.4.2. Pressure retarded osmosis testing

Experimentally measured water fluxes and supporting simulated values for PRO are shown in Fig. A5.6a. The power densities corresponding to those water fluxes observed/calculated in Fig. A5.6a are shown in Fig. A5.6b. The measured water flux and power density are much lower than those simulated for the ideal case of constant structural parameter and no external polarization. Upon the inclusion ECP, numerical simulation of water fluxes still over predicts power densities observed experimentally, suggesting that the significant difference between the experimental and simulated water flux is from changing support layer structural parameter caused by compaction. Fig. A5.6c shows how the structural parameter sharply increases over a range of transmembrane pressures. These changes are especially prominent at pressures above 4.5 bar. Prior studies comparing experimental and theoretical PRO performance have also observed rapid flux decline with increasing transmembrane pressure.^{11,35}

The observed increases in structural parameter are likely the result of the applied hydrostatic pressure which compact the membrane's support layer. This compaction will reduce the thickness of the support layer and likely collapse some of the membrane's internal

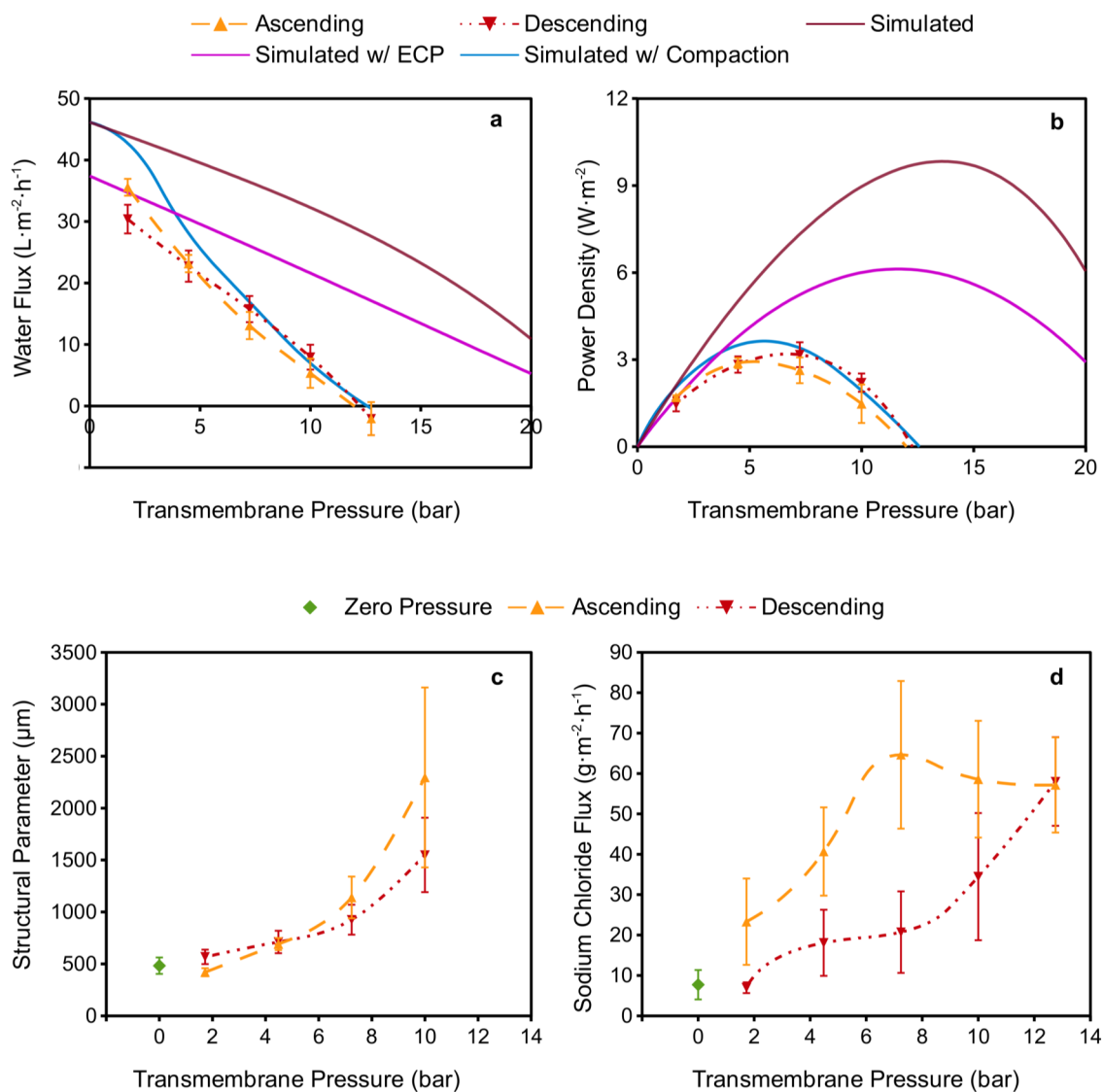


Fig. A5.6. Membrane performance in PRO showing water flux (a), power density (b), structural parameter (c), and sodium chloride reverse solute flux (d). Test conditions 0.5 M NaCl draw, DI feed, $0.25 \text{ m} \cdot \text{s}^{-1}$ draw cross-flow, and 20°C . Assumptions incorporated in the calculation of these values are in Table A5.1.

pore structure³⁷. The loss of support layer porosity is directly competitive with the reduced thickness of the support.

The impact of decreasing porosity on tortuosity is not clear because the classical relationship between porosity and tortuosity, the Bruggemann relation, is an empirical relationship shown in a generalized form in Eq. (A5.7).⁶⁵

$$\tau = \gamma \epsilon^{1-\alpha} \quad (\text{A5.7})$$

γ and α are constants relating to the morphology of the material it is possible to develop a conceptual understanding on how the tortuosity of porous membrane materials are affected by compaction. In general values for both γ and α are >1 .⁶⁵ This suggests that for the range of common values in the Bruggemann relation a loss of porosity within the membrane support layers would result in increases to the support layer tortuosity (i.e. for $\gamma=1$ and $\alpha=1.6$ a decrease in porosity from 70% to 60% would increase tortuosity from ~ 1.24 to ~ 1.36). The common range of values for the Bruggeman relation should only dictate the magnitude of tortuosity increase and not whether to tortuosity will increase with a loss of porosity.

Improved compaction tolerance could be implemented through forming membrane upon a

stiffer support structure which will not compact in PRO or one which when under compaction does not demonstrate a rapid increase in the membranes structural parameter. Support layers with a spongy structure are viewed by some as having greater tolerance to compaction making them more suitable for PRO.^{37,66}

A5.3.4.3. Ammonia-carbon dioxide water flux and rejection

The water fluxes observed from desalination tests using the $\text{NH}_3\text{-CO}_2$ draw solution with differing $\text{NH}_3\text{:CO}_2$ ratios are shown in Fig. A5.7. When compared to similar studies using this draw solution (with a 1.2:1 $\text{NH}_3\text{:CO}_2$) the observed water fluxes were higher than those observed using polydopamine (PDA) modified TFC RO membranes.⁶⁻⁸ Coinciding with observations made by Arena, there was a substantial decrease in flux when modest amounts of salt were added to the feed (0.25 M).⁶ A decrease in water flux was observed when the $\text{NH}_3\text{:CO}_2$ ratio what changed from 1.2:1 to 1.5:1. The observed water flux increased for the 2:1 ratio compared to 1.2:1 ratio. The overall change in water flux was approximately $\pm 5 \text{ L}\cdot\text{m}^{-2}\cdot\text{h}^{-1}$ when using a feed solution of DI water for the three $\text{NH}_3\text{:CO}_2$ ratios studied.

The drop in water flux for a 1.5:1 ratio is observed in spite of the higher osmotic pressure of this draw solution (Table A5.4). This suggests that the increased osmotic pressure cannot be

effectively used by the membrane, possibly

as a result of an uneven permeation of

draw solutes through the selective layer.

The key species to which the membrane is

likely fairly permeable to is ammonia,

primarily due to its similarity with water in

size and polarity, as well as its more

flexible hydration shell.⁶⁷ As ammonia that

freely crosses the membrane does not

contribute to the osmotic driving force and could alter the speciation of the draw solution at the membrane's selective layer.

The multicomponent nature of this draw solution complicates even a qualitative analysis of draw solute speciation. In general, the $\text{NH}_3:\text{CO}_2$ draw solution appears to perform best at extremes with a minimal $\text{NH}_3:\text{CO}_2$ (close to 1:1, having a low amount of aqueous NH_3) or with a large excess of NH_3 in solution, having more than 20% total molality nitrogen species as aqueous NH_3 . At the low ratios, the most abundant nitrogen species is NH_4^+ , which will not

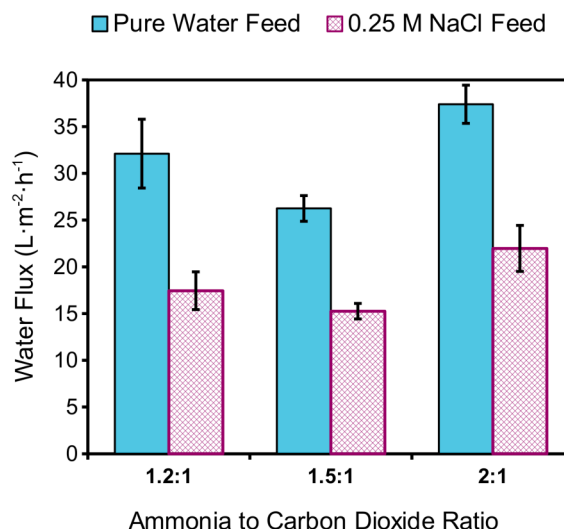


Fig. A5.7. Water flux of the membrane against a 0.25 M NaCl feed using a 2 M $\text{NH}_3\text{-CO}_2$ (based on carbon species) draw of varying $\text{NH}_3:\text{CO}_2$.

Table A5.4. Speciation of NH₃-CO₂ draw solution at 23°C.

	1.2:1 2 M _{CO₂}	1.5:1 2 M _{CO₂}	2:1 2 M _{CO₂}
pH	8.2	8.6	9.0
m _{total-N} (mol/kg _{H₂O})	2.36	2.98	4.06
m _{total-C} (mol/kg _{H₂O})	2.06	2.06	2.07
ρ _{solution} (kg/L)	1.058	1.059	1.055
m _{NH₃} (mol/kg _{H₂O})	0.0612	0.213	0.678
m _{CO₂} (mol/kg _{H₂O})	0.0632	0.0163	0.00304
m _{NH₄⁺} (mol/kg _{H₂O})	2.04	2.08	2.10
m _{HCO₃⁻} (mol/kg _{H₂O})	1.77	1.34	0.758
m _{CO₃²⁻} (mol/kg _{H₂O})	0.0113	0.0250	0.0374
m _{NH₂COO⁻} (mol/kg _{H₂O})	0.255	0.686	1.27
Ionic strength	2.05	2.10	2.14
π (bar)	50.1	74.2	116

easily cross the membrane. At higher NH₃:CO₂ ratios the draw solution comprises increasing amounts of carbamate and dissolved ammonia. Large amounts of dissolved ammonia contribute significantly to the draw solution's osmotic pressure even though some of the dissolved ammonia diffuses across the membrane. From an operational perspective, having

excess ammonia might be preferred to increase the stability and solubility of the solution.

The forward (sodium cations and chloride anions) and reverse (total ammonia species, consisting of ammonia, ammonium, and carbamate) fluxes are shown in Fig. A5.8a. For all $\text{NH}_3:\text{CO}_2$ ratios, cation fluxes (sodium and ammonium) were statistically similar. In all instances the ammonium to sodium fluxes were greater than or statistically identical to the sodium flux observed for all $\text{NH}_3:\text{CO}_2$ ratios. Ammonia species flux is higher for the 1.5:1 $\text{NH}_3:\text{CO}_2$ draw solution. This further supports the hypothesis that the low water fluxes occur due to greater ammonia flux into the feed solution. For the 2:1 ratio, the ammonia species flux stays the same, indicating that the additional dissolved ammonia effectively contributes to the osmotic driving force. The 1.2:1 $\text{NH}_3:\text{CO}_2$ draw solution has the lowest dissolved ammonia (gas) concentration (less than $0.1 \text{ mol}\cdot\text{kg}^{-1}$) and exhibits the lowest flux of ammonia species. Due to the low dissolved ammonia concentration, nearly all of ammonia species flux must occur from the transport of ammonium.

Large differences in the forward cation and anion fluxes are shown in Fig. A5.8b. Sodium flux is an order of magnitude higher than the chloride flux for all of the $\text{NH}_3:\text{CO}_2$ ratios tested. The lower chloride flux suggests that anion transport is not necessary to maintain

electroneutrality between the feed and draw solution, suggesting that sodium-ammonium cation exchange is occurring. A similar result was reported in previous work by Arena, et al. on PDA modified TFC RO membranes used with this draw solution (only in a 1.2:1 $\text{NH}_3:\text{CO}_2$).⁶ Lu, et al. also observed the occurrence of ammonium/sodium exchange across the selective layer of another iteration of this membrane.⁶⁸ This work also showed that the rate of ammonium and sodium transport can be reduced through a surface modification of the selective layer which converts carboxylic acid functional groups to amine reactive esters, which could then be reacted with aqueous ethylenediamine, effectively converting the carboxylic acid ($-\text{COOH}$) to $-\text{CONHCH}_2\text{CH}_2\text{NH}_2$.⁶⁸

The lower forward flux of anions to cations is a result of inherent negative surface functionality common to TFC membrane polyamide layers due to the presence of carboxylic acid functional groups which form from the hydrolysis of acid chloride groups from the interfacial polymerization.⁶ This behavior is not unique to the $\text{NH}_3\text{-CO}_2$ draw solution as shown in prior study by Coday et al. This study, which also used an iteration of this membrane platform, employed a NaCl draw solution and a feed of mixed electrolytes observed different rates of cation and anion transport through TFC membranes.³³

These data show that while productivity (or water flux) is an important component in forward osmosis desalination interactions between draw solutes, feed solutes, and the membrane can lower product water quality and complicate draw solution recovery. Mitigating the impact of sodium/ammonium cation exchange has been incorporated into the design of Oasys Water's osmotic brine concentrator.³⁴ Their refinements include a stripper for the feed solution to recovers draw solutes that cross the membrane through diffusion and ion exchange. Additionally, there is an RO polisher following draw solute recovery to remove the cations that cross the membrane from ion exchange. The RO permeate is clean water. The RO concentrate, containing nonvolatile cations and anions from the feed and draw solution can be

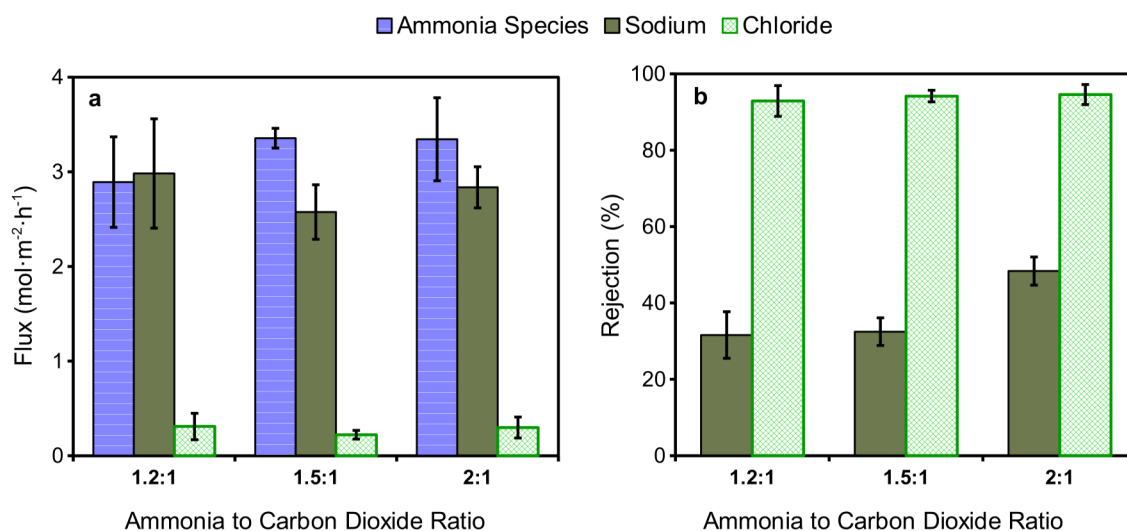


Fig. A5.8. Ion fluxes (a) and feed ion rejection (b) of a 0.25 M NaCl feed solution using a 2 M $\text{NH}_3\text{-CO}_2$ draw solution of varying $\text{NH}_3:\text{CO}_2$ ratios.

blended with the pretreated feed solution. Draw solute anions blended with the feed solution are removed with draw solute cations in the feed solution stripper.

A5.4. Conclusions

This early generation of Oasys Water's TFC membrane was demonstrated to have high water flux in FO and PRO operation. Data for PRO conditions illustrated evidence of membrane compaction under; however, evidence for ion exchange between ammonium and sodium was found in FO using the $\text{NH}_3\text{-CO}_2$ draw solution. These finding suggest that the development of low structural parameter support layers for FO and PRO now must competes with the development of membranes which are compaction tolerant and/or ion exchange resistant

References

1. Cath, T. Y.; Childress, A. E.; Elimelech, M. Forward osmosis: Principles, applications, and recent developments. *J. Membr. Sci.* **2006**, *281*, 70-87.
2. Hoover, L. A.; Phillip, W. A.; Tiraferri, A. ; Yip, N. Y.; Elimelech, M. Forward with Osmosis: Emerging Applications for Greater Sustainability. *Environ. Sci. Technol.* **2011**, *45*, 9824–9830.
3. McGinnis, R. L.; Elimelech, M. Global challenges in energy and water supply: the promise of engineered osmosis. *Environ. Sci. Technol.* **2008**, *42*, 8625-8629.

4. Chung, T.-S. ; Zhang, S. ; Wang, K. Y.; Su, J. ; Ling, M. M. Forward osmosis processes: Yesterday, today, and tomorrow. *Desalination* **2012**, *287*, 78-81.
5. Klaysom, C. ; Cath, T. Y.; Depuydt, T. ; Vankelecom, I. F. J. Forward and pressure retarded osmosis: potential solutions for global challenges in energy and water supply. *Chem. Soc. Rev.* **2013**, *42*, 6959-5989.
6. Arena, J. T.; Manickam, S. S.; Reimund, K. K.; Freeman, B. D.; McCutcheon, J. R. Solute and water transport in forward osmosis using polydopamine modified thin film composite membranes. *Desalination* **2014**, *343*, 8-16.
7. McCutcheon, J. R.; McGinnis, R. L.; Elimelech, M. A novel ammonia-carbon dioxide forward (direct) osmosis desalination process. *Desalination* **2005**, *174*, 1-11.
8. McCutcheon, J. R.; McGinnis, R. L.; Elimelech, M. Desalination by ammonia-carbon dioxide forward osmosis: Influence of draw and feed solution concentrations on process performance. *J. Membr. Sci.* **2006**, *278*, 114-123.
9. Garcia-Castello, E. M.; McCutcheon, J. R. Dewatering press liquor derived from orange production by forward osmosis. *J. Membr. Sci.* **2011**, *372*, 97-101.
10. McGinnis, R. L.; McCutcheon, J. R.; Elimelech, M. A novel ammonia-carbon dioxide osmotic heat engine for power generation. *J. Membr. Sci.* **2007**, *305*, 13-19.
11. She, Q. ; Jin, X. ; Tang, C. Y. Osmotic power production from salinity gradient resource by pressure retarded osmosis: Effects of operating conditions and reverse solute diffusion. *J. Membr. Sci.* **2012**, *401-402*, 262-273.
12. Straub, A. P.; Yip, N. Y.; Elimelech, M. Raising the Bar: Increased Hydraulic Pressure Allows Unprecedented High Power Densities in Pressure-Retarded Osmosis. *Environ. Sci. Technol. Lett.* **2014**, *1*, 55-59.
13. Stone, M. L.; Rae, C. ; Stewart, F. F.; Wilson, A. D. Switchable polarity solvents as draw solutes for forward osmosis. *Desalination* **2013**, *312*, 124-129.
14. Herron, J. Asymmetric forward osmosis membranes. United States Patent No. US 7,445,712, Nov. 4, 2008.

15. Cath, T. Y.; Adams, D. ; Childress, A. E. Membrane contactor processes for wastewater reclamation in space II. Combined direct osmosis, osmotic distillation, and membrane distillation for treatment of metabolic wastewater. *J. Membr. Sci.* **2005**, *257*, 111-119.
16. Cath, T. Y.; Gormly, S. ; Beaudry, E. G.; Flynn, M. T.; Adams, V. D.; Childress, A. E. Membrane contactor processes for wastewater reclamation in space Part I. Direct osmotic concentration as pretreatment for reverse osmosis. *J. Membr. Sci.* **2005**, *257*, 85-98.
17. Cath, T. Y.; Hancock, N. T.; Lundin, C. D.; Hoppe-Jones, C. ; Drewes, J. E. A multi-barrier osmotic dilution process for simultaneous desalination and purification of impaired water. *J. Membr. Sci.* **2010**, *362*, 417-436.
18. Ge, Q. ; Su, J. ; Chung, T.-S. ; Amy, G. Hydrophilic Superparamagnetic Nanoparticles: Synthesis, Characterization, and Performance in Forward Osmosis Processes. *Ind. Eng. Chem. Res.* **2011**, *50*, 382-288.
19. Ling, M. M.; Chung, T.-S. Desalination process using super hydrophilic nanoparticles via forward osmosis. *Desalination* **2011**, *278*, 194-202.
20. Baker, R. W. *Membrane Technology and Applications*, 2nd ed.; John Wiley & Sons Ltd: West Sussex, 2004.
21. Vos, K. D.; Burris, F. O.; Riley, R. L. Kinetic Study of the Hydrolysis of Cellulose Acetate in the pH Range of 2-10. *J. Appl. Polym. Sci.* **1966**, *10*, 825-832.
22. Watters, J. C.; Klein, E. ; Fleischman, M.; Roberts, J. S.; Hall, B. Rejection Spectra of Reverse Osmosis Membranes Degraded by Hydrolysis of Chlorine Attack. *Desalination* **1986**, *60*, 93-110.
23. Cath, T. Y.; Elimelech, M. ; McCutcheon, J. R.; McGinnis, R. L.; Achilli, A.; Anastasio, D.; Brady, A. R.; Childress, A. E.; Farr, I. V.; Hancock, N. T.; Lampi, J. ; Nghiem, L. D.; Xie, M.; Yip, N. Y. Standard Methodology for Evaluating Membrane Performance in Osmotically Driven Membrane Processes. *Desalination* **2013**, *312*, 31-38.
24. Arena, J. T.; McCloskey, B. ; Freeman, B. D.; McCutcheon, J. R. Surface modification of thin film composite membrane support layers with polydopamine: Enabling use of reverse osmosis membranes in pressure retarded osmosis. *J. Membr. Sci.* **2011**, *375*, 55-62.

25. Bui, N. N.; Lind, M. L.; Hoek, E. M. V.; McCutcheon, J. R. Electrospun nanofiber supported thin film composite membranes for engineered osmosis. *J. Membr. Sci.* **2011**, *385-386*, 10-19.
26. Bui, N. N.; McCutcheon, J. R. Hydrophilic Nanofibers as New Supports for Thin Film Composite Membranes for Engineered Osmosis. *Environ. Sci. Technol.* **2013**, *47*, 1761-1769.
27. Ren, J. ; McCutcheon, J. R. A new commercial thinfilm composite membrane for forward osmosis. *Desalination* **2014**, *343*, 187-193.
28. Wang, R. ; Shi, L. ; Tang, C. Y.; Chou, S. ; Qui, C. ; Fane, A. G. Characterization of novel forward osmosis hollow fiber membranes. *J. Membr. Sci.* **2010**, *355*, 158-167.
29. Yip, N. Y.; Tiraferri, A. ; Phillip, W. A.; Schiffman, J. D.; Elimelech, M. High Performance Thin Film Composite Forward Osmosis Membrane. *Environ. Sci. Technol.* **2010**, *44*, 3812-3818.
30. Song, X.; Lui, Z.; Sun, D. D. Nano Gives the Answer: Breaking the Bottleneck of Internal Concentration Polarization with a Nanofiber Composite Forward Osmosis Membrane for a High Water Production Rate. *Adv. Mater.* **2011**, *23*, 3256-3260.
31. Huang, L.; McCutcheon, J. R. Hydrophilic nylon 6,6 nanofibers supported thin film composite membranes for engineered osmosis. *J. Membr. Sci.* **2014**, *457*, 162-169.
32. Hoover, L. A.; Schiffman, J. D.; Elimelech, M. Nanofibers in thin-film composite membrane support layers: Enabling expanded application of forward and pressure retarded osmosis. *Desalination* **2013**, *308*, 73-81.
33. Coday, B. D.; Heil, D. M.; Xu, P. ; Cath, T. Y. Effects of Transmembrane Hydraulic Pressure on Performance of Forward Osmosis Membranes. *Environ. Sci. Technol.* **2013**, *47*, 2386-2393.
34. McGinnis, R. L.; Hancock, N. T.; Nowosielski-Slepowron, M. S.; McGurgan, G. D. Pilot Demonstration of the NH₃/CO₂ forward osmosis desalination process on high salinity brines. *Desalination* **2013**, *312*, 67-74.
35. Bui, N. N.; McCutcheon, J. R. Nanofiber Supported Thin-Film Composite Membrane for Pressure-Retarded Osmosis. *Environ. Sci. Technol.* **2014**, *48*, 4129-4136.

36. Achilli, A. ; Cath, T. Y.; Childress, A. E. Power generation with pressure retarded osmosis: An experimental and theoretical investigation. *J. Membr. Sci.* **2009**, *343*, 42-52.
37. Han, G. ; Zhang, S. ; Li, X. ; Chung, T. S. High performance thinfilm composite pressure retarded osmosis (PRO) membranes for renewable salinity-gradient energy generation. *J. Membr. Sci.* **2013**, *440*, 108-121.
38. Song, X.; Lui, Z.; Sun, D. D. Energy recovery from concentrated seawater brine by thin-film nanofiber composite pressure retarded osmosis membranes with high power density. *Energy Environ. Sci.* **2013**, *6*, 1199-1210.
39. McGinnis, R.; McGurgan, G. Forward osmosis membranes. United States Patent No. US 8,181,794, May 22, 2012.
40. Comesana, J. F.; Otero, J. J.; Camesella, E.; Correa, A. Densities and Viscosities of Ternary Systems of Water + Fructose + Sodium Chloride from 20 to 40 °C. *J. Chem. Eng. Data* **2001**, *46*, 1153-1155.
41. Lobo, V. M. M. Mutual Diffusion Coefficients in Aqueous Electrolyte Solutions. *Pure Appl. Chem.* **1993**, *65*, 2613-2640.
42. McCabe, W. L.; Smith, J. C.; Harriot, P. *Unit Operations of Chemical Engineering*, 7th ed.; McGraw-Hill: New York, 2005.
43. Manickam, S. S.; Gelb, J. ; McCutcheon, J. R. Pore structure characterization of asymmetric membranes: Non-destructive characterization of porosity and tortuosity. *J. Membr. Sci.* **2014**, *454*, 549-554.
44. Yip, N. Y.; Tiraferri, A. ; Phillip, W. A.; Schiffman, J. D.; Hoover, L. A.; Kim, Y. C.; Elimelech, M. Thin-Film Composite Pressure Retarded Osmosis Membranes for Sustainable Power Generation from Salinity Gradients. *Environ. Sci. Technol.* **2011**, *45*, 4360-4369.
45. Tiraferri, A. ; Yip, N. Y.; Straub, A. P.; Castrillon, S. R.-V.; Elimelech, M. A method for the simultaneous determination of transport and structural parameters of forward osmosis membranes. *J. Membr. Sci.* **2013**, *444*, 523-538.
46. Yip, N. Y.; Elimelech, M. Performance Limiting Effects in Power Generation from Salinity Gradients by Pressure Retarded Osmosis. *Environ. Sci. Technol.* **2011**, *45*, 10273-10282.

47. Anastasio, D. D.; Arena, J. T.; Cole, E. A.; McCutcheon, J. R. Impact of temperature on power density in closed-loop pressure retarded osmosis for grid storage. *J. Membr. Sci.* **2015**, *479*, 240-245.
48. Kawazuishi, K. ; Prausnitz, J. M. Correlation of Vapor-Liquid Equilibria for the System of Ammonia-Carbon Dioxide-Water. *Ind. Eng. Chem. Res.* **1987**, *26*, 1482-1485.
49. Edwards, T. J.; Maurer, G. ; Newman, J. ; Prausnitz, J. M. Vapor-Liquid Equilibria in Multicomponent Aqueous Solutions of Volatile Weak Electrolytes. *AIChE J.* **1978**, *24*, 966-976.
50. Pawlikowski, E. M.; Newman, J. ; Prausnitz, J. M. Phase Equilibria for Aqueous Systems of Ammonia and Carbon Dioxide. *Ind. Eng. Chem. Proc. Des. Dev.* **1982**, *21*, 764-770.
51. Buetler, D. ; Renon, H. Representation of $\text{NH}_3\text{-H}_2\text{S-H}_2\text{O}$, $\text{NH}_3\text{-CO}_2\text{-H}_2\text{O}$, and $\text{NH}_3\text{-SO}_2\text{-H}_2\text{O}$ Vapor-Liquid Equilibria. *Ind. Eng. Chem. Proc. Des. Dev.* **1978**, *17*, 220-230.
52. Robinson, R. A.; Stokes, R. H. Electrolyte Solutions, Second Revised ed.; Dover Publications: Mineola, 2002.
53. Prausnitz, J. M.; Lichtenthaler, R. N.; de Azevedo, E. G. *Molecular Thermodynamics of Fluid-Phase Equilibria*, 3rd ed.; Prentice-Hall, Inc.: Upper Saddle River, 1999.
54. Grattoni, A. ; Merlo, M. Osmotic Pressure beyond Concentration Restrictions. *J. Phys. Chem. Part B* **2007**, *111*, 11770-11775.
55. Jeffrey, G. H.; Bassett, J.; Mendham, J.; Denny, R. C. *Vogel's Textbook of Quantitative Chemical Analysis*, 5th ed.; Longman Scientific & Technical: Essex, 1989.
56. Harris, D. C. *Quantitative Chemical Analysis* , 6th ed.; W.H. Freeman and Company: New York, 2003.
57. Shi, L. ; Chou, S. R.; Wang, R. ; Fang, W. X.; Tang, C. Y.; Fane, A. G. Effect of substrate structure on the performance of thin-film composite forward osmosis hollow fiber membranes. *J. Membr. Sci.* **2011**, *382*, 116-123.
58. Tiraferri, A. ; Yip, N. Y.; Phillip, W. A.; Schiffman, J. D.; Elimelech, M. Relating performance of thin-film composite forward osmosis membranes to support layer formation and structure. *J. Membr. Sci.* **2011**, *367*, 340-352.

59. Kwak, S. Y.; Jung, S. G.; Yoon, Y. S.; Ihm, D. W. Details of Surface Features in Aromatic Polyamide Reverse Osmosis Membranes Characterized by Scanning Electron and Atomic Force Microscopy. *J. Polym. Sci. Part B Polym. Phys.* **1999**, *37*, 1429-1440.
60. Petersen, R. J. Composite reverse osmosis and nanofiltration membranes. *J. Membr. Sci.* **1993**, *83*, 81-150.
61. Green, M. M.; Wittcoff, H. A. *Organic Chemistry Principles and Industrial Practice*, 1st ed.; Wiley-VCH: Weinheim, 2003.
62. Tang, C. Y.; Kwon, Y.-N.; Leckie, J. O. Effect of membrane chemistry and coating layer on physiochemical properties of thin film composite polyamide RO and NF membranes I. FTIR and XPS characterization of polyamide and coating layer chemistry. *Desalination* **2009**, *242*, 149-167.
63. Lambert, J. B.; Shurvell, H. F.; Lightner, D. A.; Cooks, R. G. *Organic Structural Spectroscopy*; Prentice-Hall, Inc.: Upper Saddle River, 1998.
64. Speight, J. G. *Lange's Handbook of Chemistry*, 16th ed.; McGraw Hill: New York, 2005.
65. Thorat, I. V.; Stephenson, D. E.; Zacharias, N. A.; Zaghib, K. ; Harb, J. N.; Wheeler, D. R. Quantifying tortuosity in porous Li-ion battery materials. *J. Power Sources* **2009**, *188*, 592-600.
66. Widjojo, N. ; Chung, T. S.; Weber, M. ; Maletzko, C. ; Warzelhan, V. The role of sulphonated polymer and macrovoid-free structure in the support layer for thin-film composite (TFC) forward osmosis (FO) membranes. *J. Membr. Sci.* **2011**, *383*, 214-223.
67. Hesske, H. ; Gloe, K. Hydration Behavior of Alkyl Amines and Their Corresponding Protonated Forms. 1. Ammonia and Methylamine. *J. Phys. Chem.* **2007**, *111*, 9848-9853.
68. Lu, X. ; Boo, C. ; Ma, J. ; Elimelech, M. Bidirectional Diffusion of Ammonium and Sodium Cations in Forward Osmosis: Role of Membrane Active Layer Surface Chemistry and Charge. *Environ. Sci. Technol.* **2014**, *48*, 14369-14376.

Appendix 6

Numerical simulation of water flux and simultaneous determination of membrane transport parameters in forward osmosis

Initial Values and Solution options

To prevent errors restart the kernel with each calculation

```
externalPolarization = True  
FO = True  
temperature = 20 (*degrees C*)  
flowrate = 1 (*LPM*)  
feedConcentration = {0.1}
```

True

True

20

1

{0.1}

Cell dimensions

```
width = 1.0200  
height = 0.0980  
length = 3.150
```

1.02

0.098

3.15

Membrane Data

x=0 to use membrane properties from the box above

```
MPDTFC =  
  {"MPDTFC", 0, 0, 0}, {0.5, 7.087, 7.843, 7.5792}, {1, 11.376, 12.636, 12.757}, {1.5, 16.350, 15.187, 14.717}}  
EDTFC = {"EDTFC", 0, 0, 0}, {0.5, 5.020, 5.223, 5.381}, {1, 9.021, 9.558, 8.942}, {1.5, 12.029, 11.131, 11.962}}  
MPDTFCED = {"MPDTFCED", 0, 0, 0}, {0.5, 17.070, 17.159, 19.761},  
  {1, 27.046, 25.686, 29.448}, {1.5, 34.158, 31.486, 36.097}}  
  
MPDTFCfluxes = {{7.50304834, 0.5},  
  {12.256, 1},  
  {15.418, 1.5}}  
MPDTFCError = {{0.767022488, 0.5},  
  {1.0127, 1},  
  {1.073, 1.5}}  
EDTFCfluxes = {{5.208, 0.5},  
  {9.173, 1},  
  {11.707, 1.5}}  
EDTFCError = {{0.778, 0.5},  
  {0.827, 1},  
  {0.909, 1.5}}  
MPDTFCEDfluxes = {{17.996, 0.5},  
  {27.393, 1},  
  {33.914, 1.5}}  
MPDTFCEDError = {{1.668, 0.5},  
  {2.019, 1},  
  {2.410, 1.5}}  
neatFluxes = {{4.992, 0.5},  
  {8.552, 1},  
  {11.097, 1.5}}  
neatError = {{1.297, 0.5},  
  {1.663, 1},  
  {1.983, 1.5}}  
noriFluxes = {{7.959, 0.5},  
  {12.086, 1},  
  {14.590, 1.5}}  
noriError = {{0.905, 0.5},  
  {1.349, 1},  
  {1.338, 1.5}}  
HTIfluxes = {{6.356, 0.5},  
  {9.069, 1},  
  {12.165, 1.5}}  
HTIError = {{1.344, 0.5},  
  {1.667, 1},  
  {1.823, 1.5}}  
  
MPDTFCproFlux = {{3.173880277, 1.586275699}, {0.145246954, 0.032316169}}
```

```

EDTFCproFlux = {{1.37626387, 0.761689912}, {0.165231289, 0.017470961}}
MPDTFCEDproFlux = {{14.79748809, 1.693903898}, {0.504876601, 0.063864271}}
neatProFlux = {{4.691292742, 1.308923352}, {0.026162005, 0.010709922}}
noriProFlux = {{6.368370499, 1.550926069}, {0.065226358, 0.024464338}}
HTIproFlux = {{4.862822298, 1.468888233}, {0.085138034, 0.040231572}}

```

```

plot1 = ListPlot[MPDTFCfluxes, PlotStyle → Blue];
plot2 = ListPlot[EDTFCfluxes, PlotStyle → Red];
plot3 = ListPlot[MPDTFCEDfluxes, PlotStyle → Green];
plot4 = ListPlot[neatFluxes, PlotStyle → Purple];
plot5 = ListPlot[noriFluxes, PlotStyle → Orange];
plot6 = ListPlot[HTIfluxes, PlotStyle → Gray];
Show[plot1, plot2, plot3, plot4, plot5, plot6, PlotRange → All]

```

```

{{MPDTFC, 0, 0, 0}, {0.5, 7.087, 7.843, 7.5792},
 {1, 11.376, 12.636, 12.757}, {1.5, 16.35, 15.187, 14.717}}

{{EDTFC, 0, 0, 0}, {0.5, 5.02, 5.223, 5.381},
 {1, 9.021, 9.558, 8.942}, {1.5, 12.029, 11.131, 11.962}}

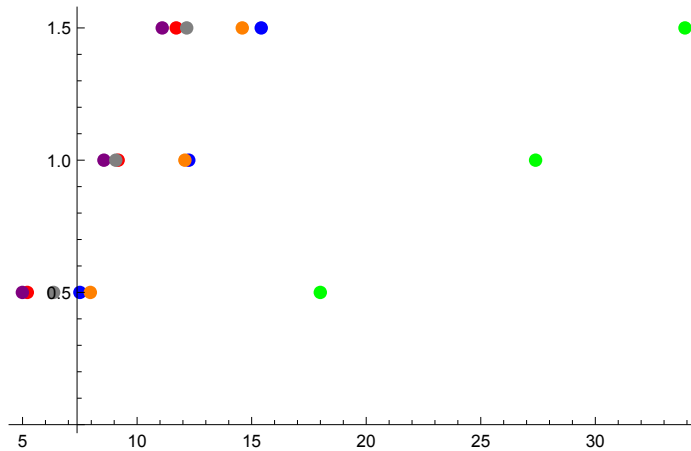
{{MPDTFCED, 0, 0, 0}, {0.5, 17.07, 17.159, 19.761},
 {1, 27.046, 25.686, 29.448}, {1.5, 34.158, 31.486, 36.097}}

{{7.50305, 0.5}, {12.256, 1}, {15.418, 1.5}}
{{0.767022, 0.5}, {1.0127, 1}, {1.073, 1.5}}
{{5.208, 0.5}, {9.173, 1}, {11.707, 1.5}}
{{0.778, 0.5}, {0.827, 1}, {0.909, 1.5}}
{{17.996, 0.5}, {27.393, 1}, {33.914, 1.5}}
{{1.668, 0.5}, {2.019, 1}, {2.41, 1.5}}
{{4.992, 0.5}, {8.552, 1}, {11.097, 1.5}}
{{1.297, 0.5}, {1.663, 1}, {1.983, 1.5}}
{{7.959, 0.5}, {12.086, 1}, {14.59, 1.5}}
{{0.905, 0.5}, {1.349, 1}, {1.338, 1.5}}
{{6.356, 0.5}, {9.069, 1}, {12.165, 1.5}}
{{1.344, 0.5}, {1.667, 1}, {1.823, 1.5}}
{{3.17388, 1.58628}, {0.145247, 0.0323162}}
{{1.37626, 0.76169}, {0.165231, 0.017471}}
{{14.7975, 1.6939}, {0.504877, 0.0638643}}
{{4.69129, 1.30892}, {0.026162, 0.0107099}}

```

$\{ \{ 6.36837, 1.55093 \}, \{ 0.0652264, 0.0244643 \} \}$

$\{ \{ 4.86282, 1.46889 \}, \{ 0.085138, 0.0402316 \} \}$



Dimensionless Values and Governing Equations

Reynolds Number

```
NRe[density_, velocity_, hydroDiam_, viscosity_] := Module[{eqn},
  eqn = (density*velocity*hydroDiam)/viscosity;
  eqn]
NRe[rho, v, d, mu]
```

$$\frac{d \rho v}{\mu}$$

Schmidt Number

```
NSc[viscosity_, density_, diffusivity_] := Module[{eqn},
  eqn = viscosity/(density*diffusivity);
  eqn]
NSc[mu, d, D]
```

$$\frac{\mu}{d D}$$

Sherwood Correlation

```
NSh[vNRe_, vNSc_, hydroDiam_, length_] := Module[{eqn},
  eqn = (1.85*(vNRe*vNSc*hydroDiam/length)^0.33);
  eqn]
NSh[Re, Sc, d, l]
```

$$1.85 \left(\frac{d Re Sc}{l} \right)^{0.33}$$

External Boundary Layer Thickness


```

boundaryThick[hydroDiam_, vNSh_] := Module[{eqn},
  eqn = hydroDiam/vNSh;
  eqn]
boundaryThick[d, Sh]

```

$\frac{d}{Sh}$

Governing Equation for Water Flux with solution for Draw solution concentration from water flux

```

fluxEqn[FOMode_, phiFunc_, wFlux_, wPerm_, sPerm_, struct_, delta_, pressureDiff_, temp_,
  concD_, concF_, diffD_, diffF_] := Module[{eqn, idGas, absTemp, dilCP, concCP, piDM, piFM},
  idGas = 8.3144621*10^(-2);
  absTemp = (temp + 273.15);
  If[FOMode, dilCP = Exp[-(wFlux * Abs[struct]) / (diffD * 3600 * 1000)],
  dilCP = Exp[-(wFlux * delta) / (diffD * 3600 * 1000)];
  If[FOMode, concCP = Exp[(wFlux * delta) / (diffF * 3600 * 1000)],
  concCP = Exp[(wFlux * Abs[struct]) / (diffF * 3600 * 1000)];
  piDM = 2 * concD * idGas * absTemp * dilCP;
  piFM = 2 * concF * idGas * absTemp * concCP;
  eqn =

  wFlux == Abs[wPerm] * ((piDM - piFM) / (1 + (Abs[sPerm] / wFlux) * (concCP - dilCP)) - pressureDiff);
  eqn]
fluxEqn[True, 1, jW, a, b, s, d, p, t, cD, cF, dD, dF]
fluxEqn[False, 1, jW, a, b, s, d, p, t, cD, cF, dD, dF]

concSol = Expand[cD /. Solve[fluxEqn[True, 1, jW, a, b, s, d, 0, t, cD, cF, dD, dF], cD][[1]]]

```

jW ==

$$\text{Abs}[a] \left(-p + \left(-0.166289 \, cF \, e^{\frac{d \, jW}{3600000 \, dF}} (273.15 + t) + 0.166289 \, cD \, e^{-\frac{jW \, \text{Abs}[s]}{3600000 \, dD}} (273.15 + t) \right) \right) /$$

$$\left(1 + \frac{\left(e^{\frac{d \, jW}{3600000 \, dF}} - e^{-\frac{jW \, \text{Abs}[s]}{3600000 \, dD}} \right) \text{Abs}[b]}{jW} \right)$$

$$\begin{aligned}
jW = & \text{Abs}[a] \left(-p + \left(0.166289 \text{ cD } e^{-\frac{d jW}{3600000 \text{ dD}}} (273.15 + t) - 0.166289 \text{ cF } e^{\frac{jW \text{ Abs}[s]}{3600000 \text{ dF}}} (273.15 + t) \right) / \right. \\
& \left. \left(1 + \frac{\left(-e^{-\frac{d jW}{3600000 \text{ dD}}} + e^{\frac{jW \text{ Abs}[s]}{3600000 \text{ dF}}} \right) \text{Abs}[b]}{jW} \right) \right) \\
& \frac{6.01362 e^{\frac{2.77778 \times 10^{-7} jW \text{ Abs}[s]}{\text{dD}}} jW}{(273.15 + t) \text{Abs}[a]} - \frac{6.01362 \text{Abs}[b]}{(273.15 + t) \text{Abs}[a]} + \frac{6.01362 e^{\frac{2.77778 \times 10^{-7} d jW}{\text{dF}}} + \frac{2.77778 \times 10^{-7} jW \text{ Abs}[s]}{\text{dD}} \text{Abs}[b]}{(273.15 + t) \text{Abs}[a]} + \\
& \frac{273.15 \text{ cF } e^{\frac{2.77778 \times 10^{-7} d jW}{\text{dF}}} + \frac{2.77778 \times 10^{-7} jW \text{ Abs}[s]}{\text{dD}}}{(273.15 + t) \left(1. + \frac{\left(e^{\frac{d jW}{3600000 \text{ dF}}} - 1. e^{-\frac{jW \text{ Abs}[s]}{3600000 \text{ dD}}} \right) \text{Abs}[b]}{jW} \right)} + \frac{1. \text{ cF } e^{\frac{2.77778 \times 10^{-7} d jW}{\text{dF}}} + \frac{2.77778 \times 10^{-7} jW \text{ Abs}[s]}{\text{dD}} t}{(273.15 + t) \left(1. + \frac{\left(e^{\frac{d jW}{3600000 \text{ dF}}} - 1. e^{-\frac{jW \text{ Abs}[s]}{3600000 \text{ dD}}} \right) \text{Abs}[b]}{jW} \right)} - \\
& \frac{273.15 \text{ cF } e^{\frac{2.77778 \times 10^{-7} d jW}{\text{dF}}} \text{Abs}[b]}{jW (273.15 + t) \left(1. + \frac{\left(e^{\frac{d jW}{3600000 \text{ dF}}} - 1. e^{-\frac{jW \text{ Abs}[s]}{3600000 \text{ dD}}} \right) \text{Abs}[b]}{jW} \right)} + \\
& \frac{273.15 \text{ cF } e^{\frac{5.55556 \times 10^{-7} d jW}{\text{dF}}} + \frac{2.77778 \times 10^{-7} jW \text{ Abs}[s]}{\text{dD}} \text{Abs}[b]}{jW (273.15 + t) \left(1. + \frac{\left(e^{\frac{d jW}{3600000 \text{ dF}}} - 1. e^{-\frac{jW \text{ Abs}[s]}{3600000 \text{ dD}}} \right) \text{Abs}[b]}{jW} \right)} - \\
& \frac{1. \text{ cF } e^{\frac{2.77778 \times 10^{-7} d jW}{\text{dF}}} t \text{Abs}[b]}{jW (273.15 + t) \left(1. + \frac{\left(e^{\frac{d jW}{3600000 \text{ dF}}} - 1. e^{-\frac{jW \text{ Abs}[s]}{3600000 \text{ dD}}} \right) \text{Abs}[b]}{jW} \right)} + \\
& \frac{1. \text{ cF } e^{\frac{5.55556 \times 10^{-7} d jW}{\text{dF}}} + \frac{2.77778 \times 10^{-7} jW \text{ Abs}[s]}{\text{dD}} t \text{Abs}[b]}{jW (273.15 + t) \left(1. + \frac{\left(e^{\frac{d jW}{3600000 \text{ dF}}} - 1. e^{-\frac{jW \text{ Abs}[s]}{3600000 \text{ dD}}} \right) \text{Abs}[b]}{jW} \right)}
\end{aligned}$$

Governing Equation for Salt Flux

```

saltFlux[FOMode_, wFlux_, sFlux_, wPerm_, sPerm_, struct_, delta_, temp_, concD_, concF_, diffD_, diffF_] :=
Module[{eqn, dilCP, concCP, concDM, concFM},
  If[FOMode, dilCP = Exp[-(wFlux * Abs[struct]) / (diffD * 3600 * 1000)],
  dilCP = Exp[-(wFlux * delta) / (diffD * 3600 * 1000)];
  If[FOMode, concCP = Exp[(wFlux * delta) / (diffF * 3600 * 1000)],
  concCP = Exp[(wFlux * Abs[struct]) / (diffF * 3600 * 1000)];
  concDM = concD * dilCP;
  concFM = concF * concCP;
  eqn =
    sFlux == Abs[sPerm] * ((concDM - concFM) / (1 + (Abs[sPerm] / wFlux) * (concCP - dilCP)));
  eqn]
saltFlux[True, jW, jS, a, b, s, d, t, cD, cF, dD, dF]
saltFlux[False, jW, jS, a, b, s, d, t, cD, cF, dD, dF]

```

$$jS = \frac{\left(-cF e^{-\frac{d jW}{3600000 dF}} + cD e^{-\frac{jW Abs[s]}{3600000 dD}} \right) Abs[b]}{1 + \frac{\left(e^{-\frac{d jW}{3600000 dF}} - e^{-\frac{jW Abs[s]}{3600000 dD}} \right) Abs[b]}{jW}}$$

$$jS = \frac{\left(cD e^{-\frac{d jW}{3600000 dD}} - cF e^{-\frac{jW Abs[s]}{3600000 dF}} \right) Abs[b]}{1 + \frac{\left(-e^{-\frac{d jW}{3600000 dD}} + e^{-\frac{jW Abs[s]}{3600000 dF}} \right) Abs[b]}{jW}}$$

Draw Solute Concentration as a Function of Water Flux

```

drawConc[wFlux_, struct_, diffD_, temp_, wPerm_, sPerm_, feedConc_, feedMass_] :=
Module[{absTemp, idGas, cD},
  absTemp = temp + 273.15;
  idGas = 8.3144621 * 10^(-2);
  cD = wFlux / Abs[wPerm] + (Abs[sPerm] / Abs[wPerm])
    (Exp[wFlux / (feedMass * 3600 * 1000)] - Exp[-(wFlux * Abs[struct]) / (diffD * 3600 * 1000)]) +
    feedConc * Exp[wFlux / (feedMass * 3600 * 1000)] * idGas * absTemp;
  cD *= Exp[(wFlux * Abs[struct]) / (diffD * 3600 * 1000)];
  cD]

drawConc[jw, s, dD, t, a, b, cF, k]
drawConc[jw, s, dD, t, a, 0, cF, k]

```

$$e^{\frac{jW Abs[s]}{3600000 dD}} \left(0.0831446 cF e^{\frac{jW}{3600000 k}} (273.15 + t) + \frac{jW}{Abs[a]} + \frac{\left(e^{\frac{jW}{3600000 k}} - e^{-\frac{jW Abs[s]}{3600000 dD}} \right) Abs[b]}{Abs[a]} \right)$$

$$e^{\frac{jW Abs[s]}{3600000 dD}} \left(0.0831446 cF e^{\frac{jW}{3600000 k}} (273.15 + t) + \frac{jW}{Abs[a]} \right)$$

Solution Physical Properties

Sodium Chloride Solution Density as a Function of Temperature and Concentration

```
denseCFunc[conc_, temp_] := Module[{eqn, densityData20, densityData30, densityData40},
  densityData20 = {998.2, 1018.5, 1037.8, 1056.4, 1074.15, 1091.3, 1107.95, 1123.8, 1139.4};
  densityData30 = {995.7, 1015.5, 1034.5, 1052.6, 1070.2, 1087.2, 1103.5, 1119.2, 1134.6};
  densityData40 = {992.2, 1011.8, 1030.4, 1048.4, 1065.8, 1082.5, 1098.7, 1114.3, 1129.6};

  eqn = ListInterpolation[{Interpolation[densityData20, (conc*2.) + 1], Interpolation[densityData30, (conc*2.) + 1],
    Interpolation[densityData40, (conc*2.) + 1]}, {20, 30, 40}, InterpolationOrder -> 2];
  eqn[temp]]

denseCFunc[1, 20]
```

1037.8

Mutual Diffusion Coefficients for a Sodium Chloride Solution as a Function of Temperature and Concentration

```
diffFunc[conc_, temp_] := Module[{eqn, diffusivity18, diffusivity25, diffusivity35,
  concentration18, concentration25, concentration35, diffFunc18, diffFunc25, diffFunc35},
  diffusivity18 = {1.26, 1.24, 1.22, 1.2, 1.21, 1.22, 1.23, 1.26, 1.29, 1.33, 1.36, 1.43}/10^9;
  diffusivity25 = {1.547, 1.503, 1.484, 1.476, 1.474, 1.476,
    1.477, 1.478, 1.483, 1.485, 1.498, 1.507, 1.517, 1.541, 1.559, 1.584, 1.591}/10^9;
  diffusivity35 = {1.882, 1.884, 1.872, 1.863, 1.857, 1.867, 1.856, 1.858,
    1.86, 1.87, 1.891, 1.958, 1.976, 1.992, 1.999}/10^9;
  concentration18 = {0.05, 0.1, 0.2, 0.4, 0.6, 0.8, 1., 1.5, 2., 2.5, 3., 4};
  concentration25 = {0.01, 0.05, 0.1, 0.2, 0.5, 0.7, 0.8, 0.9, 1., 1.2, 1.6, 1.8, 2., 2.5, 3., 3.5, 4.};
  concentration35 = {0.0792, 0.0991, 0.1476, 0.1869, 0.1977,
    0.2965, 0.3946, 0.4933, 0.5942, 0.9752, 0.14483, 2.8099, 3.2452, 3.6785, 4.0859};
  Off[InterpolatingFunction::dmval];
  diffFunc18 = ListInterpolation[diffusivity18, concentration18];
  diffFunc25 = ListInterpolation[diffusivity25, concentration25];
  diffFunc35 = ListInterpolation[diffusivity35, concentration35];
  eqn =
  ListInterpolation[{diffFunc18[conc], diffFunc25[conc], diffFunc35[conc]}, {18, 25, 35}, InterpolationOrder -> 2];
  On[InterpolatingFunction::dmval];
  eqn[temp]]

diffFunc[0, 20]
```

1.2301×10^{-9}

Sodium Chloride Solution Viscosity as a Function of Temperature and Concentration

```

viscosityFunc[conc_, temp_] := Module[{eqn, viscosity20, viscosity30, viscosity40},
  viscosity20 = {1.002, 1.047, 1.092, 1.144, 1.203, 1.272, 1.346, 1.42, 1.502}/10^3;
  viscosity30 = {0.7975, 0.834, 0.873, 0.917, 0.964, 1.015, 1.072, 1.133, 1.199}/10^3;
  viscosity40 = {0.653, 0.682, 0.716, 0.753, 0.793, 0.836, 0.836, 0.934, 0.989}/10^3;
  Off[InterpolatingFunction::dmval];

  eqn = ListInterpolation[{Interpolation[viscosity20, (conc*2.) + 1.], Interpolation[viscosity30, (conc*2.) + 1.],
    Interpolation[viscosity40, (conc*2.) + 1.]}, {20, 30, 40}, InterpolationOrder -> 2];
  On[InterpolatingFunction::dmval];
  eqn[temp]]

viscosityFunc[1, 20]

```

0.001092

Program Main Body

```

width = width*2.54/100
height = height*2.54/100
length = length*2.54/100
hydroD = 4*(width*height)/(2*width + 2*height)
flowrate /= (1000*60)
veloc = flowrate/(width*height)

```

0.025908

0.0024892

0.08001

0.00454201

$\frac{1}{60\,000}$

0.258437

```

diffFeed = {diffFunc[feedConcentration[[1]], temperature]}
viscFeed = {viscosityFunc[feedConcentration[[1]], temperature]}
denseFeed = {denseCFunc[feedConcentration[[1]], temperature]}
diffZero = {diffFunc[0, temperature]}
viscZero = {viscosityFunc[0, temperature]}
denseZero = {denseCFunc[0, temperature]}
If[FO == False, vNRe = drawConc*0];
If[FO == True, vNRe = feedConcentration*0];
vNSc = vNRe;
vNSh = vNRe;
If[FO == False, For[i = 1, i ≤ Length[drawConc], i++,
    Print[i];
    vNRe[[i]] = NRe[denseDraw[[i]], veloc, hydroD, viscDraw[[i]]];
    vNSc[[i]] = NSc[viscDraw[[i]], denseDraw[[i]], diffDraw[[i]]];
    vNSh[[i]] = NSh[vNRe[[i]], vNSc[[i]], hydroD, length]]
If[FO == True,
    vNRe[[1]] = NRe[denseFeed[[1]], veloc, hydroD, viscFeed[[1]]];
    vNSc[[1]] = NSc[viscFeed[[1]], denseFeed[[1]], diffFeed[[1]]];
    vNSh[[1]] = NSh[vNRe[[1]], vNSc[[1]], hydroD, length]]
Print[vNRe]
Print[vNSc]
Print[vNSh]
externalBoundThick = vNSh*0;
If[externalPolarization == True,
    For[i = 1, i ≤ Length[vNSh], i++, externalBoundThick[[i]] = boundaryThick[hydroD, vNSh[[i]]]]
Print[externalBoundThick]

```

{ 1.30658 × 10⁻⁹ }

{ 0.00101134 }

{ 1002.35 }

{ 1.2301 × 10⁻⁹ }

{ 0.001002 }

{ 998.2 }

66.1714

{ 1163.4 }

{ 772.216 }

{ 66.1714 }

{ 0.0000686401 }

```

membraneTested = 4
bStart = 0.7
aStart = 0.4
sStart = 500*10^-6

If[membraneTested == 1, membraneData = MPDTFCfluxes;
  membraneError = MPDTFCerror;
  membranePROdata = MPDTFCproFlux];
If[membraneTested == 2, membraneData = EDTFCfluxes;
  membraneError = EDTFCerror;
  membranePROdata = EDTFCproFlux];
If[membraneTested == 3, membraneData = MPDTFCEDfluxes;
  membraneError = MPDTFCEDerror;
  membranePROdata = MPDTFCEDproFlux];
If[membraneTested == 4, membraneData = neatFluxes;
  membraneError = neatError;
  membranePROdata = neatProFlux];
If[membraneTested == 5, membraneData = noriFluxes;
  membraneError = noriError;
  membranePROdata = noriProFlux];
If[membraneTested == 6, membraneData = HTIfluxes;
  membraneError = HTIerror;
  membranePROdata = HTIproFlux];
Print[membraneData]
Print[membraneError]

```

4

0.7

0.4

1
2000

{{4.992, 0.5}, {8.552, 1}, {11.097, 1.5}}

{{1.297, 0.5}, {1.663, 1}, {1.983, 1.5}}

```
diffFunc[membraneData[[1, 2]], 20]
diffFunc[membraneData[[2, 2]], 20]
diffFunc[membraneData[[3, 2]], 20]
Length[membraneData]
```

1.28068×10^{-9}

1.30073×10^{-9}

1.32312×10^{-9}

3

```
{fluxEqn[False, 1, membranePROdata[[1, 1]], aVal, b, s, externalBoundThick[[1]],
 0, 20, 0.1, 0, diffFeed[[1]], diffZero[[1]]], saltFlux[False, membranePROdata[[1, 1]],
 membranePROdata[[2, 1]], aVal, b, s, externalBoundThick[[1]], 20, 0.1, 0, diffFeed[[1]], diffZero[[1]]]}
```

$$\left\{ \begin{aligned} 4.69129 &= \frac{4.55221 \text{ Abs}[aVal]}{1 + 0.213161 \left(-0.933831 + e^{1059.38 \text{ Abs}[s]} \right) \text{ Abs}[b]}, \\ 0.026162 &= \frac{0.0933831 \text{ Abs}[b]}{1 + 0.213161 \left(-0.933831 + e^{1059.38 \text{ Abs}[s]} \right) \text{ Abs}[b]} \end{aligned} \right\}$$

```
eqnToSolve = concSol /. {cF → 0.1, t → 20, dF → diffFeed, d → externalBoundThick, dD → 1.3*10^-9}
outputArr = {{a, b, s, jW}}
originalData = membraneData
```

```
as = FindFit[membraneData, eqnToSolve /. b → 0, {{a, aStart}, {s, sStart}},
  jW, {MaxIterations → 10 000, PrecisionGoal → 4, AccuracyGoal → 6}]
aBool = 0;
bBool = 0;
sBool = 0;
While[aBool*bBool*sBool == 0,
  aVal = a /. as;
  sVal = s /. as;
  bVal = b /. FindRoot[saltFlux[False, membranePROdata[[1, 1]], membranePROdata[[2, 1]],
    aVal, b, sVal, externalBoundThick[[1]], 20, 0.1, 0, diffFeed[[1]], diffZero[[1]],
    {b, bStart}, {MaxIterations → 10 000, AccuracyGoal → 6, PrecisionGoal → 4}];
  as = FindFit[membraneData, eqnToSolve /. b → bVal, {{a, aStart}, {s, sStart}}, jW,
    {MaxIterations → 10 000, PrecisionGoal → 4, AccuracyGoal → 6}];
  If[Abs[oldA - aVal] ≤ 0.0001, aBool = 1, aBool = 0];
  If[Abs[oldB - bVal] ≤ 0.00001, bBool = 1, bBool = 0];
  If[Abs[oldS - sVal] ≤ (1*10^-6), sBool = 1, sBool = 0];
  oldA = aVal;
  oldB = bVal;
  oldS = sVal];
modeledPRO =
```



```

FindRoot[{fluxEqn[False, 1, jW, aVal, bVal, sVal, externalBoundThick[[1]], 0, 20, 0.1, 0, diffFeed[[1]], diffZero[[1]]],
{ jW, membranePROdata[[1, 1]]}];
Print[aVal, " ", bVal, " ", sVal, " ", jW /. modeledPRO];
AppendTo[outputArr, {aVal, bVal, sVal, jW /. modeledPRO}];

For[i = 1, i ≤ 1000, i++;
valAdjust = RandomReal[{-1, 1}];
membraneData[[1, 1]] = originalData[[1, 1]] + membraneError[[1, 1]] * valAdjust;
membraneData[[2, 1]] = originalData[[2, 1]] + membraneError[[2, 1]] * valAdjust;
membraneData[[3, 1]] = originalData[[3, 1]] + membraneError[[3, 1]] * valAdjust;
as = FindFit[membraneData, eqnToSolve /. b → 0, {{a, aStart}, {s, sStart}},
jW, {MaxIterations → 10 000, PrecisionGoal → 9, AccuracyGoal → 4}];
aBool = 0;
bBool = 0;
sBool = 0;
While[aBool * bBool * sBool == 0,
aVal = a /. as;
sVal = s /. as;
bVal = b /. FindRoot[saltFlux[False, membranePROdata[[1, 1]] + valAdjust * membranePROdata[[1, 2]],
membranePROdata[[2, 1]] + valAdjust * membranePROdata[[2, 2]], aVal,
b, sVal, externalBoundThick[[1]], 20, 0.1, 0, diffFeed[[1]], diffZero[[1]],
{b, bStart}, {MaxIterations → 10 000, AccuracyGoal → 9, PrecisionGoal → 4}];
as = FindFit[membraneData, eqnToSolve /. b → bVal, {{a, aStart}, {s, sStart}}, jW,
{MaxIterations → 10 000, PrecisionGoal → 9, AccuracyGoal → 4}];
If[Abs[oldA - aVal] ≤ 0.0001, aBool = 1, aBool = 0];
If[Abs[oldB - bVal] ≤ 0.00001, bBool = 1, bBool = 0];
If[Abs[oldS - sVal] ≤ (1 * 10^-6), sBool = 1, sBool = 0];
oldA = aVal;
oldB = bVal;
oldS = sVal];
modeledPRO =
FindRoot[{fluxEqn[False, 1, jW, aVal, bVal, sVal, externalBoundThick[[1]], 0, 20, 0.1, 0, diffFeed[[1]], diffZero[[1]]],
{ jW, membranePROdata[[1, 1]]}];
Print[aVal, " ", bVal, " ", sVal, " ", jW /. modeledPRO];
AppendTo[outputArr, {aVal, bVal, sVal, jW /. modeledPRO}];]
membranePROdata[[1, 1]]

Export["h:membrane.xls", outputArr]

```

$$\left\{ \frac{0.0205138 e^{213.675 jW \text{Abs}[s]} jW}{\text{Abs}[a]} - \frac{0.0205138 \text{Abs}[b]}{\text{Abs}[a]} + \frac{0.0205138 e^{0.0145928 jW+213.675 jW \text{Abs}[s]} \text{Abs}[b]}{\text{Abs}[a]} + \frac{0.1 e^{0.0145928 jW+213.675 jW \text{Abs}[s]}}{1. + \frac{(e^{0.0145928 jW-1.} e^{-213.675 jW \text{Abs}[s]}) \text{Abs}[b]}{jW}} - \frac{0.1 e^{0.0145928 jW} \text{Abs}[b]}{jW \left(1. + \frac{(e^{0.0145928 jW-1.} e^{-213.675 jW \text{Abs}[s]}) \text{Abs}[b]}{jW} \right)} + \frac{0.1 e^{0.0291857 jW+213.675 jW \text{Abs}[s]} \text{Abs}[b]}{jW \left(1. + \frac{(e^{0.0145928 jW-1.} e^{-213.675 jW \text{Abs}[s]}) \text{Abs}[b]}{jW} \right)} \right\}$$

{{a, b, s, jW}}

{{4.992, 0.5}, {8.552, 1}, {11.097, 1.5}}

{a → 0.433349, s → 0.000357718}

0.444786 0.289324 0.000360024 2.04372

0.578045 0.375845 0.0003657 2.60823

0.445049 0.289514 0.000360041 2.04485

0.493763 0.322229 0.000363182 2.25329

0.468083 0.305172 0.000361718 2.14372

0.494303 0.322583 0.000363208 2.25559

0.624377 0.403946 0.000366049 2.80043

0.624183 0.40383 0.000366048 2.79963

0.357702 0.226809 0.000349005 1.66463

0.443561 0.288492 0.000359919 2.03845

0.428096 0.277775 0.00035854 1.97172

0.339425 0.212904 0.000345351 1.58396

0.364631 0.232002 0.000350239 1.69511

0.647612 0.417717 0.000366028 2.89606

0.354028 0.224039 0.000348318 1.64844

0.449146 0.292323 0.000360368 2.06248

0.494972 0.323023 0.000363241 2.25844

0.434748 0.282404 0.000359158 2.00045

0.560636 0.365048 0.000365407 2.53549

0.50973 0.33266 0.000363898 2.32108

0.382668 0.245328 0.000353108 1.77419

0.542815 0.353853 0.000364999 2.46072

0.633753 0.409527 0.000366054 2.83908

0.363986 0.231521 0.000350127 1.69228

0.331996	0.207161	0.000343682	1.55105
0.473196	0.308605	0.000362041	2.16559
0.333533	0.208354	0.000344037	1.55786
0.595901	0.38678	0.000365903	2.68254
0.336421	0.210588	0.00034469	1.57066
0.654009	0.421473	0.000366003	2.92231
0.471884	0.307725	0.00036196	2.15998
0.377506	0.241542	0.000352335	1.7516
0.411749	0.266273	0.000356844	1.90091
0.321228	0.198739	0.000341052	1.50323
0.366407	0.233326	0.000350543	1.70291
0.31644	0.194957	0.000339796	1.48192
0.37245	0.237812	0.000351541	1.72944
0.594942	0.386196	0.000365894	2.67856
0.281564	0.166626	0.000328716	1.32583
0.3354	0.209799	0.000344461	1.56613
0.429729	0.278914	0.000358695	1.97878
0.280919	0.166089	0.000328474	1.32293
0.493511	0.322063	0.000363169	2.25222
0.379314	0.24287	0.00035261	1.75951
0.63885	0.412548	0.000366049	2.86005
0.375848	0.240321	0.000352078	1.74433
0.327436	0.203609	0.0003426	1.53082

-Output truncated-

4.69129

h:membrane.xls